Advanced Underseepage Analyses for Levees

Abeera Batool

Dissertation submitted to the faculty of the
Virginia Polytechnic Institute and State University
in partial fulfillment of the requirements for the degree of

Doctor of Philosophy

In
Civil and Environmental Engineering

Thomas L. Brandon - Chair
James K. Mitchell
J. Michael Duncan
Mark A. Widdowson

September 23, 2013
Blacksburg, Virginia

Keywords: levee, underseepage, finite element analysis, blanket theory, permeability, seepage berms, field test

Advanced Underseepage Analyses for Levees

By Abeera Batool

Dr. Thomas L. Brandon-Chair
Charles E. Via, Jr. Department of Civil and Environmental Engineering

ABSTRACT

The events of Hurricane Katrina in 2005 prompted the US Army Corps of Engineers (USACE) to commission studies to identify the failure mechanisms of levees and I-walls. This involves updating of the current USACE Engineering Manual (EM) 1110-2-1913, "Design and Construction of Levees," which uses *Blanket Theory* for seepage analysis. Blanket Theory entails analytical methods for calculating seepage pressures and flows beneath levees. The revision of the manual will address the design seepage criteria for levees, with a focus on incorporating new seepage analysis procedures besides Blanket Theory. Finite element analysis is one such method that has more recently become the method of choice for general seepage analyses in geotechnical engineering.

The focus of this research is mainly on underseepage analyses of levees in the lower Mississippi valley using numerical modeling, with a goal of helping engineers in making the transition from current Corps methods to finite element analysis. General guidelines are provided to conduct seepage analysis using finite element analysis for pre-defined Blanket Theory cases as well as for the design of seepage berms. In addition, the 3D finite element modeling is conducted for a full-scale field load test involving complex geometry and stratigraphy, which is useful in better understanding the response of levees and I-walls.

Dedication

This work is dedicated to my wonderful Parents, my (late) father for teaching me to dream big and my mother for supporting me to realize all those big dreams. Thank you Abboo and Ammi Jan, whatever I have achieved in this life is because of you !!!

Acknowledgements

First, I would like to thank Almighty Allah for giving me the strength to finish my research and for His countless blessings in my life.

I would like to thank my advisor Professor Brandon who has been a source of continuous inspiration for me and has helped me at every step of my research. He has not only been a great advisor but a true mentor to me, and I cannot express enough gratitude for his guidance and unwavering support. Thank you, Professor Brandon!

I would also like to thank my committee members Professor Mike Duncan, Professor James Mitchell, and Professor Mark Widdowson for their time, guidance and valuable inputs and suggestions.

Special thanks to all the geotechnical faculty and students. It was truly a great experience to be a part of this wonderful program, and to all my PhD cellmates for the invaluable discussions and brainstorms.

I had an amazing time in Blacksburg, and it was possible due to all the precious friends that I made. Some are still there in Blacksburg; others left over the years but still gave me their support and love. Special thanks to Sherif and Heba for all their support and help, and always being there for me in the time of need. I would take this opportunity to thank Kashyap, Laura, Martha, Ozgur, Abeer, Tila, and Salma for their invaluable friendship, and new friends Youssef, Maryam, Tani, and Rajat for helping me to keep going in those last few months.

Last but not least, I can't express enough gratitude to my wonderful wonderful family. My mom who has been there for me for every step of the way, giving me her love, support, and care. This degree is as much hers as mine. I would also like to thank my brothers Kashif and Wasif, for driving 8 hours to frequently see me without complaining (mostly), and always giving me their unconditional love and support, and my sister-in-law Shenaz for lending an ear when I needed it the most. Thanks to my family in Pakistan including Hajra Baji and Atif Bhai, for their prayers, and long phone calls to show their support, and all the nephews, nieces, cousins, aunts, and uncles for their love. I am truly blessed to have such wonderful people in my life.

Table of Contents

List of Figures

List of Tables

CHAPTER 1. INTRODUCTION

1.1 Background

Underseepage is a concern for many levees along the Mississippi River, especially in the lower valley due to unique geology of the soil. These levees are often characterized by the presence of a pervious stratum overlain by a top stratum of lower permeability. The seepage that takes place in the pervious stratum due to the difference in hydrostatic head of water between the riverside and the landside, and emerges on the landside of the levee is termed as underseepage. This can result in many instability problems like erosion and piping along with the sand boils. The presence of the fine-grained top stratum over the pervious material can also result in heave problems. Historically, US Army Corps of Engineers (USACE) have undergone massive studies to fully understand the problem and develop analytical solutions that best represent the conditions for the levees along the Mississippi River. This has resulted in publications of many Corps documents covering a wide variety of topics including theoretical methods to analyze seepage and stability problems of the levees. Finite element analysis has more recently become the method of choice for general seepage analyses in geotechnical engineering. The focus of this research is mainly on underseepage analyses of the levees in lower Mississippi valley using numerical modeling, and helping the engineers in making the transition from current Corps methods to Finite element analysis.

1.1.1 Geological History of Mississippi Levees

The geology of the Mississippi River Valley is unique in nature. Most of the soils in the valley were deposited by the Mississippi River due to the melting of the glacial ice during the late or postglacial times (Mansur and Kaufman 1956). During the initial period, the river mostly

carried the sands with gravel deposits from the edges of the slope and deposited them in the valley. The thickening of the valley floor took place with time and ultimately the stream slopes were reduced. This resulted in the reduction of the soil carried by the river and also decreased the grain sizes of these soils, and the type of the soil carried by the river changed to coarse sands, and then ultimately to fine sands. In the meantime, alteration of Mississippi River from braided to meandering stream also changed the soil type carried by it. The fine-grained soils were now deposited by the river instead of the coarse-grained deposits. The geology in the region is reflected by these depositions, where there are thick deposits of pervious materials overlain by the top stratum of fine-grained material. This pervious material has high permeability and can allow the water to flow through it causing underseepage and many problems associated with it.

1.1.2 Seepage Analyses

The U.S. Army Corps of Engineers (USACE) Engineering Manual (EM) 1110-2-1901, "Seepage Analysis and Control of Dams," (USACE 1986) has outlined numerous methods to conduct seepage analysis. These methods are based on having exact or approximate solutions for Laplace Equation for two-dimensional, steady state, laminar flow in an isotropic, homogeneous, porous medium. Laplace Equation can be solved by graphical methods, physical models, analog models, analytical methods or numerical models and analysis. The flow net has been a popular graphical method for two-dimensional seepage analysis which is useful in visualizing the flow regime. However, it can be hard to draw flow nets for complex scenarios and the analytical methods and numerical analysis are useful for such cases. Pavlovsky (1935), and later, Harr (1962), provided a very useful method to conduct seepage analysis by dividing the complex

seepage problem into fragments, solving the fragments independently, and then combining them together to determine the solution for the entire problem.

USACE Technical Manual (TM) 3-424, "Investigation of Underseepage and Its Control" (USACE 1956) developed the solutions for the lower Mississippi River levees based on the Method of Fragments. Some earlier work by Forchheimer (1917) and Muskat (1937) on flow through porous media also contributed to the development of these theoretical solutions. Similarly, Turnbull and Mansur (1956) investigated the underseepage along Mississippi River levees and contributed to the solutions along with work done by Bennett (1946) and Barron (1948) on the effects of semipervious blankets.

These solutions also appear in USACE Engineering Manual (EM) 1110-2-1913, "Design and Construction of Levees," (USACE 2000) and are generally termed as "Blanket Theory" solutions. These solutions are used for calculating flows under the levees and are also useful for calculating the seepage pressures. The term "blanket" is used because these solutions were especially developed for the geology along the Mississippi River where a pervious stratum is overlain by a less pervious top stratum or blanket, as explained earlier. Even if the top stratum is comprised of different layers of less pervious materials, these different permeabilities and thicknesses are transformed into a "blanket" of uniform thickness and permeability in the blanket theory solutions.

1.2 Motivation of Research

The events of Hurricane Katrina prompted USACE to undergo extensive study to identify the failure mechanisms of levees and I-walls. Interagency Performance Evaluation Taskforce (IPET) also conducted the analyses to understand the failure mechanisms and performance of

Hurricane Protection System in southeast Louisiana (IPET 2007). Current seepage analysis methods in EM 1110-2-1913 are to be updated to incorporate the lessons learned from the events of Hurricane Katrina. The revision of the manual will address the design seepage criteria for levees, with a focus on incorporating new seepage analysis procedures. There have been few changes to the methods outlined in EM 1110-2-1913 since the initial adoption, but recent failures of levees during Hurricane Katrina have prompted the revision due to its wide use across the USACE districts for seepage evaluation and design of levees.

Other methods besides blanket theory also need to be considered for performing the seepage analysis. However, guidelines should be provided in the revised engineering manual to conduct these methods. One such method is finite element analysis, which is becoming popular because of the commercially available software. Finite element analysis can also be applied to Hurricane Katrina-related problems that require more advanced seepage analysis to understand the failure mechanisms. Similarly, there is also a need of updating the Appendix C in EM 1110-2-1913, and guidelines to use finite element analysis for the design of seepage berms can be useful in this regard.

1.3 Objectives of Research

This research involves the study of blanket theory solutions, finite element analysis, seepage berm design and advanced seepage analysis for complex geometries. The purpose of the research about blanket theory is two-fold. First, there are no published proofs of the derivations of equations present in the engineering manual. Therefore, it is desirable to document the derivations and to make corrections where necessary. In addition, there are several simplifying (and sometimes limiting) assumptions made in the derivation of the equations. These

assumptions may not be appropriate for many cases, thereby reducing the applicability of the blanket theory equations for certain geometries encountered, and it is important to highlight such cases. In the EM, nine configurations (Cases 1 through 7[1]) have been addressed. An additional Case 8 is developed as part of this research to show how blanket theory can be modified to accommodate cases where sheet pile cutoffs are employed. The second objective of blanket theory study is to develop the guidelines for finite element analysis to help practicing engineers make a transition from analytical solutions to more advanced numerical modeling, which has wider applications.

Design of seepage berms is discussed in Appendix C of EM 1110-2-1913 (USACE 2000), in addition to TM 3-424, *DIV*ision *R*egulation (DIVR) 1110-1-400 (1998) and some other Corps publications. Barron (1980) also discusses the design equations for different types of berms. However, these are all theoretical solutions and similar to blanket theory, finite element guidelines are also developed for the design of seepage berms.

The advanced seepage analysis involving 3D finite element will also be conducted and numerical model will be developed for a full-scale field load test. The detailed investigation of various seepage problems using both 2D and 3D finite element analysis will provide a useful insight for better understanding the complex geometries and seepage boundary conditions, and give better perspective of limitation of various methods. Based on the results of the advanced seepage analyses, parameters are also recommended for conducting finite element analyses for levees along the London Avenue Canal in New Orleans, LA.

---

[1] Case 7 is comprised of 7a, 7b, and 7c.

1.4 Annotated Research Outline

Chapter 1: *Introduction*

This chapter provides the background information on the research topics including research objectives.

Chapter 2: *Comparison of Seepage Analysis of Levees using Blanket Theory and Finite Element Analysis*

Blanket theory is based on certain simplifying and limiting assumptions that restrict its application to relatively simple seepage problems. Blanket Theory equations presented in various Corps documents were reviewed in this chapter, and any inconsistencies in the equations were highlighted. Blanket Theory discusses seven different cases based on different types of top strata, and an additional Case 8 was developed as part of this research to increase the accuracy of seepage calculations for cases where sheet pile cutoffs are employed. EM 1110-2-1913 is in the process of being revised and as part of helping in the transition between the use of blanket theory and finite element analysis, an extensive study was performed comparing the results of finite element analyses conducted on the original blanket theory cases and guidelines were provided to conduct finite element analysis for each case separately. These guidelines could serve as a preliminary point for using finite element seepage analyses for more complicated analyses of seepage beneath levees.

Chapter 3: *Finite Element Analyses of Landside Seepage Berms*

Design of seepage berms is provided in Appendix C of EM 1110-2-1913 (USACE 2000), and the revision of the EM will also include the design of seepage berms using finite element analysis. A procedure consistent with the current design equations was developed to use finite

element analysis for the berm design, and a step-by-step method was explained to achieve this. Finite element guidelines were provided for each type of berm separately and the results were explained using multiple design examples. Cases with no top stratum were also explored in this chapter, because design equations in Appendix C are only for the cases having a blanket overlying the pervious stratum. Moreover, discrepancies in the definition of the factor of safety for each berm type were highlighted. The economics and the safety of different berm slopes were also investigated as a part of the research.

Chapter 4: *Analytical Calibration Approach to Develop a Seepage Model for the London Avenue Canal Load Test*

In addition to analyses conducted by Interagency Performance Evaluation Taskforce (IPET) to assess the performance of the Hurricane Protection System in New Orleans and southeast Louisiana (IPET 2007), USACE also carried out a load test along a portion of the London Avenue Canal following Hurricane Katrina to study the performance of levees and I-walls. London Avenue Canal load test was unique in a sense that it is very rare to have a full-scale field load test available to be compared with the numerical model, and check the validity of the finite element analysis. The London Canal load test involved a very complex geometry and provided an opportunity to perform advanced seepage analysis. Therefore, a 3D finite element model was used to depict the true geometrical nature of the load test, and a statistical calibration procedure was developed for the determination of the best possible values of the parameters having the greatest uncertainty. More than 1200 finite element runs were conducted for this approach and boundary conditions and hydraulic properties were recommended for future analyses of the London Avenue Canal, and other canals having similar subsurface conditions.

Chapter 5: *Conclusions*

This chapter provides overall concluding remarks for all the preceding chapters.

Appendix A

This appendix is the report submitted to USACE titled "Levee Seepage Analysis using Blanket Theory and Finite Element Analysis (Brandon et al. 2013)." This appendix is related to Chapter 2 of the dissertation and contains derivation of each case of blanket theory based on method of fragments, discussion about inconsistencies in blanket theory equations, evaluation of blanket theory cases with finite element analyses, general finite element guidelines to perform seepage analysis, and discussion about layered top strata. This appendix shows many additional figures presenting the results of the research.

Appendix B

This appendix is the report submitted to USACE titled "Finite Element Seepage Analysis of the London Avenue Canal Load Test (Batool and Brandon 2010)." This appendix is related to Chapter 4 of the dissertation and provides detailed discussion on determining the permeability of load test soils, numerical modeling including calibration approach and parametric analyses, 3D finite element analysis of the load test, and future recommendations.

1.5 References

Barron, R. A. (1948). "The Effect of a Slightly Pervious Top Blanket on the Performance of Relief Wells," Proceedings of the Second International Conference on Soil Mechanics and Foundation Engineering, Rotterdam, Netherlands, Vol 4, p 342.

Barron, R. A. (1980). "Mathematical analysis of landside seepage berms," Miscellaneous Paper GL-80-15, U.S. Army Engineer Waterways Experiment Station, Vicksburg, MS.

Batool, A., and Brandon, T.L. (2010). "Finite Element Seepage Analysis of the London Canal Load Test using Blanket Theory and Finite Element Analysis," Report submitted to the U. S. Army Corps of Engineers Engineering Research and Development Center, Dept. of Civil and Environmental Engineering, Virginia Tech, Blacksburg, VA, 67 pp

Bennett, P.T. (1946). "The effect of blankets on the seepage through pervious foundation." Trans. ASCE 11, p. 215

Brandon, T. L., Batool, A., Jimenez, M., and Vroman, N., (2013). "Levee Seepage Analysis using Blanket Theory and Finite Element Analysis," Report submitted to the U. S. Army Corps of Engineers Engineering Research and Development Center, Dept. of Civil and Environmental Engineering, Virginia Tech, Blacksburg, VA, 129 pp.

DIVR 1110-1-400 (1998). "Engineering and Design, Soil Mechanics Design Data, Part 6 - Landside Seepage Berms for Mississippi River and Major Tributary Levees, U.S Army Corps of Engineers, Mississippi Valley Division, Vicksburg, MS, 32 pp.

Forchheimer, P. (1917). " Zur Grundwasserbewegung nach isothermischen Kurvenscharen. (On the movement of groundwater according to sets of isothermal curves)." Sitzungsber K-K Akad der Wissenschaft 126(4):409-40 (in German).

Harr, M.E. (1962). Groundwater and seepage. McGraw-Hill, New York.

Interagency Performance Evaluation Task Force (IPET). (2007). "Performance evaluation of the New Orleans and Southeast Louisiana Hurricane protection system." Final Rep. of the Interagency Performance Evaluation Task Force, U.S. Army Corps of Engineers, (www.ipet.army.mil).

Mansur, C. I., and Kaufman, R.I. (1956). "Control of Underseepage, Mississippi River Levees, St. Louis District, CE," Journal of the Soil Mechanics and Foundations Division, 82, 864-871.

Muskat , M. (1937). The flow of homogeneous fluids through porous media. McGraw-Hill.

Pavlovsky, N.N. (1956). Collected works. Akad. Nauk USSR, Leningrad.

United States Army Corps of Engineers (USACE) (1956). “Investigating Underseepage and its Control, Lower Mississippi River Levees, Technical Memorandum 3-424,” U.S. Army Corps of Engineers, Waterway Experiment Station, Vicksburg, MS.

United States Army Corps of Engineers USACE (1986) Seepage Analysis and Control of Dams, Engineer Manual 1110-2-1901. U.S. Army Corps of Engineers, Washington, DC.

USACE (2000). “Design and Construction of Levees, Engineer Manual 1110-2-1913,” U.S. Army Corps of Engineers, Washington, DC.

CHAPTER 2. COMPARISON OF SEEPAGE ANALYSIS OF LEVEES USING BLANKET THEORY AND FINITE ELEMENT ANALYSIS

Additional information regarding research presented in this chapter can be found in Appendix A

2.1. Authors

Abeera Batool[1] and Thomas L. Brandon[1]

[1]*Dept. of Civil and Environmental Engineering, Patton Hall, Virginia Polytechnic Institute and State University (Virginia Tech), Blacksburg, VA 24061 USA*

2.2. Abstract

Blanket Theory has been used by the US Army Corps of Engineers and their contractors for over 60 years to calculate flows, hydraulic gradients, and pore pressures beneath Mississippi River levees. Finite Element Analysis has more recently become the method of choice for general seepage analyses in geotechnical engineering. As part of assisting in the transition between the use of blanket theory and finite element analysis, the authors have performed an extensive study comparing the results of finite element analyses conducted on the original blanket theory cases contained in the Corps' engineering manuals. The results have shown that for like conditions, there is a very good agreement between the two methods.

Guidelines are given for correctly assigning boundary conditions in finite element analysis to be consistent with the individual blanket theory cases. These guidelines should serve as a starting point for using finite element seepage analyses for more complex analyses of seepage beneath levees.

2.3. Introduction

The U.S. Army Corps of Engineers (USACE) Engineering Manual (EM) 1110-2-1901, "Seepage Analysis and Control of Dams," (USACE 1986) outlines several methods to perform seepage analysis. All these methods involve an exact or approximate solution of Laplace Equation. The governing Laplace Equation for two-dimensional, steady state, laminar flow in an isotropic, homogeneous, porous medium is shown in Equation 2-1, with *h* representing total hydraulic head and *x* and *y* being dimensional parameters.

$$\frac{\partial^2 h}{\partial x^2} + \frac{\partial^2 h}{\partial y^2} = 0 \tag{2-1}$$

Solutions to the Laplace Equation include graphical methods (flow nets), physical models, analog models (electrical and thermal analogy), analytical methods (mapping, semi empirical or closed form solutions) or numerical models and analysis (finite element, finite difference, etc.). The flow net has been a popular graphical method for two-dimensional seepage analysis for cases where the boundary conditions and geometry of the flow problem are known. This method is useful in visualizing the flow regime, and generations of students and engineers have been familiar with its use. However, it can be difficult to draw flow nets for complex scenarios. The use of analytical methods and numerical analysis becomes useful for such cases. Pavlovsky (1935), and later, Harr (1962), provided a very useful method to perform seepage analysis by dividing the complex seepage problem into parts or fragments, analyzing the fragments separately, and then recombining these fragments together to determine the solution for the overall problem. This method, called the "Method of Fragments," was also used by Griffith (1984) to develop the rationalized charts to estimate seepage quantities and exit gradients for

confined flow problems. These charts were developed by evaluating the accuracy of Method of Fragments using finite element analysis.

The Method of Fragments forms the basis of solutions that were developed in USACE Technical Manual (TM) 3-424, "Investigation of Underseepage and Its Control" (USACE 1956) for the lower Mississippi River levees. These solutions that also appear in USACE Engineering Manual (EM) 1110-2-1913, "Design and Construction of Levees," (USACE 2000) are commonly referred to as "Blanket Theory" solutions and are useful for calculating seepage pressures and flows beneath levees. The term "blanket" is used because these solutions were developed for levee stratigraphy where a top stratum overlies a thicker, pervious stratum. Top strata of different permeabilities and thicknesses are transformed into a "blanket" of uniform thickness and permeability. The thickness and permeability of this blanket (transformed top stratum) can be different on the landward and riverward sides.

Blanket theory involves certain simplifying and restricting assumptions that limit its application to relatively simple seepage problems. The USACE is in the process of revising its levee engineering manual (EM 1110-2-1913), and there is a need to incorporate other methods besides blanket theory into the manual for performing seepage analysis, with guidelines for their application included. A readily applicable method is the finite element analysis with commercially available software. In order to ease the transition from blanket theory to finite element analysis, the normal blanket theory cases were analyzed using both methods to examine the differences in seepage quantities and excess hydraulic heads. From these analyses, finite element boundary conditions can be specified that provide similar results as blanket theory.

2.4. Blanket Theory Cases

The blanket theory solutions were developed in TM 3-424 using a compilation of existing theories and methods such as the *Method of Fragments* (Forchheimer 1917, Muskat 1937, Pavlovsky 1935, and Harr 1962), investigation of underseepage along Mississippi River levees by Turnbull and Mansur (1956), and Bennett's (1946) and Barron's (1948) contributions on the effects of semipervious blankets. However, both TM 3-424 and EM 1110-2-1913 did not provide derivations for these solutions. Therefore, a study was conducted at Virginia Tech (Brandon et al. 2009) to provide a detailed outline of the derivations of the different cases of blanket theory and to fully document the derivations, with corrections being made, if necessary.

In the EM, solutions are given for nine different configurations of impervious and semipervious top stratum conditions. Figure 2-1 shows the general geometry of the levee used for blanket theory solutions of the different cases.

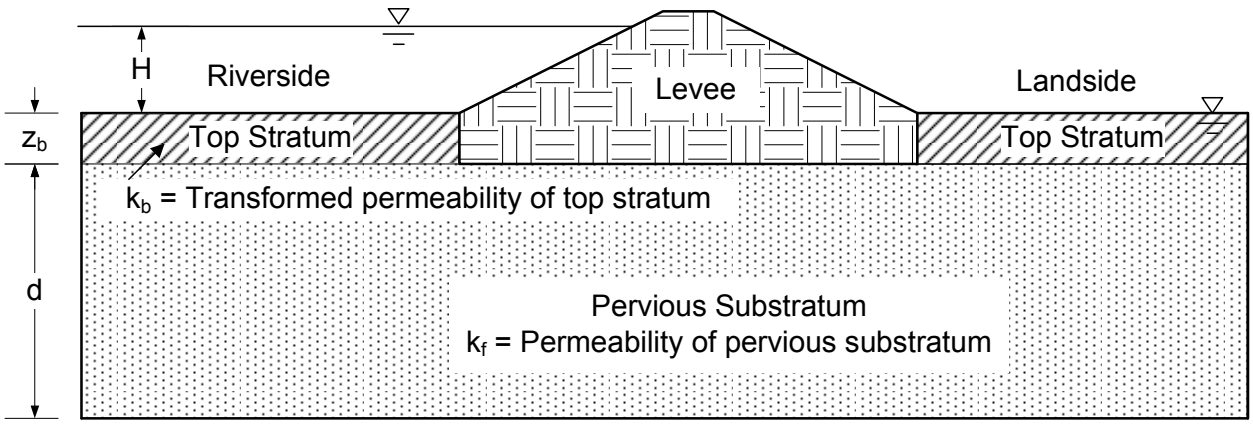

Figure 2-1 Basic geometry of a blanket theory case.

The following cases are addressed in EM 1110-2-1913:

Case 1 - No landside and riverside top stratum

Case 2 - Impervious landside and riverside top stratum

Case 3 - Impervious riverside top stratum and no landside top stratum

Case 4 - Impervious landside top stratum and no riverside top stratum

Case 5 - Semipervious riverside top stratum and no landside top stratum

Case 6 - Semipervious landside top stratum and no riverside top stratum

Case 7a - Semipervious landside and riverside top stratum (top stratum extends infinitely landward of the levee)

Case 7b - Semipervious landside and riverside top stratum (seepage block in the pervious substratum located landward of the levee, this block can be due to change in topography or geology like sharp rise in ground surface or presence of clay filled channel at landside of the levee)

Case 7c - Semipervious landside and riverside top stratum (seepage exit in the pervious substratum located landward of the levee, top stratum is of finite extent with an open seepage exit)

An additional Case 8 was developed as part of this research to increase the accuracy of seepage calculations for cases where sheet pile cutoffs are employed. The equations can be developed for different depths of sheet pile penetration into the pervious layer. Case 8 is identical to Case 7 with the sheet pile cutoff added. Both have a semipervious layer on the riverside and the landside. Similar to Case 7, Case 8 has been subdivided into 8a, 8b, and 8c as described below.

Case 8a - Semipervious landside and riverside top stratum (top stratum extends infinitely landward of the levee) with cutoff

Case 8b - Semipervious landside and riverside top stratum (seepage block in the pervious substratum located landward of the levee) with cutoff

Case 8c - Semipervious landside and riverside top stratum (seepage exit in the pervious substratum located landward of the levee) with cutoff

2.4.1. Derivations of Blanket Theory Equations based on Method of Fragments

The blanket theory equations were verified for each case and corrections were made where necessary (Brandon et al. 2009). The derivation of the new Case 8 is discussed here to demonstrate this method. Figure 2-2 shows the basic geometry for Case 8. The fundamental assumption of this method, as stated by Harr (1962), is that equipotential lines at various critical parts of the flow region can be approximated by vertical lines that divide the region into sections or *fragments*.

The application of the Method of Fragments is limited to the cases where the base width of the levee, L_2, is greater than the thickness of the pervious substratum, d, (i.e. $L_2/d \geq 1$). The assumption that the equipotential lines are vertical is often violated if $L_2/d < 1$, and hence the Method of Fragments and accordingly, blanket theory solutions, are limited to cases where $L_2/d \geq 1$.

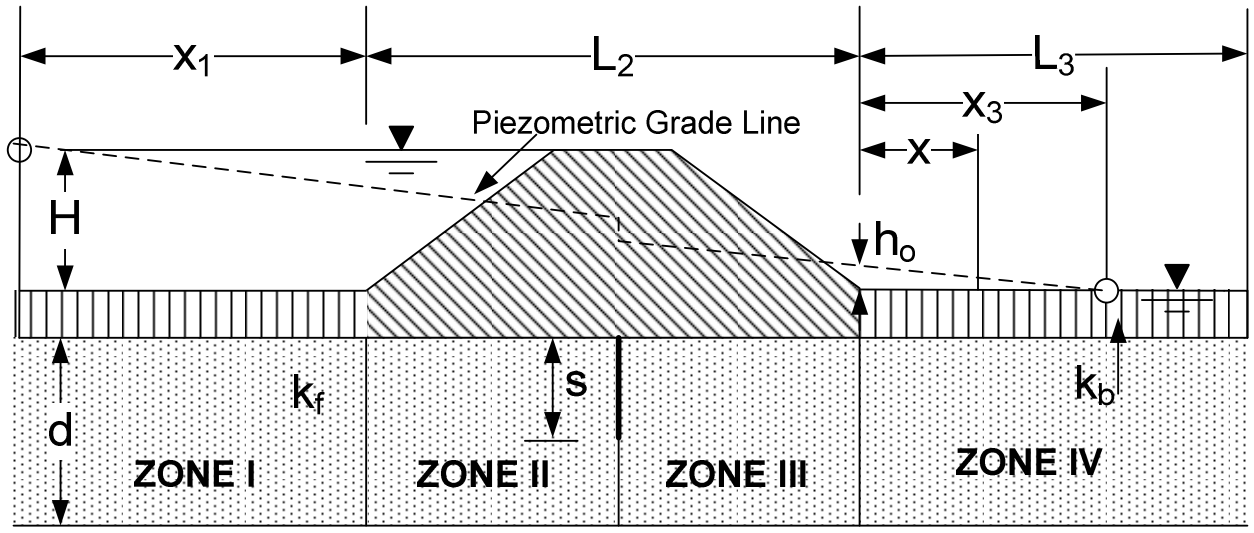

Figure 2-2 Case 8 - Semipervious top strata both riverside and landside with sheet pile at the center of levee, also showing the parameters used for blanket theory analysis.

The flow or seepage per unit length of the levee (Q_s) is computed using Equation 2-2:

$$Q_s = \frac{k_f H}{\sum \Phi} \tag{2-2}$$

Where,

k_f = Horizontal permeability of the pervious substratum

H = Net head on levee (head loss under structure)

Φ = Dimensionless form factor

Equation 2-2 is similar to the general seepage equation based on Darcy's Law, which is:

$$Q_s = \delta \cdot k_f \cdot H \tag{2-3}$$

Where,

$$\delta = \frac{1}{\Sigma \Phi} = \text{Shape factor} \tag{2-4}$$

An understanding of the correct application of the dimensionless *form factors* is necessary to properly use the Method of Fragments. The form factors were divided into different types or categories by Harr (1962) using Pavlovasky's procedure (1935). A summary of fragment types and form factors is presented in Harr (1962) and is useful as a reference to calculate the form factors of various types of zones for different seepage cases. Table 2-1 shows some examples of form factors developed by Harr (1962) for different cases.

Table 2-1 Examples of form factors for some general cases developed by Harr (1962)

Fragment Type	Illustration	Form Factor (Φ)
I	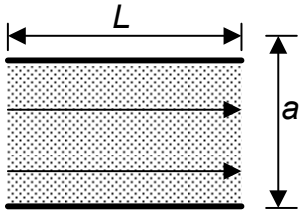	$\Phi = L/a$
II	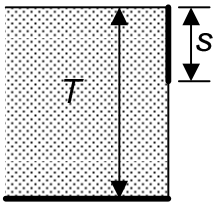	$\Phi = K/K'$ $m = \sin\frac{\pi s}{2T}$
III	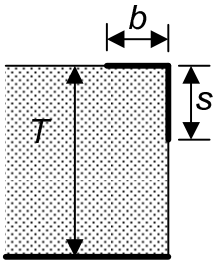	$\Phi = K/K'$ $m = \cos\frac{\pi s}{2T}\sqrt{tanh^2\frac{\pi b}{2T} + tan^2\frac{\pi s}{2T}}$

The inclusion of the cutoff requires that the section be divided into four zones or fragments as shown in Figure 2-2. It is assumed that the equipotential lines will be vertical under the sheet pile as well as under the landside and riverside slope toes of the levee.

The form factors for Zones I, II, III and IV are given by:

$\Phi_1 = x_1/d$ (Type-I Fragment)

$\Phi_2 = K/K'$ (Type-III Fragment)

$\Phi_3 = K/K'$ (Type-III Fragment)

$\Phi_4 = x_3/d$ (Type-I Fragment)

Where,

x_1 = Distance of effective seepage entry

x_3 = Distance of effective seepage exit

K/K'= Ratio of complete elliptic integral of the first kind to the complementary integral

The *modulus, m,* to determine *K/K'* is obtained using Equation 2-5 (Harr 1962):

$$m = \cos\left(\frac{\pi s}{2d}\right)\sqrt{\tanh^2\frac{\pi b}{2d} + \tan^2\frac{\pi s}{2d}} \tag{2-5}$$

Where,

s = Length of embedment of the sheet pile into the substratum

b = Half base width of the levee = $L_2 / 2$

The value of *K/K'* is determined using the tables of complete elliptic integrals of first kind (Harr 1962).

Substituting the values of the form factors in Equation 2-4:

$$\delta = \frac{1}{\Sigma\Phi} = \frac{1}{x_1/d + K/K' + K/K' + x_3/d}$$

Therefore, Equation 2-3 becomes:

$$Q_s = k_f H \frac{d}{\left(x_1 + 2d\left(\frac{K}{K'}\right) + x_3\right)} \tag{2-6}$$

Similarly, the head at the toe of the levee is determined using the Method of Fragments. The head loss in m^{th} fragment is calculated as follows:

$$h_m = \frac{H\Phi_m}{\sum\Phi} \tag{2-7}$$

Where,

Φ_m = Form factor for mth zone

$\sum\Phi$ = Summation of form factors for all the fragments (Zones I, II, III and IV in this case).

Head loss through Zone I, $h_1 = \frac{H\Phi_1}{\sum\Phi}$

Head loss through Zone II, $h_2 = \frac{H\Phi_2}{\sum\Phi}$

Head loss through Zone III, $h_3 = \frac{H\Phi_3}{\sum\Phi}$

Head loss through Zone IV, $h_4 = \frac{H\Phi_4}{\sum\Phi}$

Accordingly, the head at the toe of the structure is determined as follows:

$$h_o = H - (h_1 + h_2 + h_3) \tag{2-8}$$

Or simply,

$$h_o = h_4 = \frac{H\Phi_4}{\sum\Phi} \tag{2-9}$$

Similarly, the exit gradient can also be calculated using blanket theory as follows:

$$i = \frac{h_o}{z_b} \tag{2-10}$$

Where,

h_o = Excess hydraulic head at the toe of the levee as shown in Figure 2-2

z_b = Transformed thickness of the top stratum

There are three different subcases for Case 8, similar to Case 7, depending upon the seepage boundary conditions on the landward side. The value of x_3 is determined for each case depending upon the type of seepage exit. Similar to the above discussion, derivations of the other cases of blanket theory that are presented in the EM are available in Brandon et al. (2009).

2.4.2. Comments Regarding Blanket Theory Equations

The blanket theory equations are intended to be used with approximate values of permeability and thicknesses of the top and pervious strata. The permeability value for the pervious lower stratum should be the horizontal component of the permeability and the permeability values for the semipervious top strata should be the vertical components. In addition, it is prudent to use a range of permeability and thickness values to cover the range of variation of these parameters expected in the field. There are some inconsistencies in the way total head loss through the section (H or ΔH) and excess head at the toe of the levee (h_o) are defined in the EM 1110-2-1913, and corrections will be made in the revised manual. The incorrect definition of the head loss is only applicable for cases having blankets only on one side (Cases 3, 4, 5 and 6) shown in Figures B-5 and B-6 of Appendix B of EM 1110-2-1913. As it is shown on the figures in the EM, the head loss would be dependent on the thickness of the blanket. The value of ΔH is used to determine the seepage underneath the levee and should be the difference between the riverside and landside water level, or the total head loss from riverside to landside.

The fundamental assumption that flow through the top stratum is vertical and through the pervious substratum is horizontal is only true if the ratio of $k_f$to k_b is greater than or equal to

about 10 (Bennett 1946). Neither EM 1110-2-1913 nor TM 3-424 provides any guidelines about the ratio of permeabilities between the top stratum and pervious stratum, which would make the top stratum either impervious or semipervious. Therefore, finite element analysis can be a useful tool, in conjunction with blanket theory, to examine the range of permeability ratios where the top stratum transitions from semipervious to impervious.

2.4.3. Evaluation of Blanket Theory solutions with Finite Element Analysis

Finite element analyses have been performed on the eleven different levee seepage configurations described earlier in order to verify the blanket theory solutions and to assess potential differences in the solutions when geometrical and/or soil property values are used outside of the recommended guidelines.

The finite element analyses were performed with SLIDE (Rocscience Version 6.0) for Case 1 to Case 8 as described earlier using the same boundary conditions, layer thicknesses, and permeability values as used for the blanket theory solutions. Results were obtained for volumetric flow rates per unit of levee length (Q_s) and for excess hydraulic head (h_o) under the toe of the levee (when applicable) using both finite element analyses and blanket theory solutions.

The numbering of the first seven cases was consistent with that used in EM 1110-2-1913. Case 8 was added to model sheet pile I-walls installed in levee systems. The general boundary conditions used in Cases 1 through 8 are shown in Figure 2-3. In all analyses, the base of the levee (L_2) was assumed to be 40.2 m (132 ft). This is equivalent to a 6.1 m (20 ft) tall levee having 3H: 1V side slopes and a crest width of 3.6 m (12 ft). However, since the levee is

modeled as an impervious structure in both the finite element analysis and blanket theory analysis, the slope angles and crest width are inconsequential.

The finite element analyses were conducted with a minimum of 1500 elements. The elements used were six-noded triangles. This mesh appeared to provide accurate results with short execution times.

For Cases 1 through 4, the permeability of the pervious layer was 0.0015 m/sec (4.92×10^{-3} ft/sec). For these cases, the value of permeability is not important for comparing finite element analysis to blanket theory. The flow calculated for both methods is directly proportional to the permeability, and the excess head at the downstream toe does not depend on the value of permeability. For Cases 5 through 8, the value of permeability is more important, and values used in the analyses are discussed later.

Cases 2 through 4 have an impervious blanket, and that is modeled in finite element analysis as a *no-flow* nodal boundary condition. Both in blanket theory and in finite element analysis, this has the same effect as a blanket of zero thickness. For Cases 5 though 8, which have different combinations of riverside and landside semipervious blankets, the thickness of the blanket is an important factor, particularly in the manner in which the total head loss is defined. A comparison of blanket theory with finite element analysis (FEA) is provided only for Cases 1 and 7c in this discussion due to space constraints. The comparison of all the cases is available in Brandon et al. (2009).

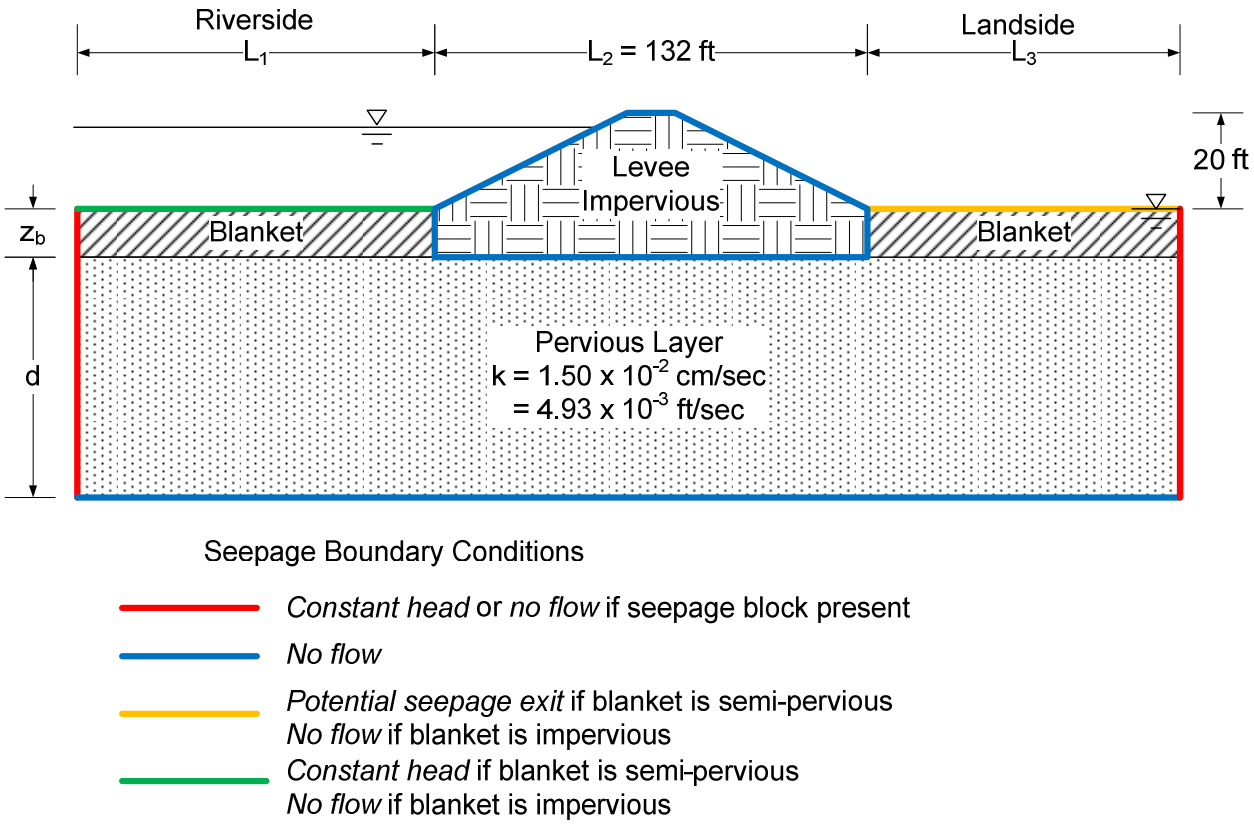

Figure 2-3 Generalized geometry and boundary conditions used in finite element analysis.

(a) Case 1 – No Landside and Riverside Top Stratum

In the FEA, the riverside nodal boundary conditions (horizontal and vertical) were set to a constant head of 6.1 m (20 ft). The landside boundary conditions (horizontal and vertical) were set to a constant head of 0 m. This analysis was done for three different thicknesses of the pervious layer (d) of 7.6 m (25 ft), 15.2 m (50 ft), and 30.5 m (100 ft). This analysis was performed considering both riverside and landside horizontal dimensions of 30.5 m (100 ft) and 457.2 m (1500 ft). For blanket theory analyses, the L_1 (distance from river to riverside levee toe) and L_3 (length of foundation and top stratum beyond landside levee toe) dimensions are considered infinite. However, for finite element analysis, these dimensions must be assigned finite lengths.

As shown in Figure 2-4, the flow (Q_s) increases with increasing thickness of the pervious layer (d), as expected. Values of L_1 and L_3 do not appear to affect the finite element results since essentially the same values of flow were calculated for L_1 and L_3 dimensions of 30.5 m (100 ft) as for L_1 and L_3 dimensions of 457.2 m (1500 ft).

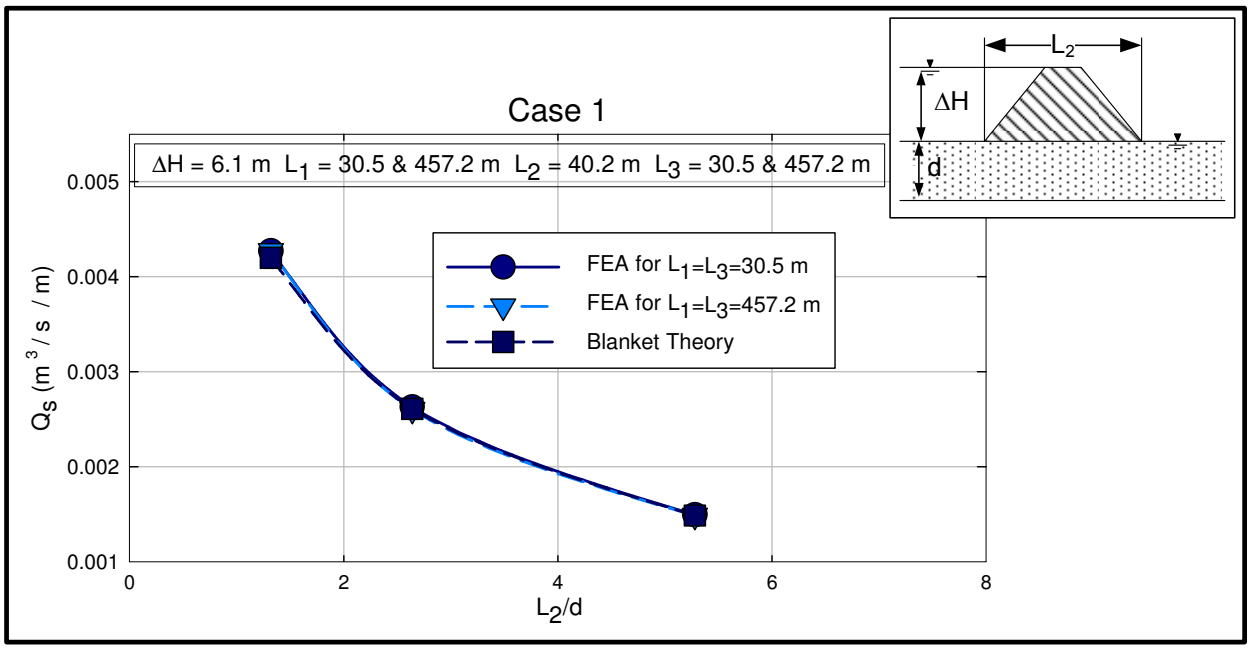

Figure 2-4 Calculated values of flow per unit length (Q_s) for different values of L_2/d using varying dimensions of L_1 and L_3 for Case 1.

There is a close agreement between the finite element analysis and blanket theory for this case. The slight difference between the two methods seems to increase with decreasing L_2/d ratio, and this is further examined in Figure 2-5. As the thickness of the pervious layer (d) becomes larger with respect to the levee width (L_2), the difference in calculated flow between FEA and blanket theory is increased. This supports the recommendation that an L_2/d ratio ≥ 1 should be used for application of blanket theory.

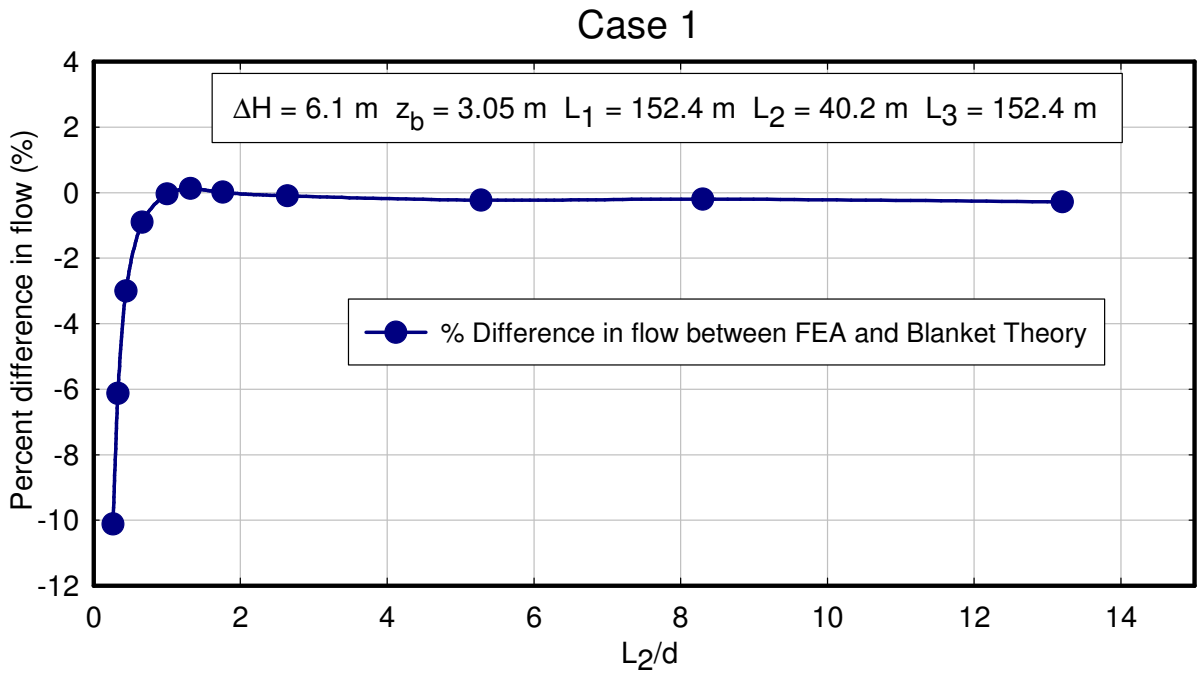

Figure 2-5 Percent difference in flow per unit length (Q_s) for blanket theory with increasing L_2/d ratios for Case 1.

2.4.4. Semipervious Top Strata

For Cases 5 and beyond, the thickness and permeability of the semipervious blanket become important factors in the analyses. For Cases 5 and 6 (semipervious blanket on riverside and landside, respectively), the thickness of the upstream blanket has an influence on the manner that the total head loss (H or ΔH) is defined. For the purpose of the finite element analysis, ΔH is defined as the change in head from the river level to the ground surface elevation on the landside. This differs from the way ΔH is shown for Cases 5 and 6 in EM 1110-2-1913 as explained earlier. For the FEA, the riverside constant head boundary condition (shown in Figure 2-3) was assigned to the elevation of ground surface such that only flow through saturated media would occur. If the constant head boundary value was assigned an elevation that corresponds to the

interface between the pervious layer and the blanket as shown in EM, then the phreatic surface could have been located within the landside blanket.

Comparison of the cases having semipervious blankets with the impervious cases allows determination of the threshold permeability values where a semipervious blanket becomes essentially impervious. The semipervious cases require evaluation of more parameter combinations than Cases 1 through 4. The permeability of the pervious layer (k_f) was assigned a value of 0.0015 m/sec (4.9 x 10^{-3} ft/sec), which is the same value used in the previous analyses. The permeability of the semipervious blanket (k_b) was varied to be a multiple of the permeability of the pervious layer (k_f). Ratios of k_f to k_b from 0.1 to 100,000 were used in the analyses.

(a) Case 7c – Semipervious landside and riverside top stratum (seepage exit in the pervious substratum located landward of the levee)

Constant head boundary conditions were assigned to the riverside ground surface and the riverside domain vertical boundary as shown in Figure 2-3. An L_1 value and an L_3 value of 152.4 m (500 ft) were used in all analyses. The thickness of the pervious layer (d) was 30.5 m (100 ft) and the thickness of the blanket (z_b) was 3 m (10 ft). The main parameter varied in these analyses was the permeability of the semipervious blankets and permeability ratios ranging from 0.1 to 100,000 were used.

The phreatic surface was assumed to be at the ground surface on the landside at the far edge of the domain. A constant head, equal to the ground surface elevation, was assigned to the far landside vertical boundary. The nodes on the horizontal landside ground surface were assigned *potential seepage exit* conditions. The riverside nodes, both on the horizontal ground surface and at the vertical domain boundary, were assigned constant heads equal to the landside head plus 6.1 m (20 ft), so that ΔH = 6.1 m (20 ft) for the analysis.

Shown in Figure 2-6 are the volumetric flow rates calculated using blanket theory and finite element analysis for the range of permeability ratios. The finite element analysis results are bracketed by the Case 1 (no top stratum) and Case 2 (impervious landside and riverside top stratum) results. The flows calculated by the blanket theory exceed the Case 1 results at a permeability ratio of about 2.

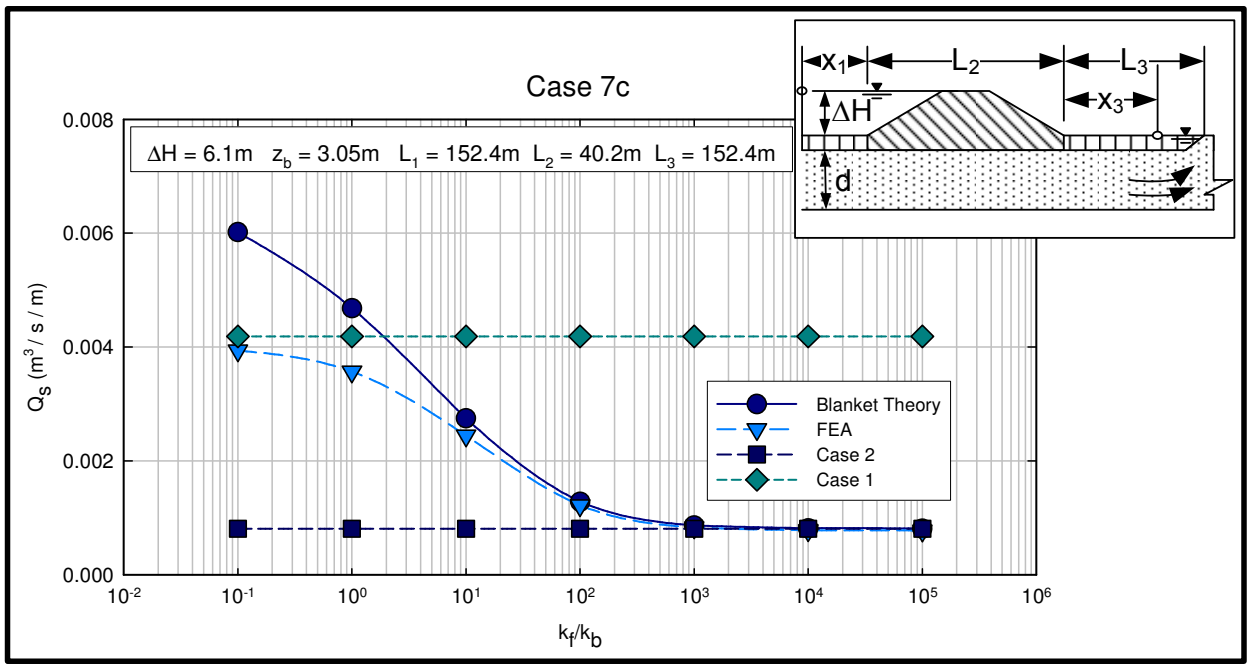

Figure 2-6 Calculated values of flow per unit length (Q_s) for various permeability ratios from blanket theory and finite element analysis for Case 7c.

Blanket theory agrees well with the FEA results for permeability ratios greater than about 100. For permeability ratios less than 100, the flows calculated by blanket theory are greater than calculated by the FEA, but that could be partially due to the way that SLIDE calculates flow values. SLIDE calculates the flow perpendicular to a vertical section placed from the horizontal midpoint of the levee extending into the pervious layer. The flow lines are not exactly horizontal beneath the midpoint of the levee, and the flow calculated by SLIDE is slightly less than the total flow beneath the levee. However, this difference is greater at lower permeability ratios, which

emphasizes the conclusion that blanket theory solutions lose their accuracy for k_f to k_b ratio of less than 10. It can be inferred from Figure 2-6 that for permeability ratios of less than 2, more accurate results are obtained assuming that a blanket is not present and doing a Case 1 analysis. Similarly, for permeability ratios of greater than or equal to 4000, accurate results can be obtained assuming that the blanket is impervious and performing a Case 2 analysis. These basic ratios were similar for comparisons of other cases as well.

Figure 2-7 shows the pressure head beneath the toe of the levee at the top of the pervious layer for different permeability ratios. Again, the heads calculated with blanket theory and FEA are in close agreement for permeability ratios greater than 100, and the difference increases for smaller values of permeability ratio. The exit gradients calculated using blanket theory would be generally greater than or equal to those calculated by FEA.

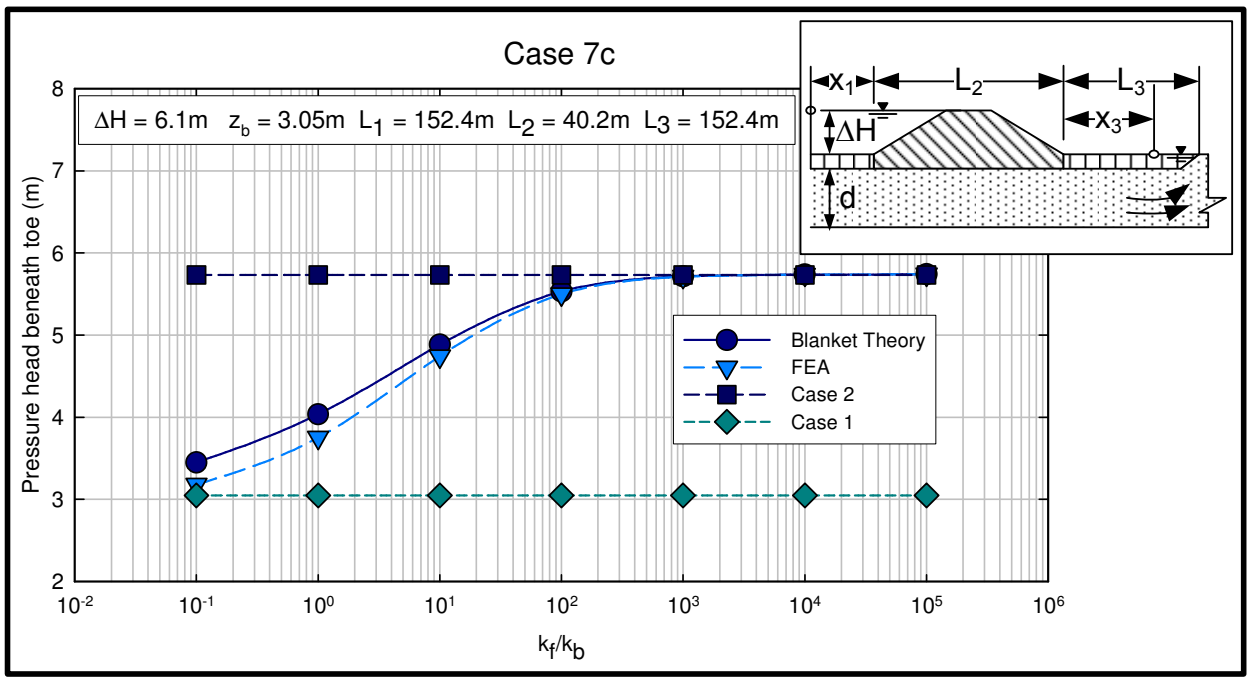

Figure 2-7 Excess head (h_o) or pressure head beneath blanket at toe for Case 7c calculated using FEA and blanket theory for different permeability ratios.

A common historical use of blanket theory has been to obtain the variation in head along the levee. This has been used to determine pore pressures for incorporation into effective stress slope stability analyses. Figure 2-8 shows the pressure head as a function of horizontal distance at the blanket/pervious layer interface calculated using blanket theory and FEA. The agreement between the two methods is excellent underneath the levee, and for a distance of about 15.2 m (50 ft) from the toe of the levee. At horizontal distances greater than 15.2 m (50 ft) from the toe, the solutions diverge. Toward the riverside, blanket theory provides higher heads than FEA. Toward the landside, FEA provides higher pressure heads than blanket theory. The agreement between blanket theory and FEA will be better with increasing permeability ratio. This would be expected since the head should vary linearly between the left and right hydraulic boundaries if the top boundary is relatively impervious.

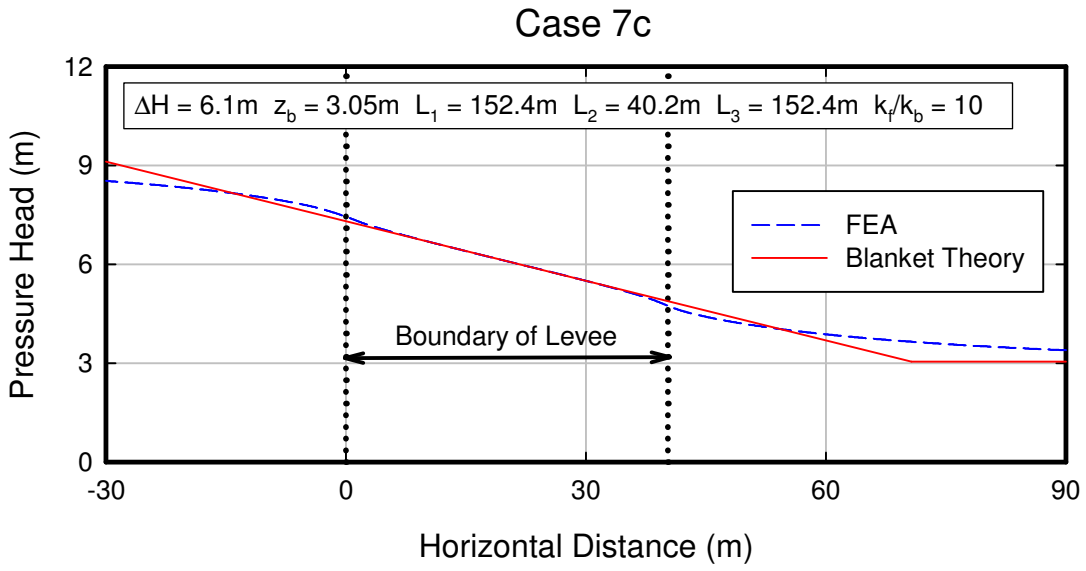

Figure 2-8 Pressure head at the top of the pervious layer for Case 7c calculated with finite element analysis and blanket theory.

2.5. General Guidelines of Finite Element Analysis of Blanket Theory Cases

Based on the results, it is clear that if finite element seepage analyses are conducted using generally the same boundary conditions as used for blanket theory, virtually identical results will be obtained from the different methods. The authors have compared all cases and subcases of blanket theory with finite element analysis, and this agreement has been consistent for all cases. The finite element method has the additional advantage that geometries more complex than that assumed in blanket theory can be easily accommodated. This section will provide guidance for assigning boundary conditions for finite element seepage analysis of the individual cases as defined in EM 1110-2-1913.

The type of boundary conditions needed, as defined in most finite element analysis programs, are the following:

- Constant head boundary with head set to riverside maximum water elevation
- Constant head boundary with head set to landside ground surface elevation
- No-flow (q = 0) boundary condition
- Potential seepage face or "unknown" boundary condition

Since the levee is considered impermeable in blanket theory, the levee does not need to be included in the finite element mesh, and the nodes at the base of the levee are assigned as a no-flow boundary condition. The nodes at the base of the domain (mesh) are also set as a no-flow boundary condition.

For each of the eight seepage cases discussed earlier, the boundary conditions will be specified for the riverside horizontal and vertical surfaces and the landside horizontal and vertical surfaces as shown in Figure 2-3. The dimensions as defined in blanket theory (L_1, L_2,

and L_3) should be the same in the finite element model as would be used in blanket theory. Table 2-2 summarizes the boundary conditions that can be used for different cases of blanket theory.

Table 2-2 Summary of boundary conditions for different cases of blanket theory

Blanket Theory Case	**Required Boundary Condition**	**Assigned Boundary Condition**
Case 1 – No top stratum	Riverside horizontal	Constant head with head assigned to riverside water elevation
	Riverside vertical	Constant head with head assigned to riverside water elevation
	Landside horizontal	Constant head with head assigned to landside ground elevation
	Landside vertical	Constant head with head assigned to landside ground elevation
Case 2 – Impervious top stratum both riverside and landside	Riverside horizontal	No-flow
	Riverside vertical	Constant head with head assigned to riverside water elevation
	Landside horizontal	No-flow
	Landside vertical	Constant head with head assigned to landside ground elevation
Case 3 – Impervious riverside top stratum and no landslide top stratum	Riverside horizontal	No-flow
	Riverside vertical	Constant head with head assigned to riverside water elevation
	Landside horizontal	Constant head with head assigned to landside ground elevation
	Landside vertical	Constant head with head assigned to landside ground elevation
Case 4 – Impervious landside top stratum and no riverside top stratum	Riverside horizontal	Constant head with head assigned to riverside water elevation
	Riverside vertical	Constant head with head assigned to riverside water elevation
	Landside horizontal	No-flow
	Landside vertical	Constant head with head assigned to landside ground elevation
Case 5 – Semipervious riverside top stratum and no landside top stratum	Riverside horizontal	Constant head with head assigned to riverside water elevation
	Riverside vertical	Constant head with head assigned to riverside water elevation

	Landside horizontal	Constant head with head assigned to landside ground elevation
	Landside vertical	Constant head with head assigned to landside ground elevation
Case 6 – Semipervious landside top stratum and no riverside top stratum	Riverside horizontal	Constant head with head assigned to riverside water elevation
	Riverside vertical	Constant head with head assigned to riverside water elevation
	Landside horizontal	Potential seepage face
	Landside vertical	Constant head with head assigned to landside ground elevation
Case 7a – Semipervious landside top strata both riverside and landside with L3 = ∞ 1	Riverside horizontal	Constant head with head assigned to riverside water elevation
	Riverside vertical	Constant head with head assigned to riverside water elevation
	Landside horizontal	Potential seepage face
	Landside vertical	Constant head with head assigned to landside ground elevation
Case 7b – Semipervious landside top strata both riverside and landside with L3 finite to a seepage block.	Riverside horizontal	Constant head with head assigned to riverside water elevation
	Riverside vertical	Constant head with head assigned to riverside water elevation
	Landside horizontal	Potential seepage face
	Landside vertical	No-flow
Case 7c – Semipervious landside top strata both riverside and landside with L3 finite to an open seepage exit.	Riverside horizontal	Constant head with head assigned to riverside water elevation
	Riverside vertical	Constant head with head assigned to riverside water elevation
	Landside horizontal	Potential seepage face
	Landside vertical	Constant head with head assigned to landside ground elevation

1Note: When L_3 is infinite then the landside vertical boundary should be sufficiently far from the levee such that an infinite landside blanket is simulated in the finite element seepage analysis. Results indicate that a landside vertical boundary of greater than 152.4 m (500 ft) from the levee toe gives an approximate infinite landside blanket condition in the finite element seepage analysis if no blanket is present. If a blanket is present, then a value of about 762 m (2500 ft) to 914.4 m (3000 ft) should be used.

2.6. Summary and Conclusions

Blanket Theory, having its origins in the *Method of Fragments* developed in the early part of the last century, has been used by the US Army Corps of Engineers and their contractors for over 60 years to calculate flows, hydraulic gradients, and pore pressures beneath levees. The results from blanket theory have been successfully incorporated in to the design and analysis of many levees on the Mississippi River and tributaries.

Finite Element Analysis has more recently become the method of choice for general seepage analyses in geotechnical engineering. As part of assisting in the transition between the use of blanket theory and finite element analysis, the authors have performed an extensive study comparing the results of finite element analyses conducted on the original blanket theory cases contained in the Corps' engineering manuals. In addition, a new Case 8 was added in this study to extend the conventional blanket theory analyses to cross sections that contain a partially penetrating sheet pile cutoff. The results have shown that for like conditions, there is a very good agreement between the two methods.

Using the original concepts of semipervious and impervious blankets originally adopted in blanket theory, the results indicate that the transition between semipervious and impervious blanket behavior occurs at a ratio of pervious layer permeability to blanket permeability between 1000 and 4000. At permeability ratios in the range of these values, the semipervious solutions (Cases 5, 6, and 7) produce essentially the same values of heads and flows as the impervious solutions.

Similarly, the transformation from a fully pervious to a semipervious blanket occurs at a ratio of pervious layer permeability to blanket permeability of about 2. In other words, the use of

the semipervious equations will produce a more accurate determination of the flow and the excess head for permeability ratios equal to or greater than 2 as compared to solutions considering the blanket as fully pervious (non-existent). For permeability ratios less than 2, the presence of the blanket may be ignored, and the solutions for cases having no blanket will generally provide more accurate results than the solutions for the semipervious cases.

Guidelines are given for correctly assigning boundary conditions in finite element analysis to be consistent with the individual blanket theory cases. These guidelines should serve as a starting point for using finite element seepage analyses for more complex analyses of seepage beneath levees. This study will also guide the practicing engineers in correlating both finite element analyses, and blanket theory equations with each other, and help them in understanding the origin of blanket theory equations that is a basis of design for existing levee systems along Mississippi River.

2.7. Acknowledgments

The authors acknowledge the support provided by US Army Corps of Engineers (USACE) for conducting this research. Mr. Noah Vroman of Vicksburg District of the Corps of Engineers, and Ms. Martha Jimenez, Graduate Student at Virginia Tech also provided valuable assistance during this research.

2.8. References

Barron, R. A. (1948). "The Effect of a Slightly Pervious Top Blanket on the Performance of Relief Wells," *Proceedings of the Second International Conference on Soil Mechanics and Foundation Engineering,* Rotterdam, Netherlands, Vol 4, p 342.

Bennett, P.T. (1946). "The effect of blankets on the seepage through pervious foundation." *Trans. ASCE* **11**, p. 215

Brandon, T. L., Batool, A., Jimenez, M., and N. Vroman (2009), "Levee Seepage Analysis using Blanket Theory and Finite Element Analysis," Report submitted to the U. S. Army Corps of Engineers Engineering Research and Development Center, Dept. of Civil and Environmental Engineering, Virginia Tech, Blacksburg, VA, 129 pp.

Forchheimer, P. (1917). " Zur Grundwasserbewegung nach isothermischen Kurvenscharen. (On the movement of groundwater according to sets of isothermal curves)." Sitzungsber K-K Akad der Wissenschaft 126(4):409-40 (in German).

Griffiths, D.V. (1984). "Rationalised charts for the method of fragments applied to confined seepage." *G´eotechnique*, 34(2), p. 229.

Harr, M.E. (1962). *Groundwater and seepage.* McGraw-Hill, New York.

Muskat , M. (1937). The flow of homogeneous fluids through porous media. McGraw-Hill.

Pavlovsky, N.N. (1956). *Collected works*. Akad. Nauk USSR, Leningrad.

Rocscience, Inc. (2010). "Slide v6.0–2D limit equilibrium slope stability analysis." Toronto.

Turnbull, W. J. and Mansur, C. I. (1959). "Investigation of Underseepage-Mississippi River Levees." *Journal of the Soil Mechanics and Foundations Division*., 85(4), 41-93.

United States Army Corps of Engineers (USACE) (1956). "Investigating Underseepage and its Control, Lower Mississippi River Levees, Technical Memorandum 3-424," U.S. Army Corps of Engineers, Waterway Experiment Station, Vicksburg, MS.

USACE (1986). "Seepage Analysis and Control of Dams, Engineer Manual 1110-2-1901," U.S. Army Corps of Engineers*,* Washington, DC.

USACE (2000). "Design and Construction of Levees, Engineer Manual 1110-2-1913," U.S. Army Corps of Engineers*,* Washington, DC.

CHAPTER 3. FINITE ELEMENT ANALYSES FOR DESIGN OF LANDSIDE SEEPAGE BERMS

3.1. Authors

Abeera Batool[1] and Thomas L. Brandon[1]

[1]*Dept. of Civil and Environmental Engineering, Patton Hall, Virginia Polytechnic Institute and State University (Virginia Tech), Blacksburg, VA 24061 USA*

3.2. Abstract

Seepage berms are a viable control measure to prevent the occurrence of underseepage-related failures of levees. Closed-form solutions have historically been used for the design of seepage berms as outlined in various US Army Corps of Engineers (USACE) manuals. However, finite element analysis (FEA) can also be useful for the design of seepage berms because of the flexibility to accommodate complex levee geometries and hydraulic properties of the soil layers. This paper provides guidelines for using the finite element method to design different types of seepage berms. Several examples are considered and berm design parameters are compared from both the existing closed-form solutions and FEA. Guidance is also provided for the design of berms for cases where no top stratum exists, and the impact of various berm slopes is discussed. Some inconsistencies in defining the factor of safety for different berm types are also identified. This paper will help practicing engineers in understanding some of the limitations of the current design methods, as well as enhance their ability to use finite element analysis as a tool for the seepage berm design.

3.3. Introduction

The foundations of Mississippi River levees, particularly in the lower Mississippi River Valley, are often characterized by having a thick pervious layer overlain by a top stratum of lower permeability. Seepage analyses for these levees have been performed using Blanket Theory (USACE 1956) specifically developed for this stratigraphy. The term "blanket" refers to a top stratum of uniform thickness and permeability. Blanket Theory is based on the Method of Fragments (Pavlovsky 1935, Harr 1962), which analyzes underseepage by dividing the problem into fragments, solving for each fragment independently, and then combining the fragments to obtain an answer for the whole problem. The US Army Corps of Engineers (USACE) Engineering Manual (EM) 1110-2-1913, *Design and Construction of Levees,* (USACE 2000) outlines the equations for seven different cases, categorized by the characteristics of the top stratum. Similarly, the finite element method can also be used to perform seepage analysis. A comparison of Blanket Theory and the finite element method for seepage analysis for levees can be found in Brandon et al. 2013. The flow under the levee, excess hydraulic heads beneath the levee toe, and ultimately, hydraulic gradients, can be calculated from either Blanket Theory or FEA. If gradients at the levee toe are too high, then seepage control measures are required. This paper focuses on the design of seepage berms as a seepage control measure. A generalized schematic of a levee and seepage berm is shown in Figure 3-1.

The conventional methods of berm design are based on theoretical and semi-empirical solutions. However, finite element analysis has become popular among geotechnical engineers due to its broad applicability to seepage problems. In addition to calculating the excess hydraulic heads to determine if seepage berms are required, it can also be used to calculate the characteristic dimensions of the seepage berms which will reduce the gradients at the levee toe

and at the berm toe to the acceptable limits. Therefore, a methodology compatible with the currently accepted design methods is proposed to use the finite element method for berm design, and a step-by-step procedure is outlined. The USACE literature describes four different types of berms: *impervious berms*, *semipervious berms*, *sand berms* and *pervious berms with collectors*. Finite element guidelines are provided for each type of berm separately. The results are explained using multiple design examples having different types of top strata with different thicknesses. The design equations available in the manuals are only for cases having a blanket overlying the pervious stratum; therefore, cases with no top stratum are also considered. In addition, inconsistencies in the definition of factor of safety for each berm type are highlighted, and final design grades for berms are also investigated.

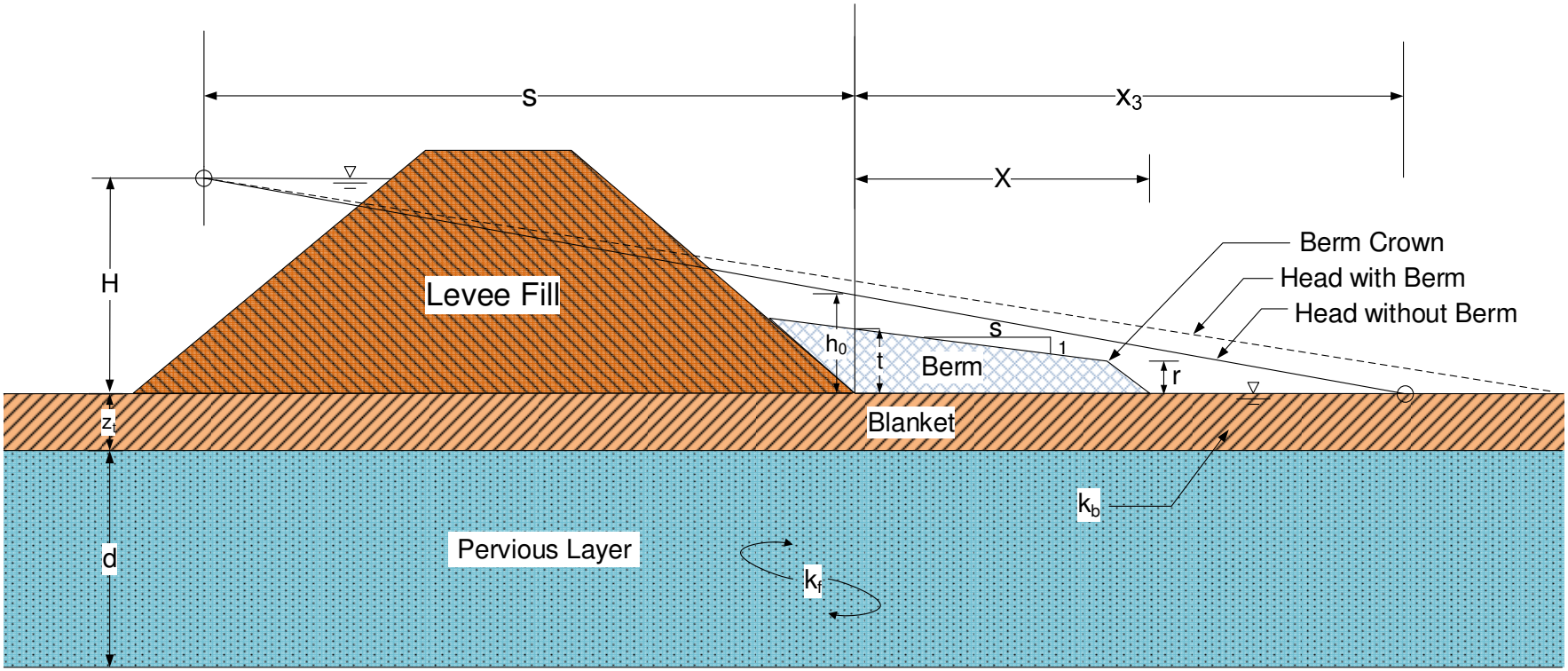

Figure 3-1 Generalized geometry of a levee with a seepage berm. (Not to scale).

3.4. Different Types of Seepage Control Measures

It is important to control underseepage to prevent or minimize excess uplift pressures and sand boils for levees founded on pervious foundations, as these phenomena can result in failure of the levees. Several control measures can be undertaken to prevent underseepage-related failures from occurring. These include impervious riverside blankets, relief wells, landside berms, drainage blankets, drainage trenches, cutoffs, and sublevees (USACE 1956). The type of foundation soil, control measure cost, site accessibility, maintenance issues, etc., can impact the selection of a specific seepage control measure. More than one control measure can be used at the same time to obtain the desired results.

Impervious riverside blankets can be used in cases where there is no top stratum on the riverside of the levee and seepage directly enters into the pervious foundation. These blankets can reduce the quantity of seepage as well as the uplift pressures on the landward side of the levee (USACE 1956). A complete or partial cutoff can be provided to reduce the quantity of seepage under the levee and reduce the chance of through-piping by adding a vertical flow component. The selection of a complete versus partial cutoff is governed by factors like the potential of backward erosion, the type of soil comprising the pervious foundation, and economic considerations (USACE 1986). Drainage blankets and trenches are provided to prevent erosion by intercepting and safely exiting seepage from the pervious stratum.

Despite the wide variety of seepage control measures, landside seepage berms and relief wells are most widely used for Mississippi River levees in practice. Landside berms are constructed on top of the top stratum to provide additional weight on the landward side of the

levee, resulting in a new thickness sufficient to resist the uplift pressures beneath the top stratum. In addition, the width of the berm also ensures the safety of the levee by shifting sand boil activity from the landward levee toe to a farther distance (USACE 1956). If the top stratum is relatively thick, landside berms may not be effective, and may create excessive uplift pressures. In practice, it is common to use landside seepage berms in conjunction with relief wells, which provide controlled channels for seepage exit at the levee toe. The result is a reduction of excess water pressures and prevention of erosion and sand boils. The relief wells should have sufficient penetration into the pervious stratum in order to effectively reduce pressures, and should be spaced close enough to limit maximum pressures between wells to the allowable values. The focus of this paper will be on the design of landside seepage berms only.

3.5. Current USACE Design Methods for Seepage Berms

The design of seepage berms is based on electrical analogy models developed by the Kansas City District of the Corps of Engineers (Mansur and Kaufman 1956). The design equations are based on Blanket Theory equations as presented by Bennett (1946). The initial case developed was for a semipervious berm having the same permeability as the top stratum. Equations were then developed for other types of berms.

Design equations for seepage berms are provided in the following Corps of Engineers publications:

1. US Army Corps of Engineers (USACE) Technical Manual (TM) 3-424, *Investigation of Underseepage and Its Control* (1956)
2. USACE Engineering Manual (EM) 1110-2-1901, *Seepage Analysis and Control of Dams* (1986)

3. USACE Engineering Manual (EM) 1110-2-1913, *Design and Construction of Levees* (2000)

Some other Corps publications, like *DIV*ision *R*egulation (DIVR) 1110-1-400 (1998) also discuss the design of seepage berms. A summary of the equations provided for the design of four different types of berms is presented in Table 3-1. The conventional design of seepage berm involves determining the width (X) and thickness (t) of the berm that will increase the factors of safety at the levee and berm toes to the desired value. One difference between the design methods presented in EM 1110-2-1913 and TM 3-424 is the required value of factor of safety against uplift at the toe of the levee, which is specified as greater than or equal to 2.8 in EM 1110-2-1913 and greater than or equal to 1.6 in TM 3-424. The design criterion used in this paper is also based on factor of safety against uplift and the minimum required values for factor of safety are specified as 1.6 and 1.0 for the levee and berm toes, respectively.

For the conventional design of seepage berms, the first step is to calculate the excess hydraulic head at the levee toe using Blanket Theory equations. Blanket Theory accommodates different types of top strata (impervious vs. semipervious), which determines the selection of the appropriate equations for the seepage analysis. The top stratum or blanket is considered as semipervious in the current discussion, which is Case 7 of Blanket Theory (USACE 2000). Case 7 can accommodate different boundary conditions on the landward side; which include an open ditch connected to the aquifer, a blocked seepage exit, or a top stratum of infinite lateral extent. Similarly, the boundary condition on the riverward side can include an open seepage entrance from the river (i.e. the river channel), or the presence of a seepage block, or hydraulic connections from riverside borrow pits.

The excess head at the levee toe (h_o) for Case 7 from Blanket Theory solutions is computed using Equation 3-1:

$$h_o = \frac{Hx_3}{x_1 + L_2 + x_3} \tag{3-1}$$

Where,

h_o = Excess head at landside levee toe

H= Net head on the levee

x_1 = Distance from the effective seepage entry to the riverside levee toe

L_2 = Base width of the levee

x_3 = Distance from the landside levee toe to the effective seepage exit

After calculating the excess head, the next step is to calculate the exit gradient and the factor of safety (F) to determine if a seepage berm is required. Therefore, the exit gradient (i) is calculated using Equation 3-2:

$$i = \frac{h_o}{z_t} \tag{3-2}$$

Where,

i = Exit gradient at landside levee toe

h_o = Excess head at landside levee toe

z_t = Thickness of the top stratum.

Similarly, the factor of safety against uplift is calculated using Equation 3-3:

$$F = \frac{\gamma'_z}{i\gamma_w} \tag{3-3}$$

Where,

F = Factor of safety against uplift

γ'_z = Submerged unit weight of the top blanket

γ_w = Unit weight of water

i = Exit gradient at landside levee toe

If the factor of safety is less than 1.6 at the levee toe, a berm needs to be provided. The required thickness (t) and width (X) of the berm can be determined from the equations in Table 3-1 for different types of berms, such that the factor of safety is at least 1.6 at the levee toe and 1.0 at the berm toe. The equations in EM 1110-2-1913 (shown in Table 3-1) to calculate thickness of the berm for all berm types are same, and are based on the gradients calculated using Equation 3-4:

$$i = \frac{h_x - t_x}{t_x + z_t} \tag{3-4}$$

Where,

i = Upward gradient at any distance x (x= 0 for landside levee toe)

h_x = Excess head at any distance x

t_x = Thickness of the berm at any distance x

z_t = Thickness of the top stratum

In addition to providing the berm thickness and width to the contractor, an appropriate slope also needs to be specified for the berm so that water is not ponded on surface of the berm. The berm slopes are generally specified as 50H:1V or steeper, with the provision that 75H:1V can be used where the foundation soil has fully consolidated under the stress imposed by the levee before the construction of the berm (USACE 2000). Similarly, the slope from the berm crown to the berm toe is specified as 3H:1V in the EM. The berm slope can be controlled by varying the berm thickness at the levee toe (t) or the thickness at the berm crown (r).

Guidance is also provided for selecting the maximum and minimum width of the seepage berm, as well as the berm thickness. EM 1110-2-1913 requires a minimum berm width of 150 ft, while the minimum thicknesses of the berm at the levee toe and berm crown are 5 ft and 2 ft, respectively. However, TM 3-424 only gives a specification for a minimum thickness of 1 ft at the berm crown. Both EM 1110-2-1913 and TM 3-424 limit the maximum width of the berm to 300 to 400 ft, with the reasoning that the levee will be safe even if sand boils occur at such far distances from the levee.

The selection of the suitable type of seepage berm is based on factors like availability of material and cost. Pervious berms will result in the smallest width of the berm as compared to impervious berms, which result in the largest width. Therefore, when feasible, a berm should be constructed of the most pervious material available to minimize the volume of material, and hopefully the cost (Barron 1980). However, in some cases, a pervious borrow material is not readily available, and the cost of importing the material is so high that the use of less pervious material available at the site may be more economical.

Table 3-1 Design Equations for Different Types of Landside Seepage Berms

Impervious Berm	Semipervious Berm	Sand Berm	Pervious Berm with Collector
$X_I = x_3\left(\frac{H}{h_a}-1\right)-s$	$X_{SP}=\frac{-A+\sqrt{A^2-24(2+r)(1+sc-H/h_a)}}{2c(2+r)}$ Where, $A=6+3sc(r+1)$ and $r=\frac{i_0}{i_1}$	$X_S=\frac{1}{3}(X_P+2X_{SP})$	$X_P=x_3\log_e\left(\frac{h'_o}{h_a}\right)$
$h'_o=H\left(\frac{x_3+X_I}{s+x_3+X_I}\right)$	$h'_o=h_a\left[1+cX_{SP}+\left(\frac{2+r}{6}\right)(cX_{SP})^2\right]$	$h'_o=h_a\left[1+cX_S+\left(\frac{2+r}{6}\right)(cX_S)^2\right]$	$h'_o=h_o=\frac{Hx_3}{s+x_3}$
$t=\frac{h'_o-z_t(\gamma'_z/F\gamma_w)}{1+(\gamma'_t/F\gamma_w)}$	$t=\frac{h'_o-z_t(\gamma'_z/F\gamma_w)}{1+(\gamma'_t/F\gamma_w)}$	$t=\frac{h'_o-z_t(\gamma'_z/F\gamma_w)}{1+(\gamma'_t/F\gamma_w)}$	$t=\frac{h'_o-z_t(\gamma'_z/F\gamma_w)}{1+(\gamma'_t/F\gamma_w)}$ $Q_s=\frac{k_f dH}{s+x_3}\left(1-e^{\frac{-X_P}{x_3}}\right)$

Notations

x_3 = Distance of effective seepage exit

s = Distance from effective seepage entry to landside toe of levee or berm

γ'_z = Submerged unit weight of top stratum

γ'_t = Submerged unit weight of berm

γ_w = Unit weight of water

h'_o = Excess head at landside toe of levee with berm

d = Thickness of pervious stratum

H = Net head on the levee

k_f = Permeability of pervious stratum

h_a = Allowable head at toe of berm = $i_1 z_t$

i_1 = Allowable upward gradient at toe of berm

i_o = Allowable upward gradient at landside toe of levee

z_t = Thickness of top stratum

$c=\sqrt{k_b/k_f z_t d}$, where k_b = Permeability of top stratum

X = Required berm width, where X_I, X_{SP}, X_S, and X_P represent widths of impervious, semipervious, sand , and pervious berms, respectively

t = Required berm thickness at levee toe

F = Factor of safety against uplift at levee toe

Q_s = Flow into berm per foot of levee

3.6. Design of Seepage Berms using Finite Element Analysis Compatible with Current Methods

The finite element analysis (FEA) method can be useful to augment or replace current design methods based on theoretical or semi-empirical solutions because it has the flexibility to accommodate complex geometries and soil properties. FEA can also address some of the limiting assumptions that are present in the equations for berm design. Finite element analysis is widely popular for seepage analysis in geotechnical engineering, and providing guidelines and procedure for the design of seepage berms will be a valuable addition. This section outlines the procedure and guidelines required to conduct finite element analyses for the seepage berm design. A comparison of finite element analysis results with conventional design calculations is conducted as a part of developing the guidelines for the berm design.

3.6.1. Guidelines for Finite Element Analysis of Levees with Berms

A simple hypothetical levee cross section is used to compare the conventional method of berm design with the proposed FEA design method. The guidelines for FEA are developed by considering different design examples. In general, the example cases differ by the permeability and thickness of the top stratum, which is considered to be present on both the landside and the riverside. DIVR 1110-1-400 (1998) specifies the values of permeability for different top stratum soil types as a function of thickness of blanket. For design purposes, the permeability of top stratum on the riverward side is considered to be less than the permeability on the landside because of the difference in the direction of flow. On the riverside, the flow direction is downward, and the top stratum becomes “silted in,” resulting in a lower permeability. The landside top stratum or blanket experiences upward flow, which can flush fines out of cracks and joints, resulting in a higher permeability. The permeability also decreases with an increase in

blanket thickness, because the thicker the blanket, the less chance that a defect will progress all the way to the pervious layer.

The soil types of the top stratum considered in the design examples are clay, silt, and silty sand, with thicknesses of 5, 10, 15 and 20 ft. The net head on the levee (H) is 20 ft, and the permeability (k_f) and thickness (d) of the pervious stratum are 3.9 x 10^{-3} ft/sec (1.2 x 10^{-1} cm/sec) and 100 ft respectively, as shown in Figure 3-2. Similarly, the base width of the levee is assumed as 132 ft. A hydraulic connection between the river and the pervious layer is assumed to be present, and the distance from river to riverside levee toe (L_1) is assumed to be 1000 ft. The length of the top stratum (L_3) is considered to be infinite for all the examples. Complete details of the design cases considered for comparison between finite element analysis and the EM solutions are summarized in Table 3-2.

As a first step, similar to conventional berm design methods, the excess head at the levee toe (h_o) is calculated using FEA for the example cases. Both FEA and Blanket Theory provide excellent agreement for values of excess head calculated at the levee toe for different types of top strata (Batool and Brandon 2013). The boundary conditions assigned in FEA will depend on the type of top stratum. Details about assigning the boundary conditions for different cases of Blanket Theory can be found in Brandon et al. (2013). The typical boundary conditions used for the calculation of excess head from FEA for cases having a semipervious top stratum on both the landside and the riverside are shown in Figure 3-2. This case is considered as the representative of all the design examples in this paper. After calculating the excess head, the next step is to calculate the exit gradient and the factor of safety to determine if a seepage berm is required.

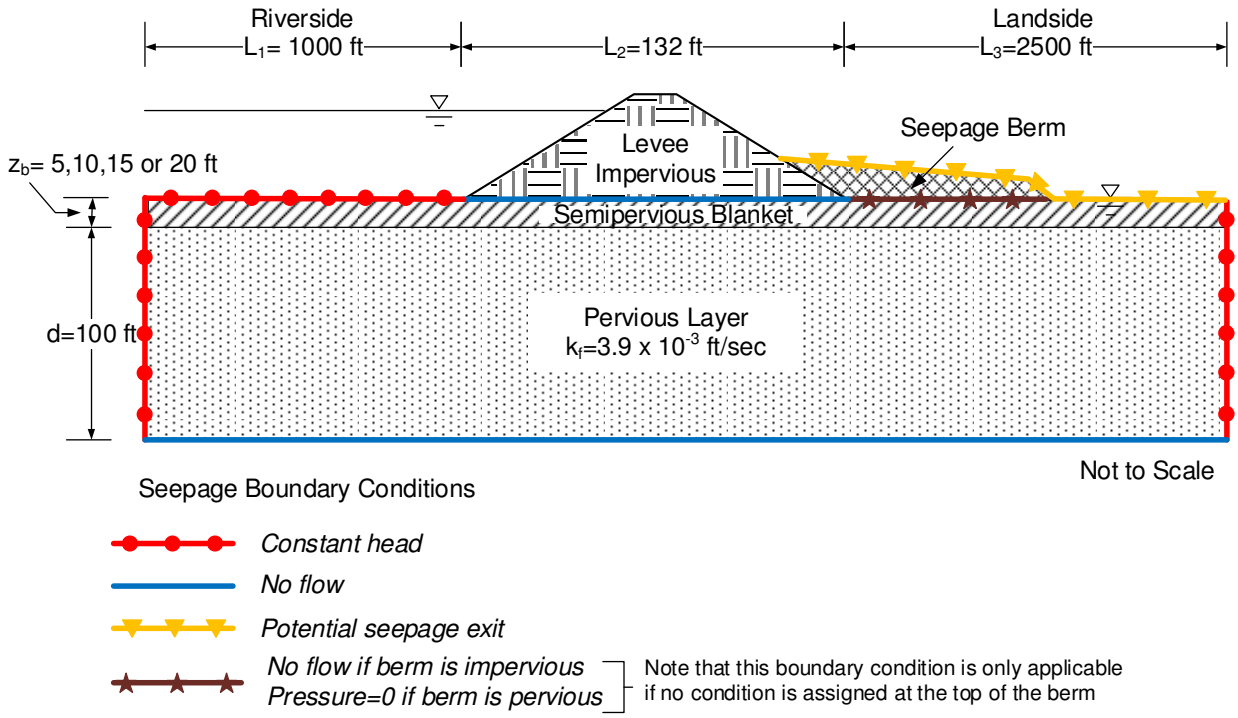

Figure 3-2 Generalized boundary conditions used for finite element analysis of the berm design for the case having a semipervious top stratum. (Not to scale).

The exit hydraulic gradient (i) can be calculated directly from FEA using the procedure explained by Duncan et al. (2011). Duncan et al. recommend that the gradient should be averaged over a defined distance. This distance can be the upper one foot of the pervious foundation, or any other suitable dimension depending on the geometry of the cross section. The cases where semipervious top strata are present, as shown in Figure 3-2, the average gradient over the thickness of the top strata can be used. The gradient can also be calculated from FEA using Equation 3-2 by substituting the value of h_o calculated from FEA. It is useful to locate nodes at the points where values of gradient or hydraulic heads are to be calculated in FEA. If nodes are not assigned at these points, the FEA program will interpolate the values at these points using the nearest nodes, and values may not be as accurate.

If the minimum criterion of factor of safety at the levee toe is not met, FEA can also be conducted to design a seepage berm similar to the conventional method. When a berm is added at the top of the blanket as shown in Figure 3-2, the boundary conditions should be modified accordingly. For the current study, analyses were conducted using the software SLIDE 6.0 (Rocscience 2010). The six-node triangular elements were used in the finite element analyses. The distance of the vertical boundary from the levee toe (L_3) which is assumed to be infinite in the examples, is modeled in FEA as 2500 ft as an approximation in this analysis. In addition to the parameters shown in Figure 3-2, other parameters required for the analyses are summarized in Table 3-2. Of course, the actual width of the levee, distance to the vertical boundaries, etc., should be used when conducting the FEA for any given field case. A brief summary of the hydraulic properties and the boundary conditions to be used for each type of berm is presented below.

(a) Impervious Berms

Impervious berms are assumed to have zero permeability in the equations present in EM 1110-2-1913. This condition is modeled in finite element analysis by assigning a value of permeability at least several orders of magnitude less than the landside top stratum. For the analyses presented, a value of 2×10^{-9} ft/sec (5×10^{-8} cm/sec) is used, which is about three orders of magnitude less than the permeabilities of the top strata considered in the examples shown in Table 3-2. The horizontal boundary on the landside of the berm is assigned an "unknown" or "potential seepage exit" boundary condition. The boundary condition for the impervious berm can be assigned in two ways: either as an "unknown" or "potential seepage exit" boundary at the top of the berm or a "no flow" boundary condition at the interface of the berm and the top

stratum (shown in dark brown in Figure 3-2). The berm does not need to be physically modeled if a "no flow" boundary condition is assigned for the length of the berm at the top of the blanket.

The horizontal distance to the vertical boundary on the landward side may affect the values of hydraulic head at the toes of the levee and the berm. This boundary should be carefully selected to best model the field conditions.

(b) Semipervious Berms

Semipervious berms are assumed to have the same permeability as the top stratum in the derivations of the equations present in EM 1110-2-1913, and they can be modeled similarly in FEA. However, an ambiguity lies in the range of the permeability of the semipervious top stratum. The Corps' Engineering Technical Letter (ETL) 1110-2-569 (USACE 2005) specifies that "Berms to be constructed as semipervious must be constructed with silty sands or fine sands and be designed using the semipervious suite of equations." The acceptable range of permeability needs to be better defined for the use of the semipervious berm equations. FEA can be useful for cases where uncertainty lies in the use of the appropriate equations, especially when exact estimation of field permeability is difficult. When conducting FEA for semipervious berms, all the boundary conditions are the same as shown in Figure 3-2, with the semipervious berm assigned an "unknown" or "potential seepage exit" boundary condition at the top of the berm. The effect of the presence of the semipervious berm, if the permeability of the berm is equal to the top stratum, is the same as increasing the thickness of the top stratum for a distance equal to the width of the berm.

(c) Sand Berms

Both EM 1110-2-1913 and TM 3-424 require the vertical permeability of a sand berm to be at least 3.3×10^{-4} ft/sec (1.0×10^{-2} cm/sec). There is no direct design equation for the width of

sand berms, and berms are approximated as being between the semipervious and pervious berm widths. Therefore, FEA can be more accurate for such types of berms. For the analyses presented, sand berms are modeled in FEA as having a permeability value of 3.9 x 10^{-3} ft/sec (1.2 x 10^{-1} cm/sec) which is same as permeability of the pervious stratum. However, this value can be changed if there is a better estimation of the permeability value or if the berms are not constructed with the same material as that of the pervious foundation. The boundary conditions for sand berms are the same as shown in Figure 3-2 with an "unknown" or "potential seepage exit" boundary condition assigned to the top of the berm.

(d) Pervious Berms with collector

Pervious berms are assumed to have an infinite permeability in the equations present in EM 1110-2-1913. This condition can be modeled in the finite element analysis by assigning the permeability as a very high value. This value is assigned as 1.0 x 10^{3} ft/sec (3.0 x 10^{4} cm/sec) for the current analysis. The part of the landside horizontal boundary after the berm is assigned an "unknown" or "potential seepage exit" boundary condition similar to the other types of berms. The boundary condition for the pervious berm can be assigned in two ways, either as an "unknown" or "potential seepage exit" boundary at the top of the berm, or a "pressure equal to zero (head equal to elevation)" boundary condition at the interface of the berm and the top stratum (shown in dark brown in Figure 3-2) assuming that the water table is at the original ground surface. The berm does not need to be physically modeled if a "pressure equal to zero" boundary condition is assigned for the length of the berm at the top of the blanket. The heads at the levee toe and berm toe are equal using both of these boundary conditions. Since, this type of berm involves a collector pipe, it is necessary to calculate the flow entering the berm so that the correct size of the collector pipe and outlet system can be designed. As most commercial FEA

programs can calculate flow across a specified boundary, this can be achieved by assigning a discharge section or flux boundary in FEA at the appropriate location. The discharge values at various locations were investigated and the horizontal section at the bottom of the berm as shown in Figure 3-3gives a good agreement with the values calculated from the closed-form equation as shown in Table 3-3.

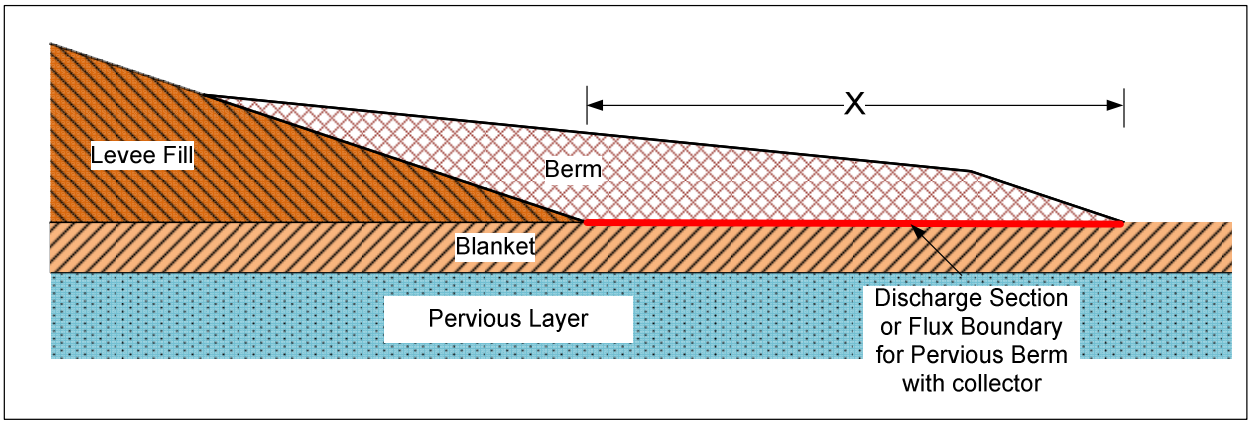

Figure 3-3 Location of the discharge section or flux boundary for Pervious Berm with Collector.

3.6.2. Steps to Determine Berm Dimensions with Finite Element Analysis

The boundary conditions presented in the above section are used to conduct the analyses for the seepage berm design. The procedure to determine required thickness and width of the berm using finite element analyses is outlined below.

1. Assume an initial berm width of 150 ft with a thickness of 5 ft at the levee toe and 2 ft at the berm crown. This represents the minimum allowed berm section. The distance from the berm crown to the berm toe will be 6 ft for the slope of 3H:1V for a crown thickness of 2 ft.
2. Compute the factors of safety at the levee and berm toes. The calculation of factor of safety differs with different berm types and it will be discussed in detail subsequently. If

the minimum requirements for both factors of safety are satisfied, the minimum berm dimensions from step 1 can be used.

3. If either of the factors of safety is not satisfied, increase either the width or the thickness of the berm, or both, for the next trial. This increase in dimensions should be as follows:

    a). If both the factors of safety at the levee and berm toes are not satisfied, increase the width and the thickness of the berm.

    b). If only the factor of safety at the levee toe is satisfied, increase the width of the berm. This increase in width can be in intervals of 100 ft until the value of factor of safety becomes close to 1.0. Smaller intervals can be used as factor of safety approaches 1.0 to optimize the design.

    c). If only the factor of safety at the berm toe is satisfied, increase the thickness of the berm. This increase in thickness can be in the intervals of 1 ft until the value of factor of safety becomes close to 1.6. Smaller intervals can be used as the factor of safety approaches 1.6 to optimize the design.

4. Increasing the thickness and width of the berm can influence the berm slopes. The berm slope is determined based on the difference of the thickness of the berm at the levee toe and berm crown for the corresponding horizontal distance. The berm dimensions should be increased in step 3a to obtain a berm slope of 50H:1V or steeper. Similarly, after calculating the desired width and thickness from steps 3b or 3c, respectively, the corresponding thickness or width should be adjusted so that the berm slope is 50H:1V or steeper. Other berm slopes such as 75H:1V and 100H:1V may also be allowed for special conditions.

5. Repeat the finite element analyses for the final dimensions of the berm. Check the factors of safety at the levee and berm toes. If both factors of safety are satisfied, and the berm slope is correct, then the dimensions satisfy the design criteria.

3.7. Comparison of Results

The design cases considered for comparison between finite element analysis and closed-form solutions are explained in the earlier section and complete details of these cases are summarized in Table 3-2. The values of distances of the effective seepage entry and exit shown in Table 3-2 are calculated from Blanket Theory equations for Case 7 having the river at distance of 1000 ft from the levee toe and top stratum of infinite extent (USACE 2000). Similarly, the excess head at the levee toe (h_o), exit gradient (i) and factor of safety (F) shown in Table 3-2 are calculated from Equations 3-1, 3-2, and 3-3, as discussed earlier.

Table 3-2 Summary of properties of design examples used for comparison between FEA and closed-form solutions

Parameters	Examples											
	Clay Stratum				Silt Stratum				Silty Sand			
Thickness, z_t (ft)	5	10	15	20	5	10	15	20	5	10	15	20
Permeability of landside top stratum, k_{bl} (cm/sec)	3.6E-04	2.5E-04	1.6E-04	9.0E-05	4.5E-04	3.4E-04	2.7E-04	2.2E-04	9.0E-04	7.6E-04	6.6E-04	6.0E-04
Permeability of riverside top stratum, k_{br} (cm/sec)	5.0E-05	3.5E-05	2.0E-05	5.0E-06	1.5E-04	1.3E-04	1.0E-04	1.0E-04	2.5E-04	2.5E-04	2.5E-04	2.5E-04
Submerged unit weight of top stratum, $\gamma' z$ (pcf)	47.5	47.5	47.5	47.5	47.5	47.5	47.5	47.5	52.5	52.5	52.5	52.5
c for landside, c_l (ft^{-1})	2.4E-03	1.5E-03	9.3E-04	6.1E-04	2.7E-03	1.7E-03	1.2E-03	9.6E-04	3.9E-03	2.5E-03	1.9E-03	1.6E-03
c for riverside, c_r (ft^{-1})	9.1E-04	5.4E-04	3.3E-04	1.4E-04	1.6E-03	1.0E-03	7.5E-04	6.5E-04	2.0E-03	1.4E-03	1.2E-03	1.0E-03
Distance to effective seepage entry, x_1 (ft)	791.5	912.9	964.5	993.1	581.1	754.6	848.4	880.9	473.6	619.6	701.7	754.6
Distance from source of seepage to levee toe, s (ft)	923.5	1044.9	1096.5	1125.1	713.1	886.6	980.4	1012.9	605.6	751.6	833.7	886.6
Distance to effective seepage exit, x_3 (ft)	410.0	687.3	1070.7	1633.0	365.1	594.1	816.5	1039.8	258.2	398.7	522.2	632.5
Excess head at levee toe, h_o (ft)	6.1	7.9	9.9	11.8	6.8	8.0	9.1	10.1	6.0	6.9	7.7	8.3
Exit Gradient at the levee toe , i	1.23	0.79	0.66	0.59	1.35	0.80	0.61	0.51	1.20	0.69	0.51	0.42
Critical Gradient , i_c	0.76	0.76	0.76	0.76	0.76	0.76	0.76	0.76	0.84	0.84	0.84	0.84
Factor of safety, F	0.62	0.96	1.16	1.29	0.56	0.95	1.26	1.50	0.70	1.21	1.64	2.02

The design criteria used in the analyses specify that if the factor of safety at the levee toe is less than 1.0, a berm should be designed to increase the factor of safety to at least 1.6 at the levee toe and 1.0 at the berm toe. These are shaded as red in Table 3-2. Similarly, if the factor of safety is between 1.0 and 1.6 at the levee toe, a berm with minimum dimensions (X = 150 ft, t = 5 ft, and r = 2 ft) can be specified. These are shaded as yellow in Table 3-2.

The examples indicate that as the thickness of the top stratum increases, excess heads beneath the toe of levee increase. However, the exit gradients at the levee toe decrease, resulting in higher factors of safety. The factor of safety is calculated to be greater than 1.0 for top stratum thicknesses of 15 ft and 20 ft for all the examples. A top stratum thickness of 10 ft also resulted in factor of safety greater than 1.0 at the levee toe for the silty sand top stratum. Berm dimensions do not need to be calculated for these cases and berms with minimum dimensions will be sufficient (berm width of 150 ft and thickness of 5 ft at levee toe). If the factor of safety is greater than 1.6 at the levee toe, as is the case with the silty sand top stratum having thicknesses of 15 and 20 ft, then no seepage control measures are required. These are shaded as green in Table 3-2.

Table 3-3 shows a comparison of the width and thickness of the berms calculated from the closed-form solutions in EM 1110-2-1913 and using FEA for a 5 ft top stratum of each soil type. Each of these cases was shaded in red in Table 3-2 indicating that a seepage berm design was warranted. The "required" values are calculated directly from the equations, while the "design" values for the berm width are rounded off and the corresponding thicknesses are modified to maintain the berm slopes of 75H:1V and 50H:1V. Therefore, the design thicknesses in Table 3-3 are often much greater than the required thicknesses to maintain the slope requirement. The slope of 75H:1V results in the lesser design thickness as compared to the steeper slope of 50H:1V for

the presented cases. However, for the berm widths of 150 and 200 ft, the thickness corresponding to 75H:1V does not meet the minimum Corps criteria for berm thickness at the levee toe as indicated in the table. Similarly, the required berm dimensions determined from FEA start from the minimum criteria specified by the Corps, as discussed in the steps to determine berm dimensions from FEA.

Table 3-3 Comparison of berm dimensions from Finite Element Analysis (FEA) and Closed-form Solutions (CS) for a top stratum thickness of 5ft and berm slopes of 50H:1V and 75H:1V.

Berm Type	Berm Dimensions (ft)		Type of top stratum					
			Clay Stratum (5ft)		Silt Stratum (5 ft)		Silty Sand (5 ft)	
			CS	FEA	CS	FEA	CS	FEA
Impervious	Required Width		821	820	841	840	364	370
	Design Width		*[a]400	*[a]400	*[a]400	*[a]400	375	375
	Required Thickness		*[b]6.1/4.7	*[b]6.2/4.7	*[b]6.9/5.4	*[b]6.9/5.4	5.1	5
	Design Thickness	75H:1V	7.1	7.1	7.1	7.1	6.9	6.9
		50H:1V	9.9	9.9	9.9	9.9	9.4	9.4
Semipervious	Required Width		264	400	287	400	117	180
	Design Width		300	400	300	400	150	200
	Required Thickness		3.1	5	3.7	5	2.6	5
	Design Thickness	75H:1V	5.8	7.1	5.8	7.1	*[c]3.9	*[c]4.5
		50H:1V	7.9	9.9	7.9	9.9	5	5.9
Sand	Required Width		241	330	261	330	108	150
	Design Width		250	350	300	350	150	150
	Required Thickness		2.8	5	3.4	5	2.5	5
	Design Thickness	75H:1V	5.2	6.5	5.8	6.5	*[c]3.9	*[c]3.9
		50H:1V	6.9	8.9	7.9	8.9	5	5
Pervious	Required Width		197	200	211	210	91	150
	Design Width		200	200	250	250	150	150
	Required Thickness		2.5	5	3	5	2.3	5
	Design Thickness	75H:1V	*[c]4.5	*[c]4.5	5.2	5.2	*[c]3.9	*[c]3.9
		50H:1V	5.9	5.9	6.9	6.9	5	5
	Flow into berm ($ft^3/sec/ft$)		0.0023	0.0022	0.0036	0.0036	0.004	0.004

*[a] Required berm width exceeds the maximum limit of 400 ft specified by the EM, therefore the width is truncated to 400 ft to satisfy the requirement and is suggested as the design width.
*[b] The two values of thickness are based on the required width, and the design width of 400 ft respectively.
*[c] The design thickness does not meet the minimum required thickness criteria of 5 ft at the levee toe for the slope of 75H:1V.

There is generally a good agreement between the berm dimensions calculated by finite element analysis and the conventional closed-form solutions for impervious and pervious berms. However, the values are different for semipervious and sand berms. The reason for the difference in the semipervious berm widths are due to the differences in the geometries involved in the derivation of the equation for this type of berm. The equation to calculate the width of the

semipervious berm is based on a triangular berm geometry considering no berm crown. The finite element analysis agrees well with the closed-form solutions if the berm crown is not considered. However, the current berm design practice requires a berm crown. The use of the closed-form solutions is unconservative if berm crown is considered, as indicated by the design dimensions shown in Table 3-3.

Barron (1980) examined the closed-form solutions for semipervious berms, and he derived a slightly different equation than that presented in EM 1110-2-1913. The value of gradient substituted in the continuity equation for the derivation of the berm width is a function of exit boundary condition distance (x_3) for the equation in EM 1110-2-1913, while it is not the case for the equation derived by Barron. The width of the semipervious berm, calculated from both closed-form solutions and finite element analyses, is very sensitive to the permeability of the top stratum and the berm. Figure 3-4 shows a significant increase in the calculated width of a berm for a slight decrease in permeability for the three solutions considering a hypothetical case with a top stratum on both the landside and riverside, and a distance from the river to the riverside levee toe of 1000 ft. The other parameters for this example are shown on Figure 3-4. The width of the berm calculated by Barron's equation is slightly less than that calculated from EM 1110-2-1913 equation. The finite element analysis gives the greatest value for the width of the berm among all methods due to the presence of berm crown as explained earlier..

A berm constructed of the same material as the top stratum is likely to be less pervious than the top stratum because the berm would be compacted and would not have the defects common in a natural top stratum. Therefore, in addition to the presence of the berm crown, the use of closed-form solutions for the semipervious berms can also be unconservative if the berm permeability value is less in the field than the one used for the berm design, as the behavior of

the berm will be approaching impervious behavior. The equations to calculate berm width in EM 1110-2-1913 only apply to cases when the permeability of the berm is equal to the permeability of the top stratum. However, finite element analyses give the flexibility of assigning a different permeability to the berm than the top stratum. The design engineer using closed-form solutions needs to be aware of the fact that the width changes rapidly with permeability, and adequate judgment is needed for the design of the semipervious berms.

The difference in the results calculated for sand berms using closed-form solutions and the finite element method is understandable as there are no equations available in the EM to calculate the width of the sand berm directly, but it is approximated as being between the widths of the semipervious and pervious berms. Therefore, if the widths of the semipervious berms are different from the EM equation and FEA, the width of the sand berm will also be different. Therefore, instead of approximating the width of a sand berm from closed-form solutions, finite element analysis should provide more reasonable results than the conventional method in this case.

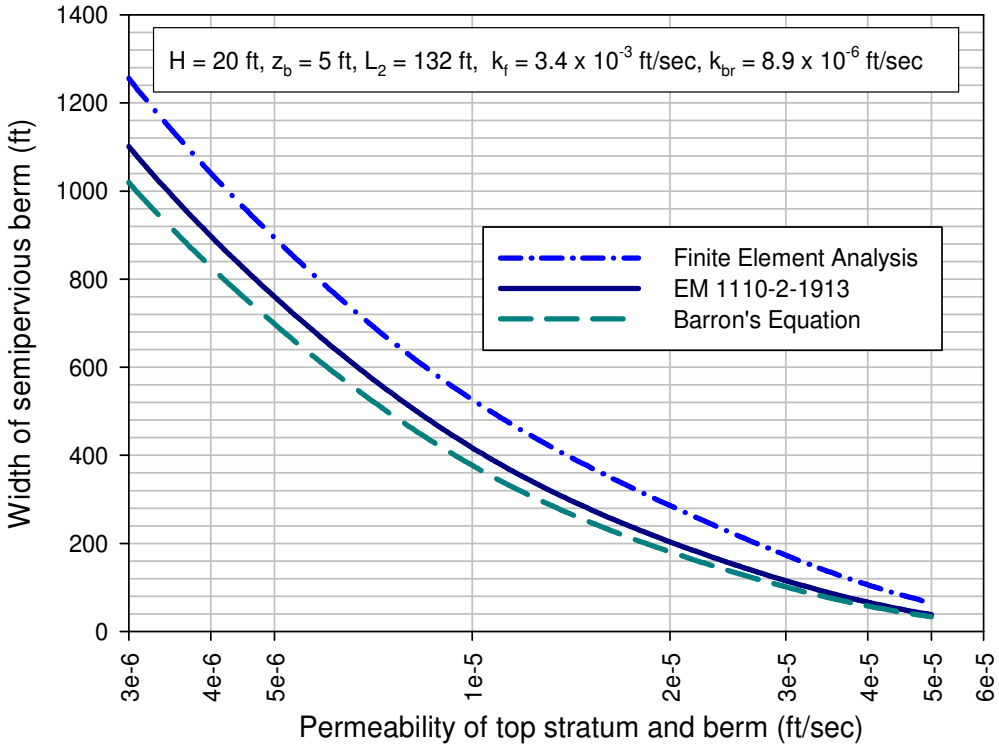

Figure 3-4 Increase in width of semipervious berm with decrease of permeability of landside top stratum and berm for different types of analyses.

3.8. Berm Surface Slopes

As indicated in Table 3-3, maintaining the desired berm slope can greatly influence the thickness of the berm. The EM generally recommends the slope of the berm to be 50H:1V or steeper to ensure adequate drainage. However, when the foundation soil has fully consolidated under the stresses imposed by the levee, it allows the use of 75H:1V for such cases. This can reduce the thickness of the berm at the toe of the levee, and can result in a smaller berm volume, resulting in less expensive berms. Similarly, if a large berm thickness is calculated from the closed-form equations, it is recommended by the EM to use the calculated thickness to construct the berm provided the berm is no flatter than 100H:1V. However, the EM does not define what constitutes as a “large” thickness and it is not clear under what circumstances will allow this flat

berm to be used. For this reason, any slope flatter than 75H:1V is not considered feasible in this discussion.

The thickness of the berm at the levee toe and the berm crown may require adjustment to meet the desired slope criteria. The minimum berm dimensions (X= 150 ft, t = 5 ft, r = 2 ft) result in a berm slope of 48H:1V, which is slightly steeper than the minimum desired flattest slope of 50H:1V by the EM. As the width of the berm increases, for a constant value of t, the berm becomes flatter, and assuring adequate drainage becomes more problematic.

Figure 3-5 shows the minimum thickness of the berm at the levee toe corresponding to the selected slopes for different berm widths. The thickness at the berm crown (r) is held constant at the minimum requirement of 2 ft in this figure. The admissible berm design must lie in the solid blue portion of the plot area, which is bounded by the minimum and maximum width requirements of 150 ft and 400 ft respectively, and the allowable slope of 50H:1V. Flatter slopes like 75H:1V are allowed if it can be shown that the soils are fully consolidated under the stress of the levee, such that the future settlement will not make the berm any flatter, and is indicated in solid yellow in the plot area. If the thickness at the levee toe controls the berm design, steeper berms are cheaper than flatter berms as indicated by the contours of the volume of the berm material plotted inside the admissible area. These contours indicate an increase in the volume of the berm material as the width of the berm increases for a constant thickness. Conversely, if the width of the berm controls the design, the thickness at the levee toe will be less for a flatter slope as compared to the steeper slope. Therefore, a flatter berm will be the more economical option in this case, as less material is required.

If the design thickness and width plot in the solid pink area, the thickness must be increased to achieve the desired slope. In this case, steeper berms will result in a greater thickness and will be less economical as indicated by the contour plots.

The following relationship can be useful to determine when the berm dimensions do not meet the desired berm slope criteria:

If $\frac{X-3r}{t-r} > 50$, then the thickness at the levee toe (t) must be increased to satisfy the slope requirement, unless it is feasible to use slope of 75H:1V as explained earlier. Then 50 should be replaced by 75 in this relationship.

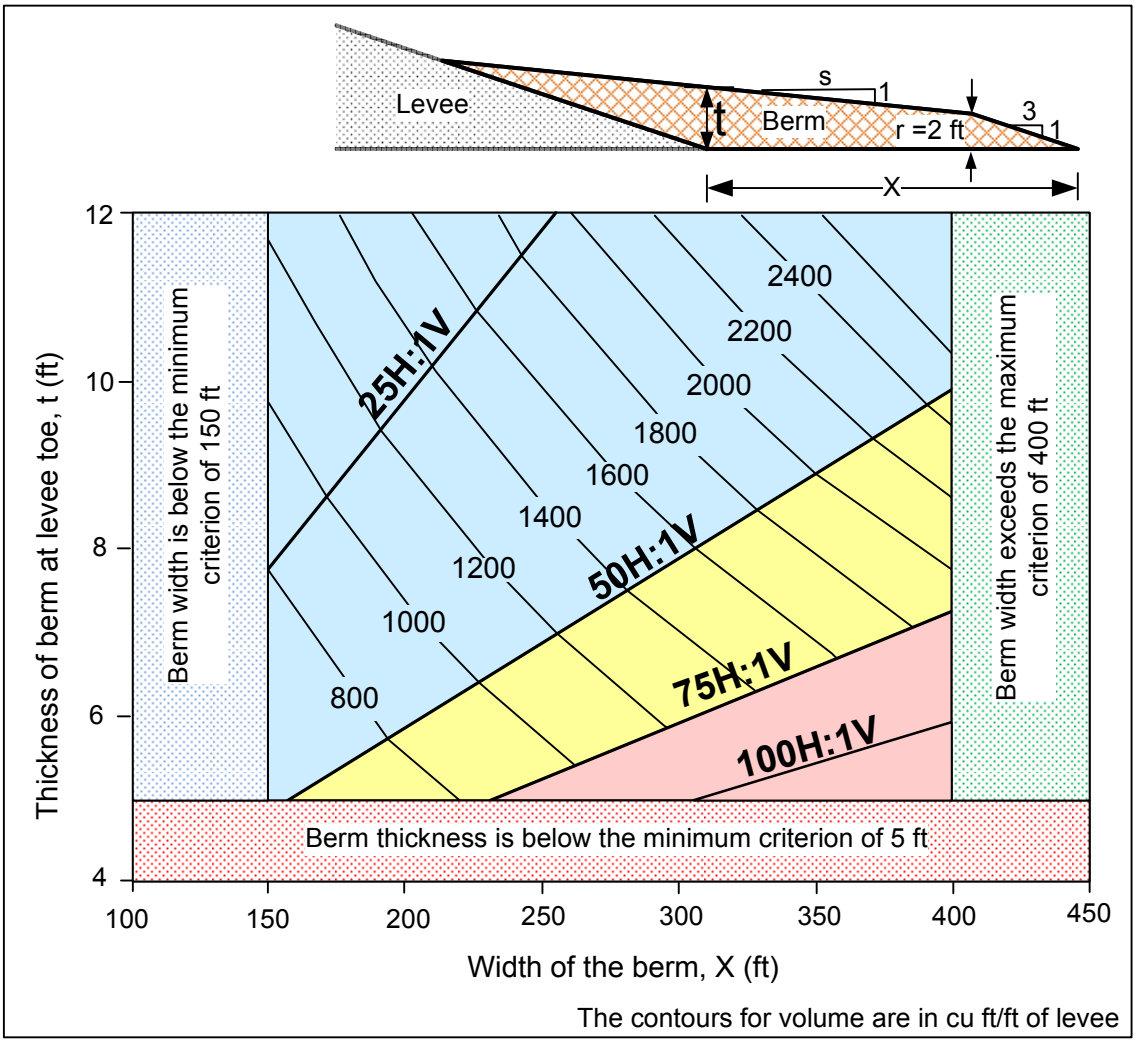

Figure 3-5 Relationship between berm thickness at levee toe and berm width for different slopes, assuming a constant berm crown thickness of 2 ft.

The red stippled area in Figure 3-5 indicates the zone where berm thickness does not meet the minimum criterion of 5 ft. Similarly, the blue and green stippled zones indicate the width ranges where the minimum and maximum width criteria are not met, respectively. Figure 3-5 can be useful in ascertaining the suitability of different slopes. It can be used with the design values of X and t determined from closed-form solutions or FEA to evaluate if the design dimensions meet the criteria for required berm slopes. The volume contours are useful for determining the economy of different slopes.

3.9. Cases with No Landside Top Stratum

The design equations present in EM 1110-2-1913 and TM 3-424 are for cases having a top stratum or blanket on the landward side, which is generally assumed to be semipervious. Therefore, these equations cannot be directly used for the design of berms for cases having no landward top stratum. However, seepage berms can still be useful for these cases and are often employed in practice. There is no closed-form Blanket Theory solution for calculating gradient for the case of no landside top stratum. In the past, flow nets were suggested for the calculation of the exit gradient, but now, finite element analysis can be a useful alternative for the design of seepage berms for such cases. DIVR 1110-1-400 suggests the use of Creep Ratio presented by Bligh (1927) for an initial determination of the need for seepage berms for cases having no landside top stratum. *Bligh's Creep Ratio*, c is defined as shown in Equation 3-5:

$$c = \frac{x_1 + L_2}{H} \tag{3-5}$$

Where,

c = Creep Ratio

x_1= Distance from effective seepage entry to riverside levee toe

H=Net head on the levee

L_2 =Base width of levee

Creep Ratios have historically been used to determine the safety of structures against erosion and piping in the absence of more exact methods. Creep Ratios relate the net head across the structure with the horizontal and vertical flow lengths from the upstream to the downstream end of the structure.

DIVR 1110-1-400 recommends that no landside seepage berm is required if Bligh's Creep Ratio is greater than or equal to 12 for coarse sand, 15 for medium sand, and 18 for very fine sand foundations. However, if the Creep Ratio is less than the above values, the DIVR suggests the use of flow nets to determine the need of landside seepage berms by calculating the exit gradients at the levee toe and comparing the value with 0.5. If the gradient exceeds 0.5, landside seepage berms are required.

Closed-form solutions can be developed to calculate the hydraulic head at the levee toe for cases having impervious berms directly on top of pervious strata. The theoretical value of head at the levee toe will remain zero if the berm is pervious, resulting in infinite gradient. The value of head at the levee toe was compared from finite element analysis and Blanket Theory for cases having no top stratum on both the landside and riverside, and impervious and semipervious top strata on the riverside. Table 3-4 shows the Blanket Theory equations to calculate the excess head at the levee toe for different cases of no top stratum and an impervious berm overlying the pervious stratum on the landside. The heads at the levee toe for these cases were in close agreement from finite element analysis and Blanket Theory. The berm width was hypothetical in

these examples and was not designed based on factor of safety but minimum design width of 150 ft was assumed just for comparison.

Table 3-4 Equations to calculate excess head at levee toe (h_o) for different cases of no top stratum and a landside impervious berm

Case	Illustration	Equation
No top stratum on both the landside and riverside	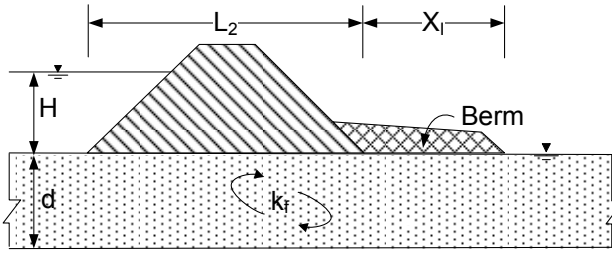	$h'_o = H\left(\frac{X_I + 0.43d}{0.86d + L_2 + X_I}\right)$
No top stratum on landside and an impervious top stratum on riverside	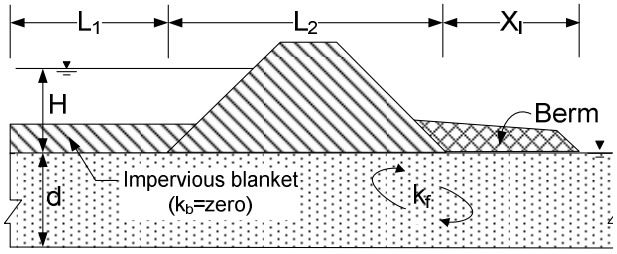	$h'_o = H\left(\frac{X_I + 0.43d}{L_1 + L_2 + X_I + 0.43d}\right)$
No top stratum on landside and a semipervious top stratum on riverside	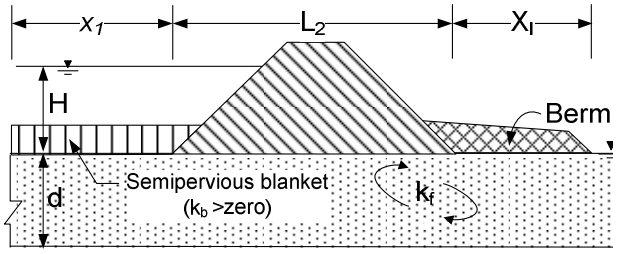	$h'_o = H\left(\frac{X_I + 0.43d}{x_1 + L_2 + X_I + 0.43d}\right)$

Notations

H = Net head on the levee
L_1 = Distance from river to riverside levee toe
h'_o = Excess head at the landside levee toe with berm
x_1 = Distance from effective seepage entry to riverside levee toe
X_1 = Width of the impervious berm
k_b = Permeability of top stratum
d = Thickness of pervious stratum
k_f = Permeability of pervious stratum
L_2 = Base width of the levee

The closed-form solutions can be modified so that they can be used for the design of seepage berms for cases having no top stratum by substituting the thickness of the top stratum (z_t) as zero in the berm equation for calculating the berm thickness as shown in Equation 3-6.

$$t = \frac{h'_o}{1 + \left(\gamma'_t / F\gamma_w\right)} \tag{3-6}$$

Where,

t = Required berm thickness at levee toe

h'_o= Excess head at landside toe of levee with berm

γ'_t = Submerged unit weight of berm

γ_w = Unit weight of water

F = Factor of safety against uplift at levee toe

However, the width of the berm (X) cannot be directly calculated from the equations in the EM, and requires drawing a flow net or finite element analysis. For calculating the required berm width, the exit gradient and the factor of safety will need to be calculated at a point where thickness of the berm is zero to determine if the minimum factor of 1.0 at the berm toe is satisfied.

Finite element analyses were conducted for the example shown in Figure 3-6 to determine if seepage berm was required. The base width of the levee is equal to 132 ft for this example. The net head on the levee is 20 ft, and thickness of pervious stratum is assumed to be 100 ft. The pervious stratum is assigned a permeability value of 3.9×10^{-3} ft/sec (1.2×10^{-1} cm/sec). The "total head" boundary condition is assigned to both the riverside horizontal and vertical boundaries. The "potential seepage exit" boundary condition is assigned to the top of the seepage berm. Similarly, the "total head" boundary condition is assigned to the portion of the landside horizontal boundary after the berm, as well as the landside vertical boundary.

The head at the levee toe was computed from finite element analysis and the gradient was calculated using the recommendations from Duncan et al. (2011) as described earlier. The gradient was calculated over a distance of 1 ft, as shown in Figure 3-6, and the value was determined as 0.7 indicating that a seepage berm is required. Similarly, Bligh's Creep Ratio is

6.6, which is less than the required value of 12 for coarse sand, which also confirms that a seepage berm is needed for this example.

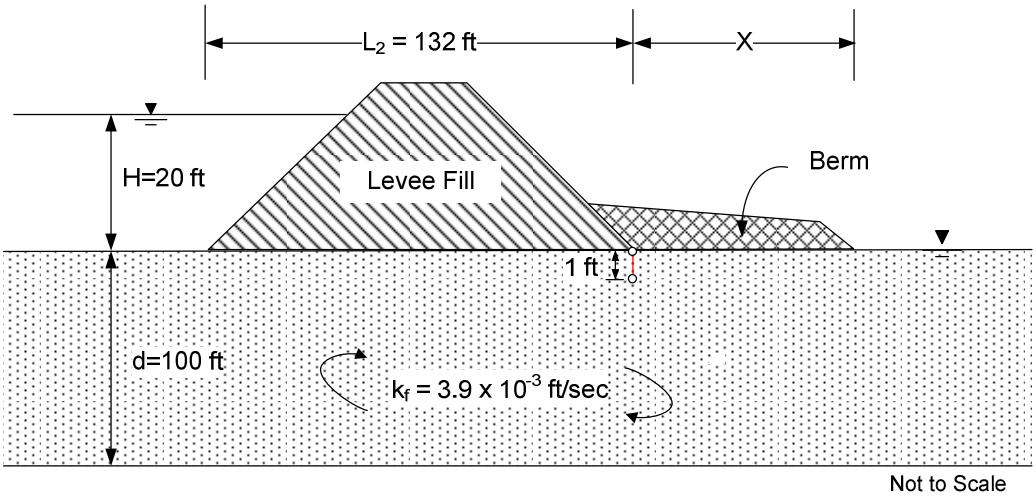

Figure 3-6 Section of the levee with no top stratum. (Not to scale).

The thickness of the impervious berm was calculated as 7.1 ft from Equation 3-6 for the example case shown in Figure 3-6. However, the width of the berm cannot be directly calculated from the closed-form solutions and requires drawing of a flow net as explained earlier. Therefore, the procedure explained in the earlier sections is followed for the design of a berm having no top stratum using FEA, and iterations were conducted to determine the required thickness and width of the berm. Similarly, semipervious berms are designed in a similar manner as impervious berms. The permeabilities of impervious and semipervious berms were assumed to be 2×10^{-9} ft/sec and 3.4×10^{-5} ft/sec, respectively, for this analysis. The design thickness and width of the impervious berm for the slope of 50H:1V were calculated as 9.7 and 390 ft, respectively for this example. Similarly, these design values reduce to 8.9 ft and 350 ft for semipervious berms. There are no direct equations to calculate the thickness of the pervious berms. Sand and pervious berms can be modeled in FEA in the same manner as explained earlier. However, it is not logical to construct seepage berms with the same permeability as that

of the pervious foundation for the levees having no top stratum. Weighted filter berms are, however, often used for such levees.

3.10. Inconsistencies in Calculating Factors of Safety

Equations to calculate factors of safety or exit gradients for seepage berms are not explicitly defined in EM 1110-2-1913. They can be inferred from the derivation of the expression for the thickness of the berm. Since the expression for calculating the thickness of the berm is same for all types of berms in the EM, it also results in the same factor of safety equation for all the berm types. However, the EM considers the semipervious berm to have same permeability and unit weight as the top stratum, so these expressions are slightly modified in the EM to incorporate this assumption. The expression in the EM for the thickness of the berm can only be obtained if the factor of safety against uplift for combined berm and top stratum is defined as shown in Equation 3-7. Similarly, it is important to calculate factor of safety for just the berm as well as the combined factor of safety for the berm and the top blanket for cases where the permeability of the berm is less than that of the top stratum. However, the EM does not explicitly provide the equation for calculating the factor of safety for the berm only.

$$F_{t+b} = \frac{\gamma'_z z_t + \gamma'_t t}{(h_o - t)\gamma_w} \tag{3-7}$$

Where,

F_{t+b} = Factor of safety against uplift for combined berm and the blanket

γ'_z = Submerged unit weight of top stratum

γ'_t = Submerged unit weight of berm

γ_w = Unit weight of water

z_t = Thickness of top stratum

h_o = Excess head at the levee toe

t = Required berm thickness at levee toe

Barron (1980) also derived the expressions for calculating berm thickness and berm width for different berm types. These derivations are also based on expressions for calculating appropriate values of factors of safety for each berm type. Barron's equations for factor of safety are different from the equations inferred from the thickness expressions present in EM 1110-2-1913 for impervious, semipervious, and pervious berms with collector. Table 3-5 shows the comparison of expressions of factors of safety for each berm type from Barron (1980) and EM 1110-2-1913.

Table 3-5 Comparison of factors of safety back-calculated from thickness equation present in EM 1110-2-1913 and presented by Barron (1980)

Berm Type	F from the EM	F by Barron (1980)	Comments
Impervious	$F_{t+b} = \frac{\gamma'_z z_t + \gamma'_t t}{(h_o - t)\gamma_w}$	$F_{t+b} = \frac{\gamma'_t t}{(h_o - t)\gamma_w}$	The factors of safety are different.
Semipervious	$k_t = k_b$ $F_{t+b} = \frac{\gamma'_t (t + z_t)}{(h_o - t)\gamma_w}$ Where, k_t = Permeability of seepage berm k_b = Permeability of top stratum	$k_t \le k_b$ For berm only, $F_t = \frac{\gamma'_t (t + \overline{K} z_t)}{(h_o - t)\gamma_w}$ Where, $\overline{K} = \frac{k_t}{k_b}$ For combined berm and blanket, $F_{t+b} = \frac{\gamma'_t \left(t + \left(\gamma'_z / \gamma'_t \right) z_t \right)}{(h_o - t)\gamma_w}$ If $\overline{K} < \frac{\gamma'_z}{\gamma'_t} \rightarrow F_t < F_{t+b}$ $\overline{K} > \frac{\gamma'_z}{\gamma'_t} \rightarrow F_t > F_{t+b}$	The factors of safety are the same if $k_t = k_b$ EM does not account for the case when k_t is different from k_b
Sand	$F_{t+b} = \frac{\gamma'_z z_t + \gamma'_t t}{(h_o - t)\gamma_w}$	$F_{t+b} = \frac{\gamma'_z z_t + \gamma'_t t}{(h_o - t)\gamma_w}$	The factors of safety are the same.
Pervious with Collector	$F_{t+b} = \frac{\gamma'_z z_t + \gamma'_t t}{(h_o - t)\gamma_w}$	$F_{t+b} = \frac{\gamma'_z z_b + \gamma'_m t}{h_o \gamma_w}$ Where, γ'_m = Moist unit weight of berm (use buyout unit weight if berm is submerged)	The factors of safety are different.

It is important to check the factor of safety against uplift for only the berm, as well as the combined factor of safety for the berm and the blanket for impervious and semipervious berms. After examining various expressions for different types of berms, it is recommended to use Equation 3-7 to calculate factor of safety against uplift for the combined berm and blanket for

semipervious and impervious berms. Equation 3-8 is recommended to calculate the factor of safety for the berm only for semipervious and impervious berms.

$$F_t = \frac{\gamma'_t \left(t + \overline{K} z_t\right)}{\left(h_o - t\right)\gamma_w} \tag{3-8}$$

Where,

F_t = Factor of safety against uplift for berm only

γ'_t = Submerged unit weight of berm

t = Required berm thickness at levee toe

$\overline{K}$ = Ratio of permeability of the seepage berm to that of the top stratum

z_t = Thickness of top stratum

h_o = Excess head at the levee toe

γ_w = Unit weight of water

F_{t+b} = Factor of safety against uplift for combined berm and the blanket

γ'_z = Submerged unit weight of top stratum

Equation 3-8 is the same as that derived by Barron for semipervious berms if the permeability of the berm is less than or equal to the top stratum. This expression may also be applied to cases where there is an impervious berm. A transformation factor ($\overline{K}$), can be used in transforming the thickness of the top stratum based on the permeability values. Therefore, a case having an impervious berm will result in very small transformation factor ($\overline{K}$), as the permeability of the impervious berm is very much less than the permeability of the top stratum,

thus making the contribution of the thickness of the top stratum very small for the calculation of the factor of safety for the berm only.

In case of sand berms, permeability of sand is greater than the permeability of the top stratum, therefore factor of safety for the combined berm and top blanket is applicable for this case, and can be calculated from Equation 3-7.

The pervious berm with collector presents an interesting case, as it does not have any effect on the seepage regime. The excess head calculated at the interface of the top and pervious stratum at the levee toe is independent of the thickness of the berm. The equation to calculate the factor of safety, and ultimately berm thickness, is different in the EM as compared to the one presented by Barron. Barron assumes that the berm is so pervious that no head loss will occur through it, giving the same value of total head at the top and bottom of the pervious seepage berm. However, the EM treats the pervious berm the same as the other types, and considers the combined effect of the berm and top stratum for calculating factor of safety. A closer look at the equations reveals that the value of the factor of safety from the EM will be greater than the value calculated from the equation presented by Barron. Similarly, the thickness of the berm calculated from Barron's equation is greater than the thickness calculated from the EM equation for pervious berms. This raises an interesting question, as to which equation is most appropriate to use for calculating factors of safety for the pervious berms.

The equation presented by Barron considers the gradient across the top stratum only, as it assumes that no head loss will occur through the pervious berm. The lower factor of safety calculated from Barron's equation is due to the fact that the mechanism involved in increasing the factor of safety, when using the pervious berm, is different than the mechanism for other berm types. The pervious berm will increase the factor of safety by increasing the net critical

gradient, while other berm types mostly increase the factor of safety by reducing the vertical gradient, thus having different impacts. The equation to calculate the factor of safety for the pervious berm presented by Barron seems more logical; however, it contradicts the conclusion in the TM, which states that the pervious berm will give the lowest thickness as compared to the other berm types. Therefore, it is important to understand the effect of the equations presented in both the EM and those presented by Barron, and use them as appropriate when designing the pervious berm with the collector.

Table 3-6 shows a comparison of design dimensions for all berm types using the EM and Barron's equations for a clay top stratum of 5 ft and the same geometry and properties as explained earlier. Both methods result in the same width for the impervious and pervious berms; however, values of thickness of the berms are different, as equations to calculate factors of safety are different for both methods from which the thickness equations are inferred. Similarly, the values are slightly different for semipervious berms because of the way the equation is solved as explained earlier. Barron presents an approximate solution for sand berms, and the values are different because the width of the semipervious berm is different from both methods. The last column in Table 3-6 represents the berm dimensions from FEA based on the recommended equations for factor of safety as presented in the preceding discussion. The factor of safety for only the berm controlled the design for impervious berm, therefore the thickness of the berm is closer to Barron's thickness in this case. Similarly, minimum allowed thickness of 5 ft is shown for other berm types from FEA, as it adheres to the Corps requirement of the 5 ft thickness at the levee toe, which serves as a starting point for FEA as explained earlier. The reasoning for a difference in the width of the semipervious and sand berm calculated from closed-form solutions and FEA was explained in the earlier sections.

Table 3-6 Comparison of required berm dimensions from different types of analyses for a clay top stratum of 5 ft for properties shown in Table 3-2.

Berm Type	Required Berm Dimensions (ft)	Analysis Type		
		EM Equations	Barron's Equations	FEA based on Recommended *F* Equations
Impervious	Width	821	821	820
	Thickness	6.1	7.7	7.7
Semipervious	Width	264	232	400
	Thickness	3.1	2.8	5
Sand	Width	241	220	330
	Thickness	2.8	2.6	5
Pervious	Width	197	197	200
	Thickness	2.5	3.6	5

3.11. Conclusions

Design of seepage berms is currently conducted using the closed-form equations outlined in the Corps of Engineers manuals. An effort is made in this paper to update these methods by introducing finite element analysis as an alternative. A methodology compatible with the current design methods is developed to use finite element analysis for the berm design, and a step-by-step procedure is outlined. Guidelines are provided for each berm type for this purpose. Berms are designed for different examples using both closed-form solutions and finite element analysis. Finite element analysis and closed-form solutions show good agreement for design of impervious and pervious berms. However, different berm design parameters are obtained for semipervious and sand berms, as the derivation of closed-form solutions for semipervious berms do not consider the presence of a berm crown. The use of the closed-form solution will be unconservative for cases when the berm crown is considered. The width of a semipervious berm

calculated from closed-form solutions is very sensitive to the permeability of the top stratum, and a slight change in permeability results in great variation in the width of the berm. Engineers designing semipervious berms using closed-form solutions need to exercise judgment to account for this rapid change in the design widths with change in permeability of the top stratum. Finite element analysis can be useful in this regard and also provides the flexibility of assigning different permeability to the berm than that of the top stratum, as opposed to the EM solutions, which assumes the same permeability. Similarly, there is no direct equation to calculate the width of the sand berm, and use of finite element method can be useful for its design.

Different berm slopes were also investigated and a diagram was developed to evaluate the feasibility of achieving different berm slopes based on the design parameters. This plot is also useful in selecting the economical berm slopes by minimizing the berm volume.

The design equations outlined in EM 1110-2-1913 are derived only for cases having a top stratum and therefore cannot be directly used for levees where no top stratum exists. Creep Ratios have historically been used to determine if berms are required, and indirect methods have to be used for the design of seepage berms for these cases. Finite element analysis can be used to good utility for the design of these berms.

Factor of safety still needs to be calculated even when designing the seepage berms using the finite element analysis. There are inconsistencies in the way factor of safety is defined in EM 1110-2-193 and by Barron (1980). Factor of safety against uplift should be calculated for only the berm, as well as for the combined berm and blanket, if the permeability of the berm is less than the top stratum. The lesser of the two values will control the berm design. However, the EM only considers the factor of safety for the combined berm and the blanket, and therefore, a general factor of safety equation derived by Barron is also recommended to be used to check the

factor of safety for the berm only for such cases. Similarly, the factor of safety for the combined berm and the top stratum is more critical for cases where the permeability of the berm is greater than the permeability of the top stratum. However, for cases where berm is completely pervious, resulting in no head through it, the equation in the EM and the equation presented by Barron result in different thicknesses of the berm, and care needs to be exercised while selecting the appropriate equation. Barron's factor of safety equation for pervious berm with collector seems more appropriate than the one presented in the EM, as it assumes that no head loss will occur through the pervious berm, which seems logical considering the berm being so pervious. This paper will serve as a useful resource for practicing engineers to understand some of the limitations of the current design methods, as well as enhance their ability to use finite element analysis as a tool for berm design.

3.12. Acknowledgments

The authors acknowledge the support provided by US Army Corps of Engineers (USACE) for conducting this research. Mr. Ken Klaus, Mr. Noah Vroman, and Dr. Joe Dunbar of the Corps of Engineers also provided valuable feedback during this research.

3.13. References

Barron, R. A. (1980). “Mathematical analysis of landside seepage berms,” Miscellaneous Paper GL-80-15, U.S. Army Engineer Waterways Experiment Station, Vicksburg, MS.

Batool, A., and Brandon, T. L. (2013). “Comparison of seepage analysis of levees using Blanket Theory and Finite Element Analysis.” (under review)

Bennett, P.T. (1946). “The effect of blankets on the seepage through pervious foundation.” Trans. ASCE **111**, pp 215-252

Bligh, W. G. (1927). The Practical Design of Irrigation Works, Van Nostrand Co., New York.

Brandon, T. L., Batool, A., Jimenez, M., and Vroman, N. (2013). "Levee Seepage Analysis using Blanket Theory and Finite Element Analysis," Report submitted to the U. S. Army Corps of Engineers Engineering Research and Development Center, Dept. of Civil and Environmental Engineering, Virginia Tech, Blacksburg, VA, 129 pp.

Duncan, J. M., O’Neil, B., Brandon, T. L., and VandenBerge, D. R. (2011). “Evaluation of Potential for Erosion in Levees and Levee Foundations," Report for Center for Geotechnical Practice and Research (CGPR#64), Dept. of Civil and Environmental Engineering, Virginia Tech, Blacksburg, VA, 40 pp

DIVR 1110-1-400 (1998). “Engineering and Design, Soil Mechanics Design Data, Part 6 - Landside Seepage Berms for Mississippi River and Major Tributary Levees, U.S Army Corps of Engineers, Mississippi Valley Division, Vicksburg, MS, 32 pp.

Federal Emergency Management Agency (FEMA 2011). “Filters for Embankment Dams - Best Practices for Design and Construction,” Federal Emergency Management Agency, Washington D.C.

Harr, M.E. (1962). Groundwater and seepage. McGraw-Hill, New York.

Mansur, C. I., and Kaufman, R.I. (1956). "Control of Underseepage, Mississippi River Levees, St. Louis District, CE," Journal of the Soil Mechanics and Foundations Division, 82, 864-871.

Pavlovsky, N.N. (1956). Collected works. Akad. Nauk USSR, Leningrad.

Rocscience, Inc. (2010). “Slide v6.0–2D limit equilibrium slope stability analysis.” Toronto.

United States Army Corps of Engineers (USACE) (1956). “Investigating Underseepage and its Control, Lower Mississippi River Levees, Technical Memorandum 3-424,” U.S. Army Corps of Engineers, Waterway Experiment Station, Vicksburg, MS.

USACE (1986). “Seepage Analysis and Control of Dams, Engineer Manual 1110-2-1901,” U.S. Army Corps of Engineers, Washington, DC.

USACE (2000). “Design and Construction of Levees, Engineer Manual 1110-2-1913,” U.S. Army Corps of Engineers, Washington, DC.

USACE (2005). “Design Guidance for Levee Underseepage, Engineer Technical Letter 1110-2-569,” U.S. Army Corps of Engineers, Washington, DC.

CHAPTER 4. ANALYTICAL CALIBRATION APPROACH TO DEVELOP A SEEPAGE MODEL FOR THE LONDON AVENUE CANAL LOAD TEST

(Published in Journal of Geotechnical and Geoenvironmental Engineering (2013)* - With Permission from ASCE)

Additional information regarding research presented in this chapter can be found in Appendix B

4.1 Authors

Abeera Batool[1] and Thomas L. Brandon[1]

[1]*Dept. of Civil and Environmental Engineering, Patton Hall, Virginia Polytechnic Institute and State University (Virginia Tech), Blacksburg, VA 24061 USA*

*Batool, A. and Brandon, T. (2013). "Analytical Calibration Approach to Develop a Seepage Model for the London Avenue Canal Load Test." *J. Geotech. Geoenviron. Eng.*, 139(5), 788–796 - With Permission from ASCE

Analytical Calibration Approach to Develop a Seepage Model for the London Avenue Canal Load Test

Abeera Batool, S.M.ASCE[1]; and Thomas L. Brandon, M.ASCE[2]

Abstract: The U.S. Army Corps of Engineers (USACE) conducted a load test along a portion of the London Avenue Canal as a part of an extensive study following the events of Hurricane Katrina to investigate the performance of I-walls and levees. A 45.7 m (150 ft) long section of the I-wall was hydraulically loaded, and pore pressures and displacements were measured in the vicinity of the I-wall through an extensive instrumentation system. The acquired data were assessed to develop a seepage model that would be applicable to the London Avenue Canal and areas where the soil conditions are similar. Two-dimensional and three-dimensional finite-element seepage analyses were conducted, a parametric study was performed, and a statistical calibration technique was developed to better estimate the actual field conditions in the numerical modeling. Based on this analysis, soil properties and finite-element boundary conditions are recommended for future analyses of the London Avenue Canal and other canals having similar subsurface conditions. **DOI: 10.1061/(ASCE)GT.1943-5606.0000810.**

CE Database subject headings: Levees and dikes; Seepage; Finite element method; Walls; Canals; Calibration; Load tests.

Author keywords: Levees; Seepage; Finite element; I-wall; Piezometer; Field test; London Canal.

Introduction

An extensive program was undertaken by the U.S. Army Corps of Engineers (USACE) following the events of Hurricane Katrina to investigate the causes of failures of I-walls and levees. This included the analyses conducted by Interagency Performance Evaluation Taskforce (IPET) to assess the performance of the Hurricane Protection System in New Orleans and southeast Louisiana [Interagency Performance Evaluation Task Force (IPET) 2007]. The USACE also conducted a load test along a portion of the London Avenue Canal to better understand the performance of I-walls in that region. The intention was to apply a water load to the I-wall and measure pore pressures and displacements in the vicinity of the I-wall through a variety of instruments.

This paper describes an assessment of the collected data related to I-wall performance and the development of a seepage model that would be applicable to the test site. Two-dimensional (2D) and three-dimensional (3D) seepage analyses were conducted, and the model was calibrated with the field test data to determine the most likely soil properties and hydraulic boundary conditions. A parametric analysis was conducted and a calibration technique was developed to provide the most accurate prediction of field conditions from the numerical modeling procedure. The method used to arrive at the optimum combination of various soil properties and hydraulic boundary conditions is presented and the results are generalized for the more common 2D seepage analyses.

[1]Ph.D. Candidate, Dept. of Civil and Environmental Engineering, Virginia Tech, Blacksburg, VA 24061 (corresponding author). E-mail: abeera@vt.edu

[2]Associate Professor, Dept. of Civil and Environmental Engineering, Virginia Tech, Blacksburg, VA 24061. E-mail: tbrandon@vt.edu

Note. This manuscript was submitted on October 25, 2011; approved on July 30, 2012; published online on August 4, 2012. Discussion period open until October 1, 2013; separate discussions must be submitted for individual papers. This paper is part of the ***Journal of Geotechnical and Geoenvironmental Engineering***, Vol. 139, No. 5, May 1, 2013. ©ASCE, ISSN 1090-0241/2013/5-788–796/$25.00.

Field Load Test Description

The load test was conducted by the USACE from August 18 to August 23, 2007. A site was selected for the load test based on an assessment of the soil stratigraphy relying on pre-Katrina borings, the dimensions of the levee embankment sections (crest width and slope angle), and the availability of adequate space for conducting the test. Based on the information available at the time, a site on the east bank south of Robert E. Lee Boulevard was selected. Fig. 1 shows the location of the site. Also visible on the figure is the location of the failure that occurred on the west bank during Hurricane Katrina, and the near failure, located directly across the canal on the east bank, directly south of Robert E. Lee Boulevard.

A detailed geotechnical investigation, consisting of borings and cone penetration tests, was completed immediately prior to the load test to provide information about the soil profile and the engineering properties of the soil layers. This information was used for the design of the load test in such a manner that it could be safely conducted without risking the integrity of the existing flood protection system. The load test was being conducted during the 2007 hurricane season, so special precautions were taken to ensure that the flood protection system would not be compromised, as is explained in the subsequent sections.

The existing I-wall consists of a driven sheet pile with a concrete cap located at the surface of the levee embankment. A sheet pile cofferdam was constructed to isolate a section of the I-wall from the rest of the canal. The cofferdam was about 45.7 m (150 ft) long and 10.7 m (35 ft) wide and the centerline of the cofferdam was located at 5772 Warrington Drive, which was the address of a then-vacant lot. The top elevation of the cofferdam was +2.4 m (+8.00 ft), NAVD88 as the maximum design water elevation to be tested inside the cofferdam was +2.3 m (+7.50 ft), NAVD88. The cofferdam isolated five of the 9.1 m (30 ft) long wall panels for testing. Fig. 2 shows an aerial view of the London Canal load test site during the test.

PZ-35 sheet piles and HP 14 × 73 piles were available to the USACE from other projects and were used in the construction of the cofferdam (Conroy 2008). Shown in Fig. 3 is a general cross section

at the test site. The cofferdam sheet piles were installed using a vibratory hammer and fully penetrated the pervious layer of beach sand to serve as a cut off to isolate the soils on the landside of the flood wall. A pump system was incorporated into the design to pump water into the interior section of the cofferdam to load the wall and to quickly dewater the cofferdam in the event of an emergency. In addition, a sluice gate was included in the cofferdam design to rapidly unload the I-wall in the test section. The crane shown on the platform in Fig. 2 was used to open the gate if required.

An extensive instrumentation system was installed at the site to measure the pressures, displacements, and water levels. Of particular interest was trying to measure the formation of a gap between the I-wall and the canal-side levee embankment. The presence of this gap was deemed important in the performance of many I-walls in the New Orleans flood protection system during Hurricane Katrina (IPET 2007; Brandon et al. 2008).

The water level in the interior section of the cofferdam and the canal water level were measured using submerged pressure transducers backed up by staff gauges. Sixteen open standpipe piezometers were installed with the screen intervals located at various depths. These piezometers were automated using pressure transducers connected to the data acquisition system. Five of the piezometers located along the centerline of the test section are indicated on Fig. 3. Fig. 4 shows a plan view of the location of all of the piezometers (PZ-1 to PZ-18) and a few survey prisms (SP-1 to SP-7).

The I-wall was heavily instrumented so that displacements could be measured as the water level inside of the cofferdam increased. The displacements were monitored at the top and base of I-wall and at the toe of slope, the mid slope, and the crest of the levee. Crackmeters were installed across the joints of the concrete I-wall caps to measure relative displacement between the panels. Inclinometers and tiltmeters were installed on the wall that could measure displacements in real time. Numerous survey prisms were affixed to the wall and the surrounding ground surface, and these were surveyed using two robotic electronic distance measuring (EDM) devices. Pressure cells were installed between the I-wall and the canal-side levee embankment to measure the reduction in earth pressure that would be caused as a gap is formed. Manual telltales, consisting of a cased rod located next to the wall, allowed a visual determination of the formation of a gap. The rods dropped into the gap as the gap was formed. Complete details of the instrumentation system can be found in URS (2007).

To conduct a test, the water level was raised in increments while the instrumentation was automatically monitored. Each water level was maintained until it was judged by a team of engineers, assessing both displacement and pore pressure measurements, that an equilibrium or steady-state condition had been achieved.

Fig. 1. Location of site for London Avenue Canal load test (Google Earth 2012)

Fig. 2. Aerial view of London Canal load test site (photograph by John McCusker 2007; with permission from The Times-Picayune)

Phase I and Phase II Test Series

The five wall panels were hydraulically loaded by increasing the water level in the cofferdam and observing the response of the I-wall and the levee. This loading process took place in two separate phases or stages, which were designed to simulate two possible mechanisms for increasing the pore pressure in the subsurface beach sand layer. If a gap is formed between the I-wall and the levee embankment, and the gap extends down to the sand layer, then the pore pressure in the sand layer can be drastically increased because of the shortened flow path (Duncan et al. 2008). This was modeled in the Phase I portion of the test. The second mechanism is created when the bottom of the canal forms a direct hydraulic connection to the sand layer because of erosion. This was modeled in the Phase II portion of the test.

Phase I of the load test was performed to isolate the formation and propagation of the gap between the I-wall and the levee embankment. The cofferdam was installed through the canal-side levee fill and marsh layers, and fully penetrated the beach sand layer. This geometry effectively replicated the condition of having an impervious material at the bottom of the canal because there was no hydraulic connection between the canal and the beach sand layer. The water level was raised in 0.15 m (0.5 ft) increments and the responses of the instruments were monitored. Once it was deemed that equilibrium conditions had indeed been achieved, based on pore pressures, wall and ground displacements, wall tilt, and so on, the water level was increased by 0.15 m (0.5 ft). The final water level achieved was 2.1 m (7 ft), NAVD88.

The Phase II loading geometry was intended to model a condition where there was a hydraulic connection between the cofferdam water level and the beach sand layer at the bottom of the canal. Twenty-nine slotted pipes were installed along the inside face of the cofferdam. The change in pore pressures in the silty sand and beach sand layers during the Phase II portion of the load test would be

J. Geotech. Geoenviron. Eng. 2013.139:788-796.

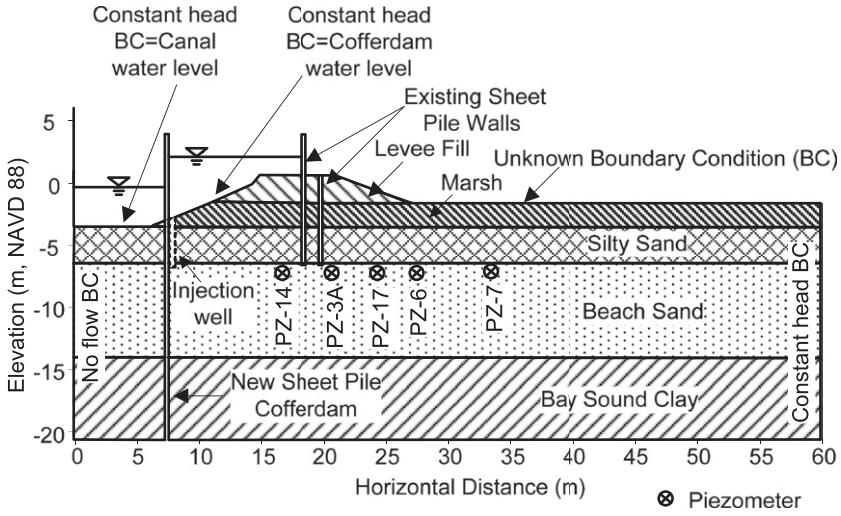

Fig. 3. Cross section of the I-wall system indicting soil layers and location of sheet pile walls including cofferdam

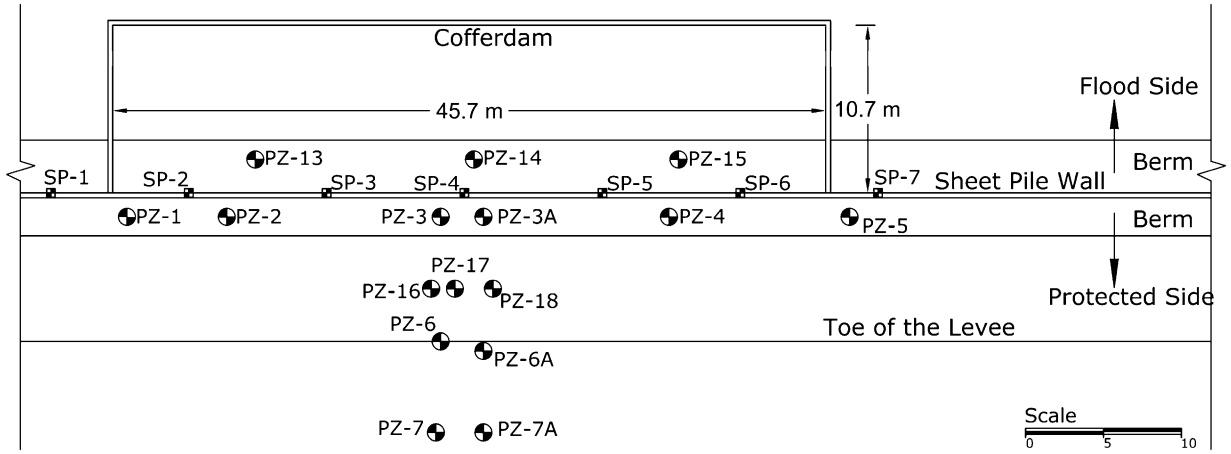

Fig. 4. Plan view of the location of the piezometers at the test site

controlled by the hydraulic connection made by these injection wells. The data acquisition, reduction, and loading procedure used in the Phase I portion of the test was also used for the Phase II portion of the test.

The analysis described in this paper focused on the Phase II results. A finite-element seepage analysis model was developed for the Phase II loading considering the injection wells for this study. Five piezometers (PZ-3A, PZ-6, PZ-7, PZ-14, and PZ-17) located at the center of the test section were used for calibration of the model. These piezometers, shown in Fig. 3, indicated the highest pore pressures measured, and were less influenced by the boundary conditions of the test section than other installed piezometers.

Model Development Challenges

The initial intention was to model the London Avenue Canal load test as a 2D seepage problem. However, scrutiny of the acquired data showed that the results were influenced by the finite boundary conditions. The following factors were judged to have made the load test differ from the ideal conditions:

1. The canal-side extent of the sheet pile cofferdam did not extend to the center of the canal. For the ideal case, the center of the canal would be a no-flow boundary condition. This led to some complicated hydraulic boundary conditions on the canal-side of the I-wall.
2. The test section was only 45.7 m (150 ft) long and the finite boundary of the cofferdam would affect the readings of the piezometers. In general, the highest pore pressures were measured in the center of the section. Fig. 5 shows that the pore pressures measured away from the centerline were smaller than the pore pressures recorded close to the centerline.
3. The pore pressures may have been influenced by changes in the canal water level as well as the changes in the water level inside of the cofferdam.
4. The displacement of the wall was greatest at the center of the section and decreased toward the boundaries. Fig. 6 shows the displacement at the top of the wall along the length of the cofferdam. The influence of a gap short-circuiting the flow would be dependent on the wall displacement (Brandon et al. 2008). This would cause an additional influence on the measured pore pressures along the length of the test section.
5. The hydraulic conductivity and general behavior of the injection wells that were used in Phase II may have changed during the course of the test because of silting in, clogging, and so on. It was not possible to accurately model the injection wells in 2D.

Based on the previously discussed information, it was inferred that the London Avenue Canal load test could not accurately be

J. Geotech. Geoenviron. Eng. 2013.139:788-796.

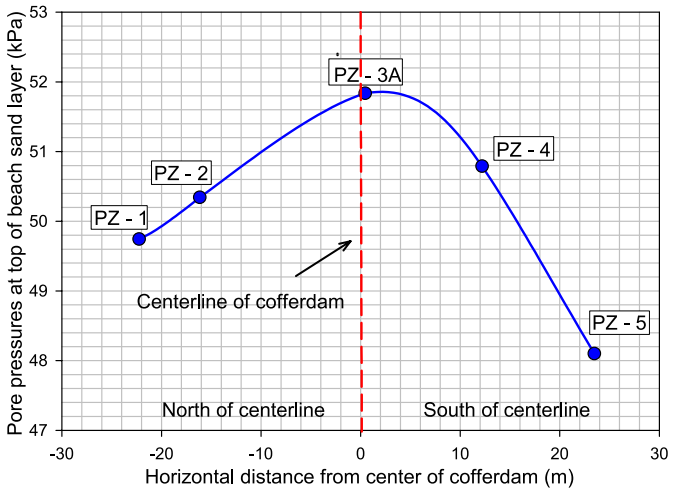

Fig. 5. Pore pressure distribution beneath the crest along the length of the cofferdam for canal water elevation of 1.2 m (4 ft), NAVD88

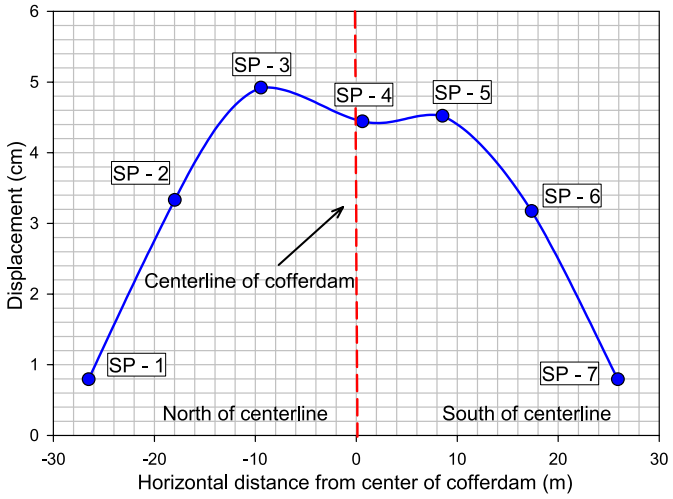

Fig. 6. Distribution of displacement at the top of the wall along the length of the cofferdam for canal water elevation of 2.1 m (7 ft), NAVD88 for the Phase II portion of the test

modeled as a 2D problem, and 3D modeling was necessary to represent the actual field conditions.

Three-Dimensional Modeling Approach

An important deviation from the ideal 2D condition was the limited length of the test section. The limited length of the test section would cause the measured pore pressures during the test to be less than those that would be expected for a full canal load test for several reasons. First, as shown in Fig. 5, the pore pressures at the boundaries of the test section are much less than those at the center, because the boundary pore pressures can be affected by the canal water level, and not just the water level inside of the cofferdam. Also, the pore pressures would be influenced by the deflection of the I-wall. If the I-wall deflects enough to cause a hydraulic connection of the canal (cofferdam) water and a subsurface pervious layer, pore pressures would be expected to increase. For a full canal test, the deflection of each wall panel would be more uniform, assuming that the stiffness of the landside embankment fill was approximately the same. However, for the load test, only five panels were loaded, and the end panels were effectively partially fixed. This would cause displacements, and likely pore pressures, to be greatest at the center or midpoint of the test section.

The previously discussed factors led to the conclusion that pore pressures measured during the load test were probably lower than the pore pressures that would have been developed for a full canal test (i.e., if the water level inside the entire canal were raised). Therefore, conducting 2D analyses of the load test was not appropriate and 3D seepage analyses were required to accurately simulate the field conditions.

The 3D seepage analyses were performed using the finite-element program *COMSOL Multiphysics* (*COMSOL Multyphysics 3.5*). The *Earth and Science Module* of this program was used to perform the seepage analysis. Initially, a 2D seepage model was developed in *COMSOL* and then the output from this model was compared with the finite-element program *SLIDE* (*Slide v6.0–2D limit equilibrium slope stability analysis*). It was observed that almost identical results were obtained from both programs and this comparison was done to validate *COMSOL* with *SLIDE*, which is a more commonly used seepage analysis program. The 3D model was developed using the load test geometry and is shown in Fig. 7. Tetrahedral elements were used in 3D model, whereas six-node triangular elements were used in 2D modeling.

Phase II of the test was the primary focus of the numerical analysis. The injection wells were modeled as slots to replicate the field conditions, allowing the hydraulic connection between the water in the cofferdam and the underlying sand stratum. The injection wells were relatively difficult to discretize, as these wells were dimensionally a very small feature with a large aspect ratio when compared with the larger domain in general. An appropriate hydraulic conductivity had to be assigned to the injection wells in the seepage model in order to establish whether the modeled injection wells were providing the desired hydraulic connection. The additional analyses were conducted; and assigning a hydraulic conductivity of the injection wells as 1.5 cm/s (0.05 ft/s) resulted in reasonable results and this value was used in all the subsequent analyses.

The cross section shown in Fig. 3 provides some of the boundary conditions assigned to the 3D model used to simulate the load test geometry. The horizontal landside boundary is assigned an unknown boundary condition, which indicates that it is a potential seepage face, and that it requires an iterative process for solution. In addition, the hydraulic conductivity of the various soil layers is also one of the most important elements in a seepage analysis. The stratigraphy at the test site included levee fill material (CL), a marsh (organic clay) layer (OH), a silty sand layer (SM), a beach sand layer (SP), and a bay sound clay layer (CH), as shown in Fig. 3 and Fig. 7. All the available field and laboratory information regarding hydraulic conductivity of each layer was examined and hydraulic conductivity values were assigned to each layer using the available data, empirical correlations with index properties, and engineering judgment. The isotropic values of hydraulic conductivity were used in the analysis and are discussed in a subsequent section of this paper. Considerable effort was put forth to determine the hydraulic boundary conditions in the vicinity of the London Avenue Canal from the 3D seepage model by calibrating the model with the pore pressures measured during the load test.

Calibration Approach

The initial analyses adopted a trial and error approach that was very time-consuming, and it became obvious that the procedure would be more efficient if a parametric analysis of the 3D model were

J. Geotech. Geoenviron. Eng. 2013.139:788-796.

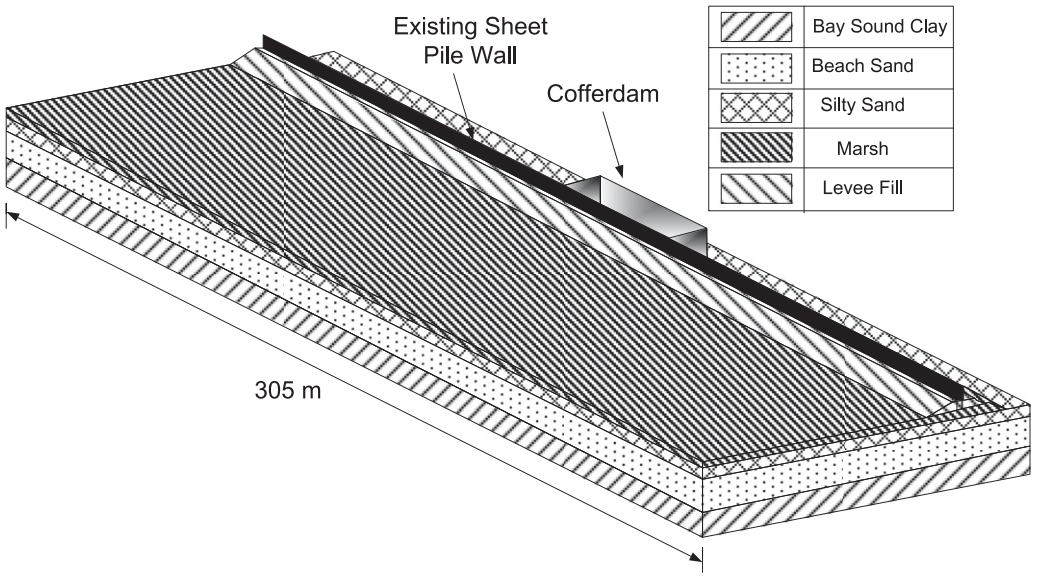

Fig. 7. 3D model of the load test geometry

performed and statistical data were obtained. After numerous runs were used to determine the general effect of changing the soil hydraulic conductivities and seepage boundary conditions on the total heads at the piezometer locations for Phase II of the load test, it was inferred that the following variables were the most important, had the greatest uncertainty, and required iteration in the analysis:

1. Hydraulic conductivity of silty sand layer;
2. Horizontal distance of the landside vertical boundary from the I-wall; and
3. Total head applied to the landside vertical boundary.

The range that the previous parameters can logically vary was selected and step sizes were determined for each parameter. Note that the horizontal distance of the landside boundary is considered from the toe of the levee in the upcoming discussion, which is located at about 12.2 m (40 ft) from the I-wall. The ranges and step sizes are summarized in Table 1.

Based on the number of parameters given in Table 1, the total number of runs was determined to be 1,260 ($6 \times 10 \times 3 \times 7$, as listed in the last column of Table 1). The next step was to generate curves for different combinations of variables to come up with the optimum values. Fig. 8 shows one such plot for illustration purposes. This plot was constructed by making use of the initial estimates obtained from the 2D analysis in order to check the viability of the approach.

Each diagonal line in Fig. 8 represents the variation of total head calculated at the location of one of the selected piezometers for different values of the constant head boundary condition at the landward edge of the domain. The piezometer readings from the actual load test are known; therefore, using the corresponding piezometer line obtained from the 3D model, the boundary condition that is required to achieve the measured piezometer values can be determined. This is done for all five selected piezometers and produces a range of the head values to be assigned on the landward side for one specific combination of parameters. Plots similar to that shown in Fig. 8 were generated for various domain widths, head values at the boundary, canal water levels, and hydraulic conductivity of the silty sand layer, as indicated in Table 1.

The range of the appropriate head values for the boundary (y-axis) can be determined by comparison with the actual piezometer readings shown on the x-axis of Fig. 8. It can be observed that

Table 1. Parameter Ranges for Parametric Analysis Iterations

Parameter	Minimum value	Maximum value	Step	Number of runs
Total head boundary condition (m, NAVD88)	−2.2	−3.7	0.305	6
Horizontal distance to vertical constant head boundary (m)	30.5	305	30.5	10
Canal water elevation (m, NAVD88)	0.61	1.22	0.305	3
Hydraulic conductivity of silty sand (cm/s)	3×10^{-5}	3×10^{-2}	3.0×10^{-5} 1.5×10^{-4} 3.0×10^{-4} 1.5×10^{-3} 3.0×10^{-3} 1.5×10^{-2} 3.0×10^{-2}	7

piezometer PZ-14, located on the canal-side of the I-wall, was problematic, as it did not fall within the range of the generated curves for this combination of parameters. Conversely, the possibility remains that the anomalous results of PZ-14 may be the case only for the previously discussed combination of parameters; and a better combination may exist for predicting the total heads closer to the measured field data for all the piezometers. Therefore, the use of parametric analysis to examine all the combinations becomes a valuable tool.

All 1,260 runs must be completed for a full application of the previously described approach. Performing numerous runs of the 3D model for the parametric analysis is a time-consuming process, but the merits and efficiency justify the use of this method. Similar plots to those shown in Fig. 8 were generated for all other combinations to assist in the statistical analysis. The purpose of generating such plots was to determine the range of best possible values, as previously explained. A summary of the results for different combinations was tabulated to determine the range of values for the landside vertical boundary conditions for each combination from parametric analysis generated using *COMSOL*.

J. Geotech. Geoenviron. Eng. 2013.139:788-796.

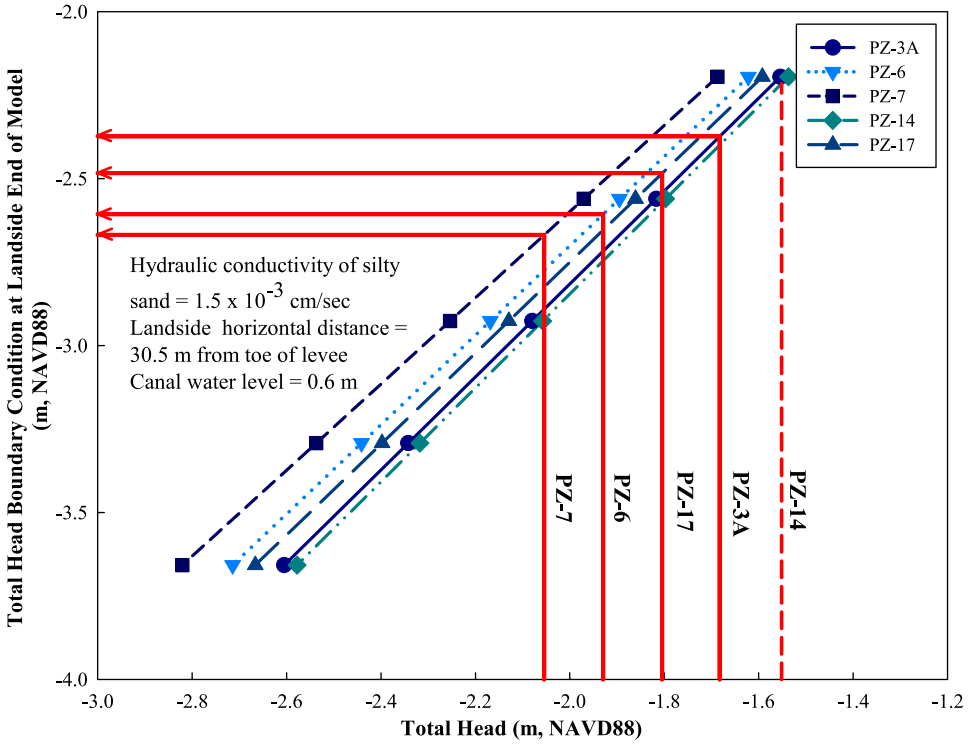

Fig. 8. Plot generated to obtain a range of total heads to be used as the landside vertical boundary condition for the indicated conditions

The head value of the landside vertical boundary that was required to obtain the same total head as measured during the field test was calculated for each piezometer in the same manner as that shown in Fig. 8. This approach determined the required head boundary condition for each individual piezometer such that using this value of head in the numerical model predicted the exact measured pore pressure. The result is a set of five values for each combination, because five centerline piezometers were considered for calibration purposes. The difference between the maximum and minimum values of the calculated total head was the range in which the boundary condition needed to be assigned to get a match of the pore pressures predicted from the model with the field readings for that particular combination. After obtaining the results for the various cofferdam water levels, the data were sorted such that the combinations having the same parameters were combined for different cofferdam water levels, because the final aim was to obtain the best combination calibrated to all the water levels at the same time.

The analyses described in the preceding sections were done considering cofferdam water levels up to 1.2 m (4 ft) only. The measured values of the piezometers indicated the development of the gap between the levee and the I-wall at higher water levels. This was inferred from a break in the pore pressure–cofferdam water elevation curve (Conroy 2008). To obtain the required boundary conditions for seepage analyses, it was decided to initially calibrate the model with the field test for the lower water levels only, because the 3D model could more accurately simulate the field conditions before the development of the gap.

The seepage analysis previously presented cannot predict the formation of the gap that is known to form between an I-wall and the levee backfill. The gap is formed when the I-wall is deflected because of the water load, and the water pressure acting between the wall and the canal-side embankment exceeds the earth pressure (Brandon et al. 2008). The soil must possess enough strength to sustain the gap. To predict the formation of the gap and its associated effect on the pore pressures, a coupled analysis, incorporating the stress-strain properties of the I-wall, levee fill, and other materials, would be required.

In this study, the modeling of the gap and its effects on the pore pressures was approached in an empirical fashion. After obtaining the most likely combination of boundary conditions for the no-gap condition, the analyses were repeated for higher water levels by incorporating the gap between the levee and the I-wall in the seepage model as constant head nodes along the sheet pile. The depth of the gap was determined by a trial-and-error procedure by incrementally changing nodes from no-flow to constant head until the pore pressures at the piezometer locations were matched. The gap was considered to be continuous in the lateral direction (along the canal). A more accurate representation would have modeled the gap as first starting at the midpoint of the test section, and progressing toward the north and south boundaries. This was more consistent with the measured wall deflections during the load test.

Assessment of the Data

After all combinations were analyzed, the results were carefully examined to begin the calibration process. At first, the ranges of the required vertical boundary condition were considered for the initial elimination of some of the combinations. The combinations that gave the smallest variation of the head at the landside boundary for all the piezometers for three different cofferdam water levels were considered to be the optimum. It was observed that analyses using horizontal distances of the landside boundary greater than 61 m (200 ft) from the toe of the levee were giving a significant variation of the required head at the boundary. Therefore, distances of 30.5 m (100 ft) and 61 m (200 ft) from the toe of the levee to the landside vertical boundary were considered for further calibration.

The processed data indicated that the silty sand hydraulic conductivity values of more than 3×10^{-3} cm/s (1×10^{-4} ft/s) for a horizontal boundary location of 30.5 m (100 ft) resulted in

J. Geotech. Geoenviron. Eng. 2013.139:788-796.

unreasonably low landside boundary heads (more than 1.5 m, or 5 ft, below the ground surface). The hydraulic conductivity value of the silty sand was further reduced to 3×10^{-4} cm/s (1×10^{-5} ft/s) if the horizontal boundary distance of 61 m (200 ft) was used in the model. The range of silty sand hydraulic conductivity is typically considered on the order of 3×10^{-4} to 3×10^{-6} cm/s (10^{-5} to 10^{-7} ft/s) (Terzaghi et al. 1996), so the results of the 3D model seemed reasonable. After reaching this conclusion, additional runs were made between the limits of 3×10^{-6} cm/s (1×10^{-7} ft/s) and 3×10^{-5} cm/s (1×10^{-6} ft/s) to further refine the hydraulic conductivity estimate. It was established that the distance of 30.5 m (100 ft) from the toe of the levee for the landside vertical boundary seemed to agree best with the field conditions and further analyses were performed for this length only.

Results

A viable method of selecting the best combination of parameters is to identify those that produce minimal values for the sum of absolute errors and SD. Table 2 summarizes the results of the analyses as well as the errors and SDs for a boundary distance of 30.5 m (100 ft) from the toe of the levee.

It was observed that the total heads obtained from the numerical modeling, especially for the lower values of hydraulic conductivity of the silty sand, were generally within 6 cm of the field values for all the piezometers considered. Minimal values of SD were obtained for the combination having a hydraulic conductivity value for the silty sand of 1.5×10^{-4} cm/s (5×10^{-6} ft/s) and a total head at the landside domain boundary of −2.8 m (−9.1 ft). While the sum of

Table 2. Analysis Results with Calculated Errors and SDs, Horizontal Boundary Distance of 30.5 m (100 ft)

CWL (m)	Head at landside boundary (m)	k (cm/s)	Absolute error for piezometer readings (m) PZ-3A	PZ-6	PZ-7	PZ-14	PZ-17	Sum of absolute errors (m)	SD
0.61	−2.61	3×10^{-6}	0.007	0.037	0.016	0.027	0.032	0.339	0.0162
0.91			0.026	0.029	0.006	0.008	0.003		
1.22			0.060	0.006	0.014	0.043	0.025		
0.61	−2.63	1.5×10^{-5}	0.003	0.038	0.015	0.032	0.034	0.331	0.0158
0.91			0.022	0.030	0.008	0.003	0.006		
1.22			0.057	0.008	0.015	0.038	0.022		
0.61	−2.65	3×10^{-5}	0.000	0.039	0.013	0.036	0.037	0.327	0.0157
0.91			0.019	0.032	0.009	0.002	0.008		
1.22			0.053	0.009	0.016	0.033	0.020		
0.61	−2.79	1.5×10^{-4}	0.007	0.032	0.010	0.051	0.037	0.358	0.0153
0.91			0.012	0.025	0.033	0.016	0.009		
1.22			0.046	0.002	0.040	0.018	0.019		
0.61	−2.91	3×10^{-4}	0.012	0.024	0.034	0.065	0.037	0.425	0.0210
0.91			0.006	0.017	0.057	0.031	0.009		
1.22			0.040	0.006	0.064	0.003	0.019		
0.61	−3.41	1.5×10^{-3}	0.034	0.010	0.133	0.131	0.034	0.940	0.0575
0.91			0.020	0.015	0.154	0.104	0.009		
1.22			0.010	0.035	0.159	0.078	0.015		
0.61	−3.69	3×10^{-3}	0.038	0.040	0.199	0.176	0.022	1.36	0.0828
0.91			0.029	0.041	0.217	0.157	0.002		
1.22			0.005	0.057	0.219	0.138	0.018		

Table 3. Best Values of Selected Parameters for Finite-Element Seepage Analysis of the London Canal (Obtained from Load Test Data Calibration)

Number	Parameters	Value: Calculated from laboratory and field tests	Value: Calculated from optimization
1	Hydraulic conductivity of the levee fill	1×10^{-6} cm/s (3.28×10^{-8} ft/s)	—
2	Hydraulic conductivity of the marsh layer	1×10^{-5} cm/s (3.28×10^{-7} ft/s)	—
3	Hydraulic conductivity of the silty sand layer	—	1.5×10^{-4} cm/s (5×10^{-6} ft/s)
4	Hydraulic conductivity of the beach sand layer	1.5×10^{-2} cm/s (4.9×10^{-4} ft/s)	—
5	Hydraulic conductivity of the bay sound clay layer	1×10^{-6} cm/s (3.28×10^{-8} ft/s)	—
6	Landside vertical boundary condition	—	−2.8 m or −9.1 ft (0.6 m below the ground surface)
7	Horizontal distance to the landside boundary domain from I-wall	—	42.7 m (140 ft)

J. Geotech. Geoenviron. Eng. 2013.139:788-796.

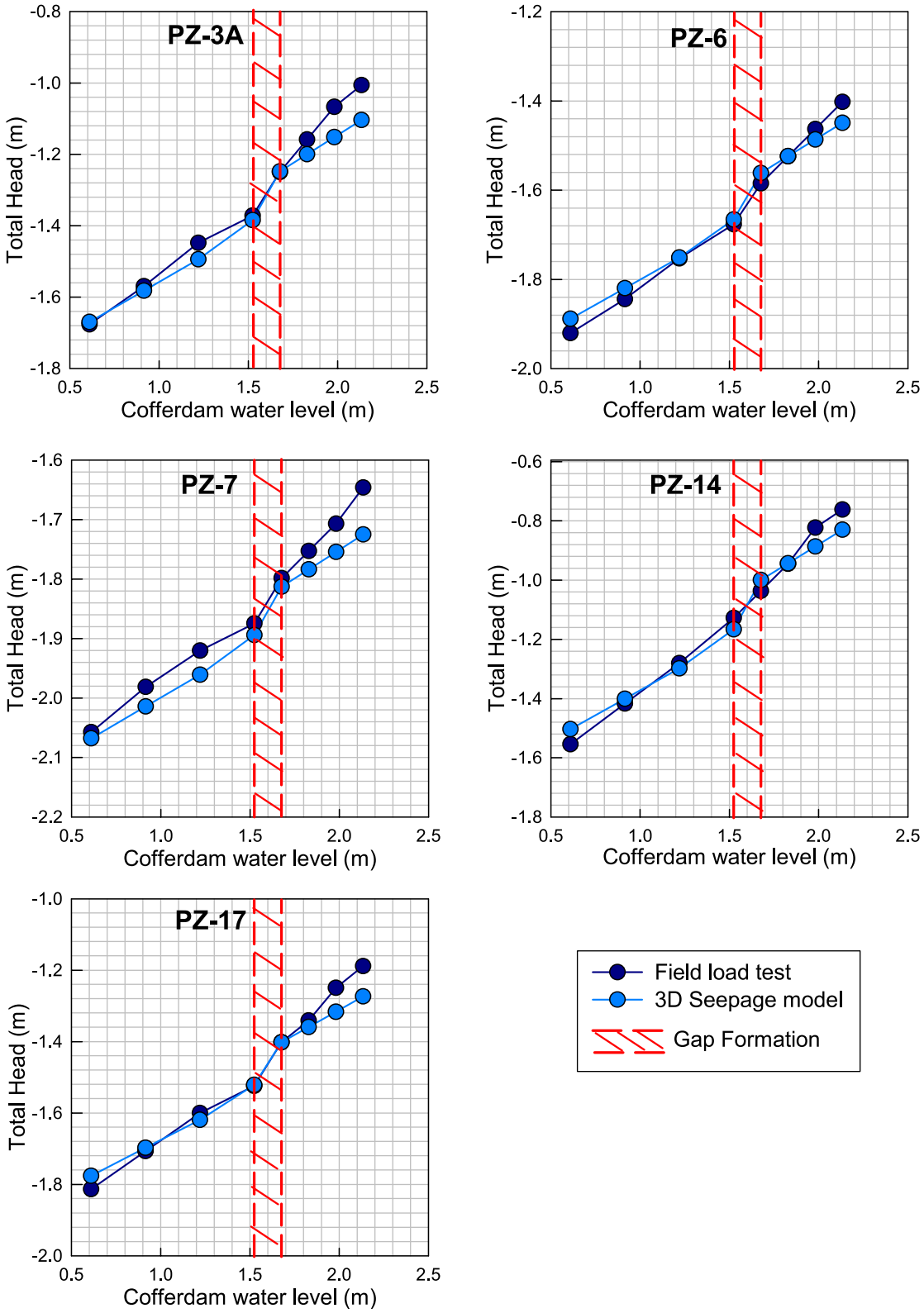

Fig. 9. Comparison of total heads obtained from London Avenue Canal load test and 3D seepage model for centerline piezometers

absolute errors for this combination is slightly more than the combinations having a lower hydraulic conductivity value of silty sand, closer inspection revealed that this combination gave an overall better agreement for all of the cofferdam water levels. Therefore, this combination was considered to be optimal in terms of the calibration with the load test data. The landside total head is significantly lower than sea level, which is logical because the ground behind the levee at this location is below sea level. A summary of the best values of various parameters for seepage analyses obtained from the calibration of the load test data is shown in Table 3. Fig. 9 shows the comparison between the total heads calculated from the 3D seepage model and the observed readings from the actual load test for the five piezometers.

J. Geotech. Geoenviron. Eng. 2013.139:788-796.

Additional analyses were conducted for the higher cofferdam water levels with the gap between the levee and the I-wall incorporated in the seepage model. The gap was initially considered to reach the top of the silty sand layer, but the output for this analysis showed that the total heads increased linearly with the canal water level using the same slope as before (i.e., for lower canal water levels without the gap). This indicated that the gap between the I-wall and the levee down to the top of the silty sand layer was not sufficient to influence the pore pressures to the degree that was measured. Therefore, it was assumed that the silty sand layer would have the ability to sustain a gap, and the gap was extended down into the silty sand layer. The depth of the gap did not extend all the way to the beach sand layer, because that would have resulted in a very significant increase of pore pressures. The results showed that the maximum absolute error for the total heads obtained from the finite-element model and the field data were within 10 cm after the development of the gap. These results seemed reasonable considering the limitations of the seepage model in simulating the gap formation. The gap formation is shown in Fig. 9 as the hatched region.

Conclusions

A load test was performed on a 45.7 m (150 ft) section of I-wall on the London Avenue Canal in New Orleans. This load test was performed on a section of I-wall located between the north and south failures that occurred during Hurricane Katrina (August 29, 2005). The section of I-wall and the surrounding soils were heavily instrumented to measure wall displacements and pore pressures as the height of water on the wall was incrementally increased.

An analysis of the acquired test data was performed to calibrate a finite-element seepage model. The available exploration and field test data were evaluated to estimate the appropriate soil parameters. The greatest uncertainty was judged to exist in the hydraulic conductivity of the silty sand layer, the location of the constant head landside domain boundary, and the value of the head at this boundary.

Assessment of the experimental results indicated that the boundary conditions of the load test deviated too much from a 2D flow condition, and that accurate results would not be obtained using 2D finite-element analysis to calibrate the seepage model. A 3D finite-element procedure was used to model the true geometric nature of the load test.

A statistical calibration procedure was used for the determination of the best possible values of the parameters having the greatest uncertainty. This approach required more than 1,200 finite-element runs to be conducted, and the results allowed for correct prediction of the centerline pore pressures measured during the test. Based on this analysis, the parameters listed in Table 3 are recommended for future analyses of the London Avenue Canal, and other canals having similar subsurface conditions such as Orleans Canal and the northeast portion of the Industrial Canal.

Acknowledgments

The authors credit the members of the team that provided the technical supervision of the London Avenue Canal Load Test for their expertise and stamina in conducting the test during one of the hottest summers in New Orleans on record. This team included Dr. Ray Martin, Dr. Bob Bachus, Mr. Pat Conroy, Mr. Neil Schwanz, and Mr. Noah Vroman. Mr. John Ashley served as the project manager of the test, and MAJ Nicholas Nazarko was the Officer in Charge. Mr. Richard Pinner and Mr. Frank Vojkovitch, both of the New Orleans District of the Corps of Engineers, provided valuable technical assistance in the design and operation of the load test.

References

Brandon, T. L., Wright, S. G., and Duncan, J. M. (2008). "Analysis of the stability of I-walls with gaps between the I-wall and levee fill." *J. Geotech. Geoenviron. Eng.*, 134(5), 692–700.

COMSOL Multyphysics 3.5 [Computer software]. Burlington, MA, COMSOL Inc.

Conroy, P. (2008). "London Avenue site specific load test report." *Technical Rep.,* U.S. Army Corps of Engineers, St. Louis, MO.

Duncan, J. M., Brandon, T. L., Wright, S. G., and Vroman, N. (2008). "Stability of I-walls in New Orleans during Hurricane Katrina." *J. Geotech. Geoenviron. Eng.*, 134(5), 681–691.

Google Earth. (2012). "5772 Warrington Dr, New Orleans, LA 70122." ⟨https://maps.google.com/maps?hl=en&q=5772+Warrington+drive+new+orleans+google+map&ie=UTF8&hq=&hnear=0x8620a8d6766a148f:0x82bc7628449995e7,5772+Warrington+Dr,+New+Orleans,+LA+70122&gl=us&ei=GHET5rLC4e09QTvwtW7Cw&oi=geocode_result&ved=0CBUQ8gEwAA⟩ (May 28, 2012).

Interagency Performance Evaluation Task Force (IPET). (2007). "Performance evaluation of the New Orleans and Southeast Louisiana hurricane protection system." *Final Rep. of the Interagency Performance Evaluation Task Force*, U.S. Army Corps of Engineers, Vicksburg, MS.

McCusker, J. (2007). "An aerial view of the Army Corps of Engineers test site on the London Avenue Canal." *Times-Picayune, Aug. 30*, ⟨http://blog.nola.com/times-picayune/2007/08/by_sheila_grissett_east_jeffer_2.html⟩ (Oct. 17, 2011).

Slide v6.0–2D limit equilibrium slope stability analysis [Computer software]. Toronto, Rocscience, Inc.

Terzaghi, K., Peck, R. B., and Mesri, G. (1996). *Soil mechanics in engineering practice*, 3rd Ed., Wiley, New York.

URS. (2007). "Structural and foundation response measured during the site specific load test on the London Avenue Outfall Canal I-wall/levee." *Technical Rep. Contract No. W912P9-05-D-0514, Task Order 6*, U.S. Army Corps of Engineers, St. Louis, 94.

J. Geotech. Geoenviron. Eng. 2013.139:788-796.

CHAPTER 5. SUMMARY AND CONCLUSIONS

The Corps of Engineers is making an effort to update the seepage methods outlined in their Engineering Manual (EM) 1110-2-1913, *Design and Construction of Levees,* (USACE 2000). The main objective of this research is to provide guidance for the Corps of Engineers in their transition from conducting underseepage analysis with Blanket Theory (USACE 2000) to using finite element analysis (FEA). Current methods outlined in the Corps documents are evaluated as part of this research and their limitations are highlighted. The review of the older methods and the associated documentation also serves as a useful resource for young engineers to understand some of the older seepage analyses present in existing reports. This research provides a step towards updating the current methods by providing general finite element guidelines for seepage analyses. In addition to blanket theory cases, guidelines are also provided for the design of seepage berms. The 3D finite element modeling of the complex geometries and strata for the London Avenue Canal is useful to better understand the response of levees and I-walls due to flood loading.

5.1. Summary of Research Accomplished

A summary of work accomplished as a part of this study is outlined below:

1. A literature review was conducted of the current Corps' methods regarding seepage analysis. Some of the older theories were also reviewed to have a better understanding of the theoretical basis of current methods.

2. The origins, assumptions, and derivations of blanket theory are not well documented. Therefore, Blanket theory equations had to be derived again to determine the assumptions and limitations.

3. An additional Case 8 was developed as part of this research to show how blanket theory can be modified to accommodate cases where sheet pile cutoffs are employed.

4. An extensive study was performed to compare the results of finite element analyses conducted on the original blanket theory cases contained in the Corps' engineering manuals to help the engineers make the transition from analytical solutions to numerical modeling.

5. Guidelines were provided to perform seepage analysis using finite element analyses in lieu of blanket theory methods for the equivalent geometries and boundary conditions.

6. A literature review was conducted of the current Corps' methods to design different types of seepage berms. Some of the limitations, including inconsistencies in the definition of factor of safety for different types of berms, were identified.

7. A methodology compatible with the currently accepted design methods was proposed using the finite element method for berm design, and a step-by-step procedure was outlined.

8. Several examples were considered and berm design parameters were compared from both the existing closed-form solutions and finite element analysis. As a result, finite element guidelines were provided for each berm type separately.

9. The design equations available in the Corps' manuals are only for cases having a blanket overlying a pervious stratum. This was extended to cases when no top stratum is present.

10. Seepage data acquired as a result of the load test conducted by the Corps of Engineers along portions of the London Avenue Canal was assessed to develop a seepage model.

11. Assessment of the experimental results indicated that the boundary conditions of the load test deviated too much from a two-dimensional (2D) flow condition; therefore, a 3D finite element procedure was used to model the true geometrical nature of the load test.

12. A parametric study was performed and more than 1200 3D runs were conducted to calibrate the model with the load test data.

13. A statistical calibration approach was developed to better estimate the actual field conditions in the numerical modeling.

5.2. Conclusions

Some of the conclusions based on the research presented in the preceding sections are outlined below:

5.2.1. Comparison of Blanket Theory Equations and Finite Element Analysis

1. There are some inconsistencies in the Blanket Theory equations presented in EM 1110-2-1913, *Design and Construction of Levees,* (USACE 2000). These include the incorrect representation of the head at the toe of the levee, the definition of net head on the levee, the determination of distance of effective seepage exit etc., and are outlined in detail in Appendix A.

2. Application of the Blanket Theory equations is limited to the cases where the ratio of width of the levee to the thickness of pervious stratum is greater than or equal to 1. The use

of Blanket Theory for cases where this assumption is violated will result in inaccurate predication of flow under the structure and excess head at the levee toe.

3. Guidelines are provided for correctly assigning boundary conditions in finite element analysis to be consistent with the individual Blanket Theory cases. These guidelines should serve as a starting point for using finite element seepage analyses for more complex analyses of seepage beneath levees.

4. The results have shown that for similar conditions, there is a very good agreement between finite element analysis and Blanket Theory solutions.

5. There is no direction provided on specifying the top blanket as an impervious vs. semipervious material, or a pervious vs. semipervious material in the blanket theory solutions outlined in the EM.

6. The correct characterization of the material type can be determined from the finite element results in that the transformation from a fully pervious to a semipervious blanket occurs at a ratio of pervious layer permeability to blanket permeability of about 2. Similarly, the results indicate that the transition between semipervious and impervious blanket behavior occurs at a ratio of pervious layer permeability to blanket permeability between 1000 and 4000. In other words, the use of the semipervious equations will produce a more accurate determination of the flow and the excess head for permeability ratios ranging from 2 to less than about 4000. Equations for impervious or for a case having no blanket can be used for ratios greater than 4000, and less than 2 respectively.

7. It is prudent to use a range of permeability and thickness values in a seepage analysis to cover the range of variation of these parameters for field cases for finite element analysis.

5.2.2. Design of Landside Seepage Berms using Finite Element Analysis

1. There is a good agreement between finite element analysis and closed-form solutions for the design of impervious and pervious berms.

2. The berm design parameters for semipervious and sand berms obtained from FEA and closed-form solutions are different.

3. The use of the closed-form solutions for semipervious berms and ultimately sand berms is unconservative if the berm crown is considered, as closed form solutions for semipervious case are based on triangular berms having no berm crown. However, finite element analysis can easily model the presence of berm crown.

4. For the case of semipervious berms, the EM solutions assume that the top stratum has the same permeability as the berm. Finite element analysis can be especially useful in designing semipervious berms because of the flexibility of assigning a different permeability to the berm than that of the top stratum.

5. The use of finite element analysis is particularly useful for sand berms, as there is no direct equation specified in the EM to calculate the width of the sand berm.

6. A plot was developed to evaluate the applicability of specifying different berm slopes based on the design parameters. This plot is also useful in selecting an economical berm slope by minimizing the berm volume.

7. Finite element analysis can be useful for the design of berms for cases where no top stratum is present, as the design equations outlined in EM 1110-2-1913 are derived only for cases having a top stratum.

8. A definition of factor of safety similar to closed-form solutions should be employed when using the finite element analysis.

9. The factor of safety against uplift should be calculated for the berm and for the combined berm and blanket if the berm is less pervious than blanket. The berm design will be controlled by the lesser of the two values.

10. Similarly, the factor of safety for the combined berm and the top stratum is more critical for cases where the permeability of the berm is greater than the permeability of the top stratum.

11. Barron's factor of safety equation for the case of a pervious berm with collector is more appropriate than the one presented in the EM, as it assumes that no head loss will occur through the pervious berm. This is a logical assumption since the berm is so pervious.

12. The guidelines provided in Chapter 3 should serve as a useful resource for practicing engineers to understand some of the limitations of the current berm design methods, as well as enhancing their ability to use finite element analysis as a tool for berm design.

5.2.3. Analysis of the London Avenue Canal Load Test

1. The London Avenue Canal load test provides a unique opportunity to check the validity of the finite element analysis, as it is very rare to have a full-scale seepage field load test available to be compared with a numerical model.

2. 3D modeling is conducted to accurately model the true geometry of the load test, as 2D modeling is unable to accurately capture the flow conditions.

3. Based on parametric analysis and statistical calibration procedures resulting in more than 1200 finite element runs, boundary conditions and other seepage model parameters are recommended for future analysis of the London Avenue Canal, and other canals having similar subsurface conditions, such as Orleans Avenue Canal and the northeast portion of the Inner Harbor Navigation Channel.

4. The 3D finite element modeling of the complex geometries and strata are helpful to afford a better understanding of the response of levees and I-walls to flood loading.

5.3. Recommendations for Future Research

During the course of the research, it became clear that additional research regarding some aspects of the study would be useful for the geotechnical practice. Some of these aspects are listed below:

1. Currently, relief well design has been handled separately from seepage. Design guidance for relief wells is provided in the USACE Engineering Manual (EM) 1110-2-1914 “Design, Construction, and Maintenance of Relief Wells” (USACE 1992). The main element for relief

well design which relies on the seepage analysis is the excess hydraulic head. If finite element analysis is to be used for underseepage analysis, then it will be convenient if it can be used for relief well design as well, and guidelines similar to blanket theory cases and landside seepage berms can be developed.

2. The factor of safety is not constant spatially around the relief wells and it is necessary to determine the most critical value in the section. It will be useful to conduct 3D finite element analysis to study the contours of the factor of safety ranging from the maximum value closer to the well and the decrease in the factor of safety as the distance from the well increases. The study of spatial variation of factors of safety should be conducted to address any ambiguity regarding a comparison of factors of safety values for relief well design with other seepage control measures like berms, which are 2D in nature.

5.4. References

USACE (1992). "Design, Construction and Maintenance of Relief Wells, Engineer Manual 1110-2-1914," U.S. Army Corps of Engineers, Washington, DC.

USACE (2000). "Design and Construction of Levees, Engineer Manual 1110-2-1913," U.S. Army Corps of Engineers, Washington, DC.

Appendix A

Levee Seepage Analysis using Blanket Theory and Finite Element Analysis

Report submitted to the U. S. Army Corps of Engineers (2013)

Authors

Thomas L. Brandon[1], Abeera Batool[1], Martha Jimenez[1] and Noah Vroman[2]

[1]*Dept. of Civil and Environmental Engineering, Patton Hall, Virginia Polytechnic Institute and State University (Virginia Tech), Blacksburg, VA 24061 USA*

[2]*U. S. Army Corps of Engineers, Vicksburg District*

Introduction

The U.S. Army Corps of Engineers Engineering Manual (EM) 1110-2-1913, "Design and Construction of Levees," dated 30 April 2000, provides closed-form (blanket theory) solutions for seepage pressures and flows beneath levees. These solutions were originally developed in the USACE Technical Manual (TM) 3-424, "Investigation of Underseepage and Its Control" (USACE 1956), and have been used by the US Army Corps of Engineers for over 50 years in various forms.

TM 3-424 developed these solutions using a compilation of existing theories and methods such as the *Method of Fragments* (Forchheimer [1](1917), Muskat[2] (1935), Pavlovsky[3] (1956) and Harr[4] (1962)), and Bennett's[5] (1946) and Barron's[6] (1948) contributions on effects of semipervious

---

[1] Forchheimer, P., Zur Grundwasserbewegung nach isothermischen Kurvenscharen. (On the movement of groundwater according to sets of isothermal curves). Sitzungsber K-K Akad der Wissenschaft 126(4):409-40 (in German), 1917

[2] Muskat , M., The flow of homogeneous fluids through porous media, McGraw-Hill, 1937

[3] Pavlovsky, N.N., "Collected works", Akad. Nauk *USSR,* Leningrad, 1956

[4] Harr, M.E., Groundwater and seepage, McGraw-Hill, New York, 1962

[5] Bennett, P.T, "The effect of blankets on the seepage through pervious foundation", *Trans. ASCE* **11**, p. 215, 1946

blankets. However, the TM did not provide derivations for these solutions, yet these solutions are still included in the EM.

The purpose of this report is two-fold. First, the original EM did not contain derivations of the different cases, and this report presents the derivations outlined in detail. Second, finite element analyses have been conducted for all cases to provide guidance for hydraulic boundary conditions when finite element analysis is used in lieu of blanket theory.

In the EM, solutions are given for nine different configurations of impervious and semi-pervious top stratum conditions. Several corrections have been made to these solutions and three additional configurations (Cases 8a, 8b and 8c) have been added.

The following cases are addressed in this report:

Case 1 - No landside and riverside top stratum

Case 2 - Impervious landside and riverside top stratum

Case 3 - Impervious riverside top stratum and no landside top stratum

Case 4 - Impervious landside top stratum and no riverside top stratum

Case 5 – Semi-pervious riverside top stratum and no landside top stratum

Case 6 – Semi-pervious landside top stratum and no riverside top stratum

Case 7a – Semi-pervious landside and riverside top stratum (top stratum extends infinitely landward of the levee)

Case 7b – Semi-pervious landside and riverside top stratum (seepage block in the pervious substratum located landward of the levee)

---

[6] Barron, R. A., "The Effect of a Slightly Pervious Top Blanket on the Performance of Relief Wells," *Proceedings of the Second International Conference on Soil Mechanics and Foundation Engineering,* Rotterdam, Netherlands, Vol 4, p 342, 1948

Case 7c - Semi-pervious landside and riverside top stratum (seepage exit in the pervious substratum located landward of the levee)

Case 8a – Semi-pervious landside and riverside top stratum (top stratum extends infinitely landward of the levee) with cutoff

Case 8b – Semi-pervious landside and riverside top stratum (seepage block in the pervious substratum located landward of the levee) with cutoff

Case 8c - Semi-pervious landside and riverside top stratum (seepage exit in the pervious substratum located landward of the levee) with cutoff

The authors benefited greatly from personal notes provided by Doug Spaulding which contained many of the derivations included in this report.

Derivation of Blanket Theory Equations Present in USACE EM 1110-2-1913

No Top Stratum (EM 1110-2-1913 – Case 1)

The following derivations are for no top stratum which is shown as Case 1 in both the USACE EM 1110-2-1913 (2000) and TM 3-424 (USACE 1956).

Case 1- No Top Stratum

Figure A-1 shows the basic geometry for Case 1. The technique to determine the flow for Case 1 was provided by M. E. Harr (1962) using the *Method of Fragments*. However, this method dates back to work done by N. N. Pavlovsky in 1935. The fundamental assumption of this method, as stated by Harr (1962), is that equipotential lines at various critical parts of the flow region can be approximated by vertical lines that divide the region into sections or *fragments*.

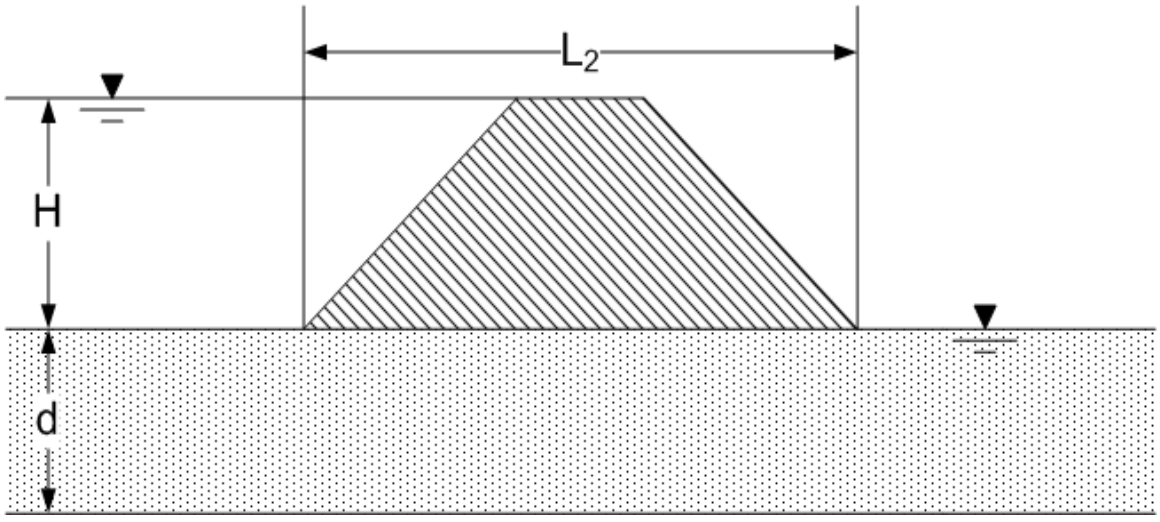

Figure A-1 Case 1 - No top stratum.

The application of the Method of Fragments is limited to the cases where the base width of the levee (L_2) is greater than the thickness of the pervious substratum, d, i.e. $L_2/d \geq 1$. This is illustrated in Figures A-2 and A-3 by showing equipotential lines determined by finite element analysis for sections having $L_2/d > 1$ and $L_2/d < 1$.

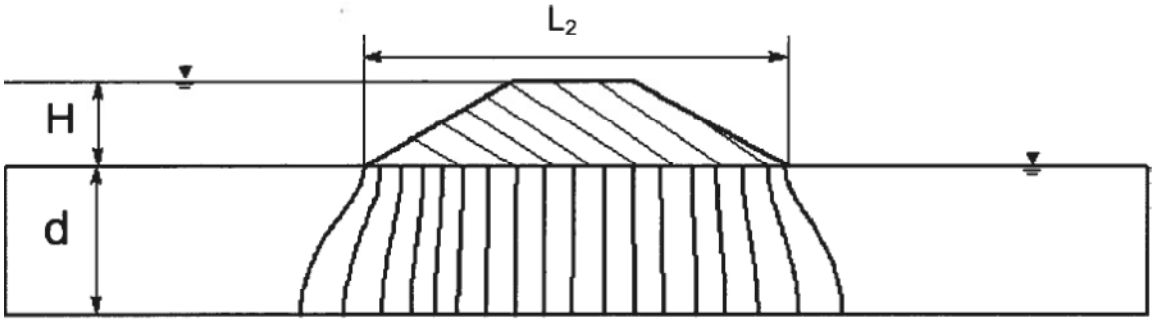

Figure A-2 Equipotential lines for levee section having $L_2/d > 1$.

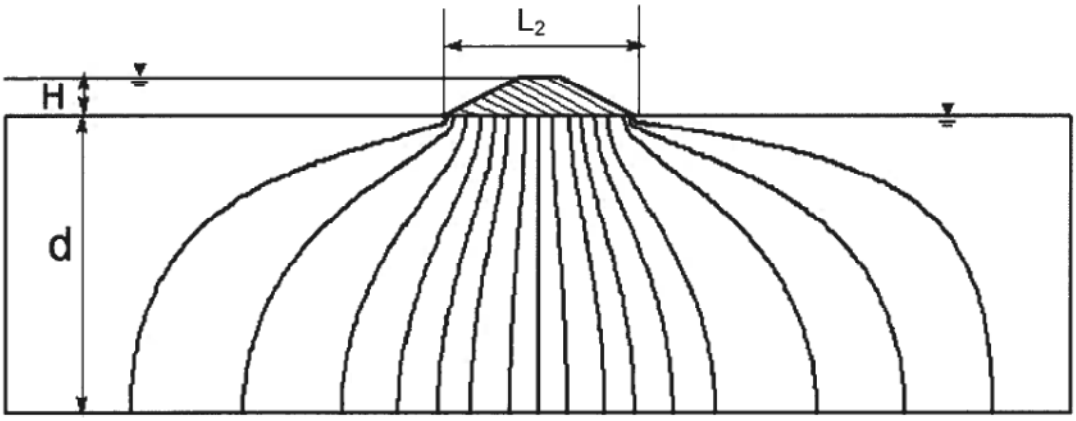

Figure A-3 Equipotential Lines for levee section having $L_2/d < 1$.

It is clear from the figures that the assumption that the equipotential lines are vertical is violated if $L_2/d < 1$ and hence the Method of Fragments and accordingly, blanket theory solutions, are limited to the case where $L_2/d \geq 1$.

The three zones or fragments for Case 1 are shown in Figure A-4.

The flow or seepage per unit length of the levee is computed using the following equation:

$$Q_s = \frac{k_f H}{\sum \Phi} \qquad \text{(A-1)}$$

Where:

k_f = Horizontal permeability of the pervious sub-stratum

H = Net head on levee

Φ = Dimensionless form factor

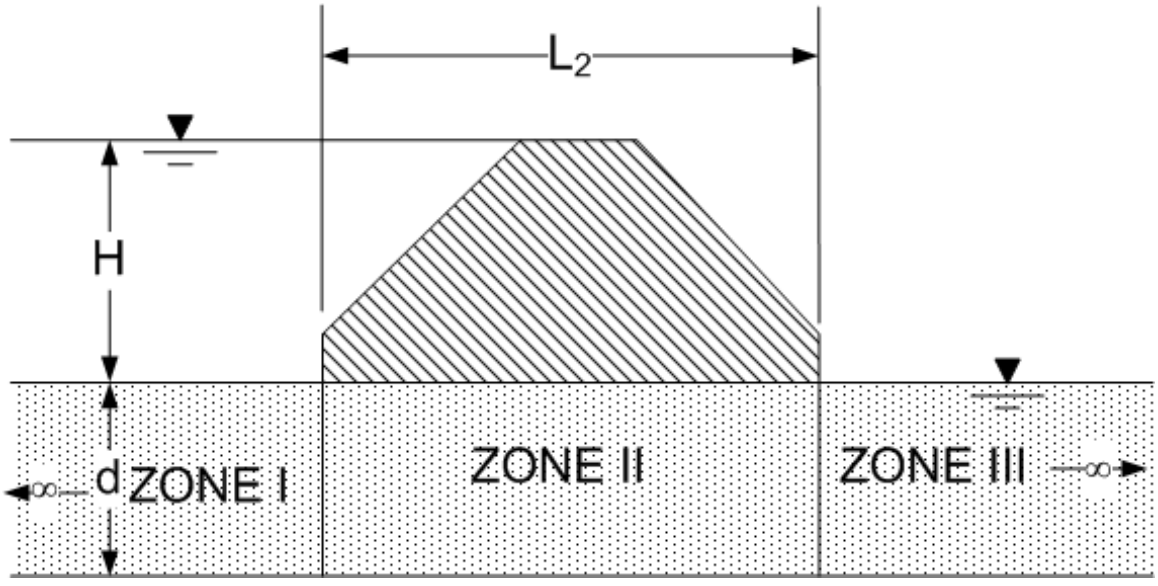

Figure A-4 Case 1 - No top stratum with three zones of fragments.

Note that the above equation is same as the general seepage equation based on Darcy's Law which is:

$$Q_s = \delta \cdot k_f \cdot H \qquad \text{(A-2)}$$

Where,

$$\delta = \frac{1}{\Sigma\Phi} = \text{Shape factor} \qquad \text{(A-3)}$$

It is important to understand the correct application of the dimensionless *form factors* in order to use the Method of Fragments. The form factors were divided into different types or categories by M. E. Harr (1962) using N. N. Pavlovasky's procedure (1935) and the related table is presented in Appendix I. This table is used as a reference to calculate form factors of various types of zones for the different cases addressed using blanket theory.

The form factor for zone II is:

$\Phi_2 = {}^{L_2}\!/_{d}$ (Type-I Fragment)

Similarly, the form factors for zones I and III are:

$\Phi_1 = \Phi_3 = 0.43$ (Special case of Type-II Fragment with s = 0)

The above-mentioned form factor is not present in the table in Appendix I. However, considerable effort was expended to trace the origin of this. It was observed that an equation similar to Case-1 of blanket theory is present in Muskat (1937) with a reference to work done by Forchheimer (1917). Some discussion related to work by Forchheimer (1917) is presented in Appendix II.

Substituting values of form factors into Equation (A-3):

$$\delta = \frac{1}{\Sigma\Phi} = \frac{1}{0.43 + L_2/d + 0.43} \qquad \text{(A-4)}$$

$$\delta = \frac{1}{0.86 + L_2/d} \qquad \text{(A-5)}$$

$$\delta = \frac{d}{0.86d + L_2} \qquad \text{(A-6)}$$

Therefore, equation (A-2) becomes:

$$Q_s = k_f H \frac{d}{(0.86d + L_2)} \qquad \text{(A-7)}$$

Where L_2 = Base width of levee

d = Thickness of pervious substratum

Equation A-7 is the same equation shown in the EM for computation of seepage beneath the levee for Case 1.

Impervious Top Stratum (EM 1110-2-1913 – Cases 2, 3, and 4)

The following derivations are for impervious top stratum conditions. An impervious top stratum on both the riverside and landside of the levee is considered in Case 2, an impervious top stratum on only the riverside is considered in Case 3 while an impervious top stratum on only the landside is considered in Case 4. These case numbers are the same in both the EM and TM.

Case 2- Impervious Top Stratum Both Riverside and Landside

The geometry for Case 2 is shown in Figure A-5 below.

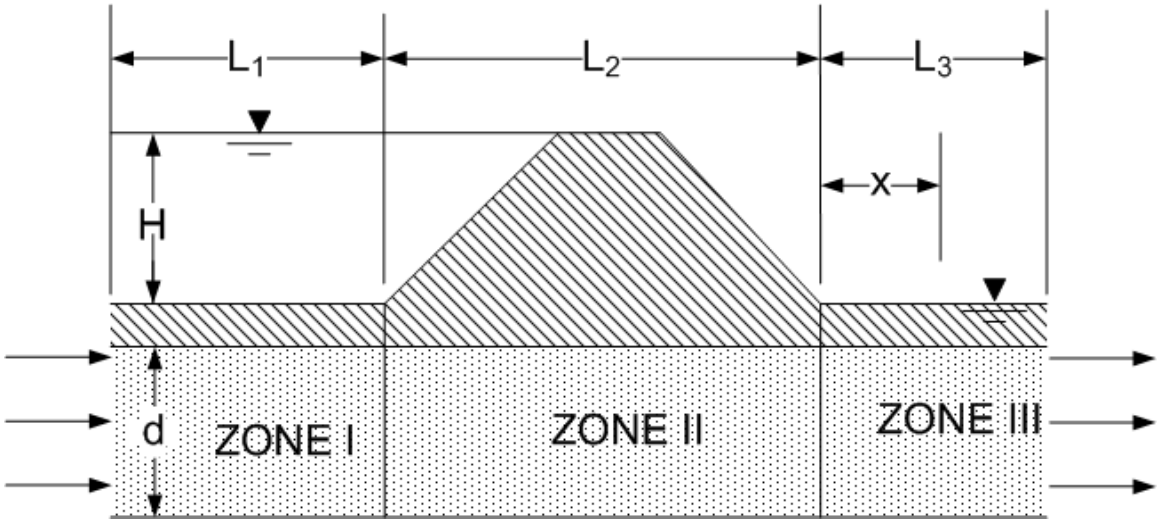

Figure A-5 Case 2 - Impervious top stratum on both riverside and landside.

Case 2 is simply a direct application of Darcy's Law for confined flow conditions, similar to flow through a pipe. However, flow can also be determined using the form factors as discussed above. The form factors for zones I, II and III are given by:

$\Phi_1 = L_1/d$ (Type-I Fragment)

$\Phi_2 = L_2/d$ (Type-I Fragment)

$\Phi_3 = L_3/d$ (Type-I Fragment)

Substituting the values of the form factors in equation (A-3):

$$\delta = \frac{1}{\Sigma\Phi} = \frac{1}{L_1/d + L_2/d + L_3/d} \qquad \text{(A-8)}$$

$$\delta = \frac{d}{L_1 + L_2 + L_3} \qquad \text{(A-9)}$$

Equation (2) becomes:

$$Q_s = k_f H \frac{d}{(L_1 + L_2 + L_3)} \qquad \text{(A-10)}$$

Where L_1 = Distance from river to riverside levee toe

L_3 = Length of foundation and top stratum beyond landside levee toe

Similarly, the head at the toe of the levee is found by considering the pressure diagram (Piezometric Grade Line or PGL) as shown in Figure A-6. The flow in the pervious layer is assumed to be solely horizontal; therefore the head loss is linear with horizontal distance.

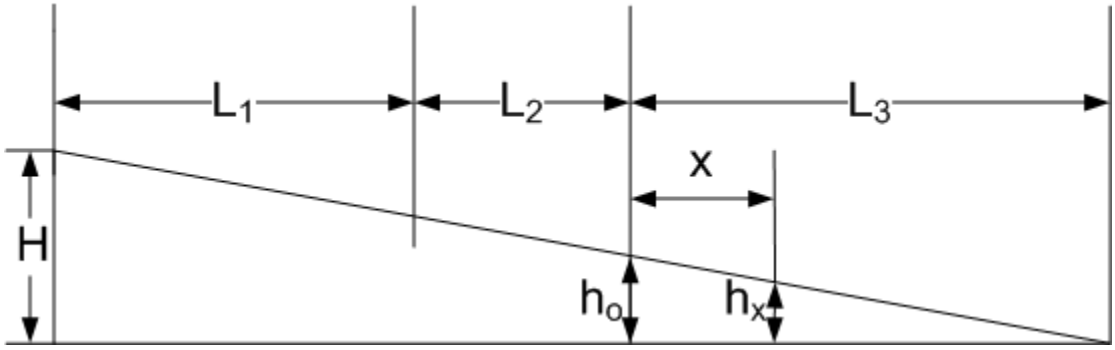

Figure A- 6 Pressure diagram for confined flow condition.

The pressure head becomes zero at a distance L_3 from the landside toe of the levee. Using the concept of similar triangles:

$$\frac{h_o}{H} = \frac{L_3}{L_1 + L_2 + L_3} \qquad \text{(A-11)}$$

$$h_o = H\left(\frac{L_3}{L_1 + L_2 + L_3}\right) \qquad \text{(A-12)}$$

Where h_o = Excess head at landside levee toe[7].

Similarly, the head at any distance x from the toe of the levee is determined by

$$h_x = h_o\left(\frac{L_3 - x}{L_3}\right) \quad \text{For } x \le L_3 \qquad \text{(A-13)}$$

$$h_x = 0 \qquad \text{For } x \ge L_3 \qquad \text{(A-14)}$$

Case 3- Impervious Riverside Top Stratum and No Landside Top Stratum

The geometry for Case 3 is shown in Figure A-7 below.

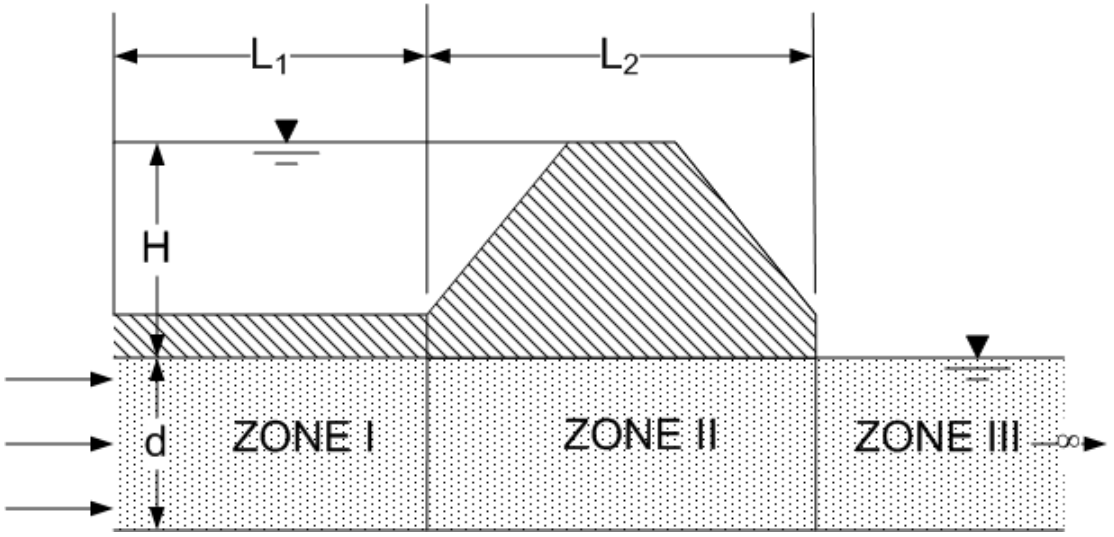

[7] This value is defined incorrectly for several cases presented in EM 1110-2-1913.

Figure A-7 Case 3 - Impervious riverside top stratum and no landside top stratum.

The total head loss (H) for Case 3 shown in Figure B-5 of Appendix B of EM 1110-2-1913 is incorrect. As it is shown on the figure in the EM, the head loss would be dependent on the thickness of the blanket. The corrected value of H is shown in Figure A-7. The value of H is used to determine the seepage underneath the levee and should be the difference between riverside and landside water level, or the total head loss from riverside to landside.

The flow can be determined by using the form factors as discussed previously. The form factors for zones I, II and III are given by:

$\Phi_1 = L_1/d$ (Type-I Fragment)

$\Phi_2 = L_2/d$ (Type-I Fragment)

$\Phi_3 = 0.43$ (Special case of Type-II Fragment with s = 0)

Substituting the values of the form factors in equation (A-3):

$$\delta = \frac{1}{\Sigma\Phi} = \frac{1}{L_1/d + L_2/d + 0.43} \qquad \text{(A-15)}$$

$$\delta = \frac{d}{L_1 + L_2 + 0.43d} \qquad \text{(A-16)}$$

Equation (A-2) becomes:

$$Q_s = k_f H \frac{d}{(L_1 + L_2 + 0.43d)} \qquad \text{(A-17)}$$

Case 4- Impervious Landside Top Stratum and No Riverside Top Stratum

The geometry for Case 4 is shown in Figure A-8. The value of H shown in Figure AII-5 of Appendix B of EM-1110-2-1913 for Case 4 is incorrect and *is not* the difference between riverside and landside water level. The corrected H is shown in the figure below.

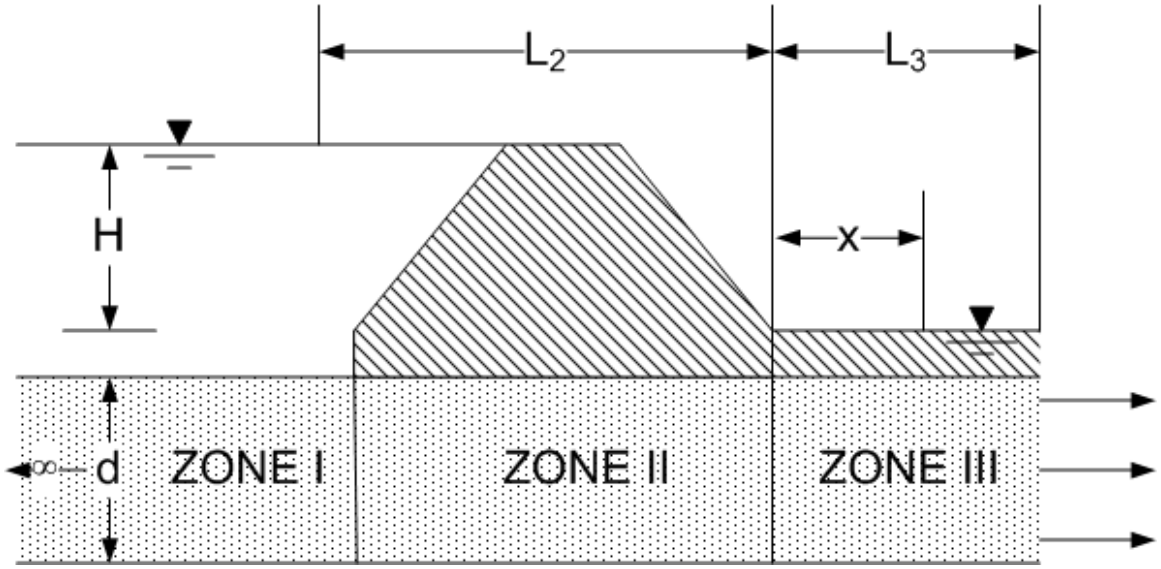

Figure A-8 Case 4 - Impervious landside top stratum and no riverside top stratum.

The flow can be determined by using the form factors as discussed previously. The form factors for zones I, II and III are:

$\Phi_1 = 0.43$ (Special case of Type-II Fragment with s = 0)

$\Phi_2 = L_2/d$ (Type-I Fragment)

$\Phi_3 = L_3/d$ (Type-I Fragment)

Substituting the values of form factors in equation (A-3):

$$\delta = \frac{1}{\Sigma\Phi} = \frac{1}{0.43 + L_2/d + L_3/d} \qquad \text{(A-18)}$$

$$\delta = \frac{d}{0.43d + L_2 + L_3} \qquad \text{(A-19)}$$

Equation (A-2) becomes:

$$Q_s = k_f H \frac{d}{(0.43d + L_2 + L_3)} \qquad \text{(A-20)}$$

Similarly, the head at the toe of the levee is found using the Method of Fragments. The head loss in m^{th} fragment is calculated as follows:

$$h_m = \frac{H\Phi_m}{\sum \Phi}$$

Where,

Φ_m = Form factor for the m^{th} zone

$\Sigma\Phi$ = Summation of form factors for all the fragments (zones I, II and III in this case).

So, head at the toe of the structure is determined as follows:

$$h_o = H - (h_1 + h_2)$$

Or simply,

$$h_o = h_3 = \frac{H\Phi_3}{\sum \Phi} \qquad \text{(A-21)}$$

So, the form factors for zones I, II and III as described above are given by

$\Phi_1 = 0.43$

$\Phi_2 = L_2/d$

$\Phi_3 = L_3/d$

Substituting the values of form factors into equation (A-21):

$$h_o = \frac{H\Phi_3}{\sum \Phi} = \frac{H(L_3/d)}{0.43 + (L_2/d) + (L_3/d)}$$

$$\frac{h_o}{H} = \frac{L_3}{0.43d + L_2 + L_3}$$

$$h_o = H\left(\frac{L_3}{0.43d + L_2 + L_3}\right) \qquad \text{(A-22)}$$

Similarly, the head at any distance x from the landside toe of the levee is determined by:

$$h_x = h_o\left(\frac{L_3 - x}{L_3}\right) \qquad \text{(A-23)}$$

Semipervious Top Stratum (EM 1110-2-1913 – Cases 5, 6, and 7, and New Case 8)

The following derivations are for semipervious top stratum conditions. A semipervious top stratum on only the riverside is considered in Case 5, a semipervious top stratum on only the landside represents Case 6; a semipervious top stratum on both the riverside and landside is considered in Case 7 and an additional configuration of Case 7 with a sheet pile at the center of the levee is considered in Case 8. Cases 7a, 7b, and 7c are shown in the TM as Cases 5, 6, and 7 respectively. Case 8 is an added configuration not shown in the EM.

Case 5- Semipervious Riverside Top Stratum and No Landside Top Stratum

The geometry for Case 5 is shown in Figure A-9. Again, the value of H shown in Figure B-6 of Appendix B of EM-1110-2-1913 for Case 5 is incorrect and is a function of the thickness of blanket on the riverward side. As H is shown on the figure in the EM, it is not the difference between landside and riverside water levels. The corrected H for Case 5 is shown in Figure A-9.

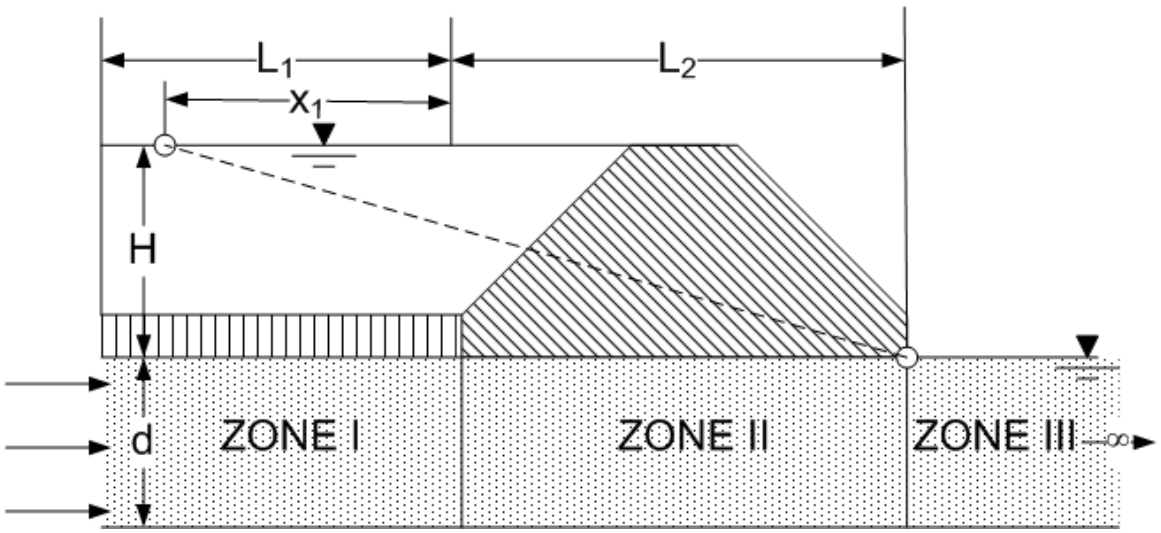

Figure A-9 Case 5 - Semipervious riverside top stratum and no landside top stratum.

The difference between Case 3 and 5 is that there was an impervious top stratum on the riverside in Case 3, while in Case 5, the top stratum is semipervious. Therefore, the distance from the river to the riverside levee toe (L_1) will no longer be equal to the effective seepage entry distance (x_1).

To simplify the calculations, the semipervious top stratum will be replaced by an equivalent impervious top stratum such that the seepage beneath the levee with be the same. This is accomplished by computing x_1, where x_1 is actually the equivalent length of an equivalent impervious top stratum for a semipervious stratum of length L_1 on riverward side. Similarly, x_3 is the equivalent length of an impervious top stratum for a semipervious stratum of length L_3 on the landward side. So, x_1 and x_3 were equal to L_1 and L_3 for impervious cases, but the flow in the pervious layer will no longer be completely horizontal for cases having a semipervious top stratum, as there will also be some vertical flow occurring through the top stratum. Therefore, x_1 and x_3 must be calculated separately. This becomes very useful for applying Method of Fragments to calculate flow as well as determining head at the toe of the levee for cases having

semipervious blankets (Cases 5 through 8). This is because confined flow conditions will only occur underneath the levee (since the levee is assumed to be completely impervious) and cannot be used elsewhere for these cases without assuming an equivalent impervious blanket.

The value of x_1 is determined from the following equations depending upon the type of seepage entrance. The complete derivations of these equations are shown in Appendix AII. Two different seepage entrance types are given below.

1. If the distance to the river from the riverside levee toe L_1 is known and no riverside borrow pits or seepage block exists, x_1 is estimated as follows:

$$x_1 = \frac{\tanh(cL_1)}{c} \qquad \text{(A-24)}$$

With c defined as:

$$c = \sqrt{\frac{k_{br}}{k_f z_{br} d}} \qquad \text{(A-25)}$$

Where k_{br} = Transformed vertical permeability of riverside top stratum

k_f = Horizontal permeability of pervious substratum

d = Thickness of pervious substratum

z_{br} = Transformed thickness of riverside top stratum

2. If a seepage block exists between the riverside levee toe and the river that prevents any seepage entrance into pervious foundation beyond the seepage block, x_1 can be estimated from the following equation:

$$x_1 = \frac{1}{c\tanh(cL_1)} \qquad \text{(A-26)}$$

The next step after determining x_1 is to calculate flow for Case 5. The same procedure as described for the first four cases will be used. The only difference is that the form factor will be defined in terms of the distance to the effective seepage entrance (as calculated above) as opposed to L_1.

The form factors for zones I, II and III are given by

$\Phi_1 = x_1/d$ (Type-I Fragment)

$\Phi_2 = L_2/d$ (Type-I Fragment)

$\Phi_3 = 0.43$ (Special case of Type-II Fragment with s = 0)

Substituting the values of the form factors into equation (A-3):

$$\delta = \frac{1}{\Sigma\Phi} = \frac{1}{x_1/d + L_2/d + 0.43} \qquad \text{(A-27)}$$

$$\delta = \frac{d}{x_1 + L_2 + 0.43d} \qquad \text{(A-28)}$$

Equation (2) becomes:

$$Q_s = k_f H \frac{d}{(x_1 + L_2 + 0.43d)} \qquad \text{(A-29)}$$

Case 6- Semipervious Landside Top Stratum and no Riverside Top Stratum

The geometry for Case 6 is shown in Figure A- 10 below. Again, the value of H shown for Case 6 in Figure B-6 of Appendix B of EM-1110-2-1913 is incorrect and *is not* the difference between landside and riverside water levels. If the water level is considered as shown in EM, then it becomes a *free surface problem,* since the phreatic surface would be present within the protected

side top stratum. This should not be the case if blanket theory is to be used. The error regarding the net head on levee is corrected in figure below.

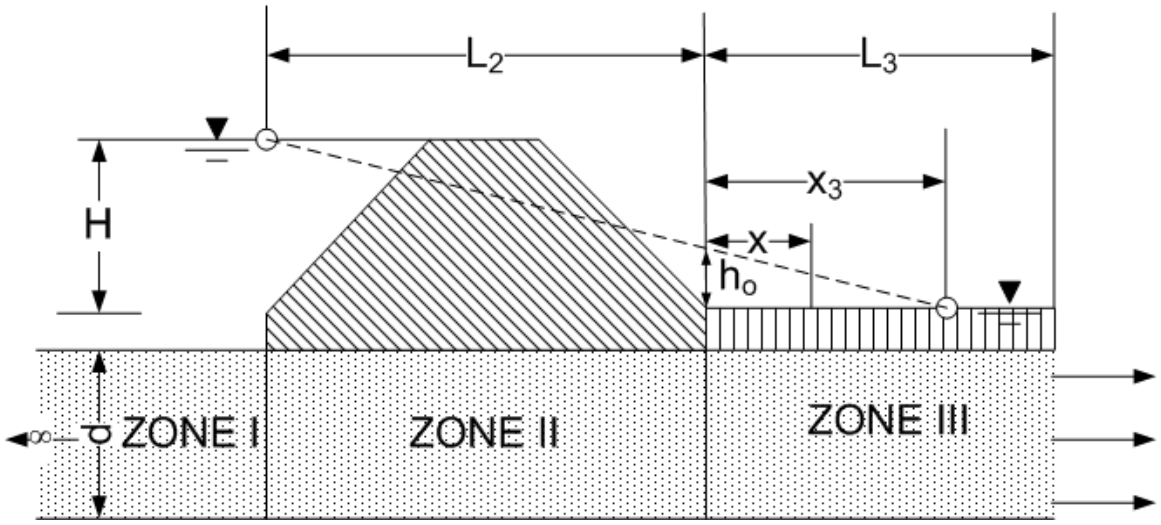

Figure A-10 Case 6 - Semipervious landside top stratum and no riverside top stratum.

Case 6 is similar to Case 4, except that the top stratum is impervious in Case 4 and semipervious in Case 6. Hence, effective seepage exit (x_3) will no longer be equal to the length of the top stratum beyond the levee toe (L_3) as explained in Case 5, and must be calculated separately.

The value of the equivalent length (x_3) of the impervious blanket is determined from the following equations, depending upon the type of seepage exit. The complete derivations of these equations are shown in Case 7 section of this report.

1. For L_3= infinite distance

$$x_3 = 1/c = \sqrt{\frac{k_f z_{bl} d}{k_{bl}}} \qquad \text{(A-30)}$$

Where,

$$c = \sqrt{\frac{k_{bl}}{k_f z_{bl} d}} \qquad \text{(A-31)}$$

Where k_{bl} = Transformed vertical permeability of the landside top stratum

k_f = Horizontal permeability of the pervious substratum

d = Thickness of the pervious substratum

z_{bl}= Transformed thickness of the landside top stratum

2. For L_3 = finite distance to a seepage block

$$x_3 = \frac{1}{c \tanh(cL_3)} \qquad \text{(A-32)}$$

Where c is as defined above.

3. For L_3= finite distance to an open seepage exit

$$x_3 = \frac{\tanh(cL_3)}{c} \qquad \text{(A-33)}$$

Calculating the flow for Case 6 is similar to that described for the impervious blanket cases. However, the form factors will be defined in terms of the distance of the effective seepage exit x_3 (as calculated above) as opposed to L_3.

The form factors for zones I, II and III are given by:

Φ_1 = 0.43 (Special case of Type-II Fragment with s = 0)

$\Phi_2 = L_2/d$ (Type-I Fragment)

$\Phi_3 = x_3/d$ (Type-I Fragment

Substituting the values of form factors in equation (A-3):

$$\delta = \frac{1}{\Sigma\Phi} = \frac{1}{0.43 + L_2/d + x_3/d} \qquad \text{(A-34)}$$

$$\delta = \frac{d}{0.43d + L_2 + x_3} \qquad \text{(A-35)}$$

Equation (A-2) becomes:

$$Q_s = k_f H \frac{d}{(0.43d + L_2 + x_3)} \qquad \text{(A-36)}$$

Similarly, the excess head at the toe of the levee is found using the Method of Fragments in a similar manner as explained in Case 4, but with L_3 being replaced by x_3 :

$$\frac{h_o}{H} = \frac{x_3}{0.43d + L_2 + x_3} \qquad \text{(A-37)}$$

$$h_o = H\left(\frac{x_3}{0.43d + L_2 + x_3}\right) \qquad \text{(A-38)}$$

The head at any distance x from the toe of the levee is incorrectly shown in the EM 1110-2-1913 by:

$$h_x = h_o\left(\frac{x_3 - x}{x_3}\right)$$

However, this is not correct as the head loss will no longer be linear because of semipervious (compared to impervious) blanket on the landside. The approach of pro-rating the heads as done above will not be useful in this case to determine the head at a distance x. For Case 6, the semipervious blanket of length L_3 can be taken as an impervious blanket of equivalent length x_3. This can be a useful approach to determine the head at toe of the levee as well as under the levee

because flow will be confined in this case and linear Piezometric Grade Line (PGL) can be obtained. However, this cannot be used to determine the head at any distance x from the toe of the levee as the linear PGL plotted for the equivalent impervious top stratum will be different than actual PGL for semipervious stratum beyond the levee toe (which will be non-linear because of flow occurring vertically through the semipervious top stratum).

The head at any distance x can be calculated in a similar manner as will be shown for Case 7 by considering the landward side of the levee, and the complete derivation of these equations will be discussed then. However, if we assume that an open seepage exit is present on the landside for Case 6, as it appears to be shown in Figure B-6 of Appendix B of EM-1110-2-1913, then this becomes similar to Case 7c, and then the head at any distance x is determined by:

$$h_x = \frac{h_o \sinh\left(c\left(L_3 - x\right)\right)}{\sinh\left(cL_3\right)} \qquad \text{(A-39)}$$

Case 7- Semipervious Top Strata both Riverside and Landside

The basic geometry for Case 7 is shown in Figure A-11.

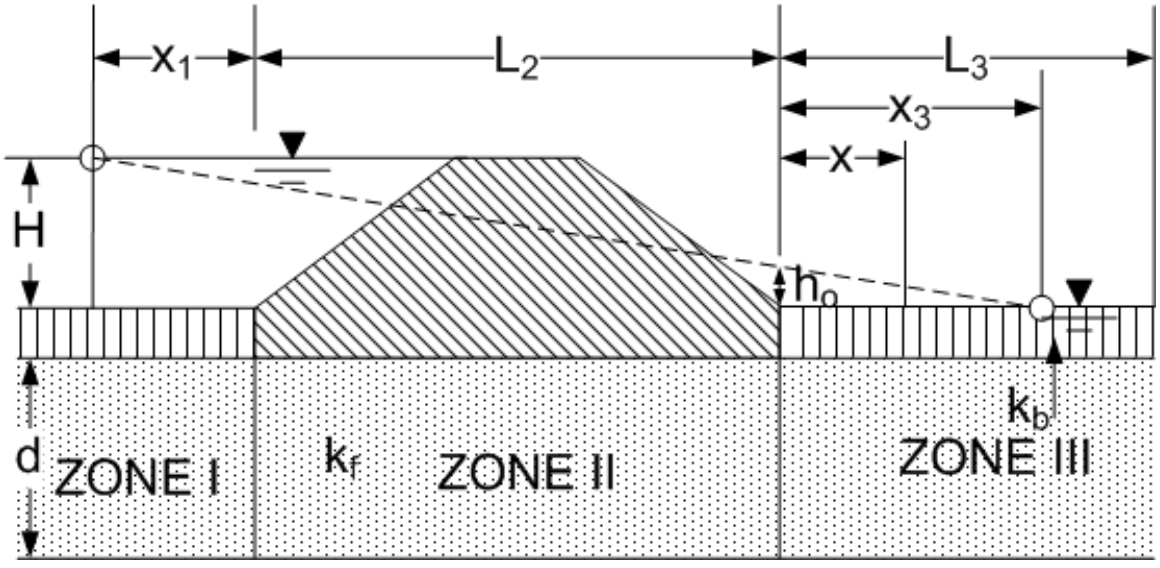

Figure A-11 Case 7 - Semipervious top strata both riverside and landside.

The same procedures as described earlier in this report will be used to determine the quantity of underseepage for Case 7. As the semipervious strata is present on both landward and riverward sides, L_1 and L_3 will be replaced by x_1 and x_3 respectively to calculate the form factors.

Therefore, the form factors for zones I, II and III are given by:

$\Phi_1 = x_1/d$ (Type-I Fragment)

$\Phi_2 = L_2/d$ (Type-I Fragment)

$\Phi_3 = x_3/d$ (Type-I Fragment)

Putting the values of the form factors in equation (A-3):

$$\delta = \frac{1}{\Sigma\Phi} = \frac{1}{x_1/d + L_2/d + x_3/d} \qquad \text{(A-40)}$$

$$\delta = \frac{d}{x_1 + L_2 + x_3} \qquad \text{(A-41)}$$

Hence, equation (A-2) becomes:

$$Q_s = k_f H \frac{d}{(x_1 + L_2 + x_3)} \qquad \text{(A-42)}$$

Similarly, the head at the toe of the levee is found using the Method of Fragments and from similar triangles as follows:

$$\frac{h_o}{H} = \frac{x_3}{x_1 + L_2 + x_3} \qquad \text{(A-43)}$$

$$h_o = H\left(\frac{x_3}{x_1 + L_2 + x_3}\right) \qquad \text{(A-44)}$$

There are three different subcases for Case 7 depending upon the boundary conditions on landward side. The value of x_3 is determined for each case depending upon the type of seepage exit.

Case 7a ($L_3 = \infty$)

Figure A-12 shows the geometry for Case 7a. This subcase is assumed to have an infinite horizontal dimension (L_3) on the landward side.

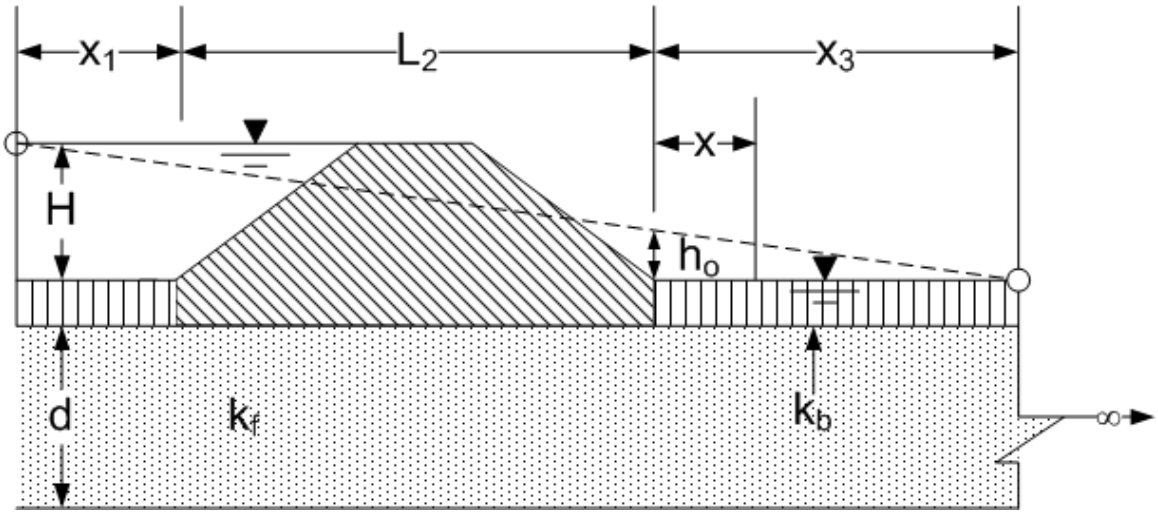

Figure A-12 Case 7a - Semipervious top strata both riverside and landside with L_3 as infinite.

The basic two assumptions made for this case are:

1. The flow through the top stratum is vertical, and the permeability of the top stratum (k_b) is the vertical component of the permeability. This is considered to occur when the contrast in permeabilities between the top stratum and substratum is about an order of magnitude or greater (Bennett 1946).

2. The flow through the pervious substratum is horizontal. This is considered to occur when the contrast in permeabilities between the top stratum and substratum is about an order of magnitude or greater (Bennett 1946).

Consider the landward side of the levee, as shown in Figure A-13, to illustrate the derivation.

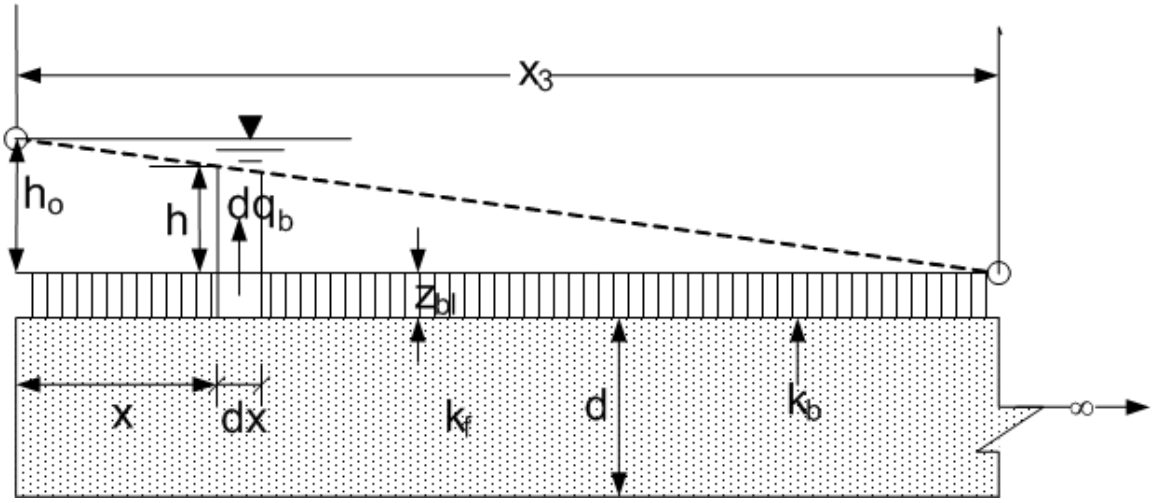

Figure A-13 Landward side of the levee.

From Darcy's Law, the vertical flow through the top stratum will be:

$$q = kiA$$

$$dq_b = k_{bl}\frac{h}{z_{bl}}dx$$

$$\frac{dq_b}{dx} = k_{bl}\frac{h}{z_{bl}} \qquad \text{(A-45)}$$

Similarly, the horizontal flow through the pervious substratum is:

$$q_f = k_f d\frac{dh}{dx}$$

$$\frac{dq_f}{dx} = k_f d \frac{d^2h}{dx^2} \qquad \text{(A-46)}$$

The continuity equation for steady state will be:

$$\frac{dq_f}{dx} + \frac{dq_b}{dx} = 0 \qquad \text{(A-47)}$$

Substituting the values of $\frac{dq_f}{dx}$ and $\frac{dq_b}{dx}$ from equations (47) and (45) respectively:

$$k_f d \frac{d^2h}{dx^2} - k_{bl} \frac{h}{z_{bl}} = 0$$

Dividing $k_f d$ on both sides of the equation:

$$\frac{d^2h}{dx^2} - \frac{k_{bl}}{k_f d z_{bl}} h = 0$$

$$\frac{d^2h}{dx^2} - c^2 h = 0 \qquad \text{(A-48)}$$

Where, $c = \sqrt{\frac{k_{bl}}{k_f z_{bl} d}}$

The differential equation is solved as shown below.

Let $p = \frac{dh}{dx}$ and the auxiliary equation is:

$$p^2 - c^2 = 0 \qquad \left(p^1 = \frac{dh}{dx}, p^2 = \frac{d^2h}{dx^2}, p^0 = h = 1 \right)$$

The roots of the above equation are *c* and -*c*.

The solution of the above differential equation is:

$$h = me^{cx} + ne^{-cx} \qquad \text{(A-49)}$$

Where, m and n are constants.

The boundary conditions for this case are:

For $x = 0, h = h_o$

For $x = \infty, h = 0$

Putting the first condition in equation (A-49)

$$h_o = m + n$$

Similarly, putting the second condition in equation (A-49)

$$0 = m \times \infty + n \times 0$$

From the above equation, it is clear that m must be zero to have a finite value.

So,

$$m = 0$$
$$n = h_o$$

Therefore, the equation for head becomes:

$$h = me^{cx} + ne^{-cx}$$

$$h_x = h_o e^{-cx} \qquad \text{(A-50)}$$

Where, $c = \sqrt{\dfrac{k_{bl}}{k_f z_{bl} d}}$

The distance from the landside levee toe to the effective seepage exit (x_3) can be determined by extrapolating the hydraulic grade line at $x = 0$ to the point where we have ground surface or tail water as shown in Figure A-13. Again note that the linear PGL is plotted to determine x_3 as this

distance is considered to be equivalent length of impervious blanket and hence the linear grade line can be obtained.

Now,

$$\frac{dh}{dx} = \frac{-h_o}{x_3} \qquad \text{(A-51)}$$

Also, we know that,

$$h = h_o e^{-cx}$$

So,

When $x = 0$,

$$\frac{dh}{dx} = -h_o c \qquad \text{(A-52)}$$

Equating equations (A-51) and (A-52), we get

$$\frac{-h_o}{x_3} = -h_o c$$

$$x_3 = \frac{1}{c} \qquad \text{(A-53)}$$

As $c = \sqrt{\frac{k_{bl}}{k_f z_{bl} d}}$, so

$$x_3 = \sqrt{\frac{k_f z_{bl} d}{k_{bl}}} \qquad \text{(A-54)}$$

Case 7b (L_3 = finite distance to seepage block)

Figure A-14 shows the geometry for Case 7b. For this case, a seepage block (impervious boundary) is located at a distance L_3 from the toe of the levee.

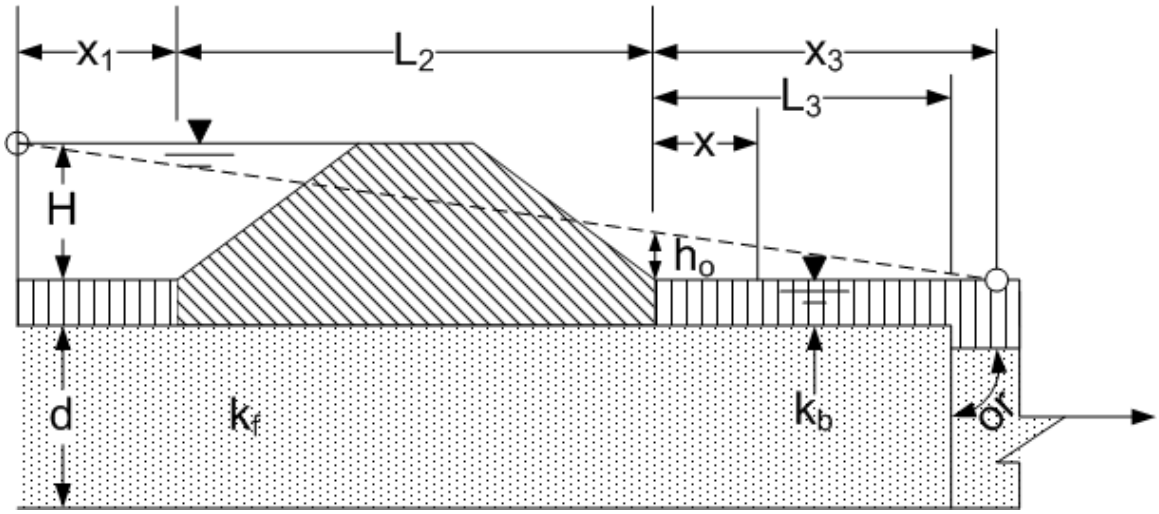

Figure A-14 Case 7b - Semipervious top strata both riverside and landside with L_3 as finite distance to seepage block.

The solution of the differential equation, as developed in Case 7a, is:

$$h = me^{cx} + ne^{-cx}$$

where, m and n are constants.

The boundary conditions for Case 7-b are:

For $x = 0, h = h_o$

For $x = L_3, \frac{dh}{dx} = 0$

Putting the first condition in equation (A-49)

$$h_o = m + n$$

$$m = h_o - n$$

Similarly, putting the second condition in equation (A-49)

$$\frac{dh}{dx} = mce^{cx} - nce^{-cx}$$

$$0 = mce^{cL_3} - nce^{-cL_3}$$

Substituting in the value of m from first boundary condition:

$$0 = (h_o - n)ce^{cL_3} - nce^{-cL_3}$$

$$0 = h_o ce^{cL_3} - nce^{cL_3} - nce^{-cL_3}$$

$$0 = h_o ce^{cL3} - nc(e^{cL_3} + e^{-cL_3})$$

$$h_o ce^{cL_3} = nc(e^{cL_3} + e^{-cL_3})$$

$$h_o e^{cL_3} = n(e^{cL_3} + e^{-cL_3})$$

Multiplying by ½ on both sides

$$\tfrac{1}{2} h_o e^{cL_3} = \tfrac{1}{2} n(e^{cL_3} + e^{-cL_3})$$

As we know that,

$$\cosh x = \frac{e^x + e^{-x}}{2}$$

So,

$$n\cosh(cL_3) = \tfrac{1}{2} h_o e^{cL_3}$$

$$n = \frac{h_o e^{cL_3}}{2\cosh(cL_3)} \qquad \text{(A-55)}$$

Putting the values of m and n in equation (A-49)

$$h = \left(h_o - \frac{h_o e^{cL_3}}{2\cosh(cL_3)} \right) e^{cx} + \left(\frac{h_o e^{cL_3}}{2\cosh(cL_3)} \right) e^{-cx}$$

$$h = h_0 e^{cx} - \left(\frac{h_o e^{cL_3}}{2\cosh(cL_3)} \right) e^{cx} + \left(\frac{h_o e^{cL_3}}{2\cosh(cL_3)} \right) e^{-cx}$$

$$h = \frac{h_o}{2\cosh(cL_3)} \left[e^{cx} 2\cosh(cL_3) - e^{cL_3} e^{cx} + e^{cL_3} e^{-cx} \right] \qquad \text{(A-56)}$$

Now,

$$e^{cx} 2\cosh(cL_3) = e^{cx} \left(e^{cL_3} + e^{-cL_3} \right) \qquad \text{Since } \cosh x = \frac{e^x + e^{-x}}{2}$$

$$e^{cx} 2\cosh(cL_3) = e^{cx+cL_3} + e^{cx-cL_3}$$

Putting the value of the above expression in equation (56)

$$h = \frac{h_o}{2\cosh(cL_3)} \left[e^{cx+cL_3} + e^{cx-cL_3} - e^{cx+cL_3} + e^{-cx+cL_3} \right]$$

$$h = \frac{h_o}{\cosh(cL_3)} \frac{\left[e^{-c(-x+L_3)} + e^{c(-x+L_3)} \right]}{2}$$

$$h_x = \frac{h_o \cosh(c(L_3 - x))}{\cosh(cL_3)} \qquad \text{(A-57)}$$

For $x = L_3$

$$h_x = \frac{h_o}{\cosh(cL_3)} \quad \text{since cosh(0) = 1} \qquad \text{(A-58)}$$

The distance from the landside levee toe to the effective seepage exit (x_3) can be determined in a same manner as done for Case 7a.

So,

$$\frac{dh}{dx} = \frac{-h_o}{x_3}$$

Also, we know that,

$$h = \frac{h_o \cosh(c(L_3 - x))}{\cosh(cL_3)}$$

$$\frac{dh}{dx} = \frac{h_o}{\cosh(cL_3)} \frac{d}{dx}(\cosh(c(L_3 - x))) \qquad \text{(A-59)}$$

Now,

$$\cosh(c(L_3 - x)) = \frac{e^{cL_3} e^{-cx} + e^{-cL_3} e^{cx}}{2}$$

$$\frac{d}{dx}\cosh(c(L_3 - x)) = \frac{e^{cL_3}(-c)e^{-cx} + e^{-cL_3}(c)e^{cx}}{2}$$

$$\frac{d}{dx}\cosh(c(L_3 - x)) = \frac{-c}{2}\left[e^{c(-x+L_3)} - e^{-c(-x+L_3)}\right]$$

$$\frac{d}{dx}\cosh(c(L_3 - x)) = -c\sinh c(L_3 - x) \qquad \sinh x = \frac{e^x - e^{-x}}{2}$$

For $x = 0$,

$$\frac{d}{dx}\cosh(c(L_3 - x)) = -c\sinh cL_3$$

Now, putting the value of above expression in equation (59)

$$\frac{dh}{dx} = \frac{h_o}{\cosh(cL_3)} - c\sinh cL_3$$

$$\frac{dh}{dx} = -ch_o \tanh cL_3 \qquad \text{(A-60)}$$

As we know that,

$$\frac{dh}{dx} = \frac{-h_o}{x_3}$$

Putting the value of $\frac{dh}{dx}$ as derived in equation (A-60).

$$-ch_o \tanh cL_3 = \frac{-h_o}{x_3}$$

$$x_3 = \frac{1}{c\tanh(cL_3)} \qquad \text{(A-61)}$$

Where, $c = \sqrt{\frac{k_{bl}}{k_f z_{bl} d}}$

Case 7c (L_3 = finite distance to an open seepage exit)

Figure A-15 shows the geometry for Case 7c. In this case, an open seepage exit is located at a distance L_3 from the landside levee toe.

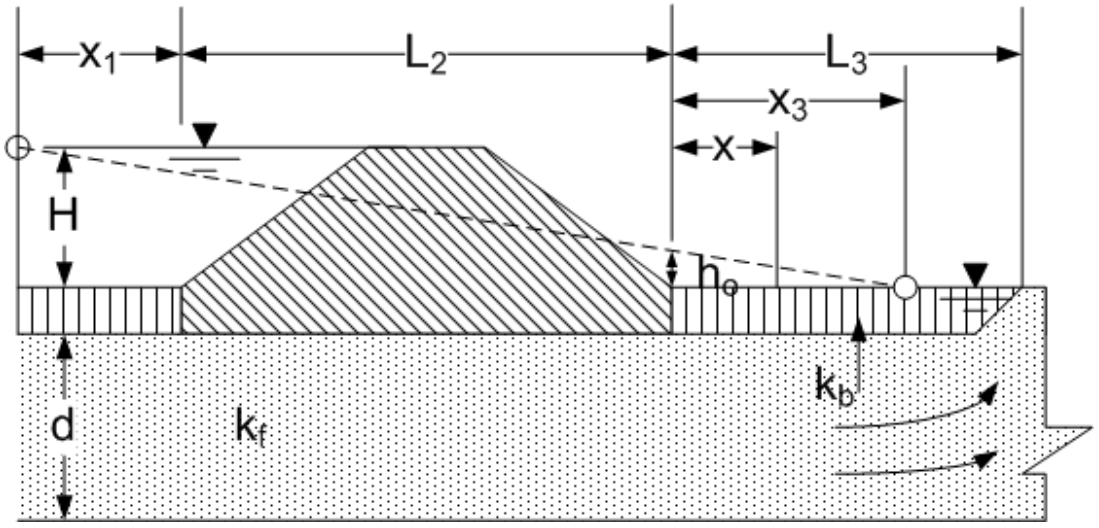

Figure A-15 Case 7c - Semipervious top strata both riverside and landside with L_3 as a finite distance to an open seepage exit.

The solution of the differential equation as developed in Case 7a is $h = me^{cx} + ne^{-cx}$ where, m and n are constants.

The boundary conditions for Case 7c are as follows:

For $x = 0, h = h_o$

For $x = L_3, h = 0$

Putting the first condition in equation (A-49)

$$h_o = m + n$$

$$m = h_o - n$$

Similarly, putting the second condition in equation (A-49)

$$h = me^{cx} + ne^{-cx}$$

$$0 = me^{cL_3} + ne^{-cL_3}$$

Putting the value of m in the above equation

$$0 = (h_o - n)e^{cL_3} + ne^{-cL_3}$$

$$0 = h_o e^{cL_3} - ne^{cL_3} + ne^{-cL_3}$$

$$0 = h_o e^{cL_3} - n\left(e^{cL_3} - e^{-cL_3}\right)$$

$$h_o e^{cL_3} = n\left(e^{cL_3} - e^{-cL_3}\right)$$

$$n = \frac{h_o e^{cL_3}}{\left(e^{cL_3} - e^{-cL_3}\right)}$$

As, $\sinh x = \dfrac{e^x - e^{-x}}{2}$

$$n = \frac{h_o e^{cL_3}}{2\sinh(cL_3)} \qquad \text{(A-62)}$$

Putting the values of m and n in equation (A-49)

$$h = \left(h_o - \frac{h_o e^{cL_3}}{2\sinh(cL_3)} \right) e^{cx} + \frac{h_o e^{cL_3}}{2\sinh(cL_3)} e^{-cx}$$

$$h = \frac{h_o}{2\sinh(cL_3)} \left(2e^{cx} \sinh(cL_3) - e^{cL_3} e^{cx} + e^{cL_3} e^{-cx} \right) \qquad \text{(A-63)}$$

Now,

$$e^{cx} 2\sinh(cL_3) = e^{cx} \left(e^{cL_3} - e^{-cL_3} \right)$$

Since, $\sinh x = \frac{e^x - e^{-x}}{2}$

$$e^{cx} 2\sinh(cL_3) = e^{cx+cL_3} - e^{cx-cL_3}$$

Putting the value of the above expression in equation (A-63)

$$h = \frac{h_o}{2\sinh(cL_3)} \left(e^{cx+cL_3} - e^{cx-cL_3} - e^{cL_3+cx} + e^{cL_3-cx} \right)$$

$$h = \frac{h_o}{\sinh(cL_3)} \frac{\left(e^{c(L_3-x)} - e^{-c(L_3-x)} \right)}{2}$$

$$h_x = \frac{h_o \sinh(c(L_3 - x))}{\sinh(cL_3)} \qquad \text{(A-64)}$$

The distance from the landside levee toe to the effective seepage exit (x_3) can be determined in a same manner as done for Case 7a.

So,

$$\frac{dh}{dx} = \frac{-h_o}{x_3}$$

Also, we know that,

$$h = \frac{h_o \sinh\left(c\left(L_3 - x\right)\right)}{\sinh\left(cL_3\right)}$$

$$\frac{dh}{dx} = \frac{h_o}{\sinh\left(cL_3\right)} \frac{d}{dx}\left(\sinh\left(c\left(L_3 - x\right)\right)\right) \qquad \text{(A-65)}$$

Now,

$$\sinh\left(c\left(L_3 - x\right)\right) = \frac{e^{cL_3} e^{-cx} - e^{-cL_3} e^{cx}}{2}$$

$$\frac{d}{dx}\sinh\left(c\left(L_3 - x\right)\right) = \frac{e^{cL_3}\left(-c\right)e^{-cx} - e^{-cL_3}\left(c\right)e^{cx}}{2}$$

$$\frac{d}{dx}\sinh\left(c\left(L_3 - x\right)\right) = \frac{-c}{2}\left[e^{c\left(-x+L_3\right)} + e^{-c\left(-x+L_3\right)}\right]$$

$$\frac{d}{dx}\sinh\left(c\left(L_3 - x\right)\right) = -c\cosh c\left(L_3 - x\right) \qquad \cosh x = \frac{e^{x} + e^{-x}}{2}$$

Now, substituting the value of above expression in equation (65)

$$\frac{dh}{dx} = \frac{h_o}{\sinh\left(cL_3\right)} - c\cosh c\left(L_3 - x\right)$$

For x=0,

$$\frac{dh}{dx} = \frac{h_o}{\sinh\left(cL_3\right)} - c\cosh\left(cL_3\right)$$

$$\frac{dh}{dx} = \frac{-ch_o}{\tanh cL_3} \qquad \text{(A-66)}$$

As we know that,

$$\frac{dh}{dx} = \frac{-h_o}{x_3}$$

Putting the value of $\frac{dh}{dx}$ in equation (A-66)

$$\frac{-ch_o}{\tanh cL_3} = \frac{-h_o}{x_3}$$

$$x_3 = \frac{\tanh(cL_3)}{c} \qquad \text{(A-67)}$$

Where, $c = \sqrt{\frac{k_{bl}}{k_f z_{bl} d}}$

Case 8- Semipervious Top Strata both Riverside and Landside with sheet pile at the center of levee

Figure A-16 shows the geometry for a new case, Case 8 which is not included in the EM. Case 8 is similar to Case 7, except that a sheet pile cutoff is located beneath the center of the levee. This case was introduced to model I-walls and partially penetrating slurry walls.

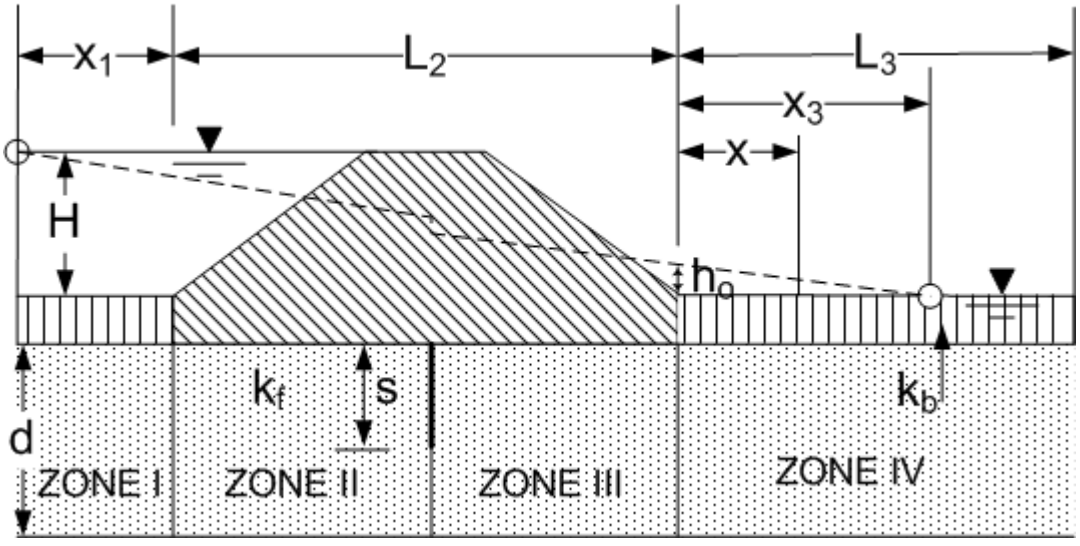

Figure A-16 Case 8 - Semipervious top strata both riverside and landside with sheet pile at the center of levee.

The same procedures as described previously will be used to determine the quantity of underseepage for Case 8. Note that the inclusion of the cutoff requires that the section be divided into four zones or fragments. It is assumed that the equipotential lines will be vertical under the sheet pile as well as under the start and end points of the levee. This assumption will only be appropriate if the base width of the levee is much greater than depth of the pervious sub-stratum as explained in Case 1.

Hence, the form factors for zones I, II, III and IV are given by:

$\Phi_1 = x_1/d$ (Type-I Fragment)

$\Phi_2 = K/K'$ (Type-III Fragment)

$\Phi_3 = K/K'$ (Type-III Fragment)

$\Phi_4 = x_3/d$ (Type-I Fragment)

The *modulus* to determine K/K' is obtained using the following equation (Harr 1962):

$$m = \cos\left(\frac{\pi s}{2d}\right)\sqrt{\tanh^2\frac{\pi b}{2d} + \tan^2\frac{\pi s}{2d}} \qquad \text{(A-68)}$$

Where,

s = Length of embedment of the sheet pile into the sub-stratum

b = Half base width of the levee = $L_2/2$

The modulus is found from equation 68 and then the value of K/K' is determined using the tables of complete elliptic integrals of first kind. One such table is provided in Appendix I.

Substituting the values of the form factors in equation (A-3):

$$\delta = \frac{1}{\Sigma\Phi} = \frac{1}{x_1/d + K/K' + K/K' + x_3/d}$$

$$\delta = \frac{1}{x_1/d + 2K/K' + x_3/d}$$

Therefore, equation (A-2) becomes:

$$Q_s = k_f H \frac{d}{\left(x_1 + 2d\left(\frac{K}{K'}\right) + x_3\right)} \qquad \text{(A-69)}$$

Similarly, the head at the toe of the levee is found using Method of Fragments. The head loss in m^{th} fragment is calculated as follows:

$$h_m = \frac{H\Phi_m}{\sum\Phi} \qquad \text{(A-70)}$$

Where,

Φ_m = Form factor for m^{th} zone

$\sum\Phi$ = Summation of form factors for all the fragments (zones I, II, III and IV in this case).

Head loss through zone I, $h_1 = \frac{H\Phi_1}{\sum\Phi}$

Head loss through zone II, $h_2 = \frac{H\Phi_2}{\sum\Phi}$

Head loss through zone III, $h_3 = \frac{H\Phi_3}{\sum\Phi}$

Head loss through zone IV, $h_4 = \frac{H\Phi_4}{\sum\Phi}$

Accordingly, the head at the toe of the structure is determined as follows:

$$h_o = H - (h_1 + h_2 + h_3) \qquad \text{(A-71)}$$

Or simply,

$$h_o = h_4 = \frac{H\Phi_4}{\sum \Phi} \qquad \text{(A-72)}$$

There are three different subcases for Case 8, similar to Case 7, depending upon the seepage boundary conditions on the landward side. The value of x_3 is determined for each case depending upon the type of seepage exit.

Case 8a ($L_3 = \infty$)

Figure A-17 shows the geometry for Case 8a. For this case, the horizontal distance from the landside levee toe is considered to be infinite.

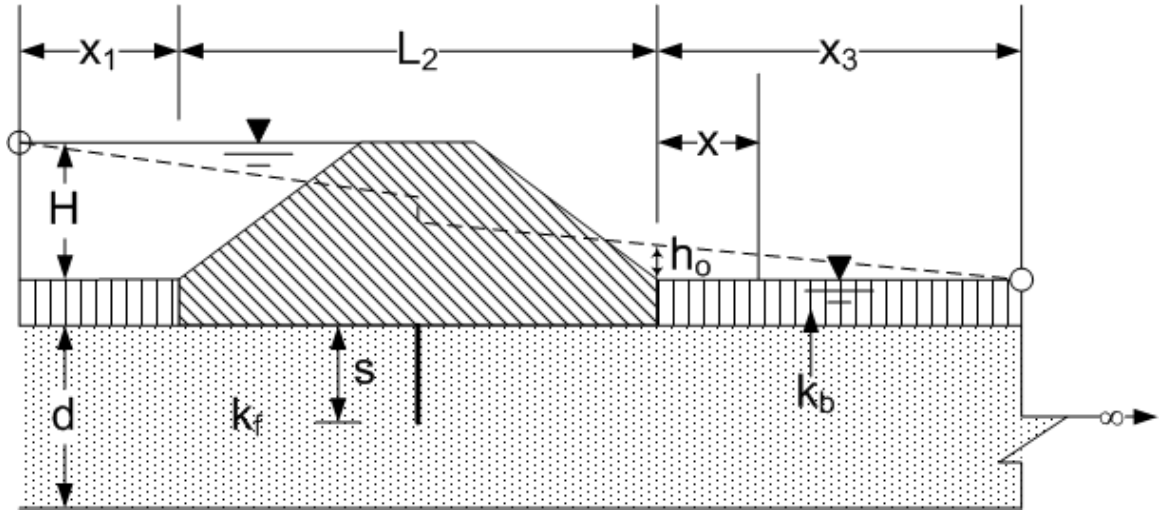

Figure A-17 Case 8a - Semipervious top strata both riverside and landside with sheet pile at the center of levee and L_3 as infinite.

It is clear from the above figure that the landward side of Case 8a is identical to the landward side of Case 7a. Therefore, the equation to determine the head at any distance x will be the same for both cases. The equation for the head at distance = x is as follows:

$$h_x = h_0 e^{-cx} \qquad \text{(A-73)}$$

where, $c = \sqrt{\frac{k_{bl}}{k_f z_{bl} d}}$ and h_o is determined from either equations (A-71) or (A-72).

The derivation of the above equation is explained in detail in the section of this report addressing Case 7a. The distance from the landside levee toe to the effective seepage exit (x_3) is also determined in a similar manner as in Case 7a and the equation is as follows:

$$x_3 = \frac{1}{c} = \sqrt{\frac{k_f z_b d}{k_b}}$$

Case 8b (L_3 = finite distance to seepage block)

Figure A-18 shows the basic geometry for Case 8b, in which seepage block is located a distance L_3 from the landward levee toe.

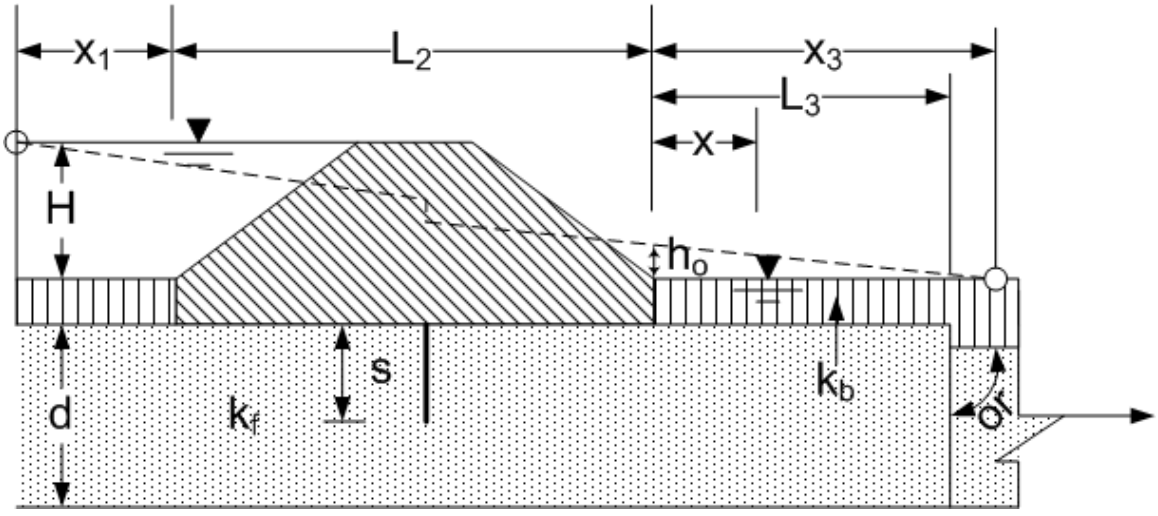

Figure A-18 Case 8b - Semipervious top strata both riverside and landside with sheet pile at the center of levee and L_3 as finite distance to seepage block.

It is again clear from the above figure that the landward side of Case 8b is identical to the landward side of Case 7b. Therefore, the equation to determine the head at any distance x will be the same. The equation for the head at distance = x is:

$$h_x = \frac{h_o \cosh(c(L_3 - x))}{\cosh(cL_3)} \qquad \text{(A-74)}$$

For $x = L_3$

$$h_x = \frac{h_o}{\cosh(cL_3)} \quad \text{since} \cosh(0) = 1$$

The distance from the landside levee toe to the effective seepage exit (x_3) is also determined in a similar manner as in Case 7b and the equation is:

$$x_3 = \frac{1}{c \tanh(cL_3)}$$

Case 8c (L3 = finite distance to an open seepage exit)

Figure A-19 shows the basic geometry used for the development of the equations for Case 8c. This case has an open seepage exit located a distance L_3 from the landward levee toe.

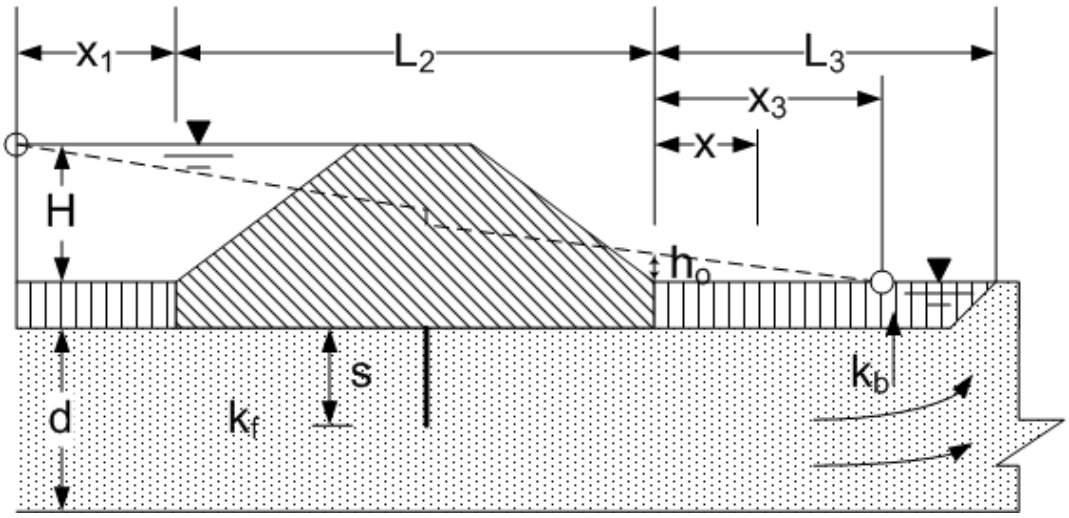

Figure A-19 Case 8c - Semipervious top strata both riverside and landside with sheet pile at the center of levee and L_3 as finite distance to an open seepage exit.

The seepage boundary conditions for Case 8c are the same as for Case 7c, therefore the equation to determine the head at any distance x is also the same. The equation for the head at distance = x is as follows:

$$h_x = \frac{h_o \sinh(c(L_3 - x))}{\sinh(cL_3)} \qquad \text{(A-75)}$$

The distance from the landside levee toe to the effective seepage exit (x_3) is also determined in the same manner as for Case 7c by the following equation:

$$x_3 = \frac{\tanh(cL_3)}{c}$$

A summary of the equations, along with their respective figures for Cases 1 through 8, are shown in the following figures. Figure A-20 summarizes Cases 1 through 4; Figure A-21 is the summary of Cases 5 and 6 while Figures A-22 and A-23 represent the summary of Cases 7 and 8 respectively.

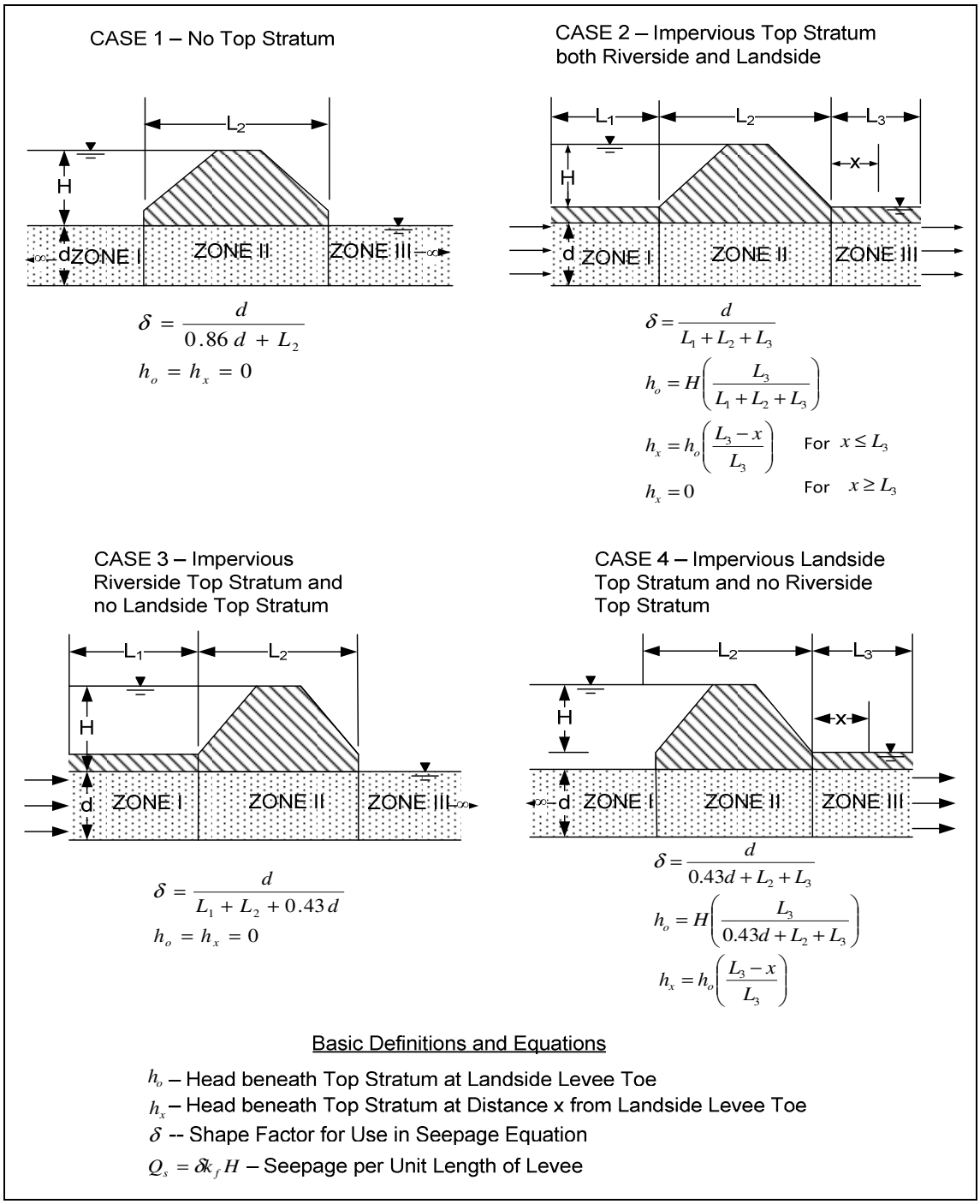

Figure A-20 Equations for computation of underseepage flow and substratum pressures for Cases 1 through 4.

CASE 5 – Semipervious Riverside Top Stratum and No Landside Top Stratum

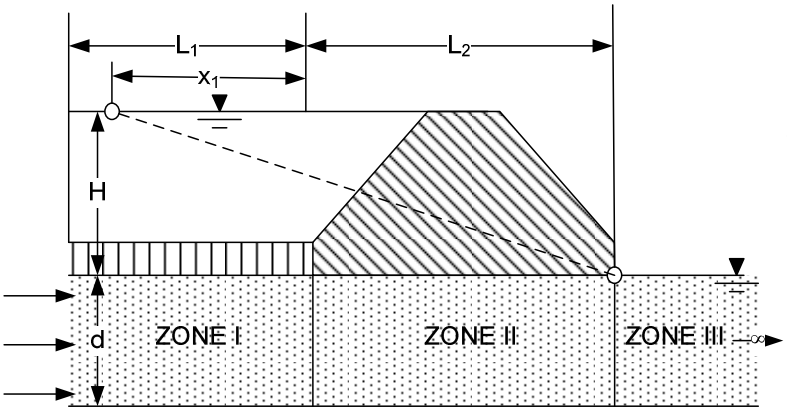

$$\delta = \frac{d}{x_1 + L_2 + 0.43d}$$

$$h_o = h_x = 0$$

CASE 6 – Semipervious Landside Top Stratum and No Riverside Top Stratum

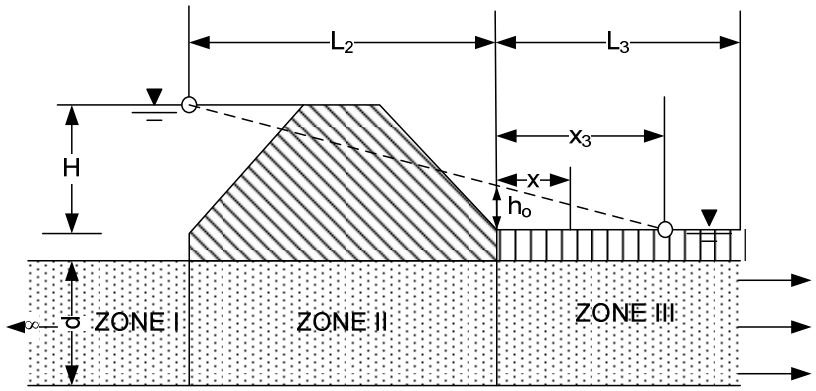

$$\delta = \frac{d}{0.43d + L_2 + x_3}$$

$$h_o = H\left(\frac{x_3}{0.43d + L_2 + x_3}\right)$$

$$h_x = \frac{h_o \sinh\left(c\left(L_3 - x\right)\right)}{\sinh\left(cL_3\right)}$$

Basic Definitions and Equations

h_o – Head beneath Top Stratum at Landside Levee Toe

h_x – Head beneath Top Stratum at Distance x from Landside Levee Toe

δ -- Shape Factor for Use in Seepage Equation

$Q_s = \delta k_f H$ – Seepage per Unit Length of Levee

Figure A-21 Equations for computation of underseepage flow and substratum pressures for Cases 5 and 6.

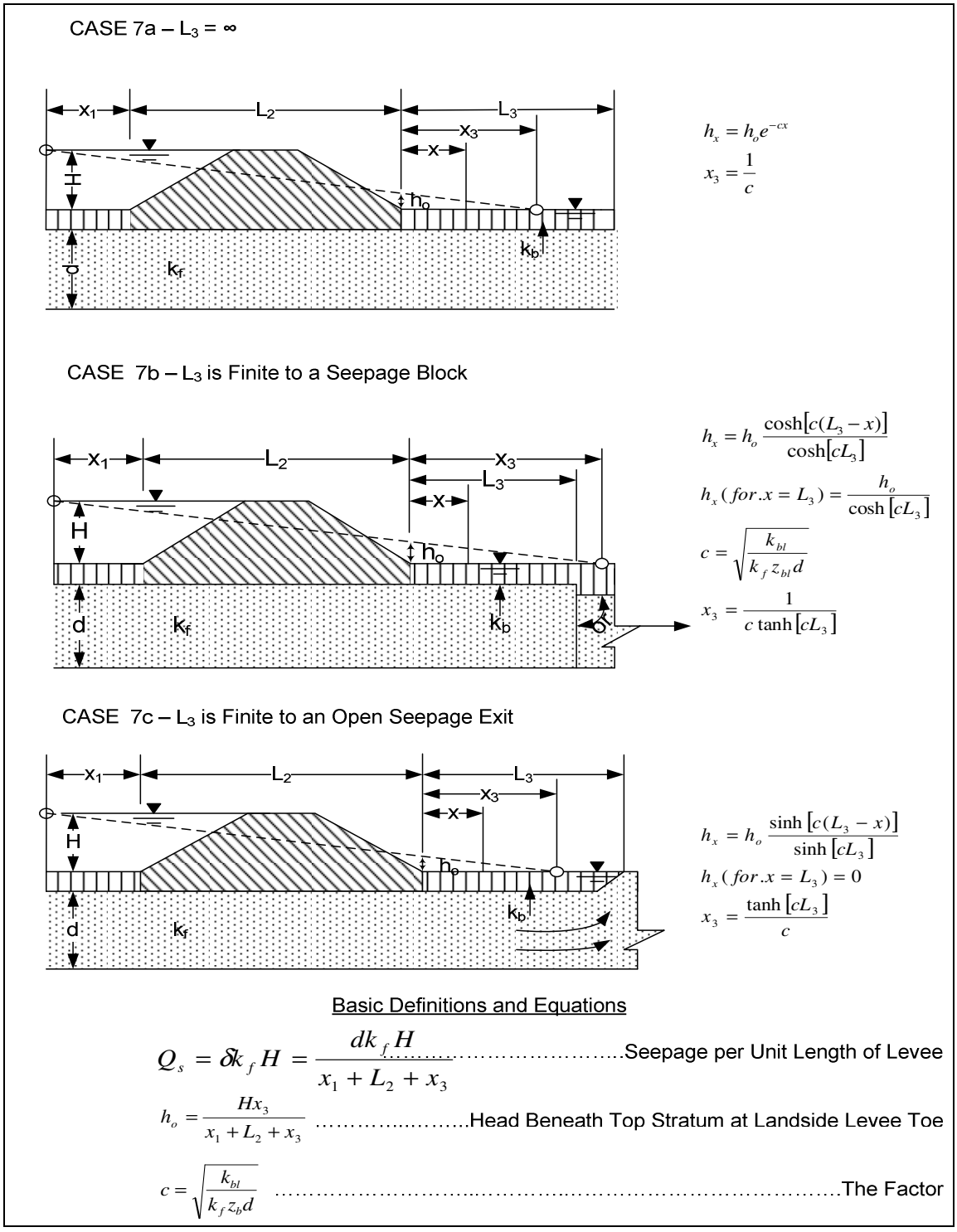

Figure A-22 Equations for computation of underseepage flow and substratum pressures for Case 7.

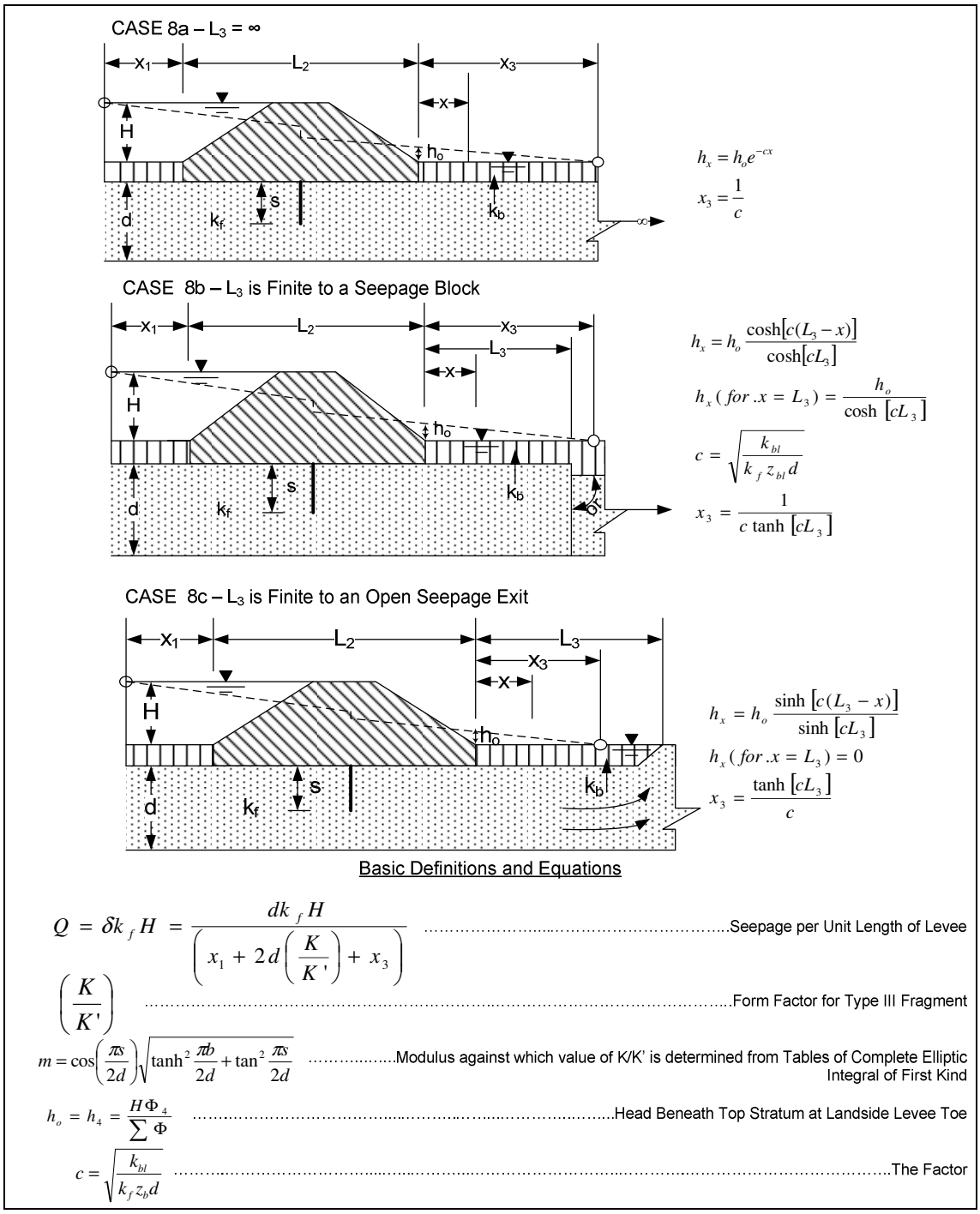

Figure A-23 Equations for computation of underseepage flow and substratum pressures for Case 8.

Comments Regarding Blanket Theory Equations

1) The blanket theory equations are based on approximate values of permeability and thicknesses of the top and pervious strata. The permeability value for the pervious stratum should be the horizontal component of the permeability. The permeability value for the semipervious stratum should be the vertical component of the permeability. Also, it is prudent to use a range of permeability and thickness values to cover the range of variation of these parameters for field cases.

2) There is a discrepancy in the manner that the total head loss through the section (ΔH or H) is defined for many cases in EM 1110-2-1913. The corrections for these errors are made in this report as shown in Figures A-7, A-8, A-9 and A-10 for Cases 3, 4, 5 and 6, respectively.

3) The equations presented in Appendix B of EM 1110-2-1913 are said to be derived from the information contained in TM 3-424. However, the transformed permeability of the top stratum is defined differently in TM 3-424, in which a weighted average is taken to determine k_b. In Appendix B of the EM, the permeability of the most impervious stratum is taken as the transformed permeability of the top stratum.

4) Similarly, the head at the toe of the levee (h_o) is shown incorrectly in the EM as compared to TM. It is indicated at the bottom of the top stratum at the toe of the levee as total head in EM, whereas, blanket theory finds the excess head which corresponds to the point located at the top of the top stratum.

5) It is not clear from the EM or TM what ratio of permeabilities between the pervious layer and the top blanket make the top blanket essentially impervious. In other words, no guidance is provided to select when the top blanket is considered to be impervious vs. semipervious.

6) The concept of a transformed thickness of the top stratum is only applicable to semipervious top stratum cases and not for impervious top stratum cases. Of the impervious cases, the top blanket essentially has zero thickness and is only a factor when computing the uplift gradient.

7) The constant $c = \sqrt{\frac{k_f z_b d}{k_b}}$ is defined only in terms of the landward stratum in Appendix B of the EM. However, it should also be stated in terms of riverward side to determine x_1.

8) The fundamental assumption that flow through top stratum is vertical and through pervious sub-stratum is horizontal is only true if the ratio of k_f to k_b is greater than or equal to 10. The validity of the assumptions becomes questionable for lower ratio of permeabilities.

9) The value of k_f used in Blanket Theory is the horizontal component of permeability of the pervious layer. The value of k_b is the vertical component of permeability.

10) The application of the Blanket Theory equations is limited to the cases where $\frac{L_2}{d} \geq 1$. This constraint is necessary to ensure that the equipotential lines are essentially vertical, which is one of the fundamental assumptions of the Method of Fragments.

Evaluation of Blanket Theory Solutions with Finite Elements Analyses

Introduction

Finite element analyses were performed on the eleven different seepage configurations in order to (1) verify the blanket theory solutions and (2) to assess potential errors in the solutions when geometrical and soil property values are used outside of the recommend guidelines.

The finite element analyses were performed with SLIDE (Rocscience Version 6.0) for Case 1 to Case 8. A comparison of SLIDE and SEEP/W (Geo-Studio Version 7.13) was performed and is presented after all cases are discussed. The finite element analyses were performed using the same boundary conditions, layer thicknesses, and permeability values as used for the blanket theory solutions. Results are presented for volumetric flow rates per unit of levee length (Q_s) and for excess hydraulic head (h_o) under the toe of the levee (when applicable) using finite element analyses and closed-form solutions. The following cases were analyzed:

Case 1 - No landside and riverside top stratum

Case 2 - Impervious landside and riverside top stratum

Case 3 - Impervious riverside top stratum and no landside top stratum

Case 4 - Impervious landside top stratum and no riverside top stratum

Case 5 – Semi-pervious riverside top stratum and no landside top stratum

Case 6 – Semi-pervious landside top stratum and no riverside top stratum

Case 7a – Semi-pervious landside and riverside top stratum (top stratum extends infinitely landward of the levee)

Case 7b – Semi-pervious landside and riverside top stratum (seepage block in the pervious substratum located landward of the levee)

Case 7c - Semi-pervious landside and riverside top stratum (seepage exit in the pervious substratum located landward of the levee)

Case 8b – Semi-pervious landside and riverside top stratum (seepage block in the pervious substratum located landward of the levee) with cutoff

Case 8c - Semi-pervious landside and riverside top stratum (seepage exit in the pervious substratum located landward of the levee) with cutoff

The general boundary conditions used in Cases 1 through Case 8 are shown in Figure A-24. In all analyses, the base of the levee (L_2) was assumed to be 132 ft. This is equivalent to a 20 ft tall levee having 3:1 slopes and a crest width of 12 ft. However, since the levee is modeled as an impervious structure in both the finite element analysis and blanket theory analysis, the true dimensions are inconsequential.

The finite element analyses were conducted with a minimum of 1500 elements. The elements used were six-noded triangles. This mesh appeared to provide accurate results with short execution times.

For Cases 1 through 4, the permeability of the pervious layer was 4.92×10^{-3} ft/sec (0.15 cm/sec). For these cases, the value of permeability is not important for comparing finite element analysis to blanket theory. The flow calculated for both methods is directly proportional to the permeability, and the excess head at the downstream toe does not depend on the value of permeability. For Cases 5 through 8, the value of permeability is more important, and values are given during the discussion of each case.

Cases 2 through 4 have an impervious blanket, and that is modeled in finite element analysis as a *no-flow* nodal boundary conditions. Both in blanket theory and in finite element analysis, this has the same effect as a blanket of zero thickness. For Cases 5 through 8, which have different

combinations of riverside and landside semi-pervious blankets, the thickness of the blanket is an important factor, particularly in the manner in which the total head loss is defined.

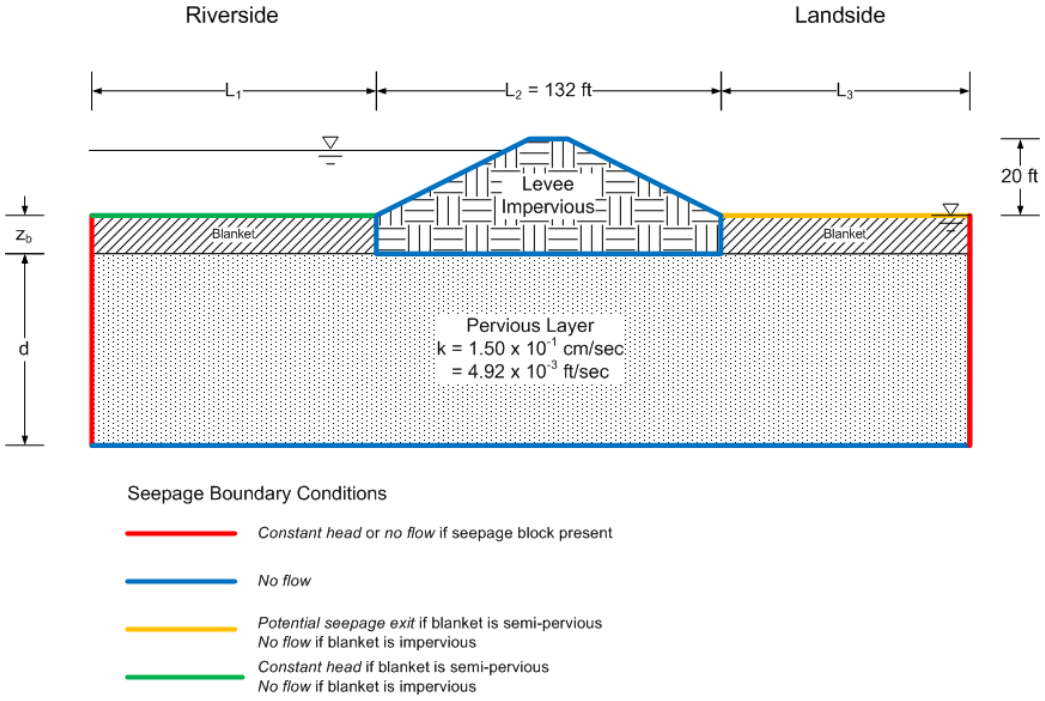

Figure A-24 Generalized geometry and boundary conditions used in finite element analysis.

Case 1 – No Landside and Riverside Top Stratum

Figure A-25 shows the basic geometry used for the FE analysis of Case 1. This analysis was done for three different thicknesses of the pervious layer (d) of 25 ft, 50 ft, and 100 ft. This analysis was performed considering both riverside and landside dimensions of 100 ft and 1500 ft. For blanket theory analyses, the L_1 and L_3 dimensions are considered to be infinite. However, for finite element analysis, these dimensions must be assigned finite lengths.

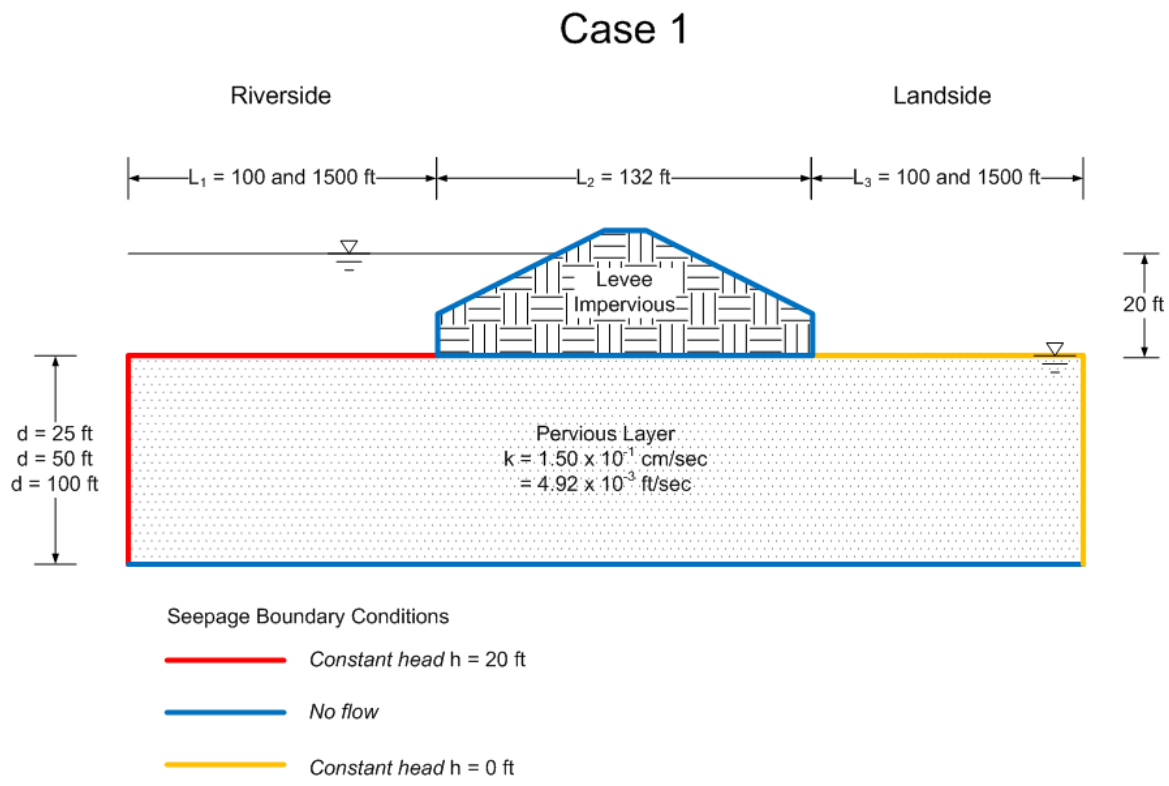

Figure A-25 Geometry for Case 1 - No landside and riverside top stratum.

In the FEA, the riverside nodal boundary conditions (horizontal and vertical) were set to a constant head of 20 ft. The landside boundary conditions (horizontal and vertical) were set to a constant head of 0 ft.

As shown in Figure A-26, the flow (Q_s) increases with increasing thickness of the pervious layer (d), as expected. Values of L_1 and L_3 do not appear to affect the finite element results. Essentially the same values of flow were calculated for L_1 and L_3 dimensions of 100 ft as for L_1 and L_3 dimensions of 1500 ft as shown in Figure A-27.

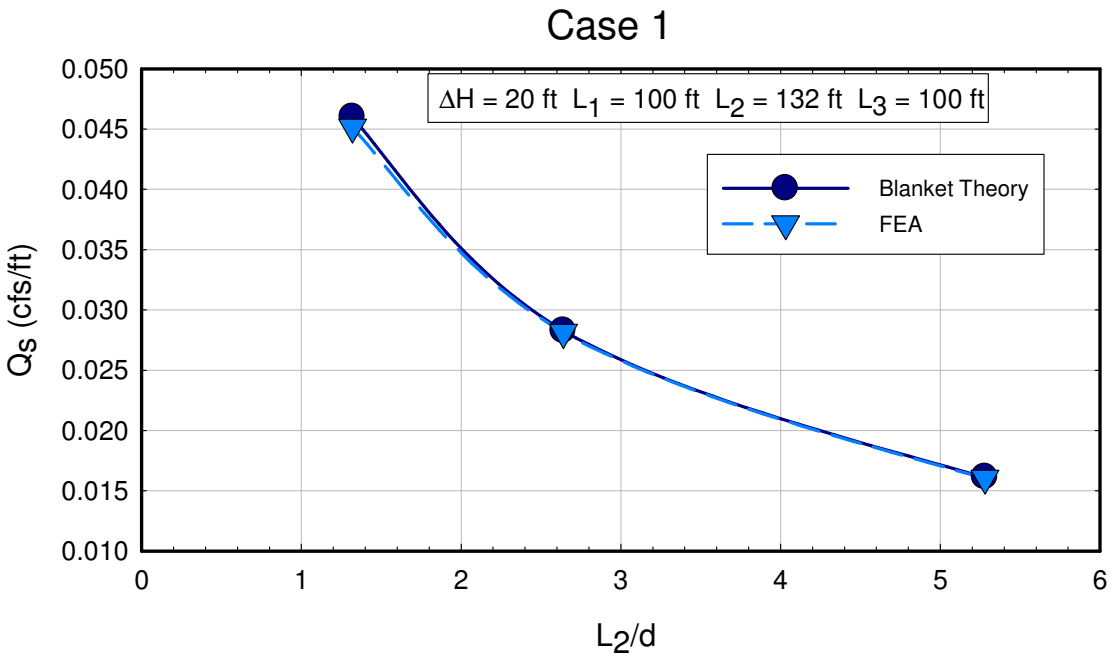

Figure A-26 Calculated values of flow per unit length (Q_s) for different values of L_2/d for Case 1.

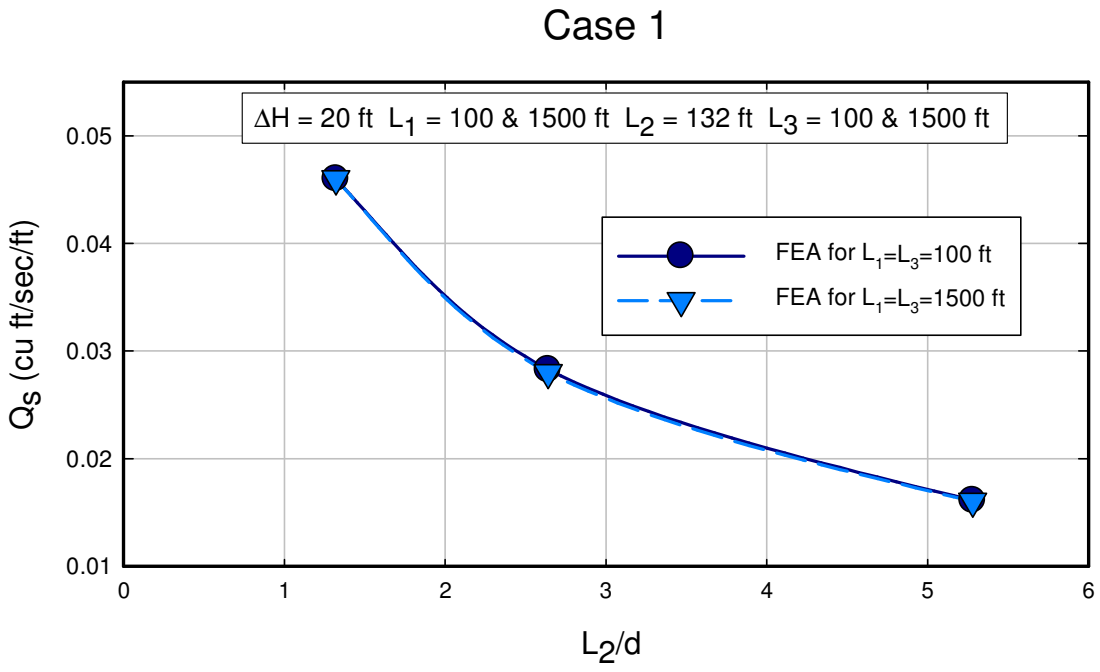

Figure A-27 Comparison of different values of L_1 and L_3 for FEA

There is close agreement between the finite element analysis and blanket theory for this case. The difference between the two methods seems to increase with decreasing L_2/d ratio as shown in Figure A-28. This supports the recommendations given in the first section that L_2/d ratio ≥ 1 for application of blanket theory, as it seems to underestimate the flow for smaller ratios.

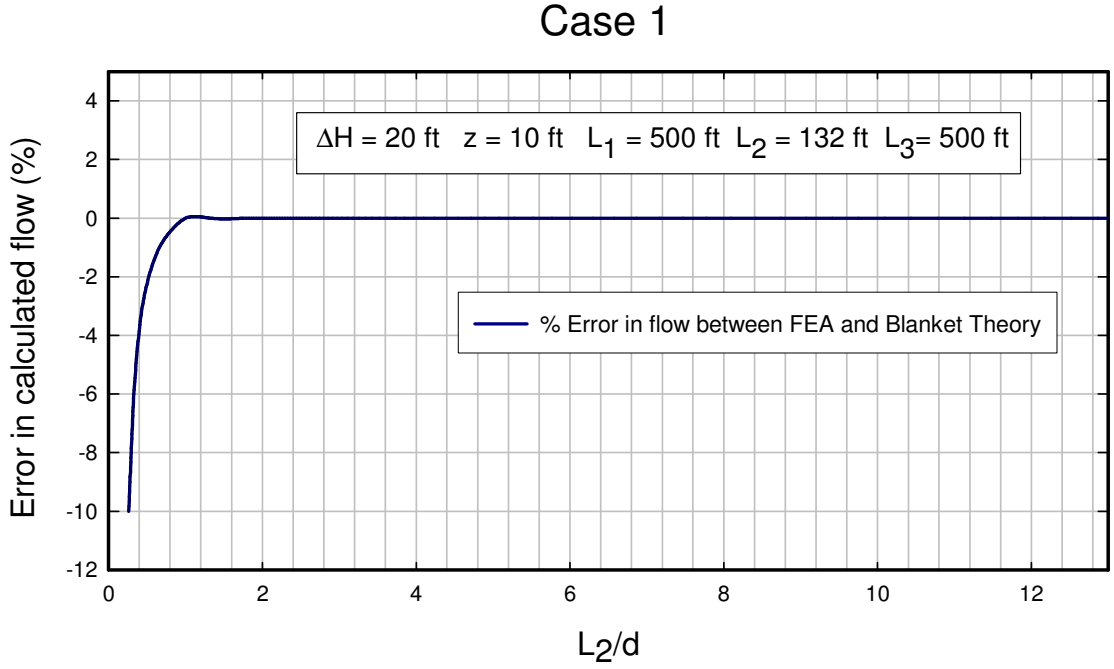

Figure A-28 Percent error in calculated flow per unit length (Q_s) for blanket theory with increasing L_2/d ratios.

Case 2 – Impervious Landside and Riverside Top Stratum:

Figure A-29 shows the geometry used for Case 2. The boundary conditions were the same as for Case 1, except that the landside and riverside horizontal ground surfaces were assigned "no flow" boundary conditions to model an impervious top stratum. In this analysis, L_3 values of 700 ft, 1300 ft, and 1500 ft were used. A constant value of L_1 equal to 2000 ft was used in all analyses.

Analyses were done for values of d equal to 25 ft and 100 ft. The seepage per unit length beneath the levee (Q_s) and the pressure head at the toe of the levee was compared for the FEA

and blanket theory solutions. For the geometry shown in Figure A-29, the excess head at the toe (h_o) is equal to the pressure head at the toe since the far landside phreatic surface is at the ground surface.

Figure A-30 shows the calculated values of Q_s for the different values of L_3 for both d = 25 ft and d = 100 ft. The value of flow decreases with increasing L_3 and decreasing d. The values of flow calculated from FEA and blanket theory were essentially equal.

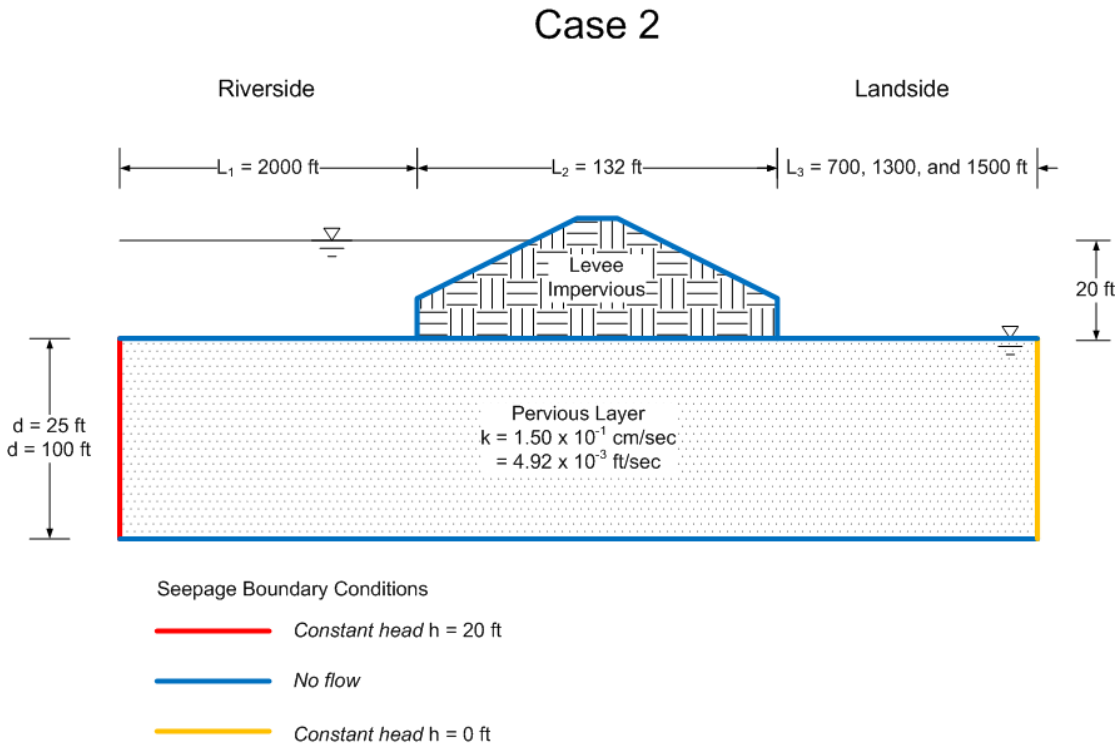

Figure A-29 Geometry for Case 2 - Impervious landside and riverside top stratum.

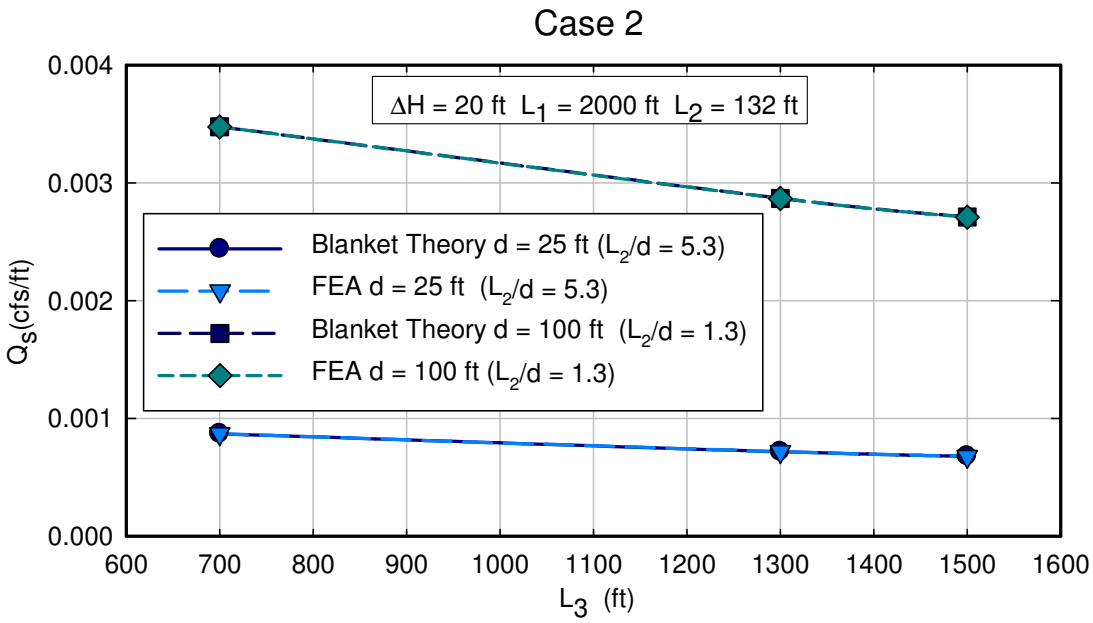

Figure A-30 Calculated values of flow per unit length (Q_s) from blanket theory and finite element analysis for different values of L_3 for Case 2.

Figure A-31 shows the variation of the pressure head (excess head) at the toe for different values of L_3. The value of head plotted corresponds to the head at the node at the toe of the levee. The value of excess head determined using FEA and blanket theory are essentially the same, regardless of the value of the thickness of the pervious layer. As indicated in the theory portion of this report, the excess head beneath the blanket is not dependent on the thickness of the pervious substratum for blanket theory, and that result is substantiated by the FEA.

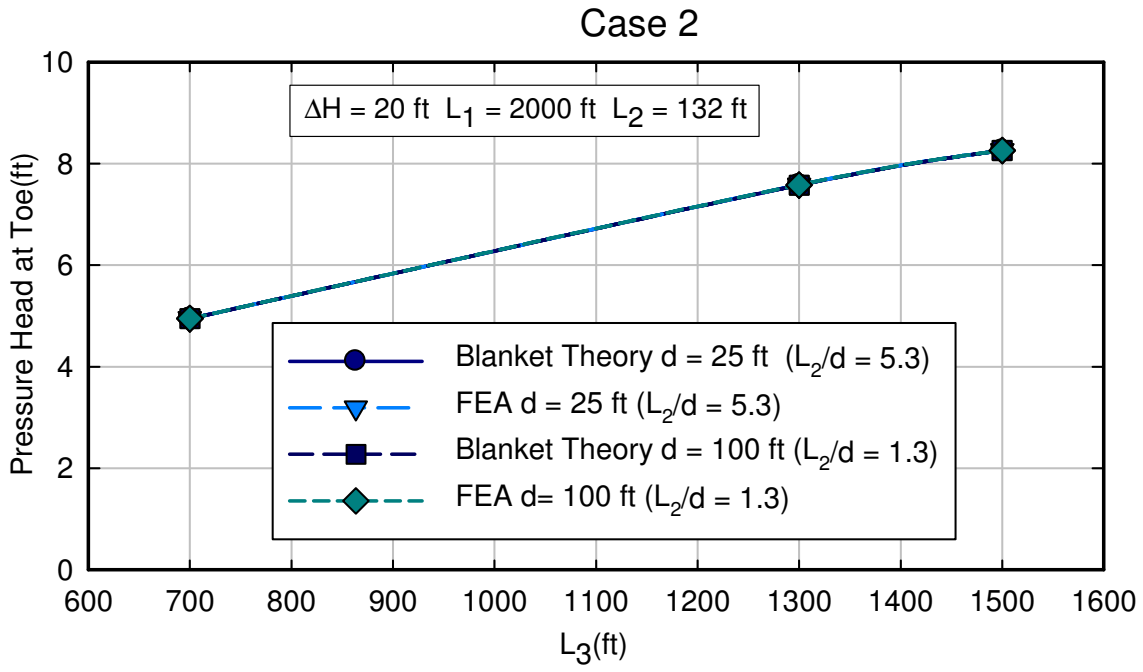

Figure A-31 Excess head (h_o) or pressure head beneath blanket at toe for Case 2 calculated using FEA and blanket theory for different values of L_3 for d = 25 ft and d = 100 ft.

Case 3 - Impervious Riverside Top Stratum and No Landside Top Stratum:

The geometry and finite element boundary conditions for Case 3 (impervious riverside top stratum and no landside top stratum) are shown in Figure A-32. The hydraulic boundary conditions are the same as for Case 1, except that *no-flow* nodal boundary conditions were assigned to the riverside ground surface to model an impermeable blanket. In the blanket theory derivation, the L_3 dimension is infinite. In order to approximate this with finite element analysis, a value of L_3 equal to 1500 ft was used in the analysis. Based on the results of Case 1, this is justified since the L_3 values of 100 ft to 1500 ft produced the same calculated flows. L_1 values of 200 ft, 500 ft, and 1000 ft were used in the FE analyses, and values of d equal to 25 ft and 100 ft were used.

Figure A-33 shows the calculated flow per unit length (Q_s) as a function of L_1. The flow decreases, as expected, with increasing magnitude of L_1 and with decreasing magnitude of d. Again, the blanket theory results and the finite element results are in exact agreement.

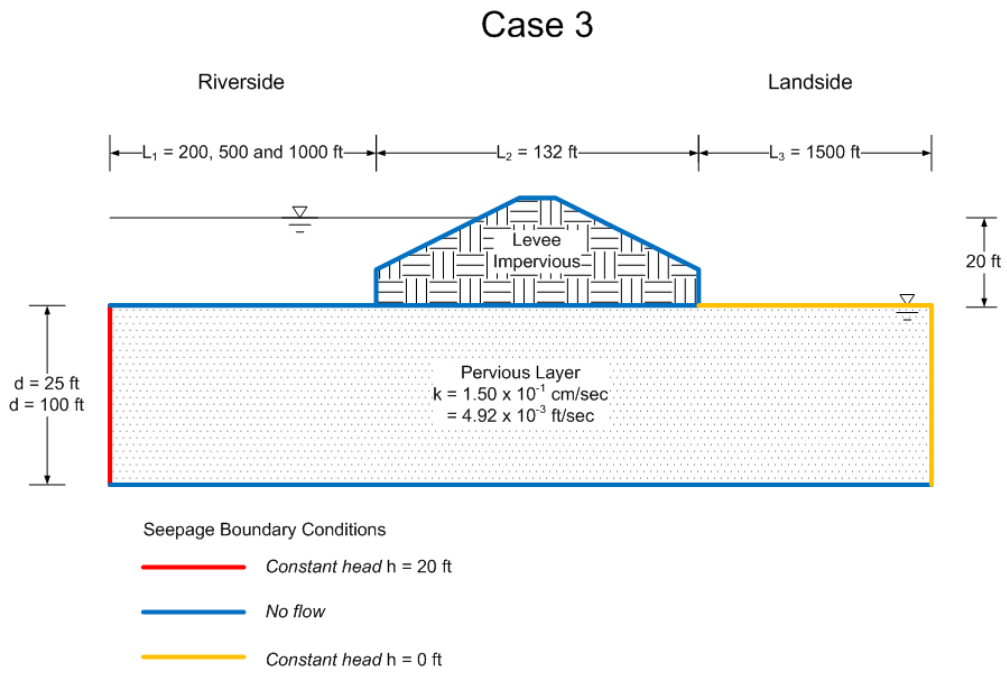

Figure A-32 Geometry for Case 3 - Impervious riverside top stratum and no landside top stratum.

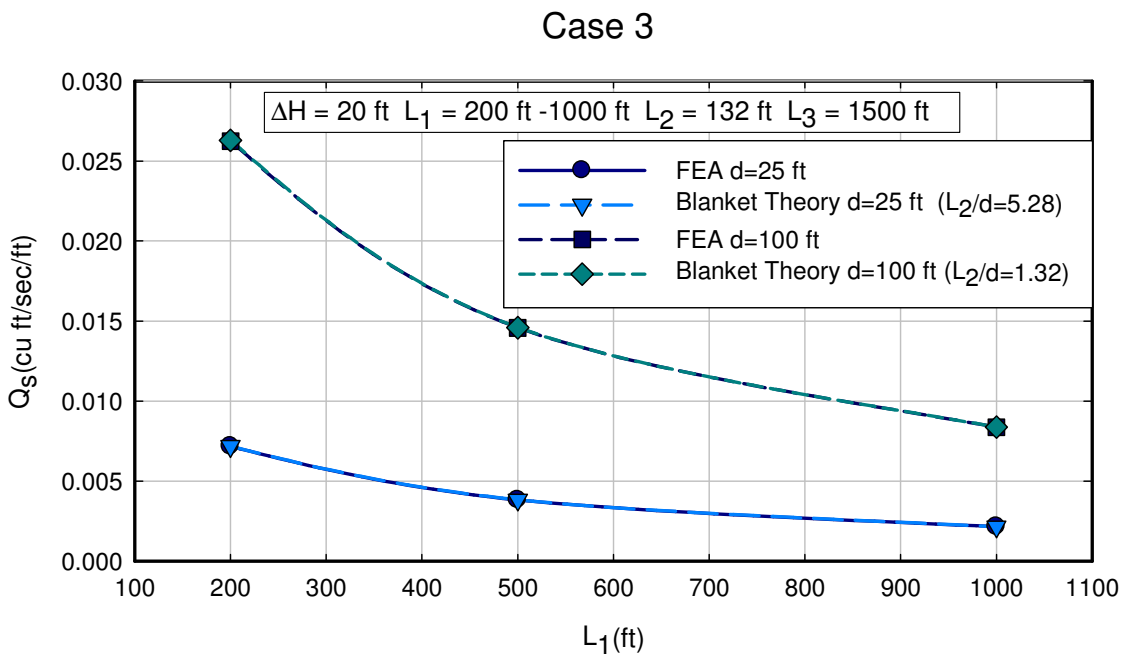

Figure A-33 Calculated values of flow per unit length (Q_s) from blanket theory and finite-element analysis for different values of L_1 for Case 3.

Case 4 - Impervious Landside Top Stratum and No Riverside Top Stratum:

The geometry for Case 4 (impervious landside top stratum and no riverside top stratum) is shown in Figure A-34. The hydraulic boundary conditions are the same as for Case 1, except that *no-flow* nodal boundary conditions were assigned to the landside ground surface to model an impermeable blanket.

Similar to the previous example, in the blanket theory derivation, the L_1 dimension is infinite. In order to approximate this with finite element analysis, a value of L_1 equal to 3100 ft was used in the analysis. For the Case 4 analysis, L_3 values of 500 ft, 1000 ft, and 1600 ft were used and values of d equal to 25 ft and 100 ft were used.

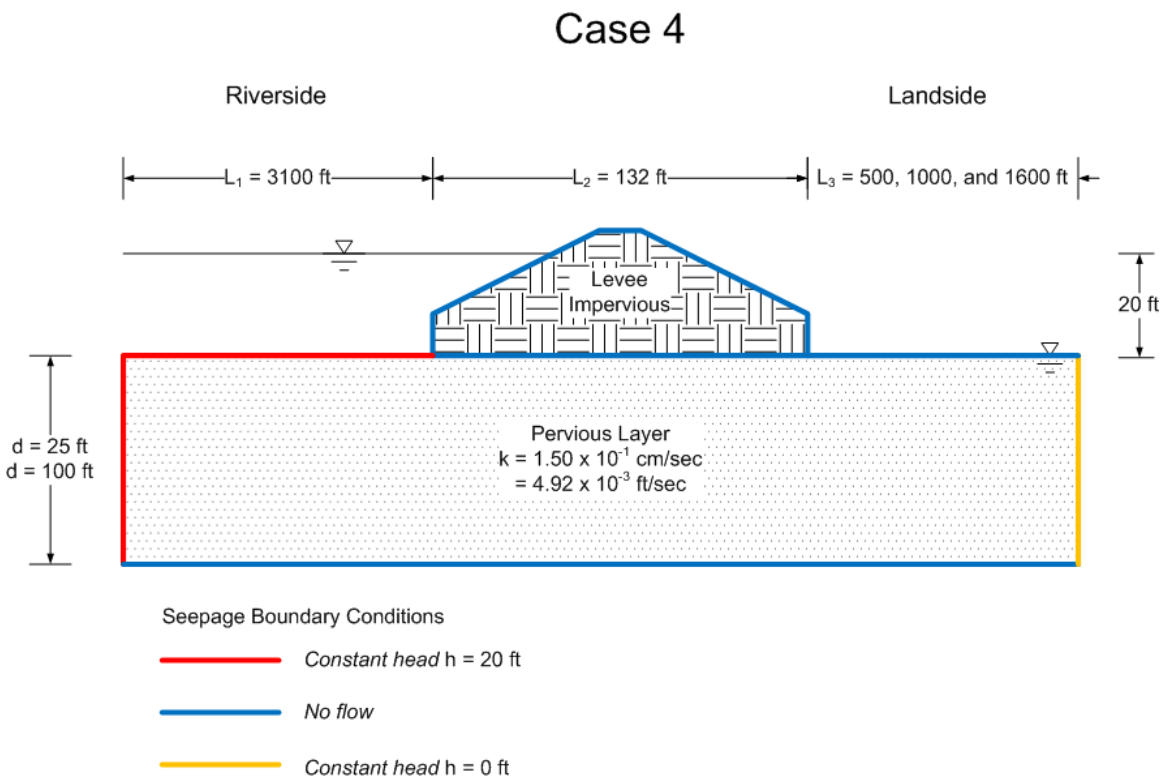

Figure A-34 Geometry for Case 4 - Impervious landside top stratum and no riverside top stratum.

Figure A-35 shows the calculated flow per unit length (Q_s) beneath the levee for different values of L_3. The results from FEA and blanket theory are essentially identical. Figure A-36 shows the value of excess head (pressure head) at the toe of the levee for the same cases. Again, there is no difference between the values calculated using blanket theory and the values calculated using FEA.

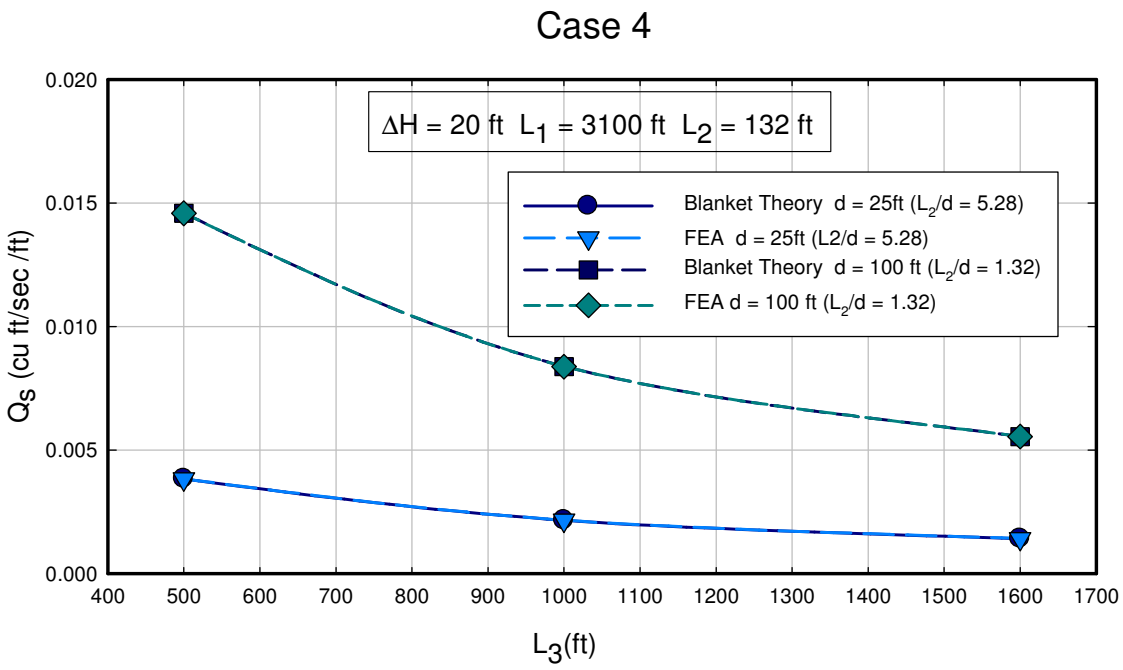

Figure A-35 Calculated values of flow per unit length (Q_s) from blanket theory and finite element analysis for different values of L_3 for Case 4.

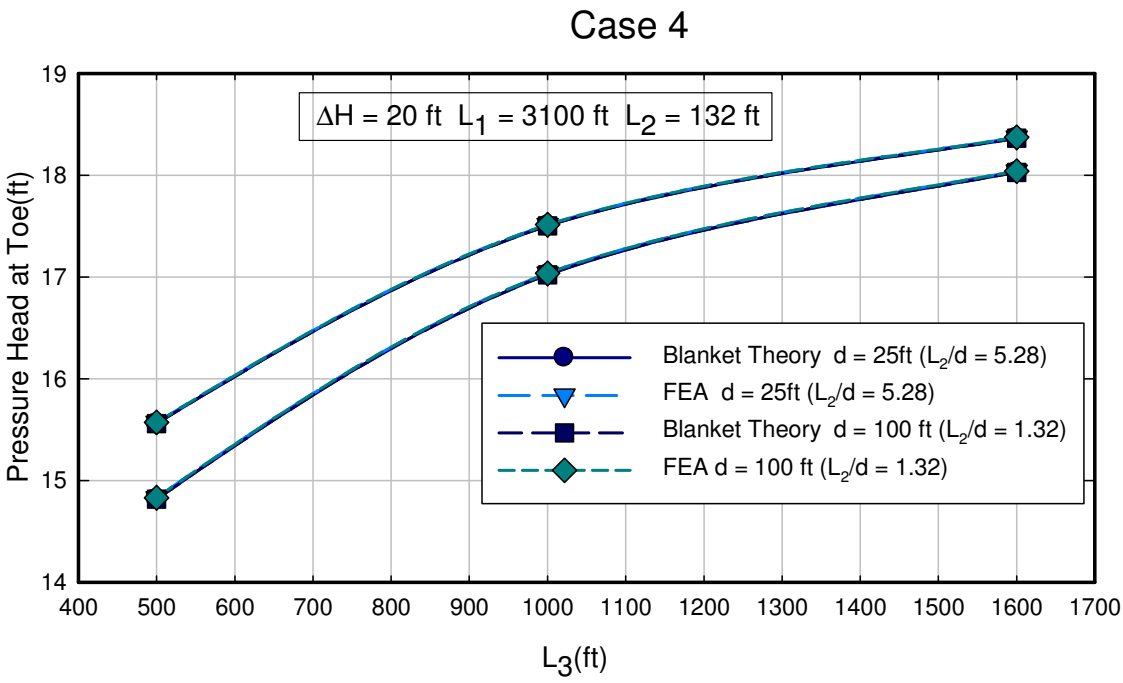

Figure A-36 Excess head (h_o) or pressure head at toe calculated using FEA and blanket theory for different values of L_3.

Case 5 - Semipervious Riverside Top Stratum and No Landside Top Stratum:

Case 5 is the first case having a semi-pervious blanket. For cases similar to Case 5, the thickness and permeability of the semi-pervious blanket become important factors in the analyses. For the geometry shown in Figure A-37, the thickness of the upstream blanket has an influence on the manner that the total head loss (H or ΔH) is defined. For the purpose of the finite element analysis, ΔH is defined as the change in head from the river level to the ground surface elevation on the landside. This differs from the way the ΔH is shown for Case 5 in EM 1110-2-1913, where ΔH is incorrectly defined as the distance from the top of the blanket to the river level.

Comparison of the cases having semi-pervious blankets with the impervious cases allows a determination of the threshold permeability values where a semi-pervious blanket becomes essentially impervious.

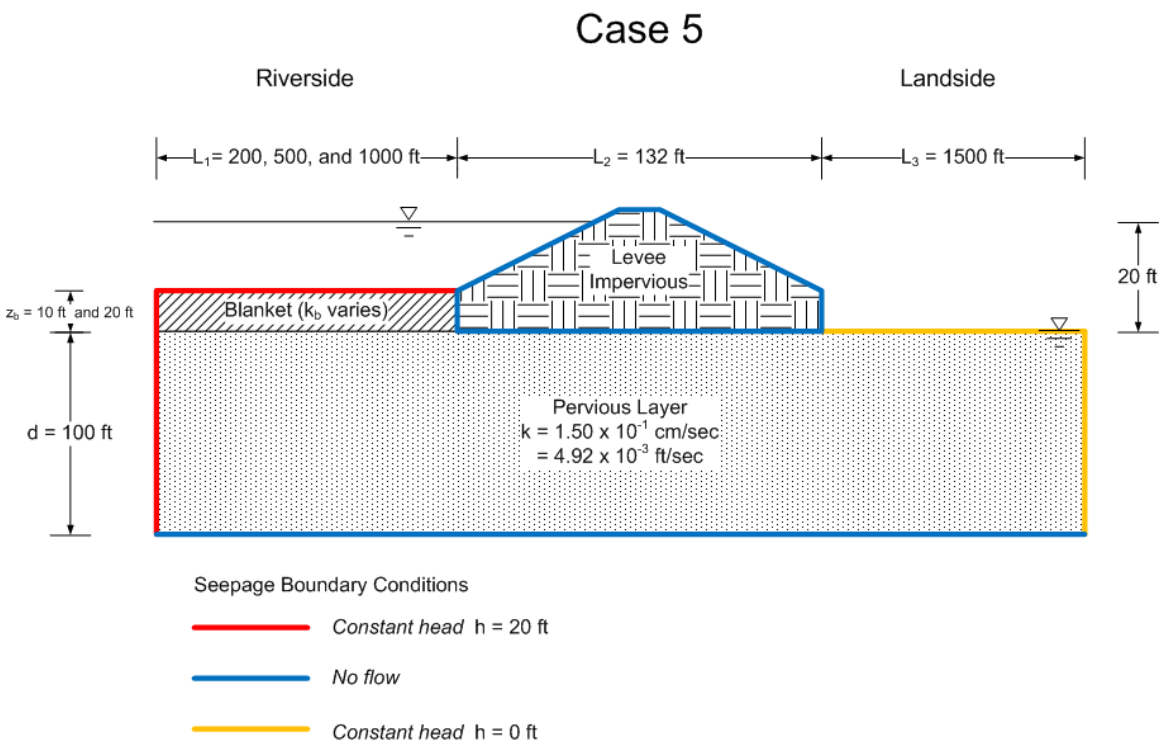

Figure A-37 Geometry of Case 5 - Semi-pervious riverside top stratum and no landside top stratum.

The semi-pervious cases require evaluation of more parameter combinations than Cases 1 through 4. The permeability of the pervious layer (k_f) was assigned a value of 4.92 x 10^{-3} ft/sec (0.15 cm/sec), which is the same value used in the previous analyses. The permeability of the semi-pervious blanket (k_b) was varied to be a multiple of the permeability of the pervious layer. Ratios of k_f to k_b from 0.1 to 100,000 were used in the analysis.

Analyses were performed for a blanket thickness (z_b) equal to 10 ft and 20 ft. The value of L_3 for the blanket theory derivations is equal to infinity, and a value of 1500 ft was used in the FEA to effectively model this condition. L_1 values of 200 ft, 500 ft, and 1000 ft were analyzed for all permeability combinations. Constant head boundary conditions (h = 20 ft) were assigned to all nodes on the riverside horizontal ground surface and the vertical riverside boundary. The landside ground surface and vertical boundary were assigned constant head values of 0 ft.

Shown in Figure A-38 are the calculated volumetric flow values for a blanket thickness of 10 ft and L_1 equal to 200 ft. Also plotted on this figure are the results from Case 1 and from Case 3 with L_1 also equal to 200 ft. Several important elements can be gleaned from the figure.

The results of the FEA are bracketed by the results for Case 1 and Case 3. This should be expected since for k_f/k_b ratios < 1, the semi-pervious blanket is effectively removed from the flow regime, and Case 5 becomes a Case 1 problem. Likewise, for large values of k_f/k_b, the blanket is essentially impervious, and the calculated flow should be the same as Case 3. For k_f/k_b ratios of about 4000, the semi-pervious blanket behaves as an impervious blanket. In other words, if the semipervious blanket has permeability of about 4000 times less than the pervious layer, then the Case 3 analysis is more appropriate than the Case 5 analysis.

For a permeability ratio of about 50 and above, blanket theory and finite element analysis are in excellent agreement. For permeability ratios less than 50, blanket theory predicts larger flow values than finite element analysis. Although the FEA correctly converges to the Case 1 solution, the flows predicted by blanket theory exceed the Case 1 values for permeability ratios of about 2 and greater.

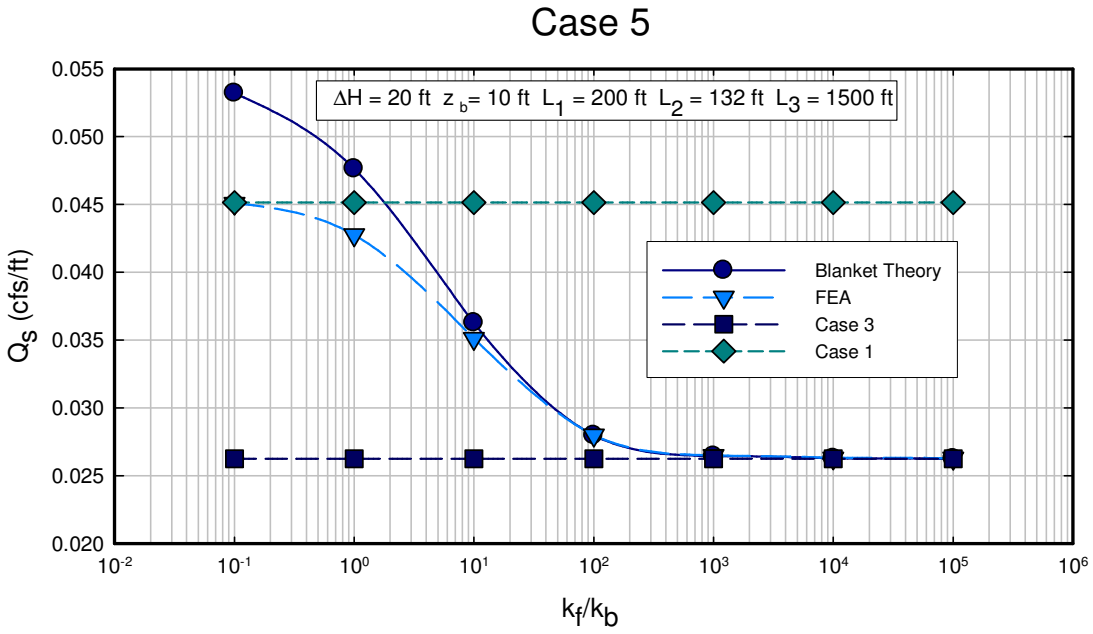

Figure A-38 Calculated values of flow per unit length (Q_s) for various permeability ratios from blanket theory and finite element analysis for Case 5 for z_b = 10 ft and L_1 = 200 ft.

Shown in Figure A-39 is a similar plot for all of the same boundary conditions, except that L_1 has been increased to 1000 ft. As expected, the volume of flow is decreased. There appears to be closer agreement with the FEA and blanket theory results for this geometry.

Figure A-40 shows the results of a similar analysis for a blanket thickness (z_b) equal to 20 ft and L_1 equal to 200 ft. This analysis shows a certain peculiarity of flow measurements using SLIDE. For this analysis, a vertical "flux section" was placed from the horizontal midpoint of the levee extending through the pervious layer. SLIDE calculates the flow perpendicular to this vertical

section. For the case of L_1 = 200 ft, the flow lines are not exactly horizontal beneath the midpoint of the levee, and the flow calculated by SLIDE is slightly less than the total flow beneath the levee. This can be remedied by drawing the flux section parallel to the total head contours at this point beneath the levee.

This artifact of SLIDE is further shown in Figure A-41. These analyses were performed for the same boundary conditions as the previous figure, except that the length of the semipervious blanket has been increased to 1000 ft. The net result of this is to decrease the flow, and the equipotential lines are vertical in the location of the flux section. This causes the calculated flow to be the same as blanket theory for high permeability ratios. A comparison of the way that SLIDE and SEEP/W calculate flows is provided later in this report.

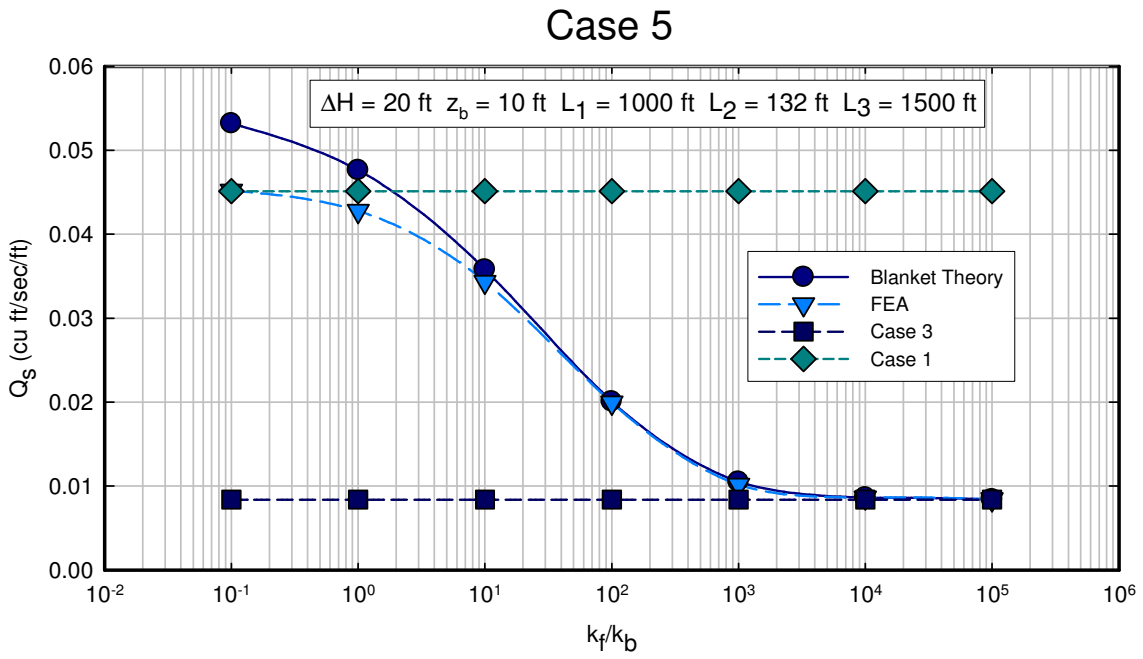

Figure A-39 Calculated values of flow per unit length (Q_s) for various permeability ratios from blanket theory and finite element analysis for Case 5 for z_b = 10 ft and L_1 = 1000 ft.

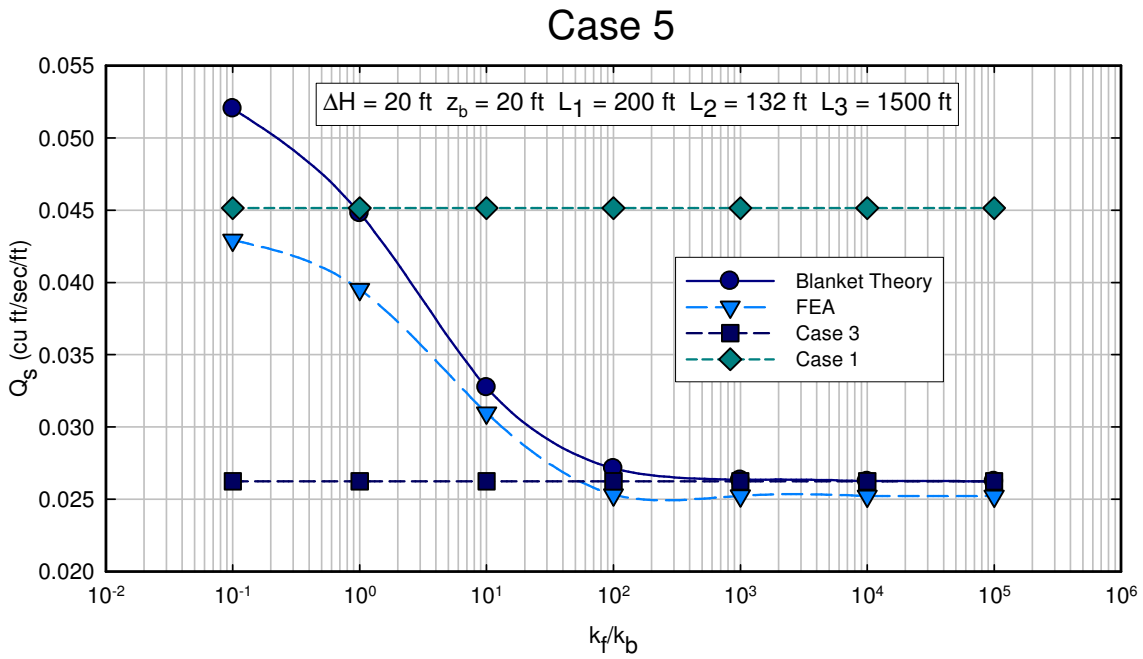

Figure A-40 Calculated values of flow per unit length (Q_s) for various permeability ratios from blanket theory and finite element analysis for Case 5 for z_b = 20 ft and L_1 = 200 ft.

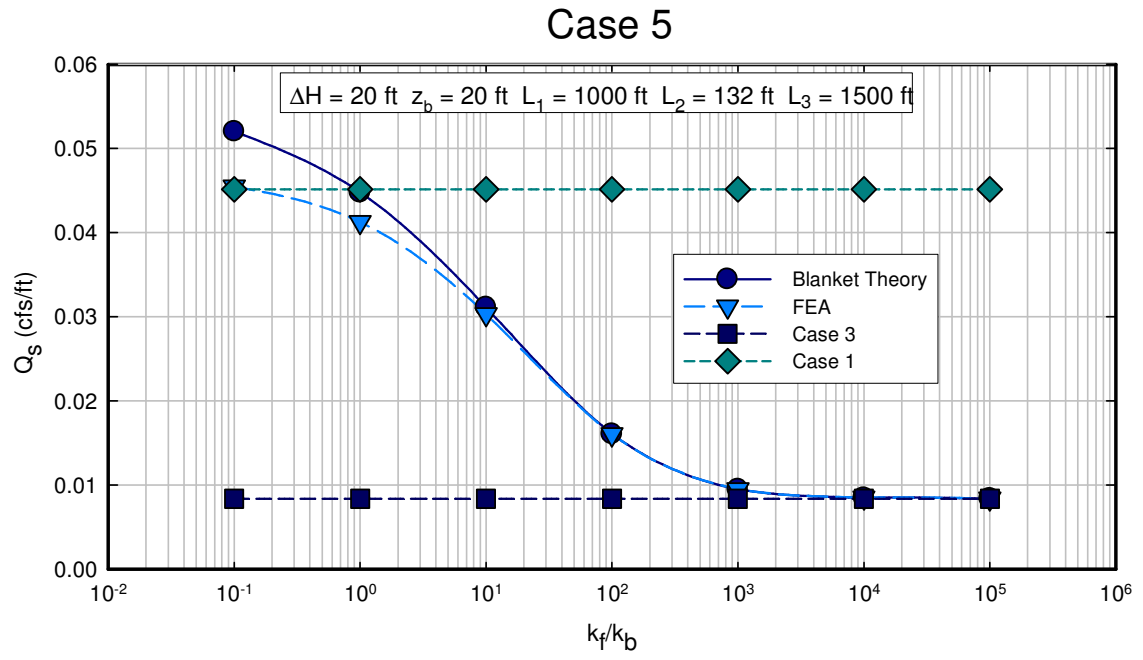

Figure A-41 Calculated values of flow per unit length (Qs) for various permeability ratios from blanket theory and finite element analysis for Case 5 for z_b = 20 ft and L_1 = 1000 ft.

Case 6 - Semipervious Landside Top Stratum and No Riverside Top Stratum

The geometry and finite element boundary conditions for Case 6 are shown in Figure A-42. This case has an L_1 dimension of infinity. An L_1 dimension of 1000 ft was used in the finite element model, because as shown earlier, that provides results that correctly approximate those of an infinite boundary condition for cases where no blanket exists.

As indicated in the "theory" section of this report, there is an inconsistency in EM 1110-2-1913 regarding the Case 6 solution. The head at a distance x cannot be calculated by assuming a linear head loss. The head is dependent on the landward side boundary conditions (i.e., infinite length of landside top stratum, open or blocked seepage exit). However, for this analysis, finite values of L_3 were used because an open seepage exit is shown in the figure B-6 of EM-1110-2-1913. The analyses were performed with L_3 values of 200 ft, 500 ft, and 1000 ft. Blanket thicknesses of 10 ft and 20 ft were analyzed, and permeability ratios (k_f/k_b) from 0.1 to 100,000 were used.

The phreatic surface on the protected side was assigned to the ground surface at the far vertical boundary. This is different than that shown in EM 1110-2-1913 on Figure B-6 on page B-15. Based on the way that the change in head is defined, the phreatic surface on the landside would have to be at the interface between the blanket and the pervious layer. For the FEA, the phreatic surface was assigned to the ground surface such that only flow through saturated media would occur. If the phreatic surface was set at the interface between the pervious layer and the blanket, then the analysis would have been a free surface analysis, with the phreatic surface being within the landside blanket.

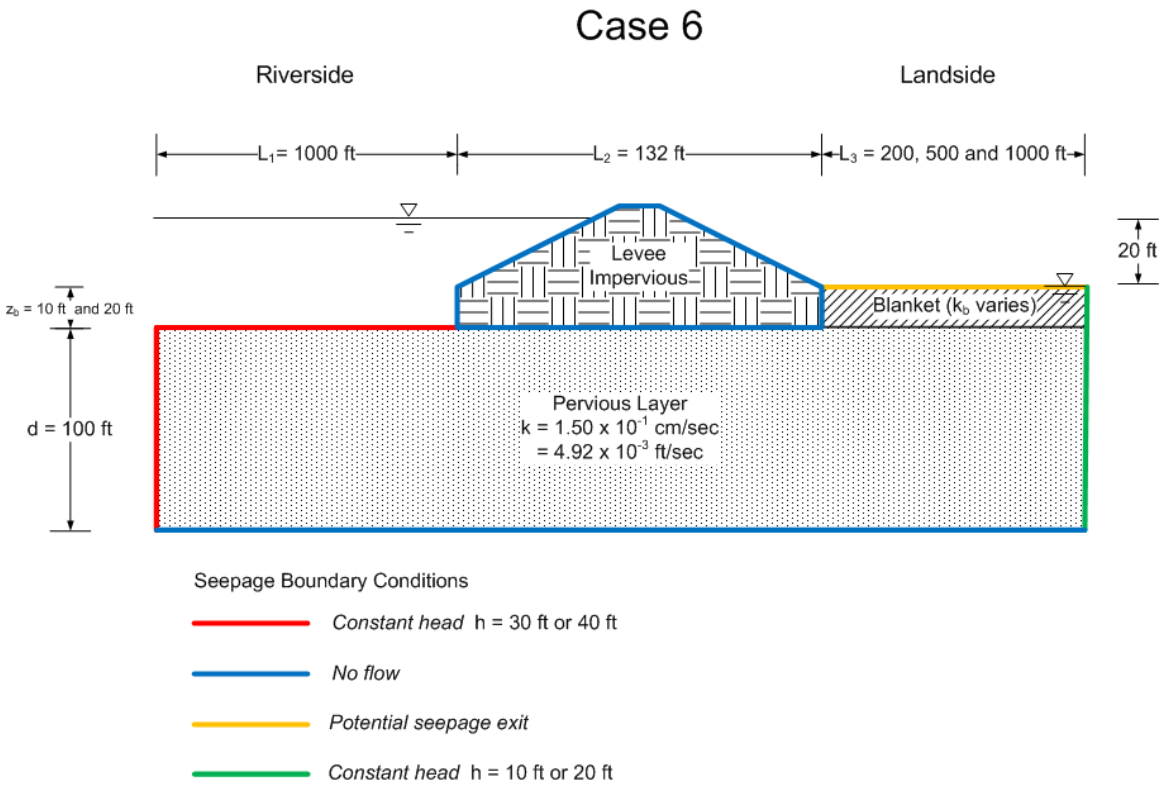

Figure A-42 Geometry for Case 6 - Semi-pervious landside top stratum and no riverside top stratum.

Shown in Figure A-43 are the calculated volumetric flow rates (Q_s) for L_3 = 1000 ft and z_b = 10 ft. As was the case for Case 5, the finite element results are bracketed by the results for Case 1 (no blankets) and Case 4 (impervious landside blanket). At a permeability ratio of about 4000, the landside blanket is effectively impervious, and the solution for Case 4 would apply.

Figure A-44 shows the results for a similar analysis with a blanket thickness of 20 ft. The results of all combinations of blanket thicknesses and L_3 dimensions produced reasonable results, with flow values decreasing with increasing values of z_b and L_3.

For Case 6 and Case 7, the value of the excess head at the toe of the levee is perhaps the most important value calculated from a seepage analysis since this parameter affects the factor of safety for heave and for erosion. The head directly beneath the toe of the levee at the interface

between the semipervious blanket and the pervious layer was calculated using FEA and blanket theory, and the results for z_b = 10 ft and L_3 = 1000 ft are shown in Figure A-45. As was the case with the calculated flows, the excess head at the toe is bracketed by the results of the Case 1 and Case 4 solutions.

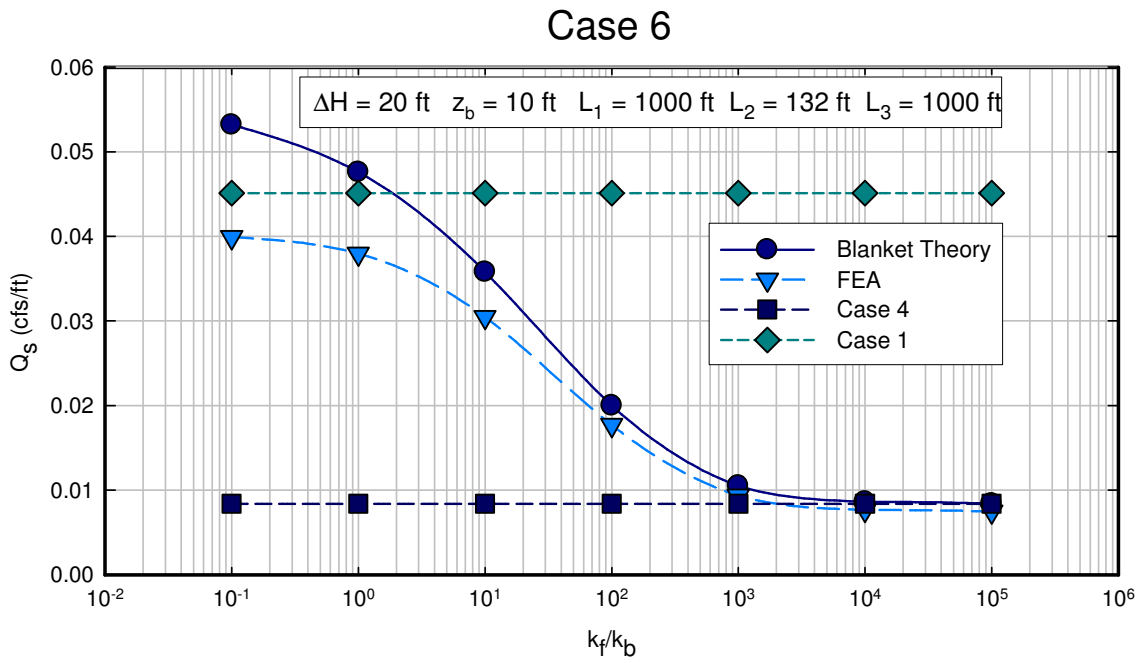

Figure A-43 Calculated values of flow per unit length (Q_s) for various permeability ratios from blanket theory and finite element analysis for Case 6 for z_b = 10 ft and L_3 = 1000 ft.

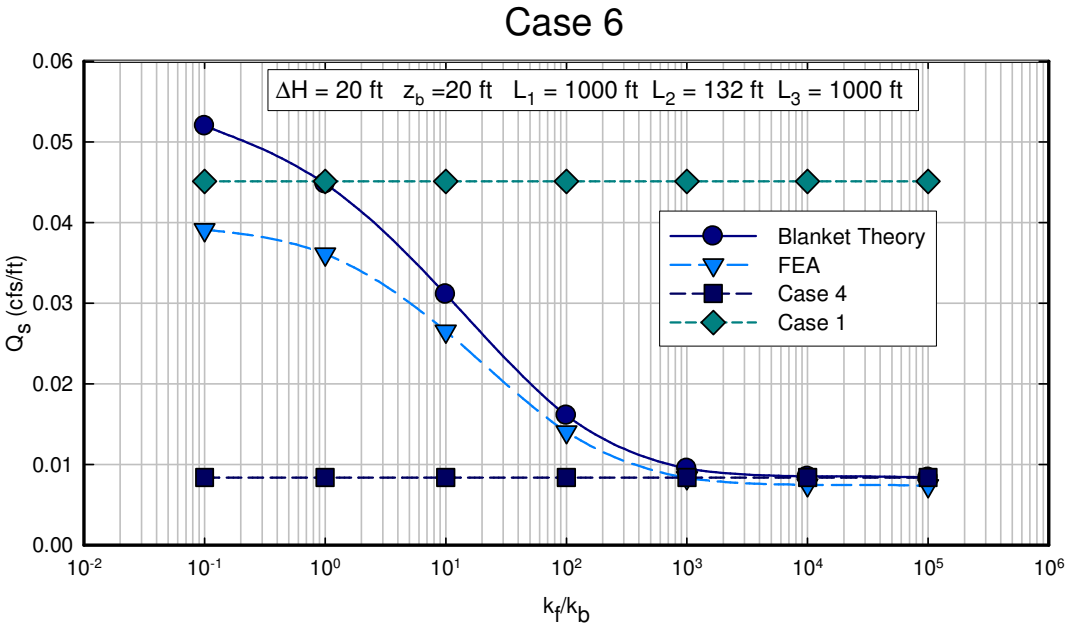

Figure A-44 Calculated values of flow per unit length (Q_s) for various permeability ratios from blanket theory and finite element analysis for Case 6 for z_b = 20 ft and L_3 = 1000 ft.

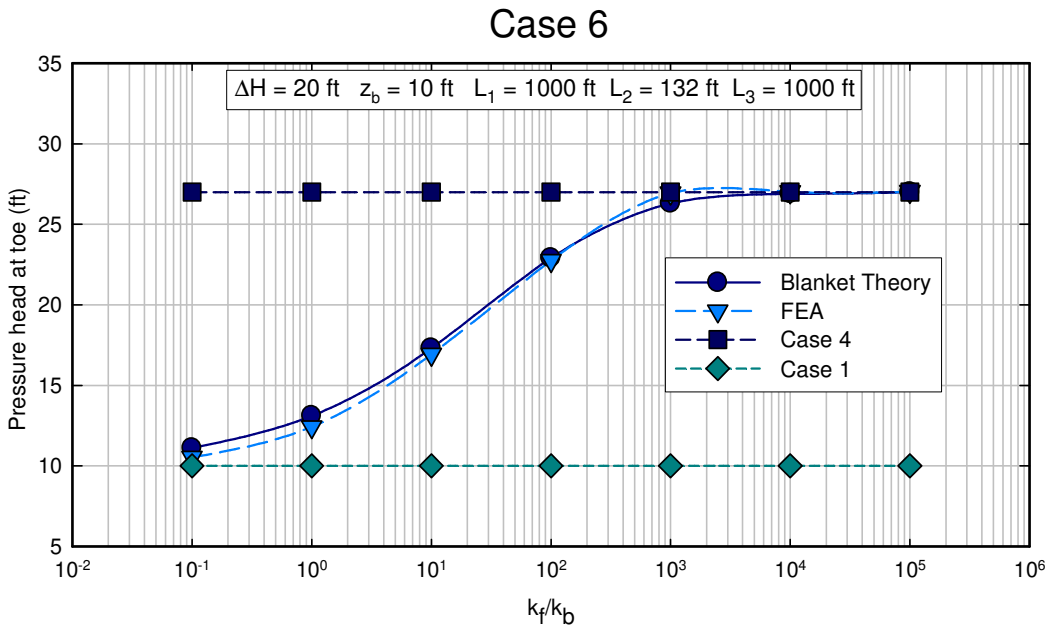

Figure A-45 Excess head (h_o) or pressure head beneath blanket at toe for Case 6 calculated using FEA and blanket theory for different permeability ratios for z_b = 10 ft and L_3 = 1000 ft.

The agreement between blanket theory and finite element analysis for Case 6 is very close. The calculated heads are closer than the flow values presented earlier because the heads are not influenced by the specific technicalities of the flow calculations used in SLIDE. Figure A-46 shows the calculated head values for the same boundary conditions, except the thickness of the blanket is increased to 20 ft. Again, the agreement between FEA and blanket theory is very good. The results of the Case 6 analyses indicate that if the geometry of the problem is similar to that assumed in the blanket theory derivations, correct values of excess head at the toe, and the associated factors of safety for erosion and heave, would be the same for FEA and blanket theory for the same hydraulic boundary conditions. When the permeability of the blanket is about 4000 times less than the pervious layer, the blanket is essentially impervious, and the Case 4 equations can be used.

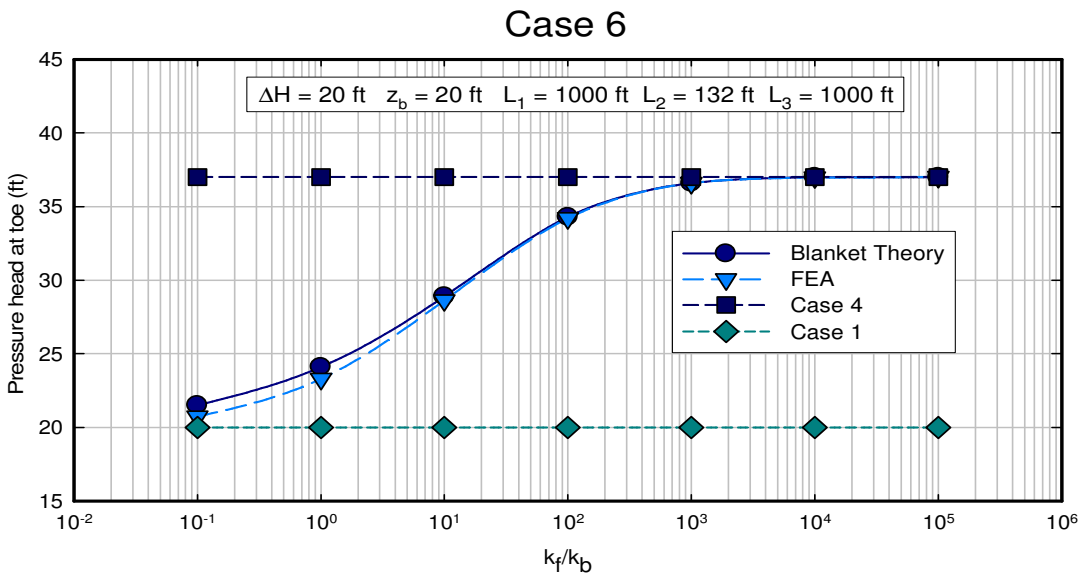

Figure A-46 Pressure head beneath blanket at toe for Case 6 calculated using FEA and blanket theory for different permeability ratios for z_b = 20 ft and L_3 = 1000 ft.

The FEA can further be compared to blanket theory for Cases 6 by examining the values of x_3. The value of x_3 is defined as the horizontal distance from the landside toe of the levee to the

location where the head at the bottom of the blanket is equal to the landside phreatic surface. This value is important because x_3 would be used as a coordinate for the piezometric grade line (PGL) to model the pore pressures in the pervious layer for a slope stability analysis. Instead of comparing only the value of x_3, it is convenient to compare blanket theory with FEA by plotting the hydraulic head at the interface between the pervious layer and blanket. For Case 6, this would be a linear relationship for blanket theory (based on current equation present in EM), from a value of $\Delta H + z_b$ at the riverside toe of the levee to a head value of z_b at the x_3 distance. However, if we use the equation similar to Case 7c for Case 6 to determine head at distance x as explained in "theory" portion of the report, this would no longer be linear due to the vertical flow occurring through semipervious top stratum. Hence two separate lines are plotted in the Figures A-47 through A-49 to indicate these two scenarios. The line labeled "Blanket Theory" is based on current equation present in EM while the line labeled "Corrected Blanket Theory" is based on the equation calculating head in a similar manner as Case 7c.Similarly, the line labeled as "FEA" shows the head values for the nodes at the interface and will also be non-linear.

Shown in Figure A-47 is the PGL for Case 6 where L_3 = 200 ft, z_b = 10 ft, and k_f/k_b = 10. Beneath the levee, the PGL for blanket theory is above that determined from FEA. At a point about 60 ft landward from the levee toe, the head predicted by blanket theory is less than that predicted by FEA. In general, the PGL predicted using blanket theory appears to be a conservative approximation of the true PGL. This would mean that the pore pressures calculated using the blanket theory PGL would be greater than those determined by FEA, and lower factors of safety would result from slope stability analyses. However, the PGL predicted by corrected blanket theory is closer to FEA than by blanket theory and becomes equal to FEA at about 120 ft landward of the levee toe and beyond.

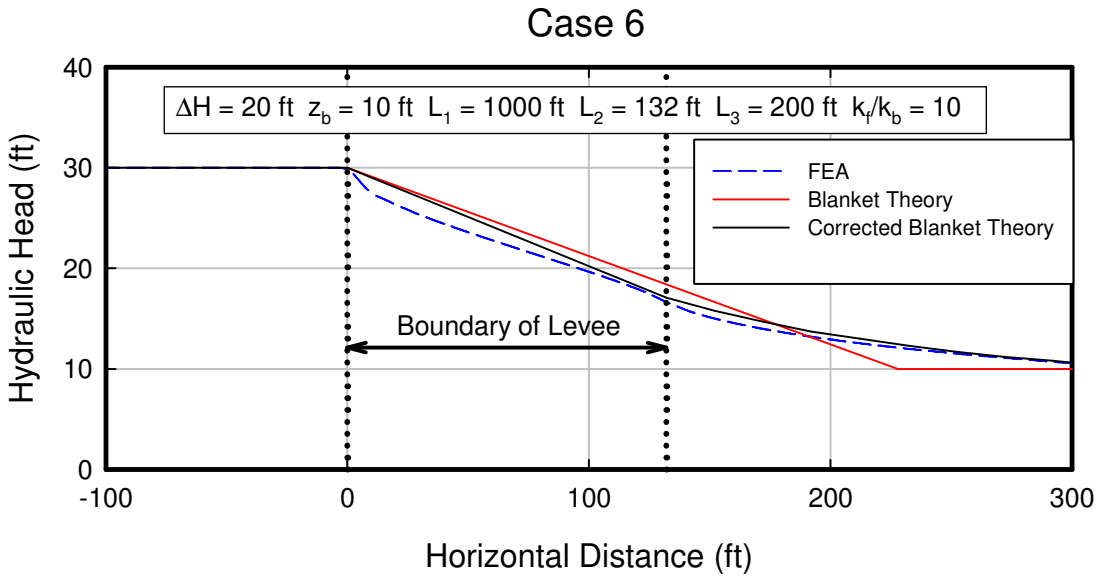

Figure A-47 Piezometric grade line for Case 6 where L_3 = 200 ft, z_b = 10 ft, and k_f/k_b = 10.

Figure A-48 shows a similar plot, except that the permeability ratio is equal to 1000. As the permeability ratio increases, the value of x_3 increases, and the point where the PGL from blanket theory exceeds the PGL from FEA increases. For these boundary conditions, the PGLs cross at about 170 ft landward from the toe of the levee. As was the case for the previous example, the PGL determined using blanket theory appears to be a conservative approximation of the true piezometric surface.

Figure A-49 shows the results from the same analysis, except that L_3 was increased to 500 ft. Increasing the value of L_3 also serves to increase the distance where the PGL predicted by blanket theory and FEA are equivalent.

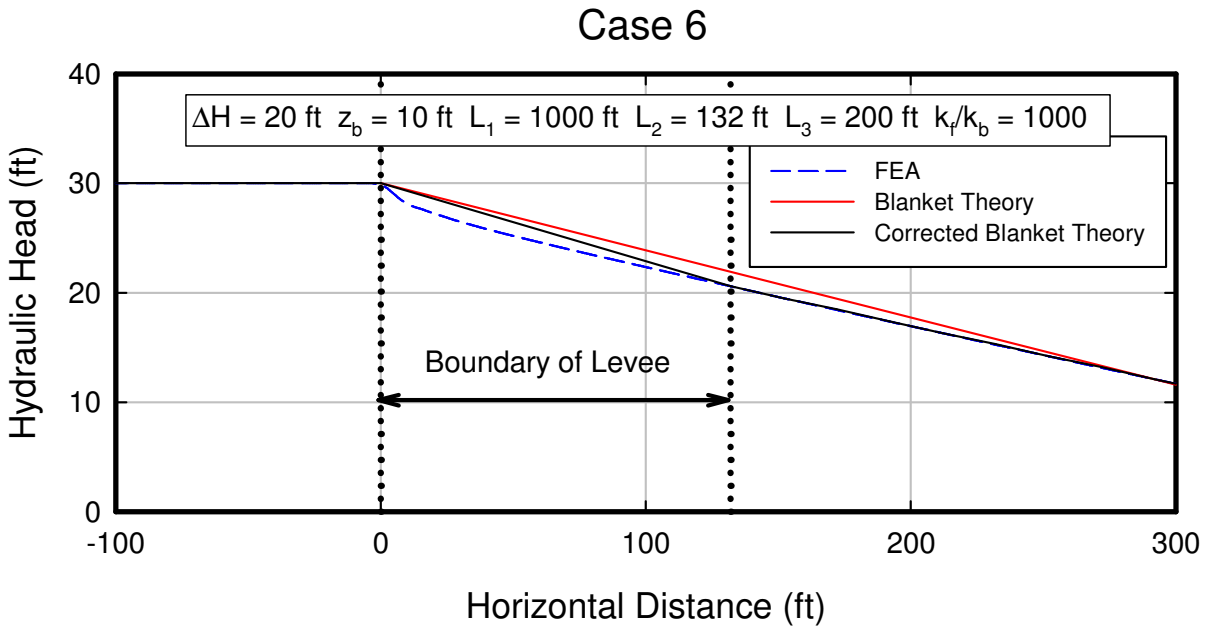

Figure A-48 Piezometric grade line for Case 6 where L_3 = 200 ft, z_b = 10 ft, and k_f/k_b = 1000.

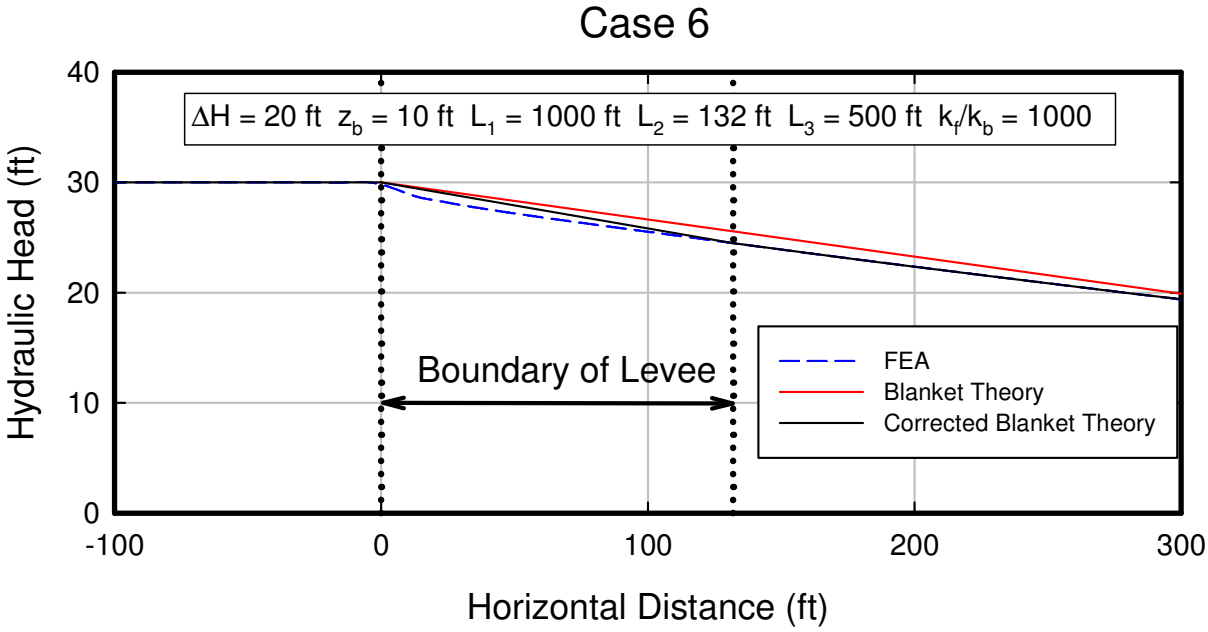

Figure A-49 Piezometric grade line for Case 6 where L_3 = 500 ft, z_b = 10 ft, and k_f/k_b = 1000.

Case 7 – Semipervious Top Strata on Riverside and Landside.

Case 7, as defined in EM 1110-2-1913, is subdivided into three subcases depending on the landside boundary conditions. Case 7a has an infinite L_3 dimension. Case 7b contains a seepage block (impervious boundary) at a distance L_3 from the toe. Case 7c assumes a defined value of L_3. These cases will be described separately in the following text.

Case 7a – Semi-pervious landside and riverside top stratum (top stratum extends infinitely landward of the levee)

Figure A-50 shows the basic geometry for Case 7a. Constant head boundary conditions were assigned to the riverside ground surface and the riverside domain vertical boundary. An L_1 value of 500 ft was used in all analyses. An L_3 value of 2500 ft was used in the finite element analysis to simulate an infinite boundary condition for the case of a blanket overlying a pervious layer. The thickness of the pervious layer (d) was 100 ft in all analyses.

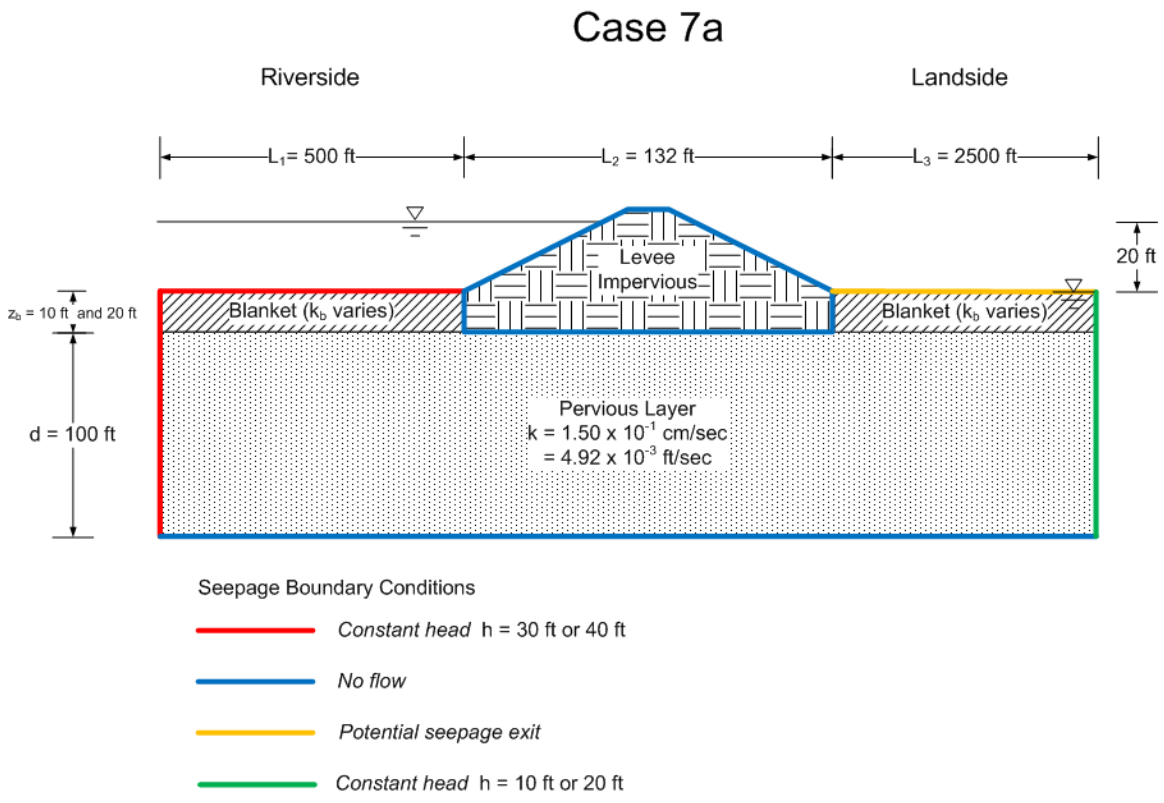

Figure A-50 Geometry and finite element boundary conditions for Case 7a.

The main parameter varied in these analyses was the permeability of the semipervious blankets. Permeability ratios (k_f/k_b) ranging from 0.1 to 100,000 were used. The same permeability was applied to both the upstream and downstream blankets.

The phreatic surface was assumed to be at the ground surface on the landside. A constant head, equal to the ground surface elevation, was assigned to the far landside vertical boundary. The nodes on the horizontal landside ground surface were assigned *potential seepage exit* conditions. The riverside nodes, both on the horizontal ground surface and at the vertical domain boundary, were assigned constant heads equal to the landside head plus 20 ft, so that ΔH = 20 ft for the analysis.

The calculated volumetric flow rate per unit length (Q_s) is plotted in Figure A-51 for both the finite element and blanket theory solutions as a function of permeability ratio. The finite element analysis results are bracketed by the Case 1 and Case 2 results. The flows calculated by the blanket theory exceed the Case 1 results at a permeability ratio of about 2. The Case 2 results shown on the figure were calculated assuming an L_3 = 2500 ft to be consistent with the FEA. Blanket theory agrees well with the FEA results for permeability ratios greater than about 100. For permeability ratios less than 100, the flows calculated by blanket theory are greater than calculated by the FEA, but that could be partially due to the way that SLIDE calculates flow values.

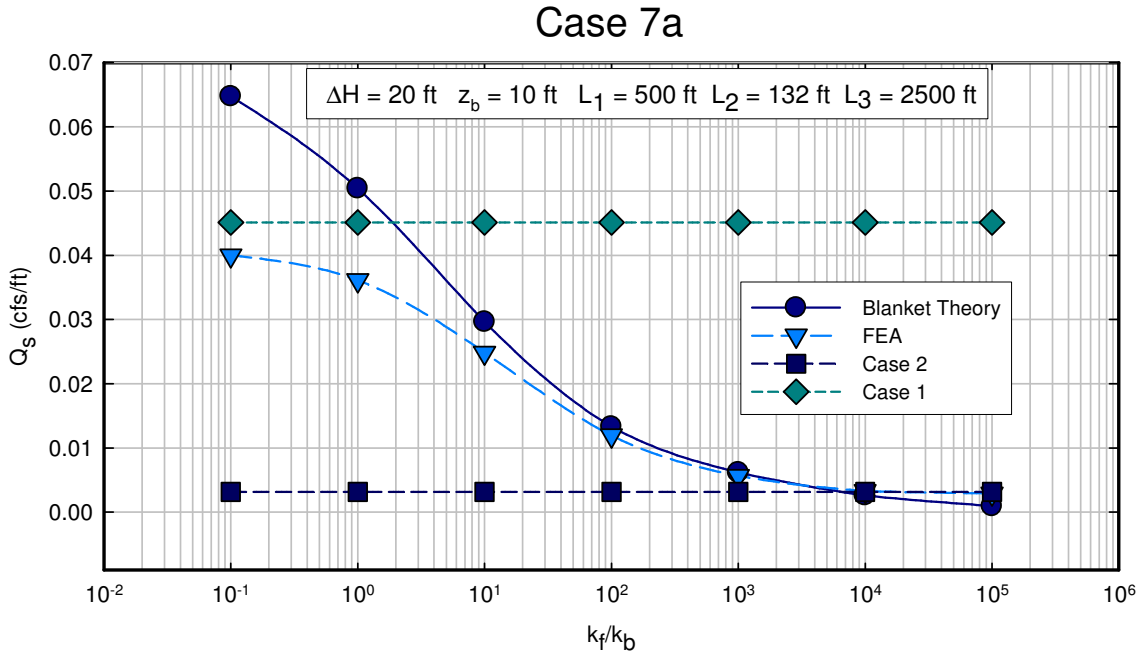

Figure A-51 Calculated values of flow per unit length (Q_s) for various permeability ratios from blanket theory and finite element analysis for Case 7a for z_b = 10 ft and L_1 = 500 ft.

Shown in Figure A-52 is an analysis identical to the previous one, but the thickness of the riverside and landside blankets has been increased to 20 ft. The results are similar to that

obtained for a blanket thickness of 10 ft, except that the Case 5 blanket theory intersects the Case 2 results at a permeability ratio of 1. Again, good agreement is obtained between blanket theory and FEA.

Figure A-53 shows the calculated pressure head beneath the toe of the levee at the top of the pervious layer for a blanket thickness of 10 ft. There is generally good agreement between blanket theory and FEA. The difference above permeability ratios of about 10,000 may be due to the fact that an L_3 = 2500 ft may not have been large enough to model infinity. However, this permeability ratio is outside of the range that Case 7a would be applicable. Overall, these results indicated that equivalent exit gradients would be obtained using either blanket theory or FEA.

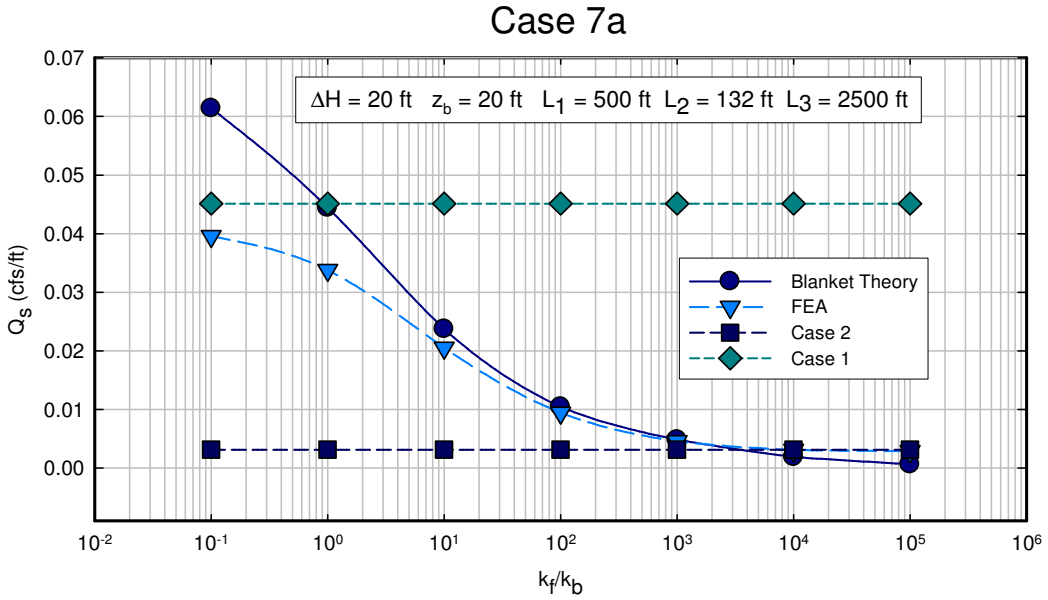

Figure A-52 Calculated values of flow per unit length (Q_s) for various permeability ratios from blanket theory and finite element analysis for Case 7a for z_b = 20 ft and L_1 = 500 ft.

Figure A-54 shows essentially the same results for a blanket thickness of 20 ft. Again, there is good agreement between blanket theory and FEA for the boundary conditions used.

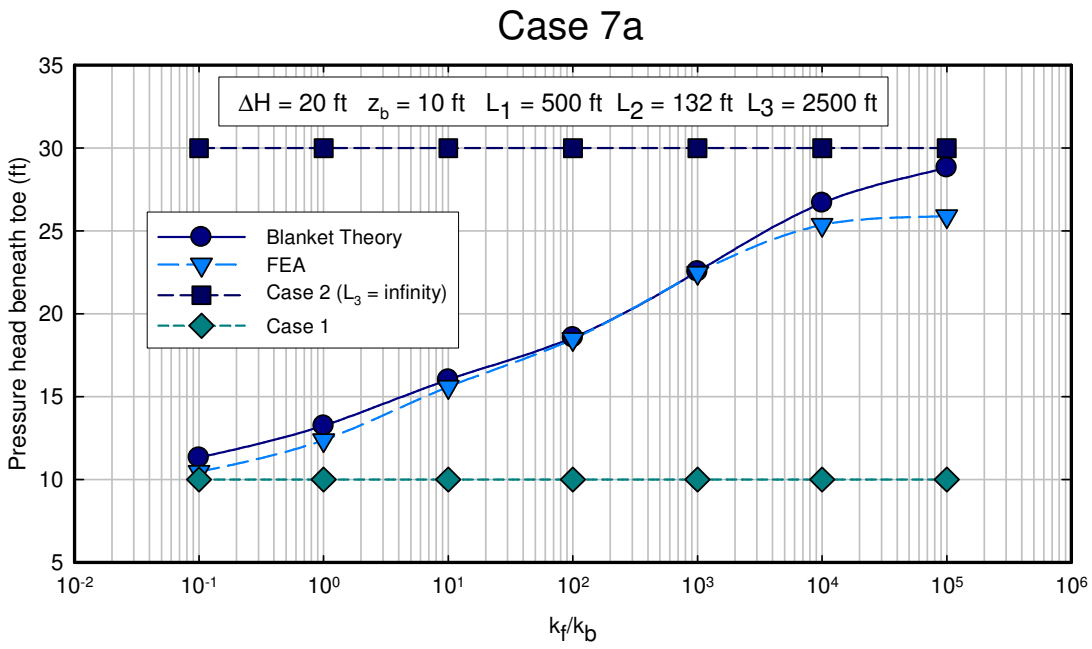

Figure A-53 Excess head (h_o) or pressure head beneath blanket at toe for Case 7a calculated using FEA and blanket theory for different permeability ratios for z_b = 10 ft and L_1 = 500 ft.

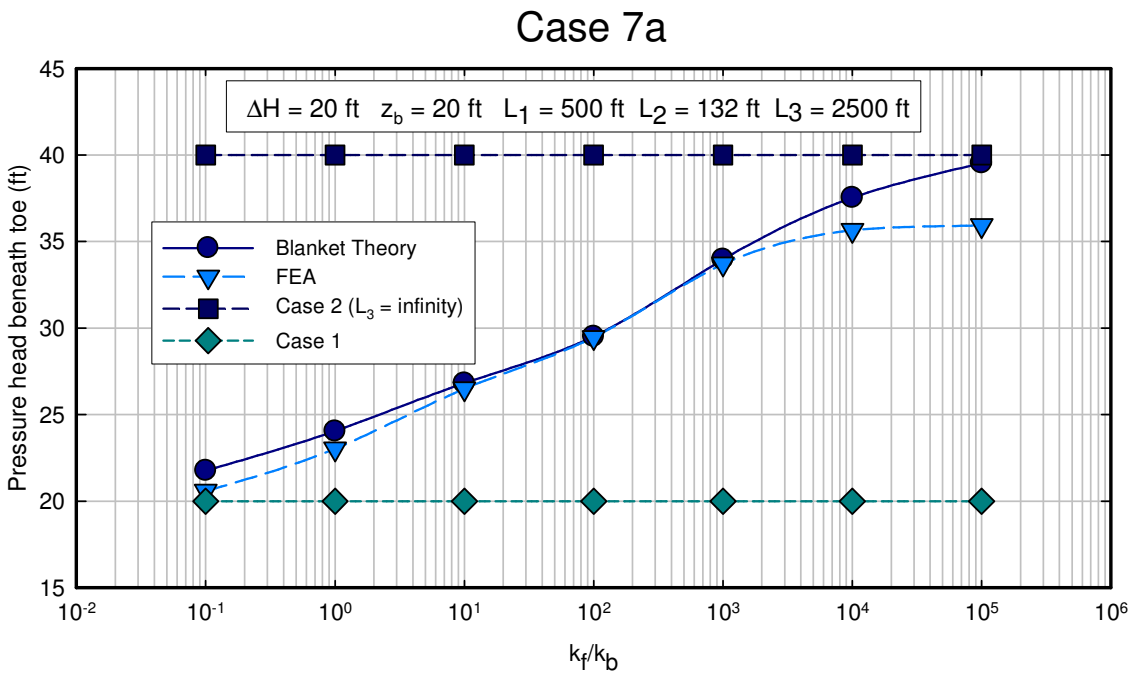

Figure A-54 Excess head (h_o) or pressure head beneath blanket at toe for Case 7a calculated using FEA and blanket theory for different permeability ratios for z_b = 20 ft and L_1 = 500 ft.

The PGL that is predicted using blanket theory for Case 7a can be assessed using the results of the FEA. Since a finite value of L_3 was used in the FEA to model an infinite boundary condition, it is more logical to compare the PGL for Cases 7b and 7c since both of these cases use a finite value of L_3.

Case 7b – Semi-pervious landside and riverside top stratum (seepage block in the pervious substratum located landward of the levee)

Figure A-55 shows the basic geometry for Case 7b. This case differs from Case 7a in that a seepage block (impervious vertical boundary) is located at a distance L_3 from the landside levee toe. In order for this to be modeled using the finite element method, the far nodes on the vertical boundary were assigned *no-flow* boundary conditions. The nodes on the horizontal landside ground surface were assigned *potential seepage exit* conditions. The riverside nodes, both on the horizontal ground surface and at the vertical domain boundary, were assigned constant heads equal to the landside head plus 20 ft, so that $\Delta H = 20$ ft for the analysis.

An L_1 value and an L_3 value of 500 ft were used in all analyses. The thickness of the pervious layer (d) was 100 ft. The main parameter varied in these analyses was the permeability of the semipervious blankets. Permeability ratios (k_f/k_b) ranging from 0.1 to 100,000 were used. The same permeability was applied to both the upstream and downstream blankets.

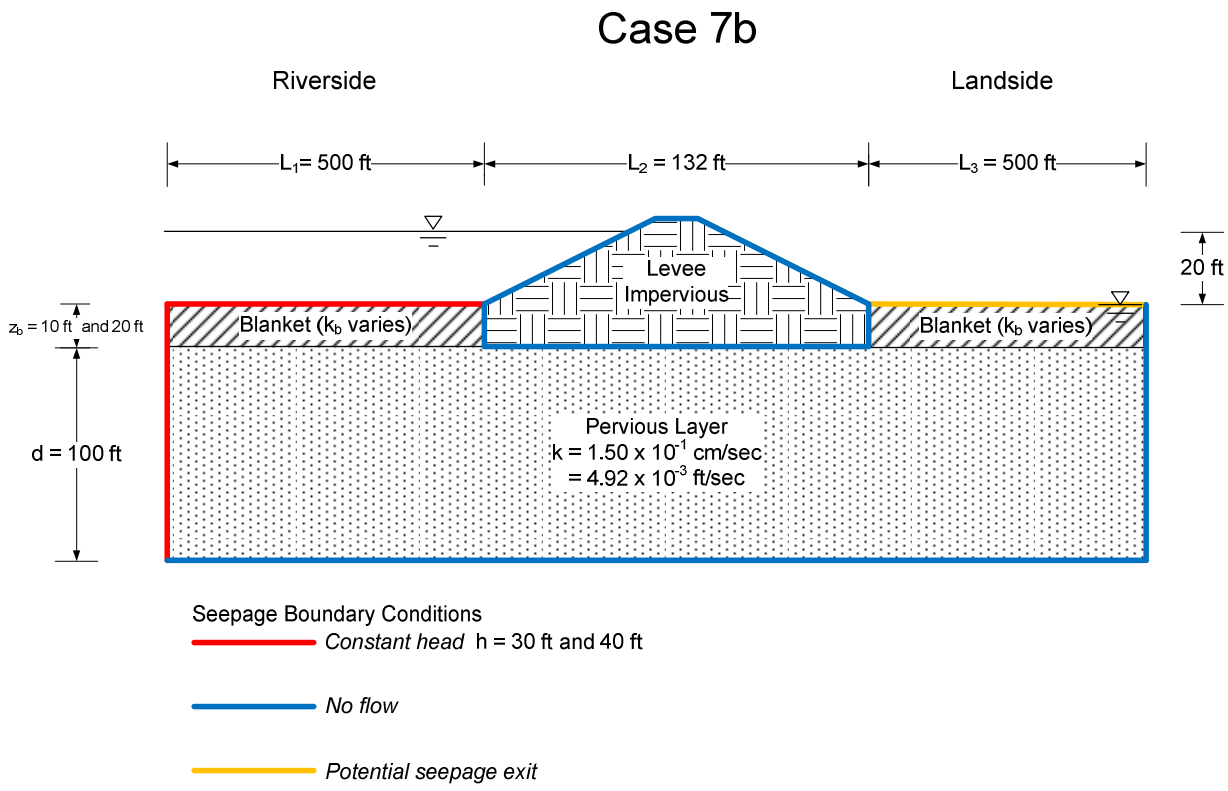

Figure A-55 Geometry and finite element boundary conditions for Case 7b.

The calculated volumetric flow rate per unit length (Q_s) is plotted in Figure A-56 for both the finite element and blanket theory solutions as a function of permeability ratio. The finite element analysis results reach an approximate asymptote at the Case 1 solution. However, similar to what was found for Case 7a, the flows calculated by the blanket theory exceed the Case 1 results at a permeability ratio of about 2. For permeability ratios less than about 100, blanket theory produces larger flows than FEA. For permeability ratios greater than this, the calculated flow is approximately the same.

Figure A-57 shows the same general analysis, but with the thickness of the riverside and landside blanket increased to 20 ft. The agreement between the blanket theory and FEA flow values are generally very good for permeability ratios greater than about 100.

Figure A-58 shows the heads beneath the toe of the levee for blanket theory and FEA for a blanket thickness of 10 ft. As can be seen, the head values agree very well. Figure A-59 shows the results for the same boundary conditions for a blanket thickness of 20 ft. Again, there is generally a good agreement between the pressure heads calculated using blanket theory and FEA.

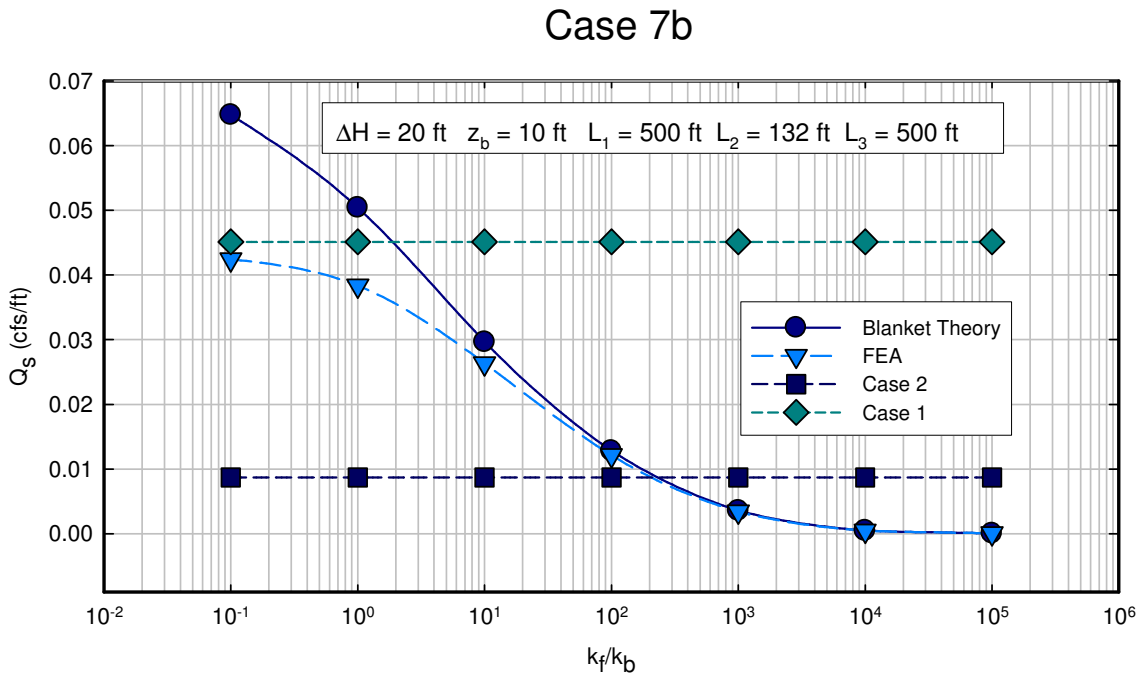

Figure A-56 Calculated values of flow per unit length (Q_s) for various permeability ratios from blanket theory and finite element analysis for Case 7b for z_b = 10 ft and L_1 = 500 ft and L_3 = 500 ft.

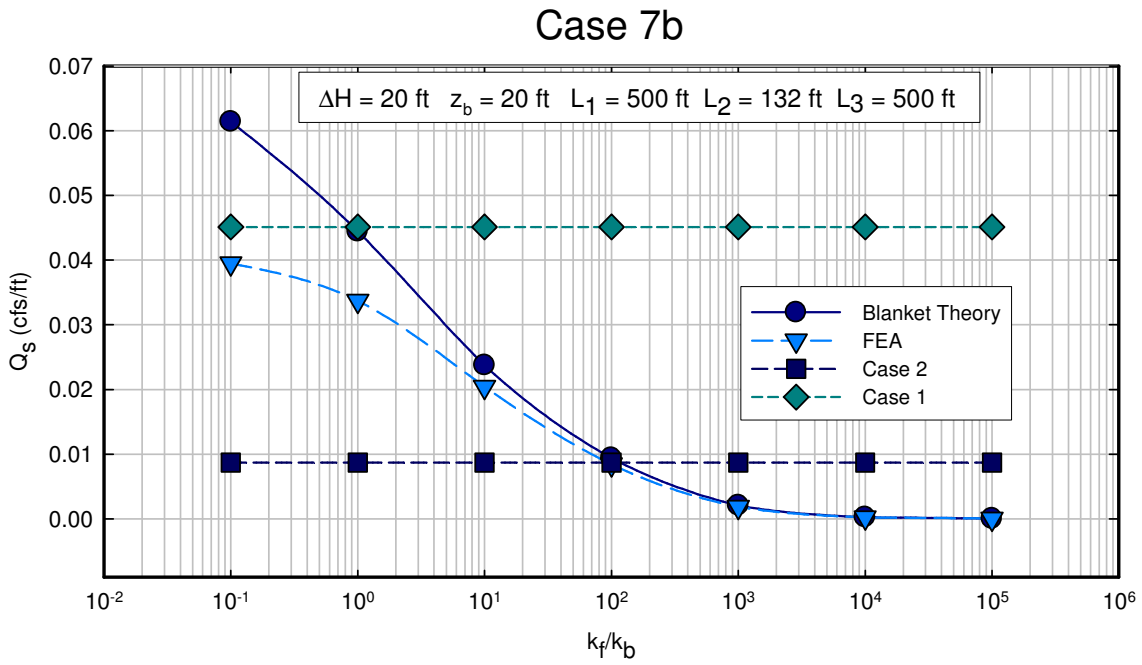

Figure A-57 Calculated values of flow per unit length (Q_s) for various permeability ratios from blanket theory and finite element analysis for Case 7b for z_b = 20 ft and L_1 = 500 ft and L_3 = 500 ft.

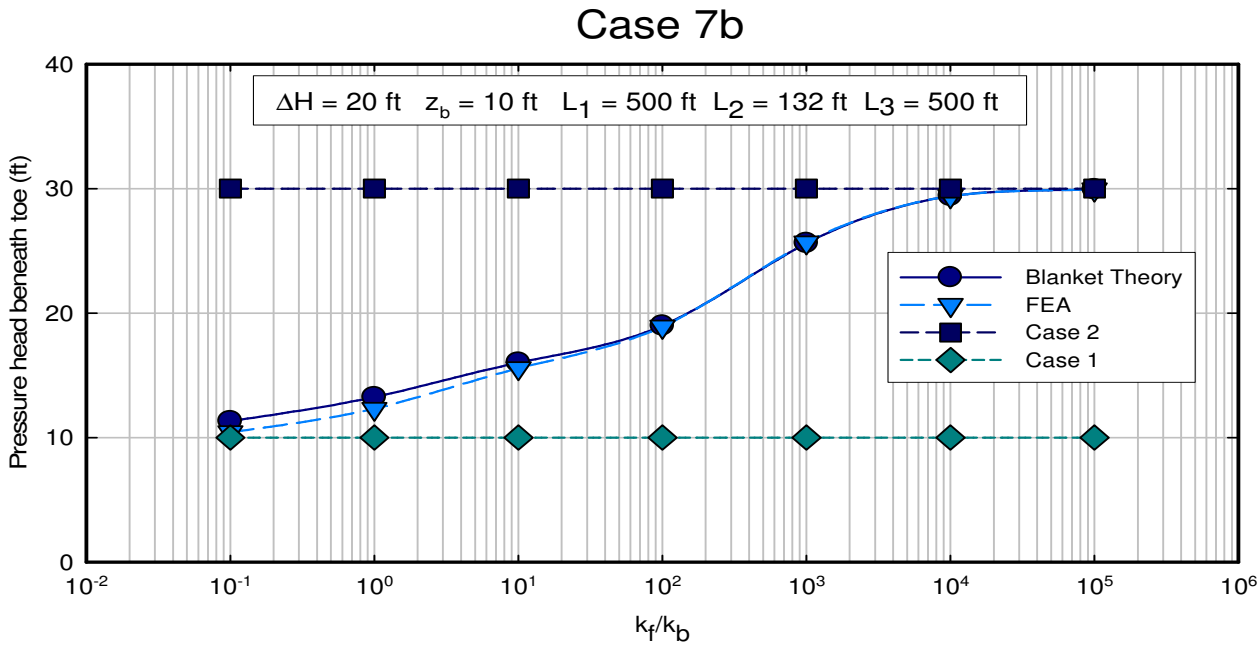

Figure A-58 Excess head (h_o) or pressure head beneath blanket at toe for Case 7b calculated using FEA and blanket theory for different permeability ratios for z_b = 10 ft, L_1 = 500 ft, and L_3 = 500 ft.

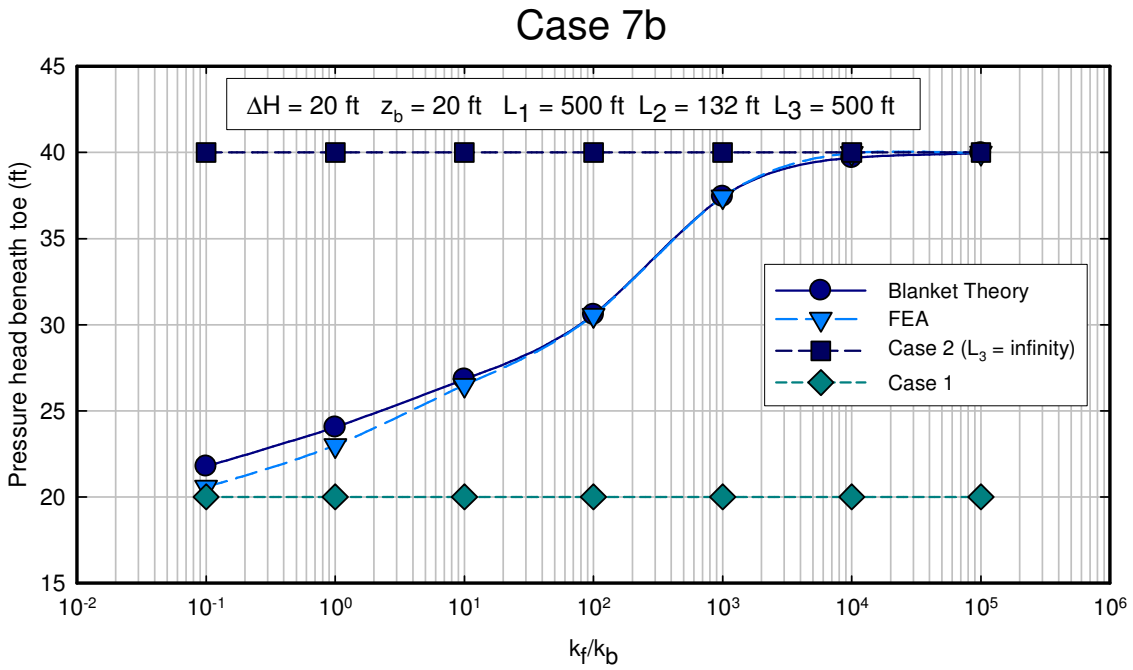

Figure A-59 Excess head (h_o) or pressure head beneath blanket at toe for Case 7b calculated using FEA and blanket theory for different permeability ratios for z_b = 20 ft, L_1 = 500 ft, and L_3 = 500 ft.

Case 7c - Semi-pervious landside and riverside top stratum (seepage exit in the pervious substratum located landward of the levee)

The geometry and finite element boundary conditions for Case 7c are shown in Figure A-60. This case is essentially the same as Case 7a except that a finite value of L_3 is used. The general boundary conditions are the same for Case 7c as for Case 7a.

For Case 7c, an L_1 value of 500 ft and an L_3 value of 500 ft were used in the analysis. The thickness of the pervious layer (d) was 100 ft and the thickness of the blanket (z_b) was 10 ft and 20 ft. The permeability of the blanket was varied in the analysis, and permeability ratios ranging from 0.1 to 100,000 were used.

Shown in Figure A-61 are the volumetric flow rates calculated using blanket theory and finite element analysis for the range of permeability ratios. There is excellent agreement between blanket theory and FEA for permeability ratios greater than 100, and both methods converge to the Case 2 solution (impervious blanket). The difference between blanket theory and FEA increases as the permeability of the blanket becomes closer to the permeability of the pervious layer. The FEA approximately converges to the Case 1 solution, but the blanket theory predicts higher flows than the Case 1 solution for permeability ratios less than 2.

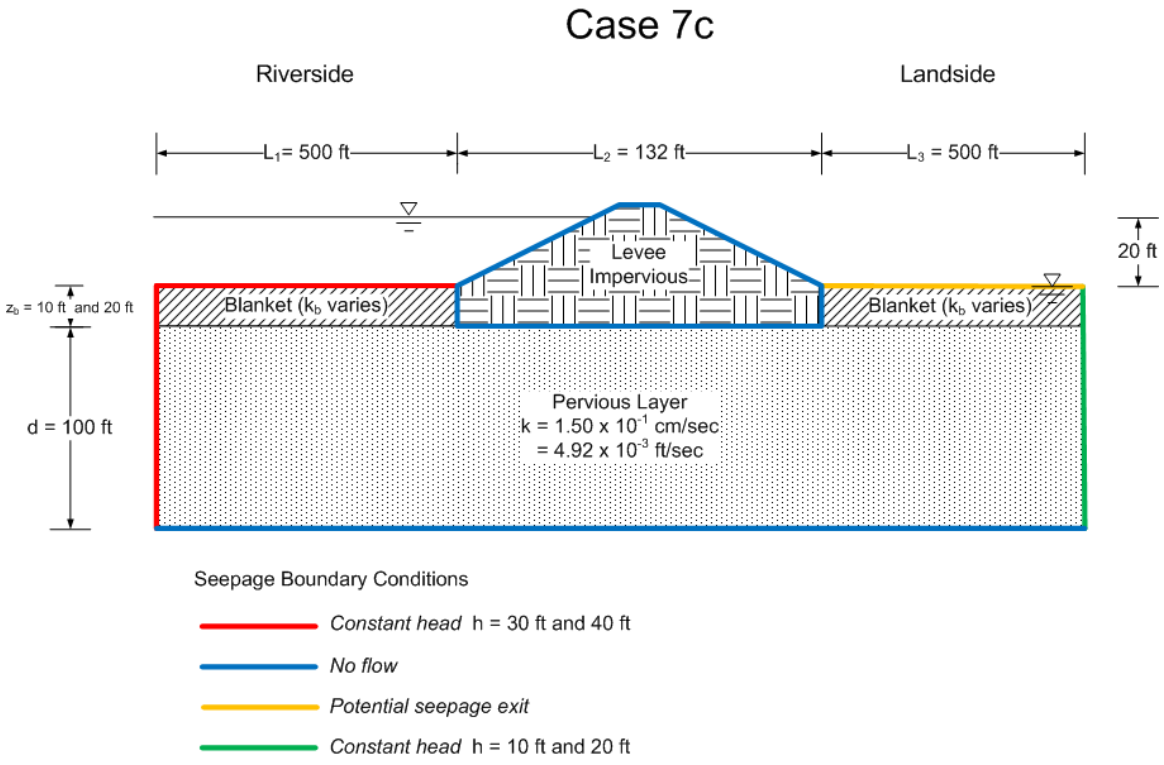

Figure A-60 Geometry and boundary conditions for Case 7c.

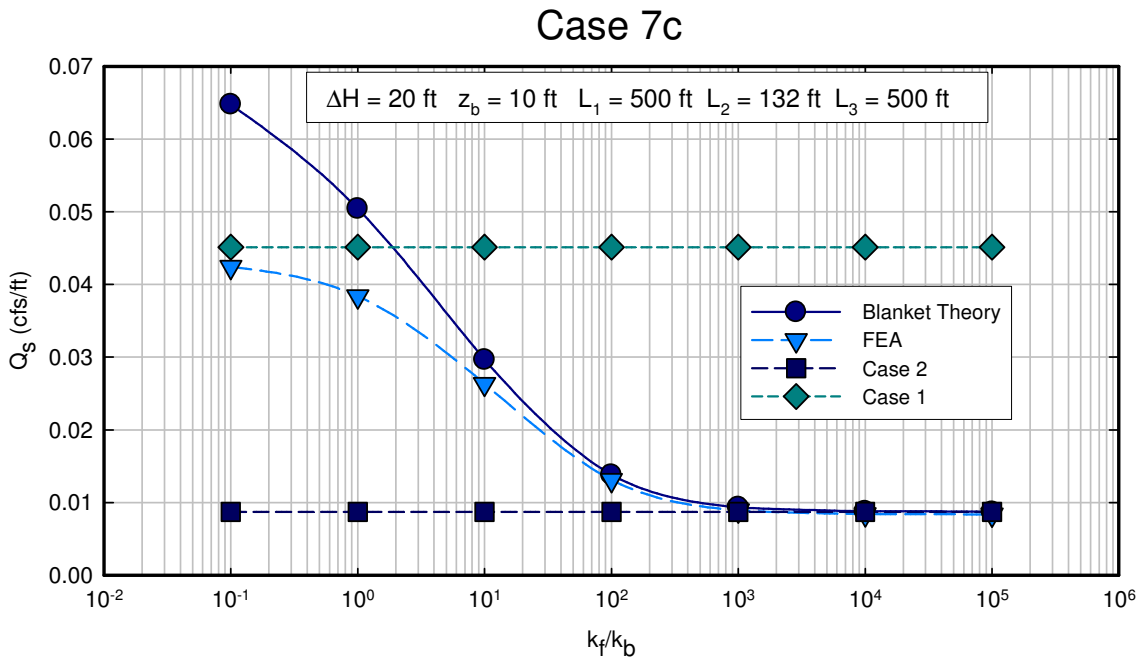

Figure A-61 Calculated values of flow per unit length (Q_s) for various permeability ratios from blanket theory and finite element analysis for Case 7c for z_b = 10 ft and L_1 = 500 ft and L_3 = 500 ft.

Figure A-62 shows a plot for the results using the same boundary conditions as the previous analysis, except that the thickness of the semipervious blanket was increased to 20 ft. As has been the rule for previous cases, the blanket theory predicts higher flows for low permeability ratios. The value of permeability ratio where the Case 7c and Case 2 analyses are equal is about unity.

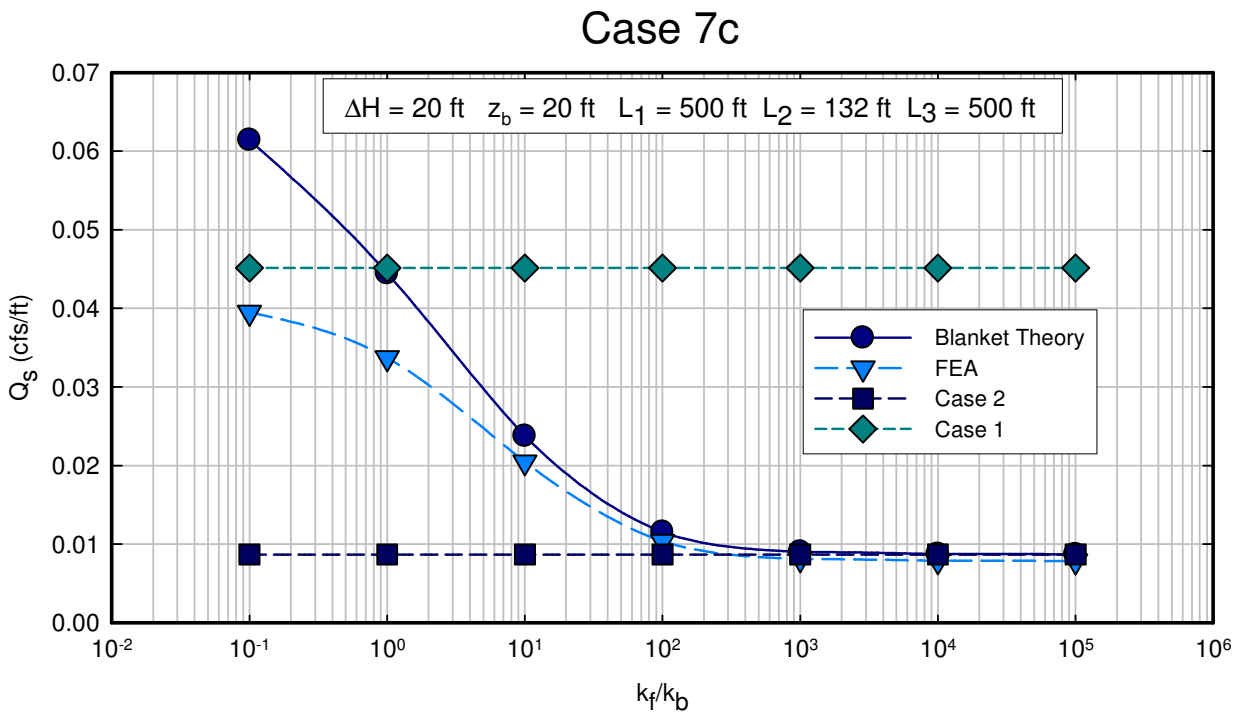

Figure A-62 Calculated values of flow per unit length (Q_s) for various permeability ratios from blanket theory and finite element analysis for Case 7c for z_b = 20 ft and L_1 = 500 ft and L_3 = 500 ft.

Figure A-63 shows the pressure head beneath the toe of the levee at the top of the pervious layer for different permeability ratios. Again, the heads calculated with blanket theory and FEA are in close agreement for permeability ratios greater than 100, and the difference increases for smaller values of permeability ratio. The exit gradients calculated using blanket theory would be generally greater than or equal to those calculated by FEA. Figure A-64 shows the results for the same conditions, except the thickness of the blanket is 20 ft. The same general trends are evident.

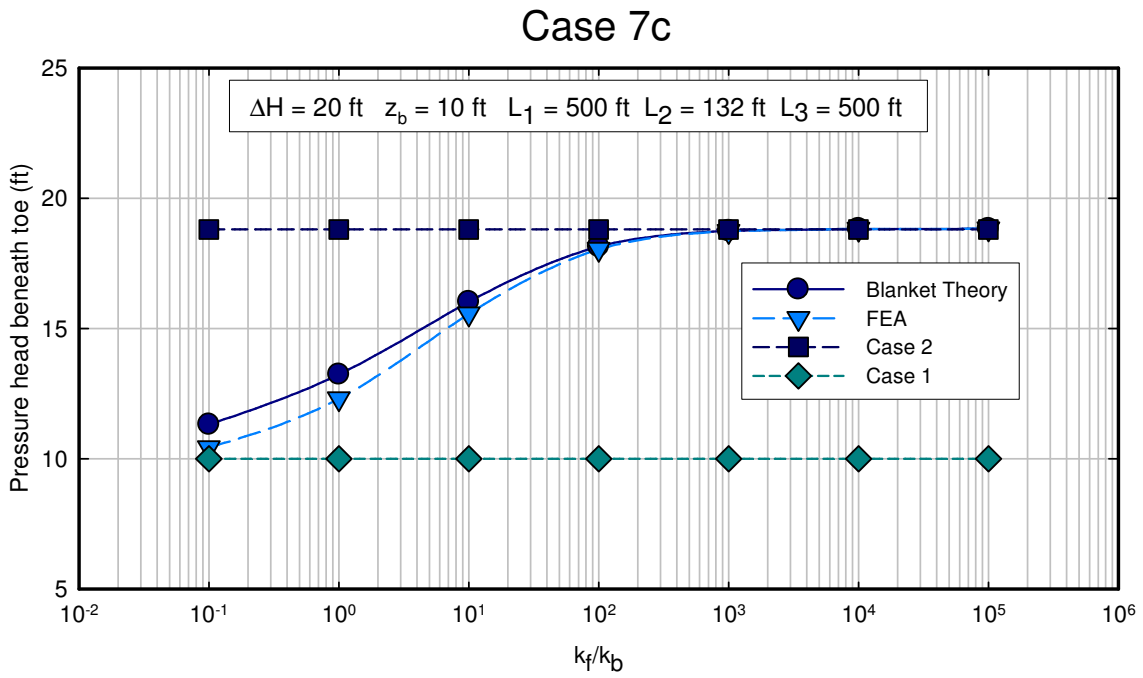

Figure A-63 Excess head (h_o) or pressure head beneath blanket at toe for Case 7c calculated using FEA and blanket theory for different permeability ratios for z_b = 10 ft, L_1 = 500 ft, and L_3 = 500 ft.

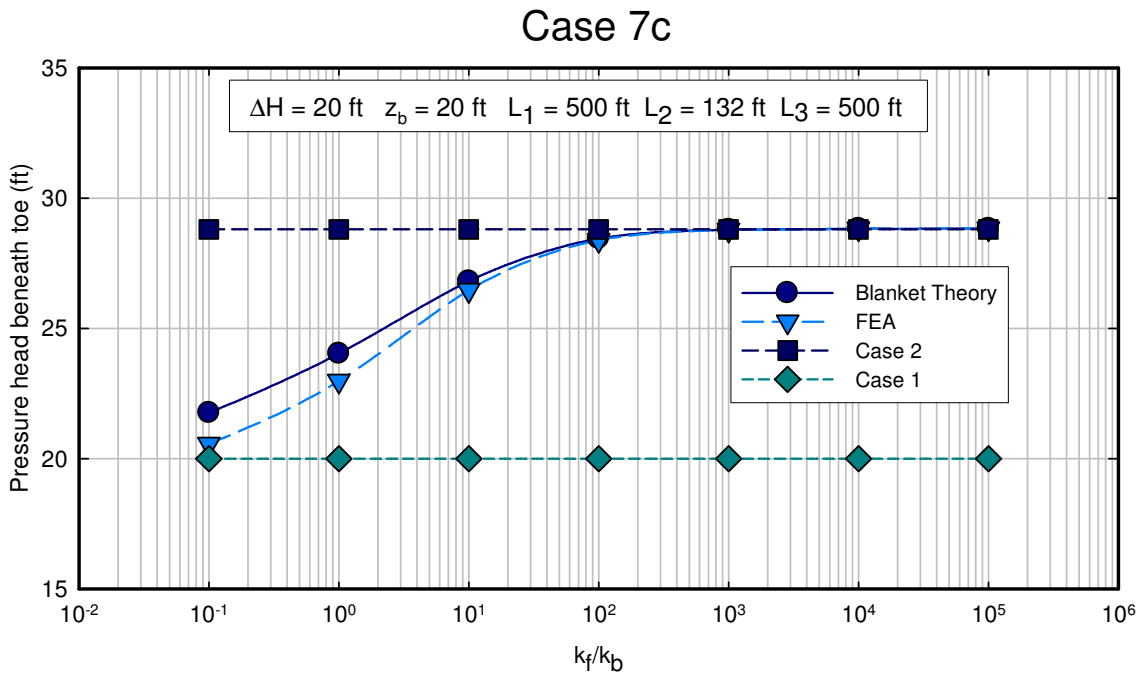

Figure A-64 Excess head (h_o) or pressure head beneath blanket at toe for Case 7c calculated using FEA and blanket theory for different permeability ratios for z_b = 20 ft, L_1 = 500 ft, and L_3 = 500 ft.

Figure A-65 shows the pressure head as a function of horizontal distance at the blanket/pervious layer interface calculated using blanket theory and FEA. The agreement between the two methods is excellent underneath the levee, and for a distance of about 50 ft from the toe of the levee. At horizontal distances greater than 50 ft from the toe, the solutions diverge. Toward the riverside, blanket theory provides higher heads than FEA. Toward the landside, FEA provides higher pressure heads than blanket theory.

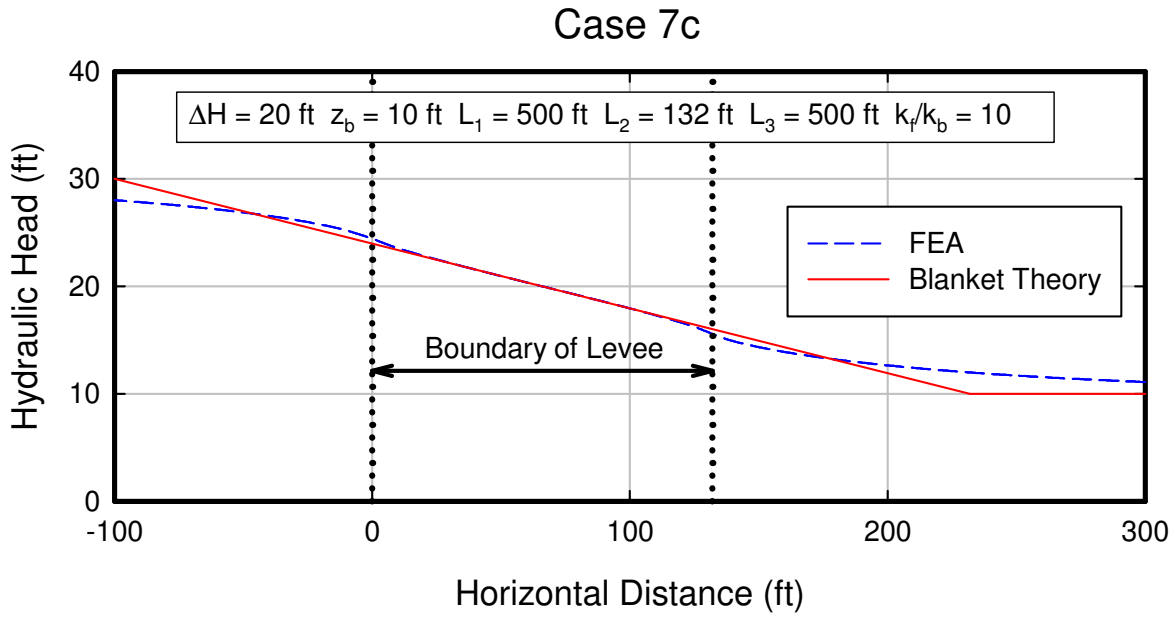

Figure A-65 Pressure head at the top of the pervious layer for Case 7c calculated with finite element analysis and blanket theory for z_b = 10 ft and k_f/k_b = 10.

The agreement between blanket theory and FEA is still better with increasing permeability ratio. Shown in Figure A-66 are the results for the same boundary condition, except that the semipervious blanket is 1000 times less permeable that the pervious layer. For the range of horizontal distances plotted in the figure, the agreement is exact.

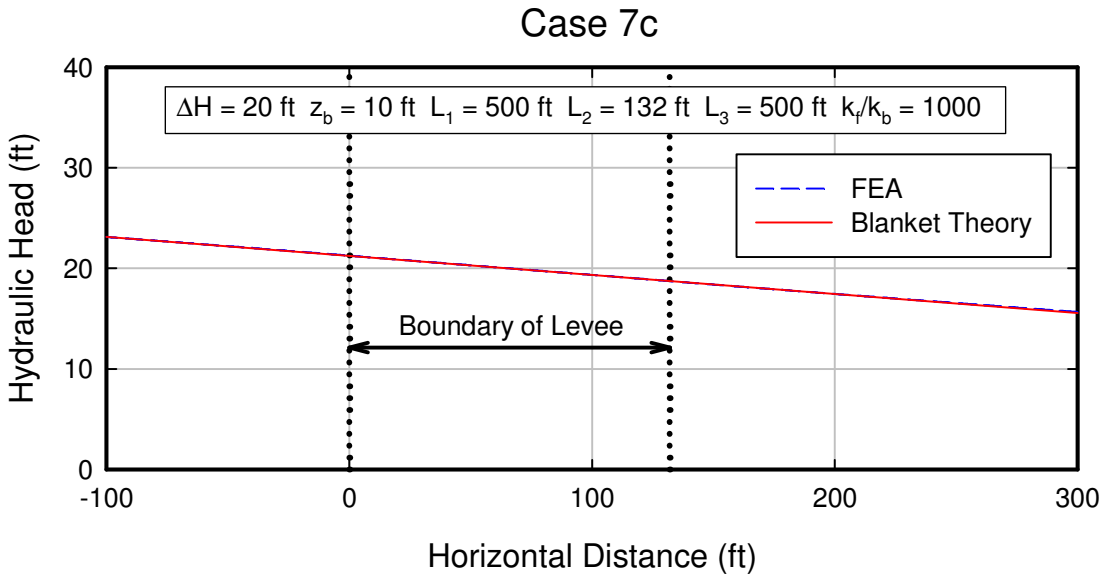

Figure A-66 Pressure head at the top of the pervious layer for Case 7c calculated with finite element analysis and blanket theory for z_b = 10 ft and k_f/k_b = 1000.

Case 8 – Semipervious Top Strata on Riverside and Landside.

Case 8 was developed as part of this study to increase the accuracy of seepage calculations for cases where sheet pile cutoffs are employed. Case 8 is basically Case 7 with the sheet pile cutoff added. Both have a semipervious layer on the riverside and the landside. Similar to Case 7, Case 8 has been subdivided into 8a (infinite landside dimension), 8b (seepage block at L_3), and 8c (finite L_3 dimension). The equations can be developed for different sheet pile penetrations into the pervious layer. The examples presented are for 50% penetration.

Since the difference between Cases 8a and Case 8c is the length of L_3, Case 8a will be omitted from the discussion. Cases 8b and 8c were analyzed with similar geometry. The only differences in the analysis are the landside boundary conditions at the edge of the domain. All analyses were conducted with L_1 and L_3 equal to 500 ft. The thickness of the pervious layer (d) was 100 ft and the thickness of the semipervious blanket was 10 ft. The permeability of the blanket was varied in the analysis, and permeability ratios ranging from 0.1 to 10,000 were used.

Comparisons of FEA and blanket theory were made based on calculated flows beneath the levee and pressure heads at the landside toe of the levee. A comparison of PGLs for FEA and blanket theory was not made for Case 8 because owing to the non-linearity of the PGL resulting from the inclusion of the cutoff wall.

Case 8b – Semi-pervious landside and riverside top stratum (seepage block in the pervious substratum located landward of the levee) with cutoff wall

Shown in

Figure A-67 are the geometry and boundary conditions for Case 8b. To model a seepage block, the landslide vertical boundary was assigned no-flow nodal boundary conditions.

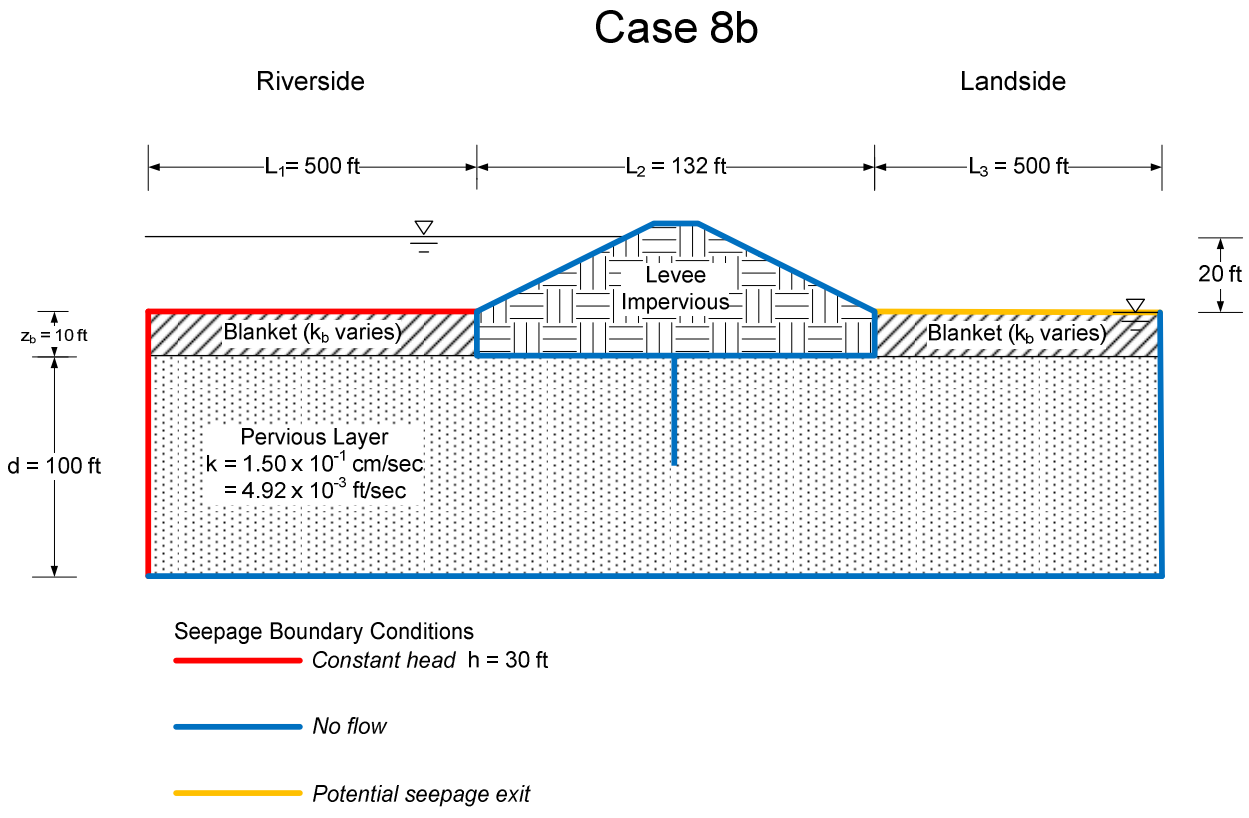

Figure A-67 Geometry and boundary conditions for Case 8b.

Figure A-68 shows the calculated flow underneath the levee as a function of permeability ratio. In general, the FEA analysis results in lower flow rates than blanket theory, as has been the case for other sections as well. Figure A-69 shows the pressure head beneath the landside toe of the levee. There is an excellent agreement between FEA and blanket theory, and both analysis methods would result in the same hydraulic gradient.

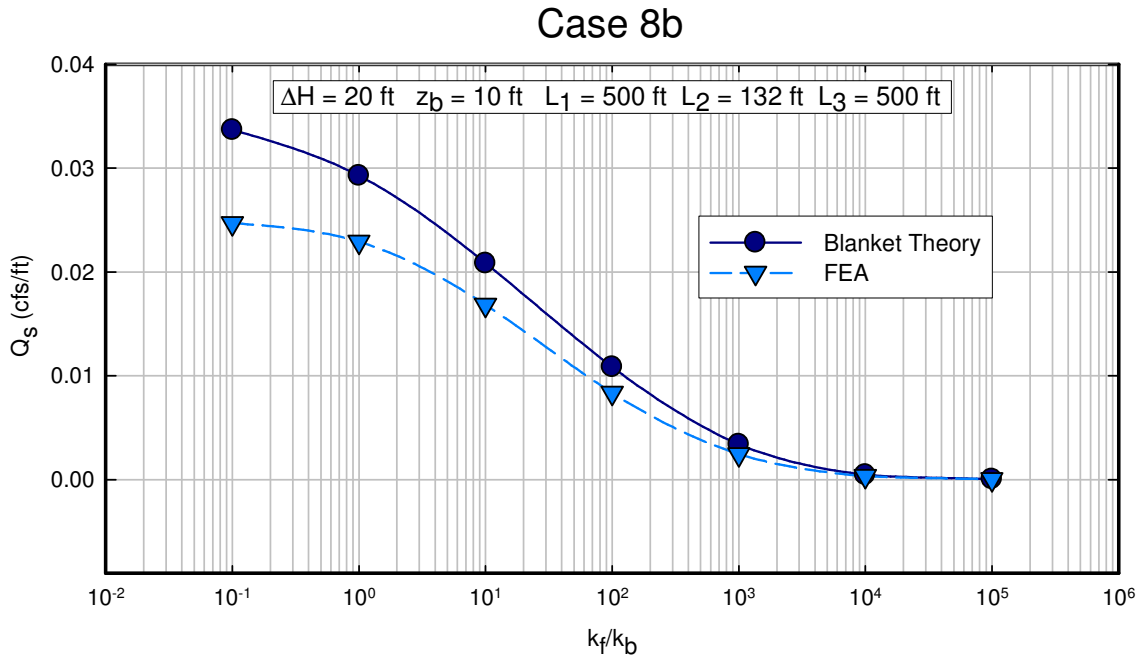

Figure A-68 Calculated values of flow per unit length (Q_s) for various permeability ratios from blanket theory and finite element analysis for Case 8b for z_b = 10 ft and L_1 = 500 ft and L_3 = 500 ft.

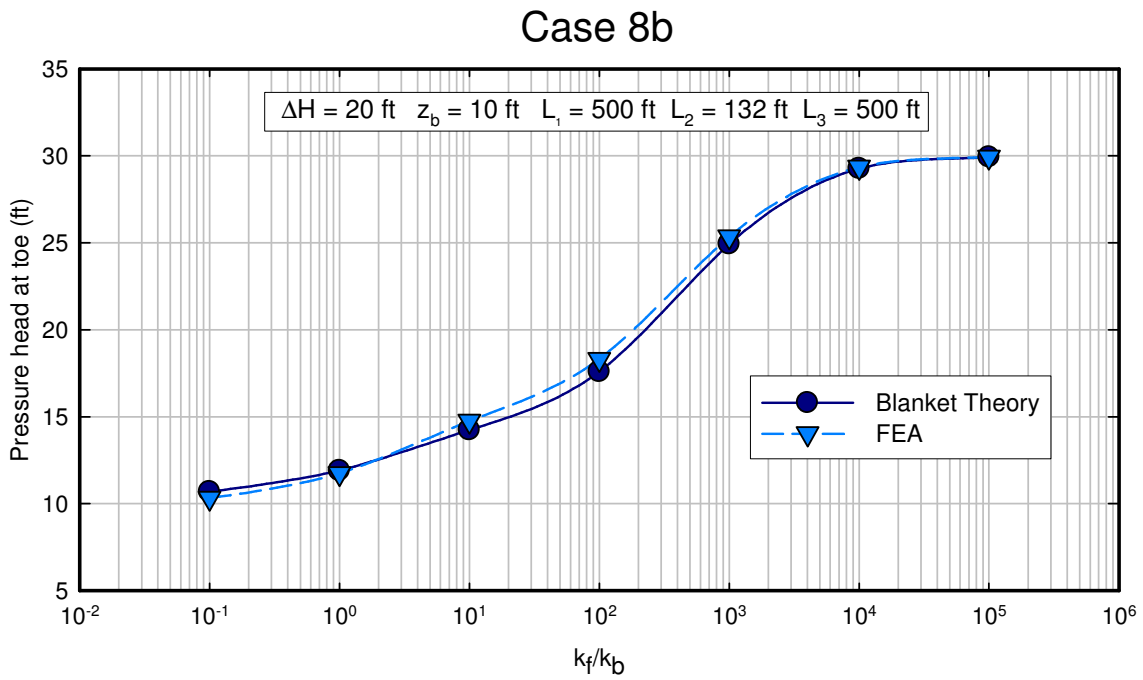

Figure A-69 Pressure head beneath blanket at toe for Case 8b calculated using FEA and blanket theory for different permeability ratios for z_b = 10 ft, L_1 = 500 ft, and L_3 = 500 ft.

Case 8c - Semi-pervious landside and riverside top stratum (seepage exit in the pervious substratum located landward of the levee) with cutoff wall

The geometry and boundary conditions for Case 8c is shown in Figure A-70. The boundary conditions are the same as for Case 7c except that no-flow boundary conditions are assigned to the cutoff wall.

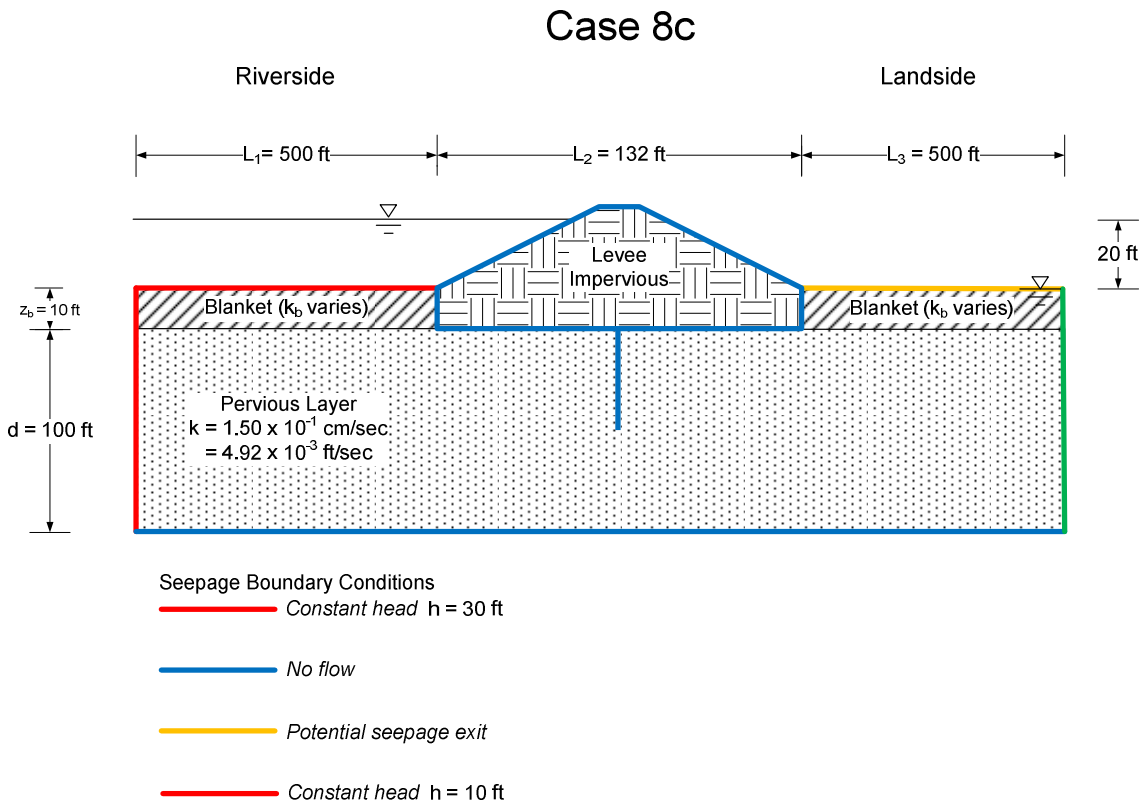

Figure A-70 Geometry and boundary conditions for Case 8c.

Figure A-71 shows flow underneath the levee calculated by FEA and blanket theory. The finite element analysis predicts less flow than blanket theory for every permeability ratio. This may possibly be due to the manner in which SLIDE calculates flow as being the flow perpendicular to a flux boundary. The agreement between blanket theory and pressure head beneath the landside toe of the levee was better (Figure A-72).

The results of the analyses conducted on Case 8 indicate that this new blanket theory case may be a viable method to calculate exit gradients and uplift pressures for cross sections containing cutoff walls, provided that the geometry is similar to that used for the derivation of the equations.

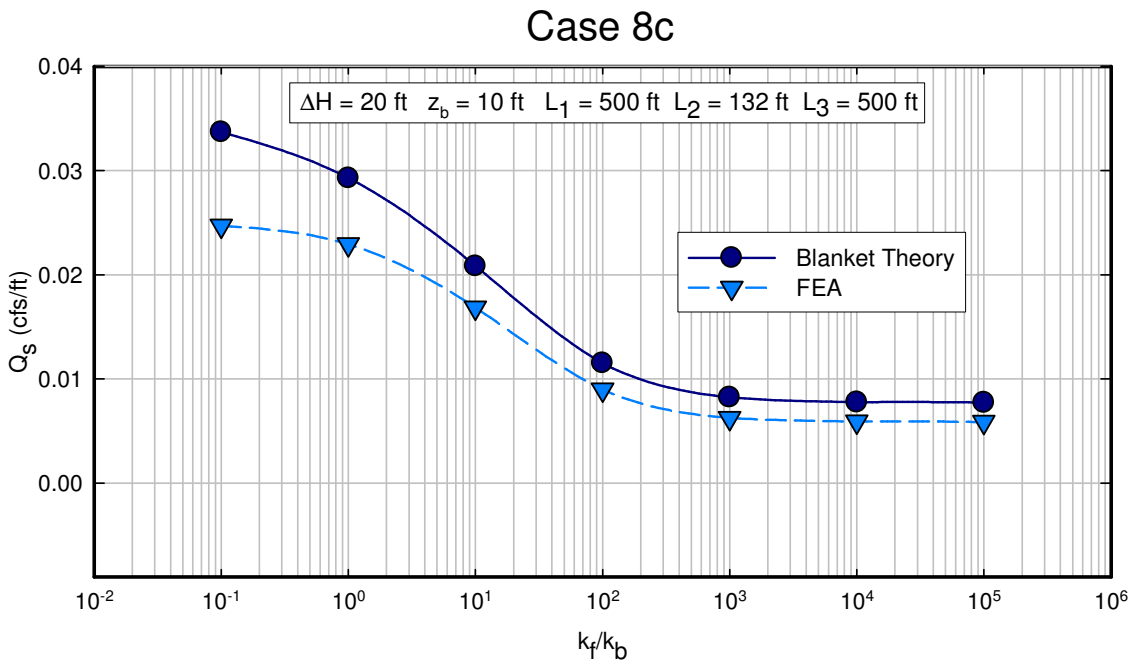

Figure A-71 Calculated values of flow per unit length (Q_s) for various permeability ratios from blanket theory and finite element analysis for Case 8c for z_b = 10 ft and L_1 = 500 ft and L_3 = 500 ft.

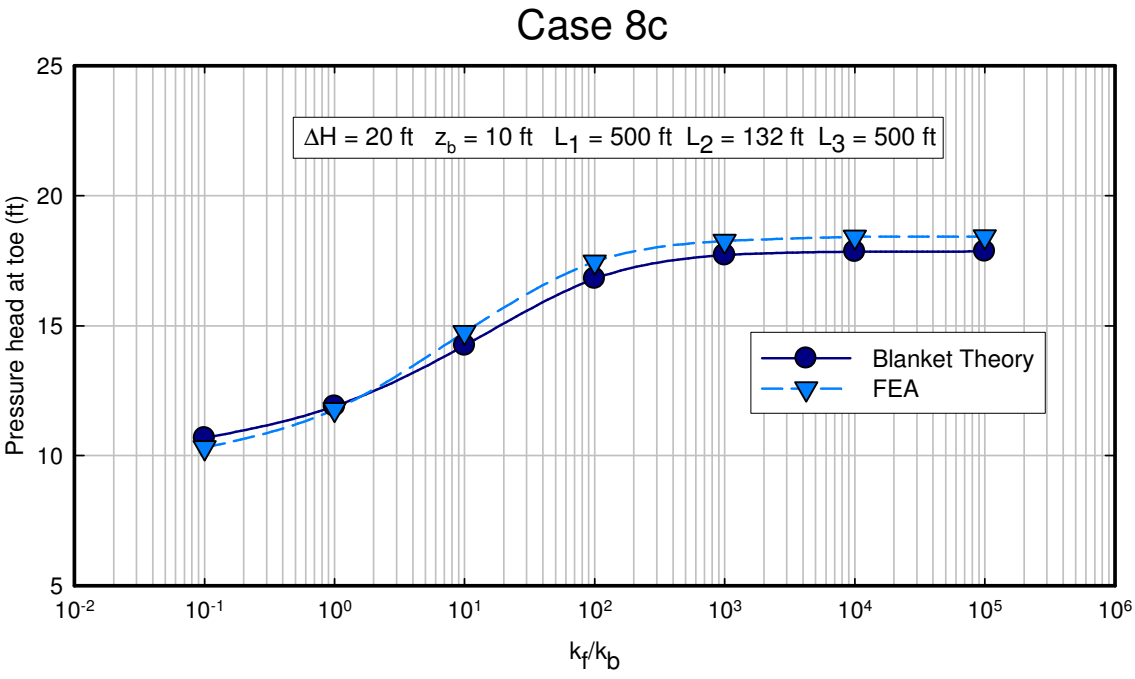

Figure A-72 Pressure head beneath blanket at toe for Case 8c calculated using FEA and blanket theory for different permeability ratios for z_b = 10 ft, L_1 = 500 ft, and L_3 = 500 ft.

Comparison of SLIDE with SEEP/W

A comparison of the results from the finite element programs SLIDE and SEEP/W were made for all cases. For cases with finite boundaries (L_1 and L_3 dimensions), SLIDE and SEEP/W provided equivalent results. As an example, shown in Figure A-73 and Figure A-74 are the results from Case 7c for the flow underneath the levee and the pressure head at the toe of the levee. There is a slight difference in the reported values of flow for the two programs due to the way that flow is reported by SLIDE and SEEP/W. For SLIDE, flow is reported as the flow perpendicular to a line drawn from the horizontal midpoint of the levee down to the bottom of the pervious layer. For SEEP/W, the total flow across the same interface is reported. The difference in flow is the greatest for cases where the blanket has a relatively high permeability, because the flow lines would not be completely horizontal, and some flow may be occurring at an angle to the interface. This would cause SLIDE to report a smaller flow than SEEP/W. For cases where the permeability of the blanket is low, the flow lines are virtually horizontal and both programs report the same flow. The values of the pressure head at the toe of the levee (Figure A-74) are the same.

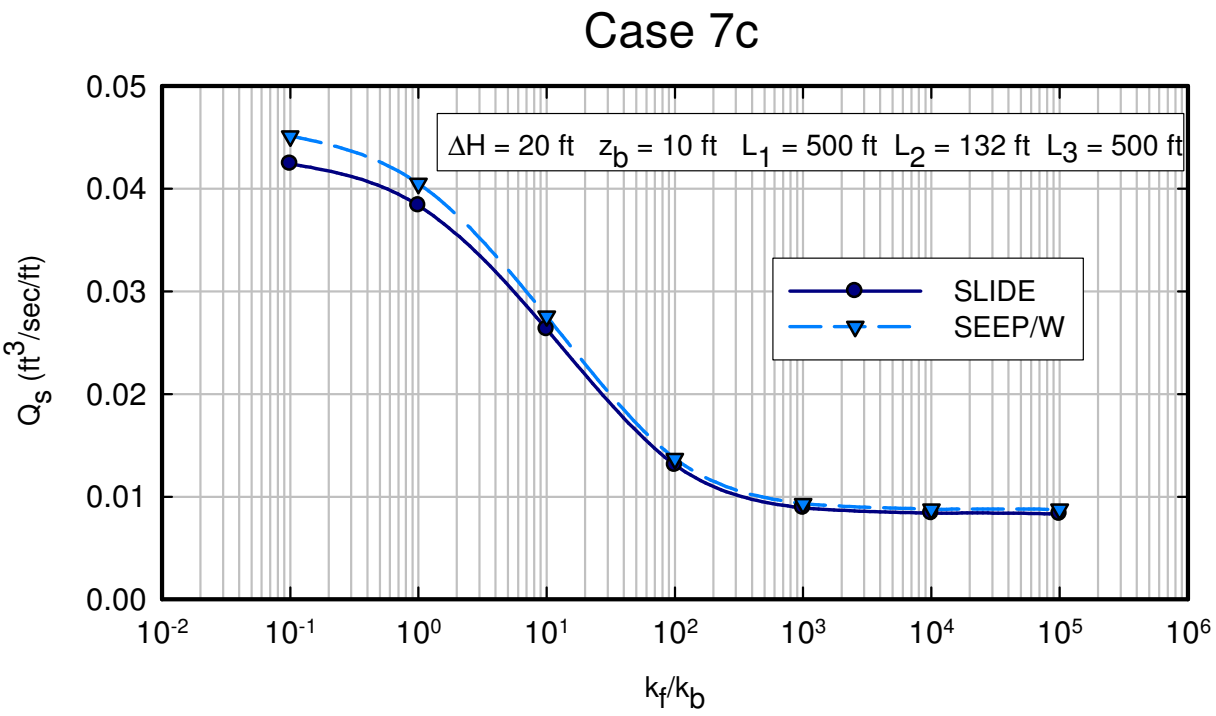

Figure A-73 Calculated flows for SLIDE and SEEP/W for Case 7c.

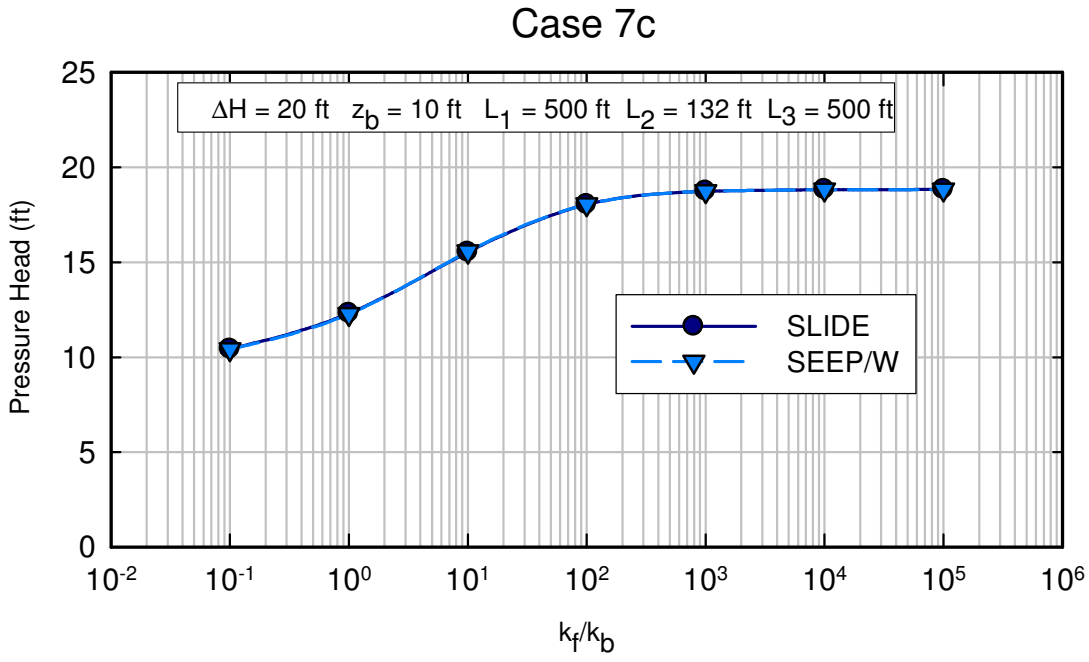

Figure A-74 Pressure head at the toe of the levee calculated by SLIDE and SEEP/W for Case 7c.

SEEP/W has a special boundary condition that allows an infinite horizontal distance to be simulated using a decay function. This boundary condition was used in SEEP/W analyses for Cases 1, 3, 4, 5, 6, and 7a. Reasonable results were obtained for cases where only one material and boundary condition were present at the vertical boundary (Cases 1, 3, 4, 5, and 6). Use of this boundary condition did not provide reasonable results for Case 7a.

Issues with Numbers of Elements

Both SLIDE and SEEP/W often produce poor results when less than 1500 elements are used in the analysis. This may be due to the fact that the domain is relative shallow compared to the length. Shown in Figure A-75 is an example from the Case 6 analyses that shows the difference in the flow calculated by SLIDE and SEEP/W. For SLIDE, the flow increases with increasing number of elements. A sensitivity study was not conducted for SEEP/W.

This sensitivity to the number of elements for SLIDE seems to be only for the calculated flow values. The head values were essentially the same for 1500 and 3000 elements.

Both programs have a default number of elements of about 1500. It may be prudent for the user to increase the number to about 3000. The larger mesh only requires marginally greater computation time, and there doesn't seem to be any other distinct disadvantages to using a larger number of elements.

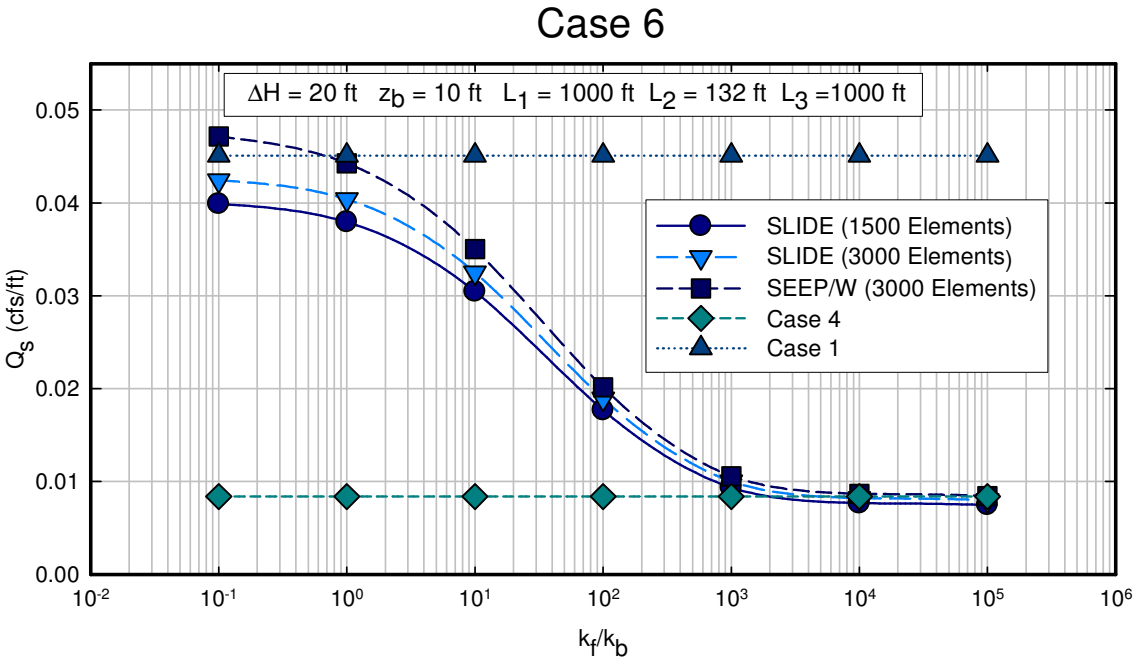

Figure A-75 Calculated flows for Case 6 showing the effect of number of elements.

General Guidelines for Finite Element Analysis

Based on the results presented in the previous section, it seems that finite element seepage analysis can be conducted using the same boundary conditions used for blanket theory, and virtually identical results will be obtained for identical conditions. The finite element method has the additional advantage that geometry more complex than that assumed in blanket theory can be easily accommodated.

This section will provide guidance for setting boundary conditions for finite element seepage analysis for the separate seepage cases as defined in EM 1110-2-1913. In addition, suggestions for boundary conditions for modeling other cases, such as outfall canals, are given.

Boundary Conditions for Blanket Theory Cases

The type of boundary conditions needed, as defined in SLIDE, SEEP/W, GMS, or other finite element analysis programs are the following:

- Constant head boundary with head set to riverside maximum water elevation
- Constant head boundary with head set to landside ground surface elevation.
- No-flow (q = 0) boundary condition
- Potential seepage face or “unknown” boundary condition.

Since the levee is considered to be impermeable in blanket theory, the levee does not need to be included in the finite element mesh, and the nodes at the base of the levee are assigned as a no-flow boundary condition. The nodes at the base of the domain (mesh) are also set as a no-flow boundary condition.

For each of the eight seepage cases presented in the previous section, the boundary conditions will be specified for the riverside horizontal and vertical surfaces and the landside horizontal and

vertical surfaces as shown in Figure A-76 below. The dimensions as defined in blanket theory (L_1, L_2, and L_3) should be the same in the finite element model as would be used in blanket theory.

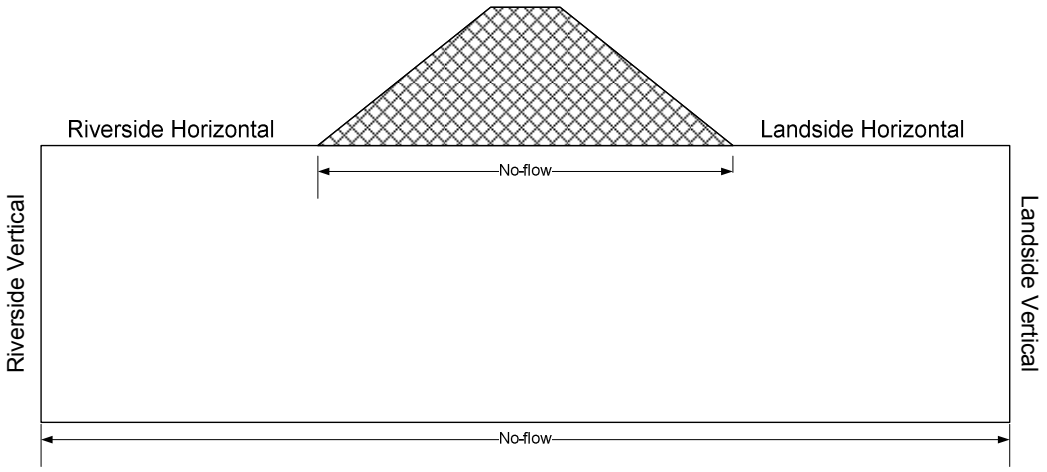

Figure A-76 Boundary conditions to be set for finite element seepage analysis.

Case 1 – no top stratum

Riverside horizontal	Constant head with head assigned to riverside water elevation
Riverside vertical	Constant head with head assigned to riverside water elevation
Landside horizontal	Constant head with head assigned to landside ground elevation
Landside vertical	Constant head with head assigned to landside ground elevation

Case 2 – Impervious top stratum both riverside and landside

Riverside horizontal	No-flow
Riverside vertical	Constant head with head assigned to riverside water elevation
Landside horizontal	No-flow
Landside vertical	Constant head with head assigned to landside ground elevation

Case 3 – Impervious riverside top stratum and no landslide top stratum

Riverside horizontal	No-flow
Riverside vertical	Constant head with head assigned to riverside water elevation
Landside horizontal	Constant head with head assigned to landside ground elevation
Landside vertical	Constant head with head assigned to landside ground elevation

Case 4 – Impervious landside top stratum and no riverside top stratum

Riverside horizontal	Constant head with head assigned to riverside water elevation
Riverside vertical	Constant head with head assigned to riverside water elevation
Landside horizontal	No-flow
Landside vertical	Constant head with head assigned to landside ground elevation

Case 5 – Semi-pervious riverside top stratum and no landside top stratum

Riverside horizontal	Constant head with head assigned to riverside water elevation
Riverside vertical	Constant head with head assigned to riverside water elevation
Landside horizontal	Constant head with head assigned to landside ground elevation
Landside vertical	Constant head with head assigned to landside ground elevation

Case 6 – Semi-pervious landside top stratum and no riverside top stratum

Riverside horizontal	Constant head with head assigned to riverside water elevation
Riverside vertical	Constant head with head assigned to riverside water elevation
Landside horizontal	Potential seepage face
Landside vertical	Constant head with head assigned to landside ground elevation

Case 7a – Semi-pervious landside top strata both riverside and landside with $L_3 = \infty$

Riverside horizontal	Constant head with head assigned to riverside water elevation
Riverside vertical	Constant head with head assigned to riverside water elevation
Landside horizontal	Potential seepage face
Landside vertical	Constant head with head assigned to landside ground elevation

Note: When L_3 is infinite then the landside vertical boundary should be sufficiently far from the levee such that an infinite landside blanket is simulated in the finite element seepage analysis. Results presented in the previous section indicate that a landside vertical boundary of greater than 500 ft from the levee toe gives an approximate infinite landside blanket condition in the finite element seepage analysis if no blanket is present. If a blanket is present, then a value of about 3000 ft should be used. Ideally, this dimension could logically be expressed as a factor of d or L_2, and that will be investigated in subsequent phases of this research. In addition, SEEP/W has an "infinite" region that possibly can be used for the landside vertical boundary, but the authors did not have success in using it on this project.

Case 7b – Semi-pervious landside top strata both riverside and landside with L_3 finite to a seepage block.

Riverside horizontal	Constant head with head assigned to riverside water elevation
Riverside vertical	Constant head with head assigned to riverside water elevation
Landside horizontal	Potential seepage face
Landside vertical	No-flow

Case 7c – Semi-pervious landside top strata both riverside and landside with L_3 finite to an open seepage exit.

Riverside horizontal	Constant head with head assigned to riverside water elevation
Riverside vertical	Constant head with head assigned to riverside water elevation
Landside horizontal	Potential seepage face
Landside vertical	Constant head with head assigned to landside ground elevation

The results presented in the previous section indicate that the transition between semi-pervious and impervious blanket behavior occurs at a ratio of pervious layer permeability to blanket permeability between 1000 and 4000. At permeability ratios in the range of these values, the semi-pervious solutions (Cases 5, 6, and 7) produce essentially the same values of heads and flows as the impervious solutions, and the results of blanket theory agree closely with finite element analysis.

Similarly, the transformation from a fully pervious to a semi-pervious blanket occurs at a ratio of pervious layer permeability to blanket permeability of about 2. In other words, the use of the semi-pervious equations will produce a more accurate determination of the flow and the excess head for permeability ratios equal to or greater than 2 as compared to solutions considering the blanket as fully pervious (non-existent). For permeability ratios less than 2, the presence of the blanket may be ignored, and the solutions for cases having no blanket will generally provide more accurate results than the solutions for the semi-pervious cases.

Case 8 was added in this study to extend the conventional blanket theory analyses to cross sections that contain a partially penetrating sheet pile cutoff. The boundary conditions for finite element analysis of Case 8 solutions is essentially the same as for Case 7, except that no-flow

boundary conditions are assigned to the nodes at the exterior of the sheet pile, or the sheet pile can be modeled as an impervious material (i.e. no material type in SEEP/W).

Layered top strata

Blanket theory transforms the top strata into one layer of uniform thickness and permeability. The comparison of the blanket theory with the finite element analyses presented in the seepage report is also for the transformed parameters. However, it is useful to study the effect of this transformation on seepage under the structure and heads at the toe of the levee. Therefore, as a next step, a two-layered top stratum is modeled as is in finite element analysis and output parameters are compared with blanket theory solutions, which will consider the transformed thickness and permeability.

The analyses are conducted for the thickness of top stratum as 20 ft. However, the top stratum is further divided into two layers as shown in Figure A-77, where k_1 and z_1 are the permeability and thickness of the top layer, while k_2 and z_2 are the permeability and thickness of the bottom layer of the blanket. Table 1 summarizes the permeabilities of different combinations used in the analyses of layered top strata having two layers of equal thicknesses of 10 ft. Combinations 1 to 6 have the permeability of bottom layer as 4.92×10^{-5} ft/sec, while the permeability of the top layer is varied from 4.92×10^{-3} ft/sec to 4.92×10^{-8} ft/sec. Similarly, the order of permeabilities is reversed for combinations 7 to 12 with top layer having the permeability as 4.92×10^{-5} ft/sec and permeability is varied for the bottom layer. Combinations 13 to 17 have the permeability of the bottom layer fixed at a very low value of 4.92×10^{-8} ft/sec and the permeability is varied from 4.92×10^{-4} ft/sec to 4.92×10^{-8} ft/sec for the top layer. Combinations 18 to 22 indicate the permeability of the bottom layer fixed at the value of 4.92×10^{-4} ft/sec (one order of magnitude higher than the pervious layer) and the permeability is again varied from 4.92×10^{-4} ft/sec to 4.92×10^{-8} ft/sec for the top layer. Similarly, Tables 2 and 3 indicate the same information for different thicknesses of two layers comprising the top strata. Table A-2 is for the thickness of top

and bottom layers of the blanket as 5 and 15 ft respectively. The thicknesses of the blanket layers are reversed in Table A-3.

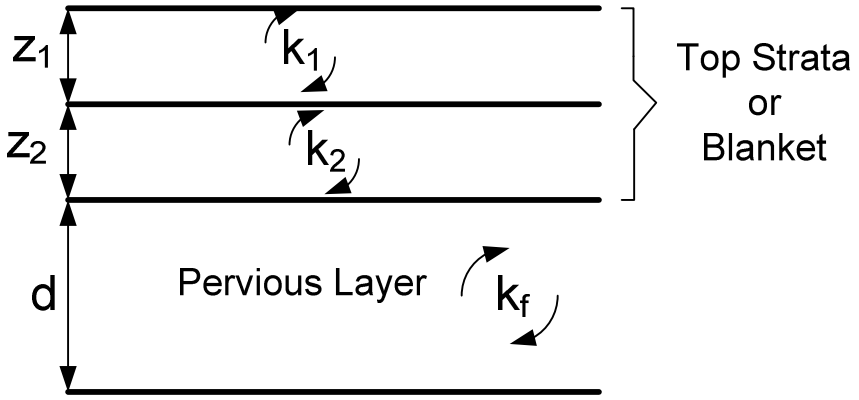

Figure A-77 General configuration of top strata used in the analyses

The boundary conditions and other hydraulic properties are considered the same as explained earlier in the discussion. The analysis is conducted for Case 6, which has top stratum on landward side and no riverside top stratum. The permeability of the pervious layer (k_f) was assigned a value of 4.92 x 10^{-3} ft/sec (0.15 cm/sec), which is the same value used in the previous analyses. The value of both L_1 and L_3 is 1000 ft, and the net head on the levee (H) is 20 ft for the analysis. Similarly, thickness of the pervious layer (d) is 100 ft. The finite element analyses were conducted in the similar manner as before for all the cases shown in Tables A-1, A-2 and A-3. The blanket theory solutions were also computed and the transformed thicknesses and permeabilities used in the analyses are indicated in Tables 1, 2and 3. The volumetric flow rates per unit of levee length (Q_s) and excess hydraulic head (h_o) under the toe of the levee were compared from both the analyses.

Shown in Figure A-78 is the comparison of volumetric flow values calculated from finite element analysis and blanket theory for combinations 1 to 22. The blanket theory analysis provides close results with finite element analysis; the greatest difference is obtained for

combination 18 that has the permeability value for top and bottom layers as 4.92 x 10^{-4} ft/sec. This gives the ratio of k_f to k_b as 10, which is exactly the borderline of the applicability of the blanket theory. Better agreement of results is obtained for higher ratios of k_f to k_b. Similarly, excellent agreement is obtained for the pressure head (excess head) beneath the toe from the two methods as shown in Figure A-79 for combinations 1 to 22. FiguresFigure A-80,Figure A-81Figure A-82 andFigure A-83 show the similar plots for combinations 23 through 66. Same trends are observed for the different thicknesses of top stratum and combination having k_f to k_b ratio of 10 shows the largest variation for volumetric flow per unit length. Again, the blanket theory results and the finite element results for pressure beneath the toe are in close agreement.

The analysis is controlled by the least pervious layer in blanket theory solutions, which also becomes true for finite element analysis if permeability of one of the layers of the blanket is very small as compared to the other layer. The analyses conducted indicate that the blanket theory provides reliable results for layered problems especially if the assumptions of the theory are not violated. However, this class of problems is better addressed in finite element analysis, which can easily incorporate the complex geometries and properties. In addition, if more than two layers are present for the blanket; finite element analysis may be more appropriate for such cases.

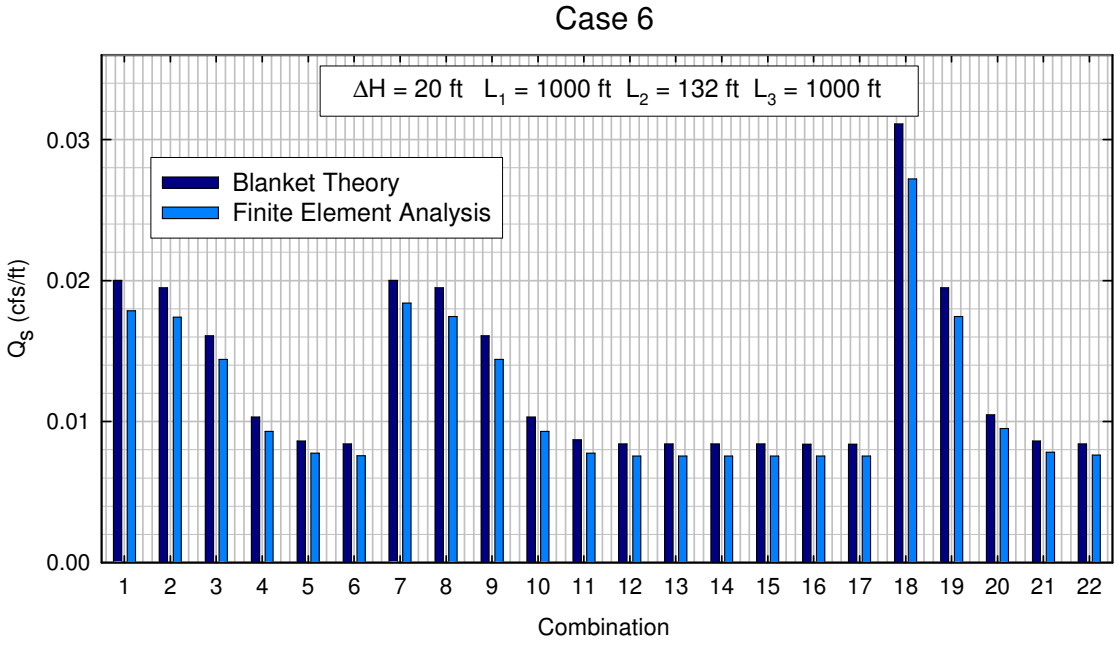

Figure A-78 Calculated values of flow per unit length (Qs) from blanket theory and finite element analysis for combinations 1 to 22 for Case 6.

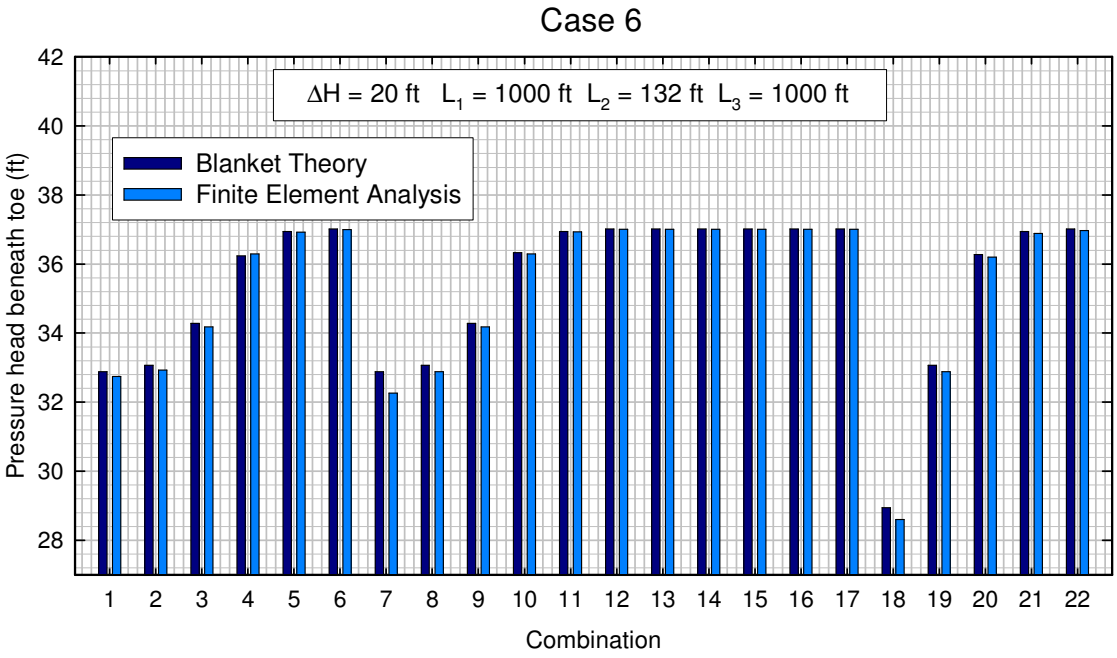

Figure A-79 Excess head (ho) or pressure head beneath blanket at toe for Case 6 calculated using FEA and blanket theory for combinations 1 to 22.

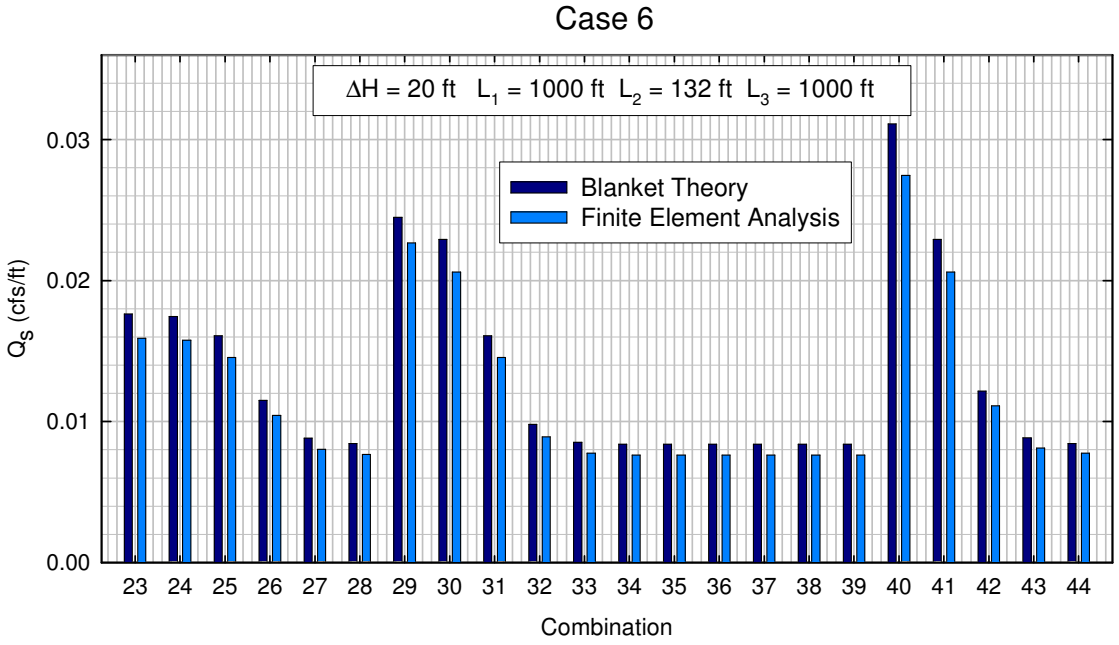

Figure A-80 Calculated values of flow per unit length (Qs) from blanket theory and finite element analysis for combinations 23 to 44 for Case 6.

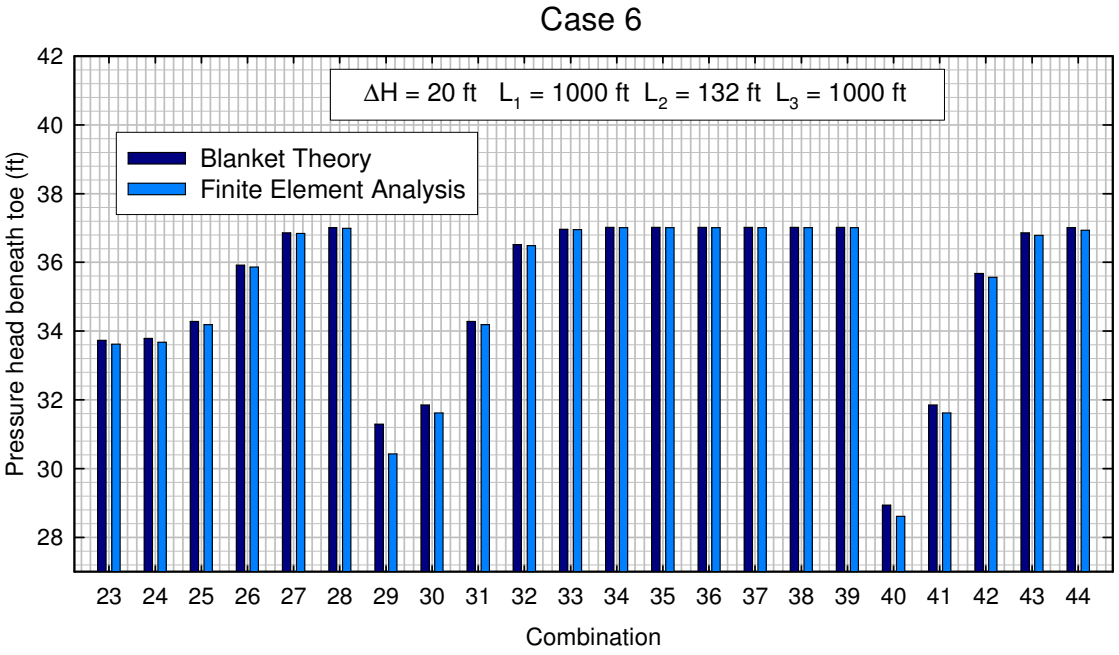

Figure A-81 Excess head (ho) or pressure head beneath blanket at toe for Case 6 calculated using FEA and blanket theory for combinations 23 to 44.

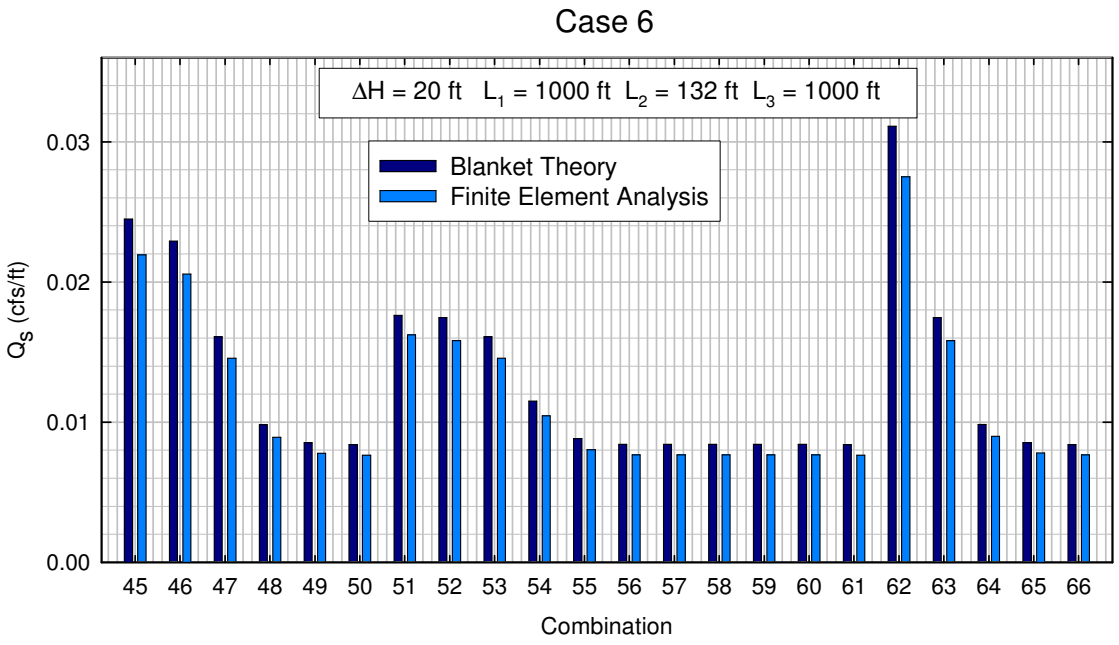

Figure A-82 Calculated values of flow per unit length (Qs) from blanket theory and finite element analysis for combinations 45 to 66 for Case 6.

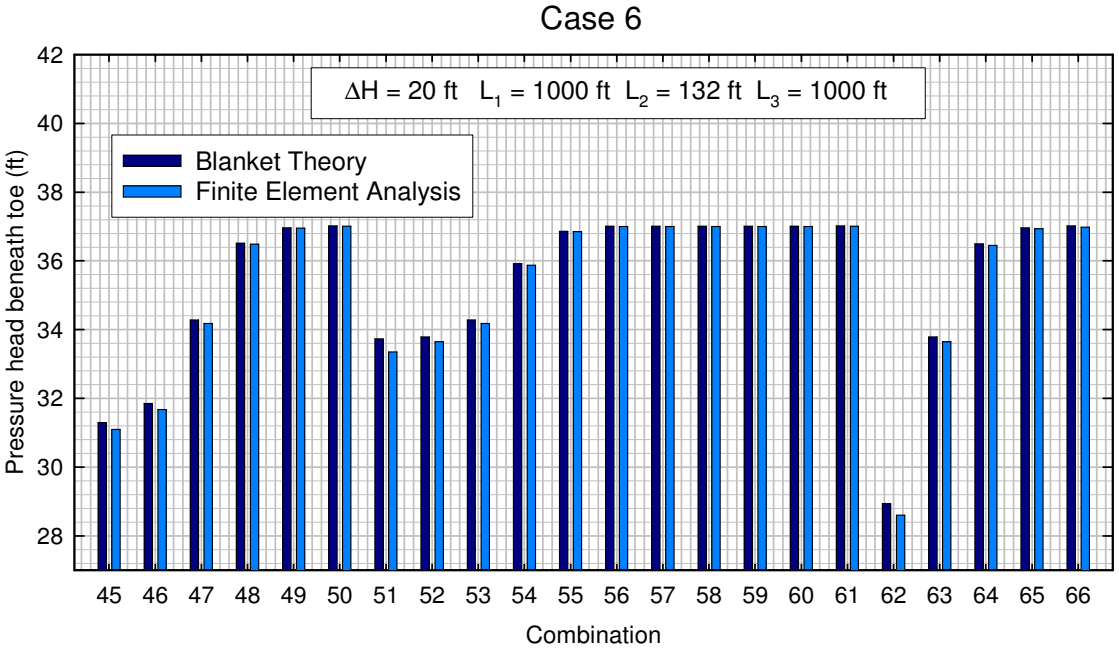

Figure A-83 Excess head (h_o) or pressure head beneath blanket at toe for Case 6 calculated using FEA and blanket theory for combinations 45 to 66.

Table A-1 Summary of parameters for combinations 1 to 22 used in the analyses of top strata having z1 = z2 = 10 ft

Case no.	Permeability		Thickness		Case no.	Permeability		Thickness	
	Original (ft/sec)	Transformed k_b (ft/sec)	Original (ft)	Transformed z_b (ft)		Original (ft/sec)	Transformed k_b (ft/sec)	Original (ft)	Transformed z_b (ft)
1	$k_1=4.92\times10^{-3}$ $k_2=4.92\times10^{-5}$	4.92×10^{-5}	$z_1=10$ $z_2=10$	10.1	12	$k_1=4.92\times10^{-5}$ $k_2=4.92\times10^{-8}$	4.92×10^{-8}	$z_1=10$ $z_2=10$	10.01
2	$k_1=4.92\times10^{-4}$ $k_2=4.92\times10^{-5}$	4.92×10^{-5}	$z_1=10$ $z_2=10$	11	13	$k_1=4.92\times10^{-4}$ $k_2=4.92\times10^{-8}$	4.92×10^{-8}	$z_1=10$ $z_2=10$	10.001
3	$k_1=4.92\times10^{-5}$ $k_2=4.92\times10^{-5}$	4.92×10^{-5}	$z_1=10$ $z_2=10$	20	14	$k_1=4.92\times10^{-5}$ $k_2=4.92\times10^{-8}$	4.92×10^{-8}	$z_1=10$ $z_2=10$	10.01
4	$k_1=4.92\times10^{-6}$ $k_2=4.92\times10^{-5}$	4.92×10^{-6}	$z_1=10$ $z_2=10$	11	15	$k_1=4.92\times10^{-6}$ $k_2=4.92\times10^{-8}$	4.92×10^{-8}	$z_1=10$ $z_2=10$	10.1
5	$k_1=4.92\times10^{-7}$ $k_2=4.92\times10^{-5}$	4.92×10^{-7}	$z_1=10$ $z_2=10$	10.1	16	$k_1=4.92\times10^{-7}$ $k_2=4.92\times10^{-8}$	4.92×10^{-8}	$z_1=10$ $z_2=10$	11
6	$k_1=4.92\times10^{-8}$ $k_2=4.92\times10^{-5}$	4.92×10^{-8}	$z_1=10$ $z_2=10$	10.01	17	$k_1=4.92\times10^{-8}$ $k_2=4.92\times10^{-8}$	4.92×10^{-8}	$z_1=10$ $z_2=10$	20
7	$k_1=4.92\times10^{-5}$ $k_2=4.92\times10^{-3}$	4.92×10^{-5}	$z_1=10$ $z_2=10$	10.1	18	$k_1=4.92\times10^{-4}$ $k_2=4.92\times10^{-4}$	4.92×10^{-4}	$z_1=10$ $z_2=10$	20
8	$k_1=4.92\times10^{-5}$ $k_2=4.92\times10^{-4}$	4.92×10^{-5}	$z_1=10$ $z_2=10$	11	19	$k_1=4.92\times10^{-5}$ $k_2=4.92\times10^{-4}$	4.92×10^{-5}	$z_1=10$ $z_2=10$	11
9	$k_1=4.92\times10^{-5}$ $k_2=4.92\times10^{-5}$	4.92×10^{-5}	$z_1=10$ $z_2=10$	20	20	$k_1=4.92\times10^{-6}$ $k_2=4.92\times10^{-4}$	4.92×10^{-6}	$z_1=10$ $z_2=10$	10.1
10	$k_1=4.92\times10^{-5}$ $k_2=4.92\times10^{-6}$	4.92×10^{-6}	$z_1=10$ $z_2=10$	11	21	$k_1=4.92\times10^{-7}$ $k_2=4.92\times10^{-4}$	4.92×10^{-7}	$z_1=10$ $z_2=10$	10.01
11	$k_1=4.92\times10^{-5}$ $k_2=4.92\times10^{-7}$	4.92×10^{-7}	$z_1=10$ $z_2=10$	10.1	22	$k_1=4.92\times10^{-8}$ $k_2=4.92\times10^{-4}$	4.92×10^{-8}	$z_1=10$ $z_2=10$	10.001

Table A-2 Summary of parameters for combinations 23 to 44 used in the analyses of top strata having z_1 =5 ft and z_2 = 15 ft

Case no.	Permeability		Thickness		Case no.	Permeability		Thickness	
	Original	Transformed	Original	Transformed		Original	Transformed	Original	Transformed
	(ft/sec)	k_b (ft/sec)	(ft)	z_b (ft)		(ft/sec)	k_b (ft/sec)	(ft)	z_b (ft)
23	k_1=4.92x10^{-3} k_2= 4.92x10^{-5}	4.92x10^{-5}	z_1= 5 z_2= 15	15.05	34	k_1= 4.92x10^{-5} k_2= 4.92x10^{-8}	4.92x10^{-8}	z_1= 5 z_2= 15	15.005
24	k_1= 4.92x10^{-4} k_2= 4.92x10^{-5}	4.92x10^{-5}	z_1= 5 z_2= 15	15.5	35	k_1= 4.92x10^{-4} k_2=4.92x10^{-8}	4.92x10^{-8}	z_1= 5 z_2= 15	15.0005
25	k_1= 4.92x10^{-5} k_2= 4.92x10^{-5}	4.92x10^{-5}	z_1= 5 z_2= 15	20	36	k_1= 4.92x10^{-5} k_2= 4.92x10^{-8}	4.92x10^{-8}	z_1= 5 z_2= 15	15.005
26	k_1= 4.92x10^{-6} k_2= 4.92x10^{-5}	4.92x10^{-6}	z_1= 5 z_2= 15	6.5	37	k_1= 4.92x10^{-6} k_2= 4.92x10^{-8}	4.92x10^{-8}	z_1= 5 z_2= 15	15.05
27	k_1= 4.92x10^{-7} k_2= 4.92x10^{-5}	4.92x10^{-7}	z_1= 5 z_2= 15	5.15	38	k_1= 4.92x10^{-7} k_2= 4.92x10^{-8}	4.92x10^{-8}	z_1= 5 z_2= 15	15.5
28	k_1= 4.92x10^{-8} k_2= 4.92x10^{-5}	4.92x10^{-8}	z_1= 5 z_2= 15	5.015	39	k_1= 4.92x10^{-8} k_2= 4.92x10^{-8}	4.92x10^{-8}	z_1= 5 z_2= 15	20
29	k_1= 4.92x10^{-5} k_2=4.92x10^{-3}	4.92x10^{-5}	z_1= 5 z_2= 15	5.15	40	k_1= 4.92x10^{-4} k_2= 4.92x10^{-4}	4.92x10^{-4}	z_1= 5 z_2= 15	20
30	k_1= 4.92x10^{-5} k_2= 4.92x10^{-4}	4.92x10^{-5}	z_1= 5 z_2= 15	6.5	41	k_1= 4.92x10^{-5} k_2= 4.92x10^{-4}	4.92x10^{-5}	z_1= 5 z_2= 15	6.5
31	k_1= 4.92x10^{-5} k_2= 4.92x10^{-5}	4.92x10^{-5}	z_1= 5 z_2= 15	20	42	k_1= 4.92x10^{-6} k_2= 4.92x10^{-4}	4.92x10^{-6}	z_1= 5 z_2= 15	5.15
32	k_1= 4.92x10^{-5} k_2= 4.92x10^{-6}	4.92x10^{-6}	z_1= 5 z_2= 15	15.5	43	k_1= 4.92x10^{-7} k_2= 4.92x10^{-4}	4.92x10^{-7}	z_1= 5 z_2= 15	5.015
33	k_1= 4.92x10^{-5} k_2= 4.92x10^{-7}	4.92x10^{-7}	z_1= 5 z_2= 15	15.05	44	k_1= 4.92x10^{-8} k_2= 4.92x10^{-4}	4.92x10^{-8}	z_1= 5 z_2= 15	5.0015

Table A-3 Summary of parameters for combinations 45 to 66 used in the analyses of top strata having $z_1 = 15$ ft and $z_2 = 5$ ft

Case no.	Permeability		Thickness		Case no.	Permeability		Thickness	
	Original (ft/sec)	Transformed k_b (ft/sec)	Original (ft)	Transformed z_b (ft)		Original (ft/sec)	Transformed k_b (ft/sec)	Original (ft)	Transformed z_b (ft)
45	$k_1=4.92\times10^{-3}$ $k_2=4.92\times10^{-5}$	4.92×10^{-5}	$z_1=15$ $z_2=5$	5.15	56	$k_1=4.92\times10^{-5}$ $k_2=4.92\times10^{-8}$	4.92×10^{-8}	$z_1=15$ $z_2=5$	5.015
46	$k_1=4.92\times10^{-4}$ $k_2=4.92\times10^{-5}$	4.92×10^{-5}	$z_1=15$ $z_2=5$	6.5	57	$k_1=4.92\times10^{-4}$ $k_2=4.92\times10^{-8}$	4.92×10^{-8}	$z_1=15$ $z_2=5$	5.0015
47	$k_1=4.92\times10^{-5}$ $k_2=4.92\times10^{-5}$	4.92×10^{-5}	$z_1=15$ $z_2=5$	20	58	$k_1=4.92\times10^{-5}$ $k_2=4.92\times10^{-8}$	4.92×10^{-8}	$z_1=15$ $z_2=5$	5.015
48	$k_1=4.92\times10^{-6}$ $k_2=4.92\times10^{-5}$	4.92×10^{-6}	$z_1=15$ $z_2=5$	15.5	59	$k_1=4.92\times10^{-6}$ $k_2=4.92\times10^{-8}$	4.92×10^{-8}	$z_1=15$ $z_2=5$	5.15
49	$k_1=4.92\times10^{-7}$ $k_2=4.92\times10^{-5}$	4.92×10^{-7}	$z_1=15$ $z_2=5$	15.05	60	$k_1=4.92\times10^{-7}$ $k_2=4.92\times10^{-8}$	4.92×10^{-8}	$z_1=15$ $z_2=5$	6.5
50	$k_1=4.92\times10^{-8}$ $k_2=4.92\times10^{-5}$	4.92×10^{-8}	$z_1=15$ $z_2=5$	15.005	61	$k_1=4.92\times10^{-8}$ $k_2=4.92\times10^{-8}$	4.92×10^{-8}	$z_1=15$ $z_2=5$	20
51	$k_1=4.92\times10^{-5}$ $k_2=4.92\times10^{-3}$	4.92×10^{-5}	$z_1=15$ $z_2=5$	15.05	62	$k_1=4.92\times10^{-4}$ $k_2=4.92\times10^{-4}$	4.92×10^{-4}	$z_1=15$ $z_2=5$	20
52	$k_1=4.92\times10^{-5}$ $k_2=4.92\times10^{-4}$	4.92×10^{-5}	$z_1=15$ $z_2=5$	15.5	63	$k_1=4.92\times10^{-5}$ $k_2=4.92\times10^{-4}$	4.92×10^{-5}	$z_1=15$ $z_2=5$	15.5
53	$k_1=4.92\times10^{-5}$ $k_2=4.92\times10^{-5}$	4.92×10^{-5}	$z_1=15$ $z_2=5$	20	64	$k_1=4.92\times10^{-6}$ $k_2=4.92\times10^{-4}$	4.92×10^{-6}	$z_1=15$ $z_2=5$	15.05
54	$k_1=4.92\times10^{-5}$ $k_2=4.92\times10^{-6}$	4.92×10^{-6}	$z_1=15$ $z_2=5$	6.5	65	$k_1=4.92\times10^{-7}$ $k_2=4.92\times10^{-4}$	4.92×10^{-7}	$z_1=15$ $z_2=5$	15.005
55	$k_1=4.92\times10^{-5}$ $k_2=4.92\times10^{-7}$	4.92×10^{-7}	$z_1=15$ $z_2=5$	5.15	66	$k_1=4.92\times10^{-8}$ $k_2=4.92\times10^{-4}$	4.92×10^{-8}	$z_1=15$ $z_2=5$	15.0005

Finite Element Boundary Conditions for Outfall Canals

Considerable judgment is required to apply blanket theory for seepage analysis of outfall canals since the seepage boundary conditions used in the derivation of the blanket theory equations are not the same as the seepage boundary conditions at the outfall canals. The vertical boundary at the centerline of the canal would be a *no-flow* boundary, and none of the original blanket theory cases have a no-flow vertical boundary on the river or flood side. It is possible, with some effort, to modify existing cases to incorporate a vertical "seepage block" on the flood side.

If the bottom of the canal has direct hydraulic communication with the pervious layer, then Case 6 might provide reasonable results even though the vertical boundary conditions differ. If the canal is "silted in," then Case 7c would be partially applicable. For the "silted in" condition, there would be some value of x_1 that could be used with Case 7c that may provide approximate results, but it is not possible to determine this value of x_1 based on site geometry since the boundary conditions for Case 7c and the outfall canals differ considerably.

IPET used finite element analysis to calculate pore pressures in the foundation sands of London Avenue Canal and Orleans Canal I-walls. In these analyses, the following boundary conditions were used:

- Constant head boundary for all points canal-side of the sheet pile to the centerline of the canal.
- No-flow vertical boundary corresponding to the centerline of the canal (L_1 dimension in blanket theory).
- Potential seepage face boundary for surfaces on the protected side of the I-wall

- Constant head vertical boundary at L_3 dimension as defined in blanket theory.
- The sheet pile was modeled as an impervious material.

In the case of a gap forming between the sheet pile and the levee fill, constant head boundary conditions, with a head equal to the canal water level, were assigned to the depth of the gap on the flood side boundary of the sheet pile. If the pervious layer is exposed in the bottom of the canal, then the presence of the gap has little effect on the calculated pore pressures. If the canal is "silted in," then the gap can increase the pore pressures in the pervious layer if the gap extends down to this layer.

The distance to set the vertical boundary on the protected side (L_3) requires some judgment. Ideally, it should be set at the minimum distance where the head is not affected by the canal water level. As the value of L_3 increases, the analysis becomes more conservative regarding the calculation of exit gradients, uplift pressures, and pore pressures. During the IPET study, the L_3 dimension was estimated based on piezometer data. A value of about 210 ft was used for London Avenue Canal analyses, and 135 ft was used for Orleans Canal analyses. Preliminary analysis performed at Virginia Tech of the London Avenue load test data indicates that an L_3 dimension of about 80 ft seems to accurately predict pore pressures in the lower sand layer for the boundary conditions and stratigraphy present at the location of the test section.

Determination of the Underseepage Factor of Safety for HDSRRS Seepage Criteria

For HDSRRS seepage criteria, the factor of safety for underseepage is computed as follows:

$$FS = \frac{\gamma' \cdot z_t}{\gamma_w \cdot h_0}$$

Where:

γ' = average effective (or buoyant) unit weight of soil = $\gamma_{sat} - \gamma_w$

γ_w = unit weight of water

γ_{sat} = total, or saturated, unit weight of soil blanket

z_t = landside blanket thickness

h_o = excess head (above hydrostatic) at toe

The excess head at the toe (h_0) from the finite element seepage analysis can be determined from the difference between the pressure head at the base of the blanket and the landside blanket thickness at the toe (see Figure A-84).

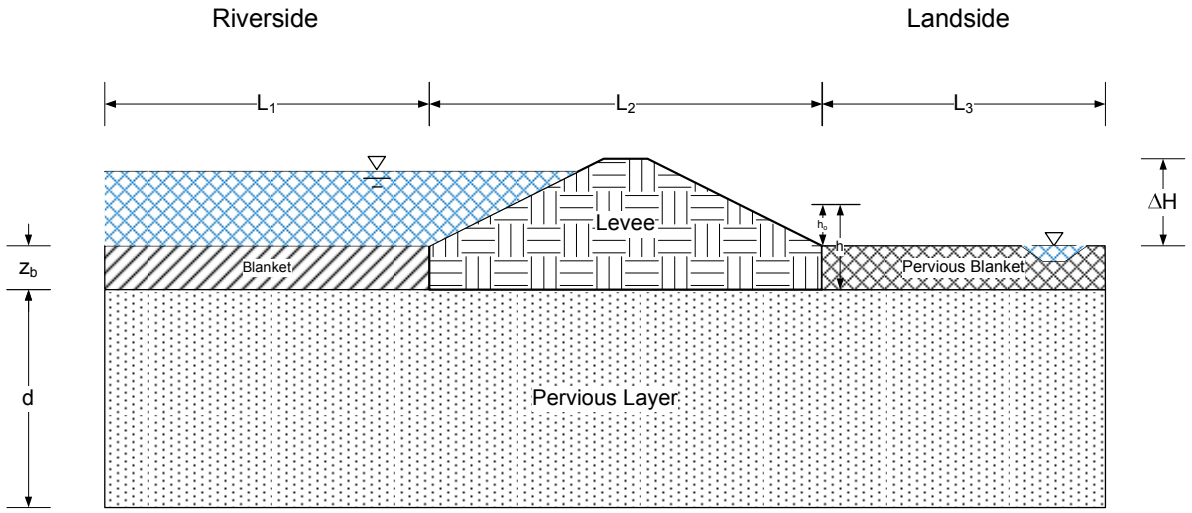

Figure A-84 Excess head at the toe (h_0) from the finite element seepage analysis.

Appendix AI

TableAI- 1 Summary of Fragment Type and Form Factors (Harr 1962-used under fair use 2013)

Fragment Type	Illustration	Form Factor (Φ)
I	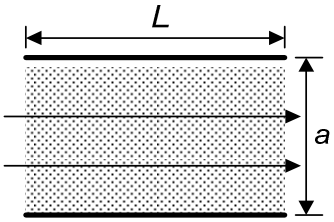	$\Phi = \frac{L}{a}$
II	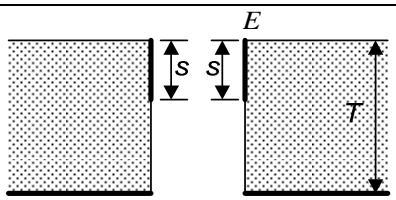 Special Case s = 0, ϕ=0.43	$\Phi = \frac{K}{K'}; m = \sin\frac{\pi s}{2T}$ $I_E = \frac{h\pi}{2KTm}$
III	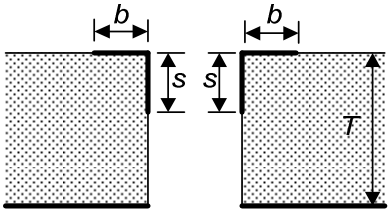	$\Phi = \frac{K}{K'}$ $m = \cos\frac{\pi s}{2T}\sqrt{tanh^2\,\frac{\pi b}{2T} + tan^2\,\frac{\pi s}{2T}}$
IV	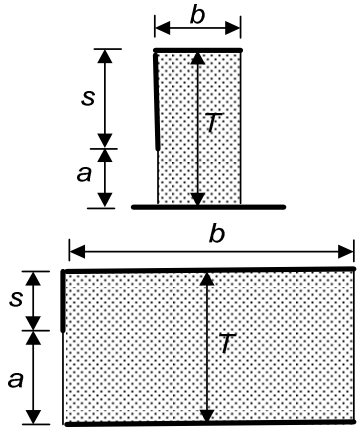	Exact solution: $\frac{\Lambda}{\Lambda'} = \frac{T}{b'}; modulus = \lambda$ $\Phi = \frac{K'(m)}{K(m)}; m = \lambda sin\left(\frac{a}{T}\Lambda, \lambda\right)$ Approximate solution: $S \geq b$: $\Phi = \ln\left(1 + \frac{b}{a}\right)$ $b \geq S$: $\Phi = \ln\left(1 + \frac{s}{a}\right) + \frac{b - s}{T}$

Fragment Type	Illustration	Form Factor (Φ)
V	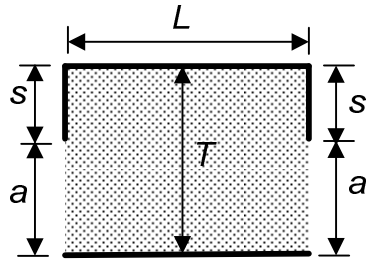	$L \le 2s$: $\Phi = \ln\left(1 + \frac{b}{2a}\right)$ $b \ge 2s$: $\Phi = 2\ln\left(1 + \frac{s}{a}\right) + \frac{b - 2s}{T}$
VI	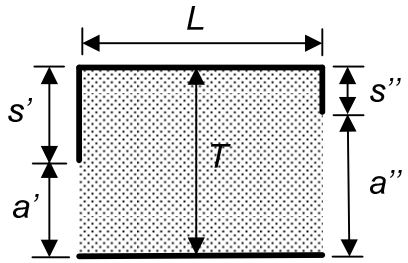 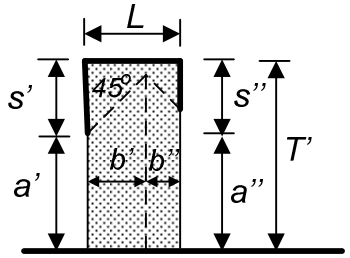	$L > s' + s''$: $\Phi = ln\left[\left(1 + \frac{s'}{a'}\right)\left(1 + \frac{s''}{a''}\right)\right] + \frac{L - (s' + s'')}{T}$ $L = s' + s''$: $\Phi = ln\left[\left(1 + \frac{s'}{a'}\right)\left(1 + \frac{s''}{a''}\right)\right]$ $L < s' + s''$: $\Phi = ln\left[\left(1 + \frac{b'}{a'}\right)\left(1 + \frac{b''}{a''}\right)\right]$ Where: $b' = \frac{L + (s' - s'')}{2}$ $b'' = \frac{L - (s' - s'')}{2}$

TableAI- 2 Complete elliptic integrals of the first kind

m^2	K/K'	m^2	K/K'	m^2	K/K'	m^2	K/K'	m^2	K/K'
0.000	0.000	0.21	0.745	0.51	1.009	0.81	1.377	0.9993	3.195
0.001	0.325	0.22	0.754	0.52	1.018	0.82	1.397	0.9994	3.244
0.002	0.349	0.23	0.763	0.53	1.028	0.83	1.416	0.9995	3.302
0.003	0.366	0.24	0.773	0.54	1.037	0.84	1.439	0.9996	3.373
0.004	0.379	0.25	0.782	0.55	1.047	0.85	1.462	0.9997	3.465
0.005	0.389	0.26	0.791	0.56	1.057	0.86	1.484	0.9998	3.594
0.006	0.398	0.27	0.800	0.57	1.066	0.87	1.511	0.9999	3.814
0.007	0.406	0.28	0.808	0.58	1.076	0.88	1.538	1	∞
0.008	0.413	0.29	0.817	0.59	1.087	0.89	1.567		
0.009	0.420	0.30	0.826	0.60	1.098	0.90	1.600		
0.01	0.426	0.31	0.834	0.61	1.107	0.91	1.634		
0.02	0.471	0.32	0.843	0.62	1.118	0.92	1.672		
0.03	0.502	0.33	0.852	0.63	1.129	0.93	1.718		
0.04	0.526	0.34	0.860	0.64	1.140	0.94	1.770		
0.05	0.547	0.35	0.869	0.65	1.151	0.95	1.828		
0.06	0.565	0.36	0.877	0.66	1.162	0.96	1.901		
0.07	0.582	0.37	0.886	0.67	1.174	0.97	1.992		
0.08	0.598	0.38	0.895	0.68	1.186	0.98	2.123		
0.09	0.612	0.39	0.903	0.69	1.198	0.990	2.347		
0.10	0.625	0.40	0.911	0.70	1.211	0.991	2.381		
0.11	0.638	0.41	0.920	0.71	1.224	0.992	2.418		
0.12	0.650	0.42	0.929	0.72	1.237	0.993	2.461		
0.13	0.662	0.43	0.938	0.73	1.251	0.994	2.510		
0.14	0.674	0.44	0.946	0.74	1.265	0.995	2.568		

0.15	0.684	0.45	0.955	0.75	1.279	0.996	2.639		
0.16	0.695	0.46	0.964	0.76	1.294	0.997	2.731		
0.17	0.706	0.47	0.973	0.77	1.310	0.998	2.860		
0.18	0.716	0.48	0.982	0.78	1.326	0.999	3.081		
0.19	0.726	0.49	0.991	0.79	1.343	0.9991	3.115		
0.20	0.735	0.50	1.000	0.80	1.360	0.9992	3.152		

Notes: *m* is the modulus. To determine K/K', compute the modulus (*m*) and then square it to find the K/K' from the above table.

Values in the table are based on values from V.I. Aravin and S. Numerov, "Seepage Computations for Hydraulic Structures," Stpoitel'stvu I Arkhitekture, Moscow, 1955.

Appendix II

Derivation of Case 1 based on Forchheimer (1917)

The paper written by Forchheimer (1917) is in archaic technical German, and it was difficult to obtain a useful translation from current German-speaking engineers at our disposal. However, an effort was made to determine the origin of the equation presented in Muskat (1937), referenced to Forchheimer, which is similar to Case 1 of blanket theory. For this purpose, terminologies present in Muskat (1937) were related to those in Forchheimer (1917) for ease of understanding. The figure and equation numbers are also presented and cited as they appear in original paper.

The case having $L_2/d > 1$ will be discussed here as blanket theory is applicable only to such cases. However, it appears as $f/2a > 1/8$ in Forchheimer (1917) which is similar to $w/h > 1$ in Muskat (1937). Referring to Figure AII-1, Forchheimer considers the width of the levee as 2f and thickness of the pervious stratum as a/2. Therefore, for the case having $f/2a > 1/8$ (i.e. $w/h>1$) where w is width of the structure and h is thickness of pervious substratum, we divide the length between x=0 and x= f (the midpoint of levee) into an outer length of a/4 and an inner length of f-a/4 as shown the Figure AII-1 (similar to Figure 11 of Forchheimer (1917)). The pressure loss is calculated for the outer and inner lengths, which is done by considering segments of f = a/8.

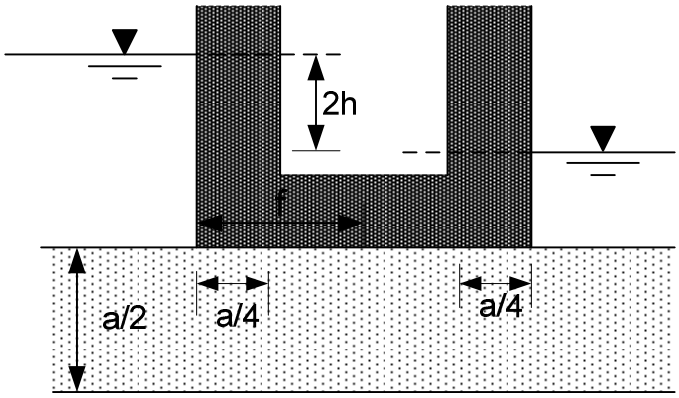

Figure AII- 1 Figure indicating the outer and inner portions of the levee.

For the outer portion, pressure loss is calculated using Equation 38 of the paper which is for the case f/2a < 1/8. This assumption is valid to some extent as the length of the outer portion is a/4 < h (a/2). Equation 38 from Forchheimer (1917) is shown below:

$$h_{\Phi} = \frac{\pi q}{k \ln \frac{\cosh\left(\frac{\pi f}{2a}\right) - 1}{3\cosh\left(\frac{\pi f}{2a}\right) - 1}} = approximately 1.364 \frac{q}{k} \frac{1}{\log \frac{\left(\frac{\pi f}{2a}\right)^2}{4 + 3\left(\frac{\pi f}{2a}\right)^2}}$$

The pressure loss for the outer portion is equal to 0.673·q/k after substituting the value of f = a/8 in Equation 38 of Forchheimer (1917).

Similarly, for the inner portion, the pressure loss is again calculated by using a segment of length equal to a/8 and Darcy's Equation is used for this purpose:

$$q = kia$$

$$q = k\left(\frac{h}{l}\right)A$$

$$h = \frac{q}{k}\frac{l}{A}$$

Where $A = (a/2)*1$ and $l = a/8$

Substituting the values of A and l in the above expression, the pressure loss for the inner portion is equal to 0.25·q/k.

Similarly, the collective pressure loss will be $0.923\frac{q}{k}$ which is very close to the actual calculated value of $0.937\frac{q}{k}$.

Note that the factor 0.937 is obtained by considering the flow net and then calculating the ratio of $\pi/2$ and mean potential difference $\left(\frac{\Phi_o+\Phi_f}{2}\right)$ as explained on Page 427 of Forchheimer (1917).

Equations 36 and 37 of Forchheimer (1917) are shown below:

$$\Phi_o = \ln\frac{\sinh\left(\frac{\pi f}{2a}\right)}{1+\cosh\left(\frac{\pi f}{2a}\right)}$$

$$\Phi_f = \ln\frac{\sinh\left(\frac{\pi f}{2a}\right)}{\cosh\left(\frac{\pi f}{2a}\right)+\sqrt{\sinh^2\left(\frac{\pi f}{2a}\right)+\cosh^2\left(\frac{\pi f}{2a}\right)}} = \ln\frac{\sinh\left(\frac{\pi f}{2a}\right)}{\cosh\left(\frac{\pi f}{2a}\right)+\sqrt{\cosh\left(\frac{\pi f}{a}\right)}}$$

Substituting the value of f/2a = 1/8 in Equations 36 and 37 of Forchheimer (1917), the mean potential difference is calculated as 1.6754 and the potential decrease (the ratio of $\pi/2$ and mean potential difference) as 0.937.

It is inferred that a correction is necessary for calculating the potential loss at the center of the structure since we are just considering segments of a/8 for the inner and outer distances and not the whole length for calculation of pressure loss.

It is presumed that correction for the outer section is incorporated in the calculated value of 0.937q/k by considering the flow from source to sink, with the source lying closer to the outer portion. However, for the correction of inner length, it is believed that the pressure loss has to be calculated for the length of f-a/4. This is again done by considering the Darcy's Law for the section of length equal to f-a/4.

$$q = kia$$

$$q = k\left(\frac{h}{l}\right)A$$

$$h = \frac{q}{k}\frac{l}{A}$$

Where $A = a/2$ and $l = f - a/4$. So, the pressure loss for this section will be:

$$\frac{q}{k}\frac{2}{a}\left(f - \frac{a}{4}\right) = \frac{q}{k}\left(\frac{2f}{a} - \frac{1}{2}\right)$$

Therefore, the pressure drop up to the center of the structure (i.e. the blanket) is calculated by using the following formula:

$$h = \frac{q}{k}\left(0.93 + \frac{2f}{a} - \frac{1}{2}\right)$$

Note that 0.93 is obtained by considering the mean of 0.923 and 0.937.

The above expression can be modified as follows:

$$h = \frac{q}{k}\left(0.43 + \frac{2f}{a}\right)$$

$$h\frac{k}{q} = \left(0.43 + \frac{2f}{a}\right)$$

$$\frac{q}{kh} = \frac{1}{\left(0.43 + \frac{2f}{a}\right)}$$

For h = a/2 and w = 2f

$$\frac{q}{\Delta\Phi} = \frac{1}{\left(0.43 + w/2h\right)}$$

$$\frac{q}{\Delta\Phi} = \frac{1}{\left(0.86 + w/h\right)}$$

The above expression is similar to one that appears in Muskat (1937) and Case 1 of the blanket theory.

Determination of distance from effective seepage entry to riverside levee toe (x_1).

Consider the riverward side of the levee as shown in Figure AII-2

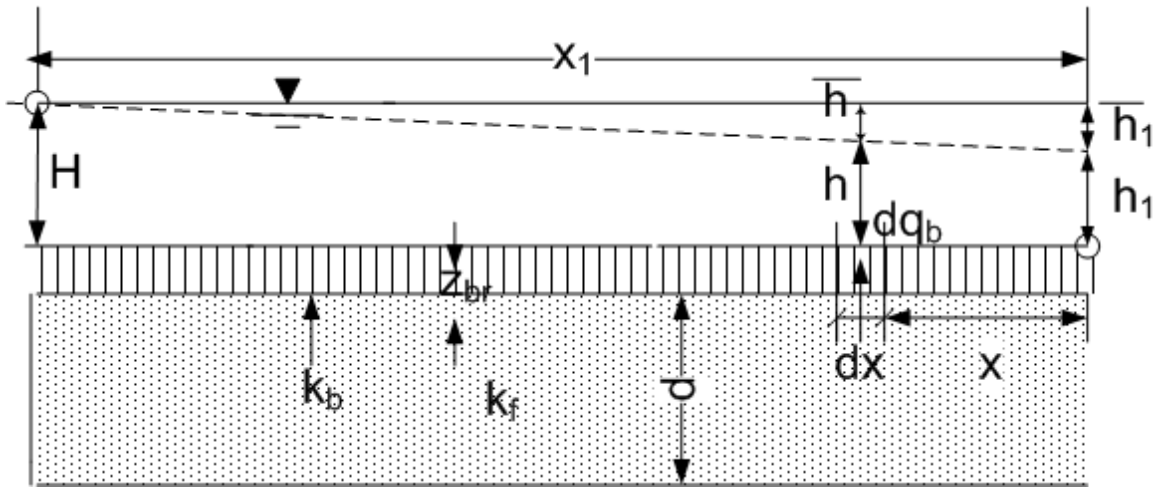

Figure AII- 2 Riverward side of the levee.

Now, from Darcy's Law, the vertical flow through the top stratum is

$q = kiA$

$$dq_b = k_{br}\left(\frac{H-h}{z_{br}}\right)dx$$

$$\frac{d_{qb}}{dx} = k_{br}\left(\frac{H-h}{z_{br}}\right) \qquad \text{(A2-1)}$$

Similarly, the horizontal flow through the pervious substratum is

$$q_f = k_f d \frac{dh}{dx}$$

$$\frac{dq_f}{dx} = k_f d \frac{d^2h}{dx^2} \qquad \text{(AII-2)}$$

The continuity equation for steady state will be:

$$\frac{dq_f}{dx} + \frac{dq_b}{dx} = 0$$

Putting the values of $\frac{dq_f}{dx}$ and $\frac{dq_b}{dx}$ from equations (1) and (2) respectively

$$k_f d \frac{d^2h}{dx^2} + k_{br}\left(\frac{H-h}{z_{br}}\right) = 0$$

Dividing $k_f d$ on both sides of the equation

$$\frac{d^2h}{dx^2} + \frac{k_{br}}{k_f dz_{br}}(H-h) = 0$$

Let $\bar{h} = H - h$ and $\frac{d^2\bar{h}}{dx^2} = -\frac{d^2h}{dx^2}$

So,

$$\frac{d^2\bar{h}}{dx^2} - c^2\bar{h} = 0 \qquad \text{(AII-3)}$$

Where, $c = \sqrt{\frac{k_{br}}{k_f z_{br} d}}$

The differential equation is solved as follows:

Let $p = \frac{d\bar{h}}{dx}$ and the auxiliary equation is:

$$p^2 - c^2 = 0 \qquad (p^1 = \frac{d\bar{h}}{dx}, p^2 = \frac{d^2\bar{h}}{dx^2}, p^0 = \bar{h} = 1)$$

The roots of the above equation are c and $-c$

The solution of the above differential equation is:

$$\bar{h} = m_1 e^{cx} + n_1 e^{-cx} \qquad \text{(AII-4)}$$

Where, m_1 and n_1 are constants

1. If the distance to the river from the riverside levee toe L_1 is known and no riverside borrow pits or seepage block exists, x_1 is determined as follows:

The boundary conditions for this case are

For $x = 0, \bar{h} = H - h_1$

For $x = L_1, \bar{h} = 0$

Putting the first condition in equation (AII-4)

$$H - h_1 = m_1 + n_1$$

Similarly, putting the second condition in equation (AII-4)

$$0 = m_1 e^{cL_1} + n_1 e^{-cL_1}$$

Putting the value of m_1 in the above equation

$$0 = (H - h_1 - n_1) e^{cL_1} + n_1 e^{-cL_1}$$

$$0 = He^{cL_1} - h_1 e^{cL_1} - n_1 e^{cL_1} + n_1 e^{-cL_1}$$

$$0 = He^{cL_1} - h_1 e^{cL_1} - n_1 \left(e^{cL_1} - e^{-cL_1}\right)$$

$$He^{cL_1} - h_1 e^{cL_1} = n_1 \left(e^{cL_1} - e^{-cL_1}\right)$$

$$n_1 = \frac{He^{cL_1} - h_1 e^{cL_1}}{\left(e^{cL_1} - e^{-cL_1}\right)}$$

As, $\sinh x = \dfrac{e^x - e^{-x}}{2}$, Also, assume, $\overline{h_1} = H - h_1$

$$n_1 = \frac{\overline{h_1} e^{cL_1}}{2\sinh(cL_1)}$$

Putting the values of m_1 and n_1 in the solution of differential equation

$$\overline{h} = \left(\overline{h_1} - \frac{\overline{h_1} e^{cL_1}}{2\sinh(cL_1)}\right) e^{cx} + \frac{\overline{h_1} e^{cL_1}}{2\sinh(cL_1)} e^{-cx}$$

$$\overline{h} = \frac{\overline{h_1}}{2\sinh(cL_1)} \left(2e^{cx}\sinh(cL_1) - e^{cL_1} e^{cx} + e^{cL_1} e^{-cx}\right) \qquad \text{(AII-5)}$$

Now,

$e^{cx} 2\sinh(cL_1) = e^{cx}\left(e^{cL_1} - e^{-cL_1}\right)$ Since, $\sinh x = \dfrac{e^x - e^{-x}}{2}$

$$e^{cx} 2\sinh(cL_1) = e^{cx + cL_1} - e^{cx - cL_1}$$

Putting the value of above expression in equation (AII-5)

$$\bar{h} = \frac{\overline{h_1}}{2\sinh(cL_1)}\left(e^{cx+cL_1} - e^{cx-cL_1} - e^{cL_1}e^{cx} + e^{cL_1}e^{-cx}\right)$$

$$\bar{h} = \frac{\overline{h_1}}{\sinh(cL_1)}\frac{\left(e^{c(L_1-x)} - e^{-c(L_1-x)}\right)}{2}$$

$$\bar{h} = \frac{\overline{h_1}\sinh(c(L_1-x))}{\sinh(cL_1)}$$

The distance from the riverside levee toe to the effective seepage entry (x_1) can be determined by extrapolating hydraulic grade line at $x = 0$ to the full head on river stage.

So,

$$\frac{d\bar{h}}{dx} = \frac{-\overline{h_1}}{x_1}$$

Also, we know that,

$$\bar{h} = \frac{\overline{h_1}\sinh(c(L_1-x))}{\sinh(cL_1)}$$

$$\frac{d\bar{h}}{dx} = \frac{\overline{h_1}}{\sinh(cL_1)}\frac{d}{dx}(\sinh(c(L_1-x))) \qquad \text{(AII-6)}$$

Now,

$$\sinh(c(L_1-x)) = \frac{e^{cL_1}e^{-cx} - e^{-cL_1}e^{cx}}{2}$$

$$\frac{d}{dx}\sinh(c(L_1-x)) = \frac{e^{cL_1}(-c)e^{-cx} - e^{-cL_1}(c)e^{cx}}{2}$$

$$\frac{d}{dx}\sinh(c(L_1-x)) = \frac{-c}{2}\left[e^{c(-x+L_1)} + e^{-c(-x+L_1)}\right]$$

$$\frac{d}{dx}\sinh(c(L_1-x)) = -c\cosh c(L_1-x) \qquad \cosh x = \frac{e^x + e^{-x}}{2}$$

Now, putting the value of above expression in equation (B-6)

$$\frac{d\bar{h}}{dx} = \frac{\overline{h_1}}{\sinh(cL_1)} - c\cosh c(L_1 - x)$$

For x=0,

$$\frac{d\bar{h}}{dx} = \frac{\overline{h_1}}{\sinh(cL_1)} - c\cosh(cL_1)$$

$$\frac{d\bar{h}}{dx} = \frac{-c\overline{h_1}}{\tanh(cL_1)} \qquad \text{(AII-7)}$$

As we know that,

$$\frac{d\bar{h}}{dx} = \frac{-\overline{h_1}}{x_1}$$

Putting the value of $\frac{d\bar{h}}{dx}$ in equation (AII-7)

$$\frac{-\overline{h_1}}{x_1} = \frac{-c\overline{h_1}}{\tanh(cL_1)}$$

$$x_1 = \frac{\tanh(cL_1)}{c}$$

where,

$$c = \sqrt{\frac{k_{br}}{k_f z_{br} d}}$$

where k_{br} =Transformed vertical permeability of riverside top stratum

k_f = Horizontal permeability of pervious substratum

d = Thickness of pervious substratum

z_{br} = Transformed thickness of riverside top stratum

2. If the seepage block exists between the riverside levee toe and the river so as to prevent any seepage entrance into pervious foundation beyond the point, x_1 can be determined as follows:

From above case, we know that

$\bar{h} = m_1 e^{cx} + n_1 e^{-cx}$ Where, m_1 and n_1 are constants.

The boundary conditions for this case are as follows:

For $x = 0, \bar{h} = H - h_1$

For $x = L_1, \frac{d\bar{h}}{dx} = 0$

Putting the first condition in equation (AII-4)

$$H - h_1 = m_1 + n_1$$

Similarly, putting the second condition in equation (AII-4)

$$\frac{d\bar{h}}{dx} = m_1 c e^{cx} - n_1 c e^{-cx}$$

$$0 = m_1 c e^{cL_1} - n_1 c e^{-cL_1}$$

Putting the value of m_1 in the above equation

$$0 = (H - h_1 - n_1) c e^{cL_1} + n_1 c e^{-cL_1}$$

$$0 = H c e^{cL_1} - h_1 c e^{cL_1} - n_1 e^{cL_1} - n_1 e^{-cL_1}$$

$$0 = H c e^{cL_1} - h_1 c e^{cL_1} - n_1 c\left(e^{cL_1} - e^{-cL_1}\right)$$

$$H c e^{cL_1} - h_1 c e^{cL_1} = n_1 c\left(e^{cL_1} + e^{-cL_1}\right)$$

Multiplying by ½ on both sides

$$\tfrac{1}{2}\left(\mathrm{Hce}^{\mathrm{cL_1}} - \mathrm{h_1 ce}^{\mathrm{cL_1}}\right) = \tfrac{1}{2}\,\mathrm{n_1 c}\left(\mathrm{e}^{\mathrm{cL_1}} + \mathrm{e}^{-\mathrm{cL_1}}\right)$$

As we know that,

$$\cosh x = \frac{e^{x} + e^{-x}}{2}$$

And we also assume $\overline{h_1} = H - h_1$

So,

$$n_1 \cosh(cL_1) = \tfrac{1}{2}\overline{h_1} e^{cL_1}$$

$$n_1 = \frac{\overline{h_1} e^{cL_1}}{2\cosh(cL_1)}$$

Substituting the values of m_1 and n_1 in the solution of differential equation

$$\overline{h} = \left(\overline{h_1} - \frac{\overline{h_1} e^{cL_1}}{2\cosh(cL_1)}\right) e^{cx} + \frac{\overline{h_1} e^{cL_1}}{2\cosh(cL_1)} e^{-cx}$$

$$\overline{h} = \frac{\overline{h_1}}{2\cosh(cL_1)}\left(2e^{cx}\cosh(cL_1) - e^{cL_1}e^{cx} + e^{cL_1}e^{-cx}\right) \qquad \text{(AII-8)}$$

Now,

$$e^{cx}\,2\cosh(cL_1) = e^{cx}\left(e^{cL_1} + e^{-cL_1}\right) \qquad \text{Since, } \cosh x = \frac{e^{x} + e^{-x}}{2}$$

$$e^{cx}\,2\cosh(cL_1) = e^{cx+cL_1} + e^{cx-cL_1}$$

Putting the value of above expression in equation (AII-8)

$$\overline{h} = \frac{\overline{h_1}}{2\cosh(cL_1)}\left(e^{cx+cL_1} + e^{cx-cL_1} - e^{cL_1}e^{cx} + e^{cL_1}e^{-cx}\right)$$

$$\bar{h} = \frac{\overline{h_1}}{\cosh(cL_1)} \frac{\left(e^{-c(-x+L_1)} + e^{c(-x+L_1)}\right)}{2}$$

$$\bar{h} = \frac{\overline{h_1}\cosh(c(L_1 - x))}{\cosh(cL_1)}$$

For $x = L_1$

$$\overline{h_x} = \frac{\overline{h_1}}{\cosh(cL_1)} \qquad (\text{since}, \cosh(0) = 1)$$

The distance from the riverside levee toe to the effective seepage entry (x_1) can be determined by extrapolating hydraulic grade line at $x = 0$ to the full head on river stage.

So,

$$\frac{d\bar{h}}{dx} = \frac{-\overline{h_1}}{x_1}$$

Also, we know that,

$$\bar{h} = \frac{\overline{h_1}\cosh(c(L_1 - x))}{\cosh(cL_1)}$$

$$\frac{d\bar{h}}{dx} = \frac{\overline{h_1}}{\cosh(cL_1)} \frac{d}{dx}(\cosh(c(L_1 - x))) \qquad (\text{AII-9})$$

Now,

$$\cosh(c(L_1 - x)) = \frac{e^{cL_1}e^{-cx} + e^{-cL_1}e^{cx}}{2}$$

$$\frac{d}{dx}\cosh(c(L_1 - x)) = \frac{e^{cL_1}(-c)e^{-cx} + e^{-cL_1}(c)e^{cx}}{2}$$

$$\frac{d}{dx}\cosh(c(L_1 - x)) = \frac{-c}{2}\left[e^{c(-x+L_1)} - e^{-c(-x+L_1)}\right]$$

$$\frac{d}{dx}\cosh\left(c\left(L_1 - x\right)\right) = -c\sinh c\left(L_1 - x\right) \qquad \sinh x = \frac{e^x - e^{-x}}{2}$$

For $x = 0$,

$$\frac{d}{dx}\cosh\left(c\left(L_1 - x\right)\right) = -c\sinh(cL_1)$$

Now, putting the value of above expression in the equation (AII-9)

$$\frac{d\bar{h}}{dx} = \frac{\bar{h_1}}{\cosh\left(cL_1\right)} - c\sinh(cL_1)$$

$$\frac{d\bar{h}}{dx} = -c\bar{h_1}\tanh(cL_1) \qquad \text{(AII-10)}$$

As we know that,

$$\frac{d\bar{h}}{dx} = \frac{-\bar{h_1}}{x_1}$$

Putting the value of $\frac{d\bar{h}}{dx}$ in equation (AII-10)

$$-\frac{\bar{h_1}}{x_1} = -c\bar{h_1}\tanh(cL_1)$$

$$x_1 = \frac{1}{c\tanh(cL_1)}$$

Where,

$$c = \sqrt{\frac{k_{br}}{k_f z_{br} d}}$$

Where k_{br} =Transformed vertical permeability of riverside top stratum

k_f = Horizontal permeability of pervious substratum

d = Thickness of pervious substratum

z_{br} = Transformed thickness of riverside top stratum.

Appendix III

Additional Figures Comparing FEA and Blanket Theory

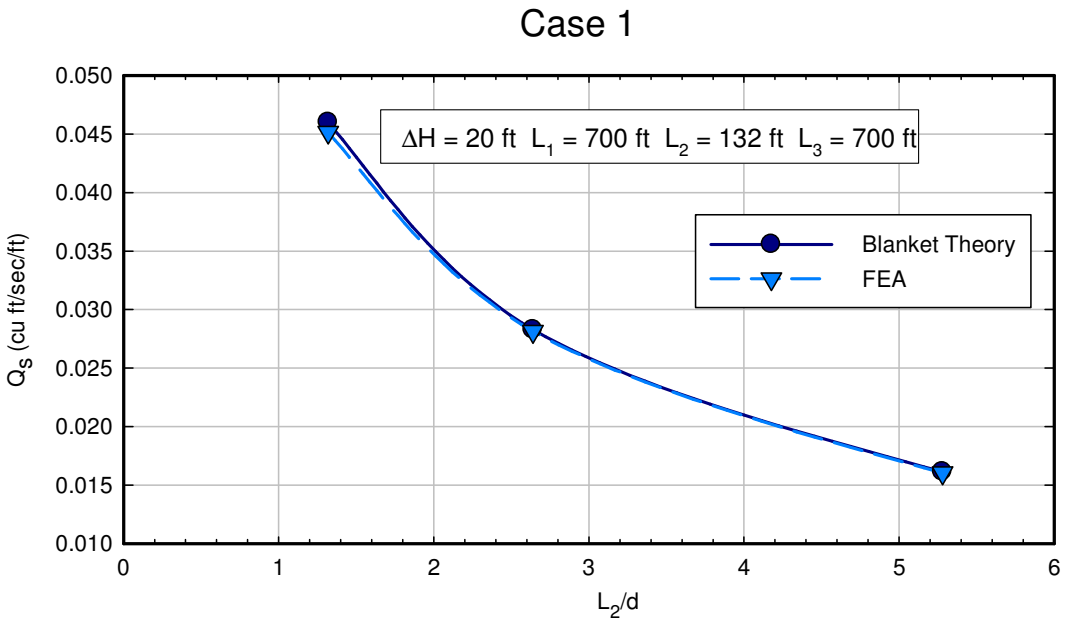

Figure AIII- 1 Calculated values of flow per unit length (Q_s) for different values of L_2/d for Case 1.

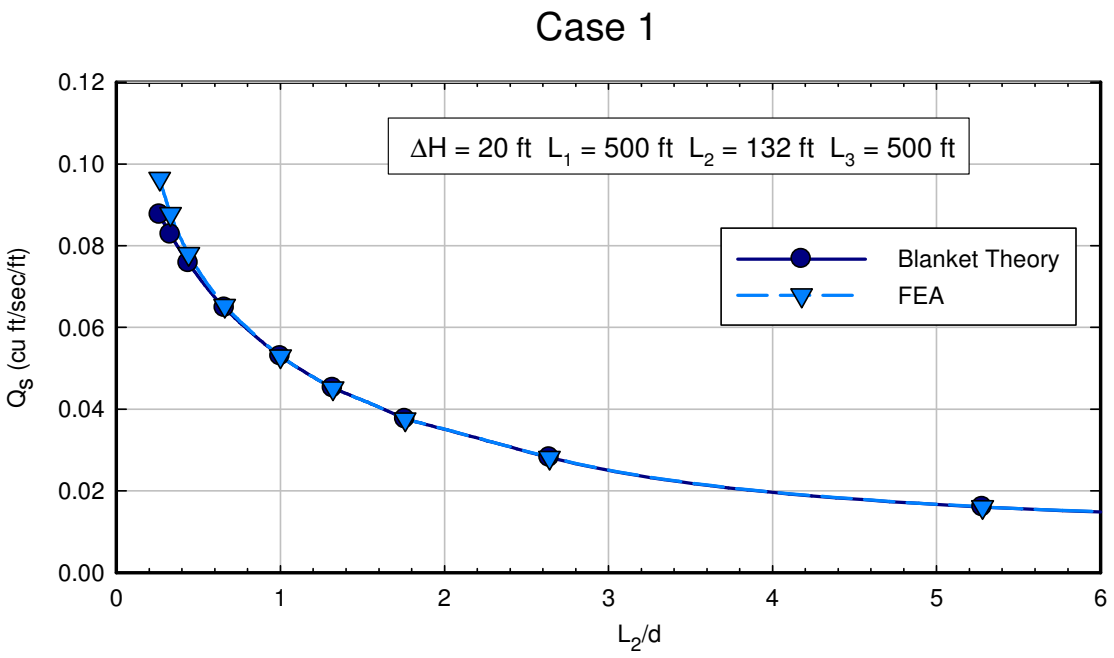

Figure AIII- 2 Calculated values of flow per unit length (Q_s) for different values of L_2/d for Case 1.

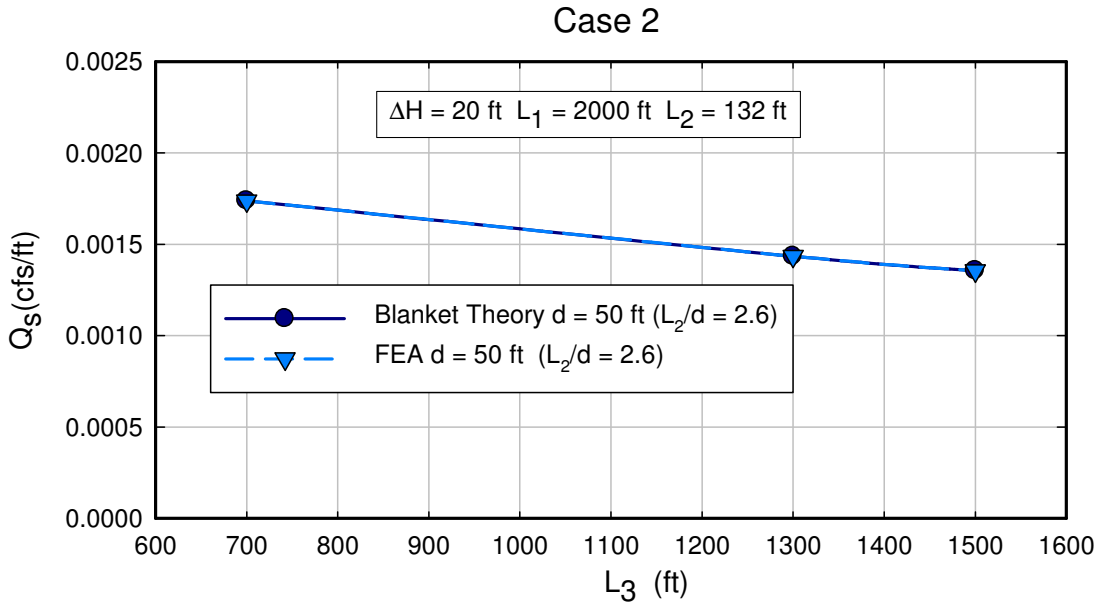

Figure AIII- 3 Calculated values of flow per unit length (Q_s) from blanket theory and finite element analysis for different values of L_3 for Case 2.

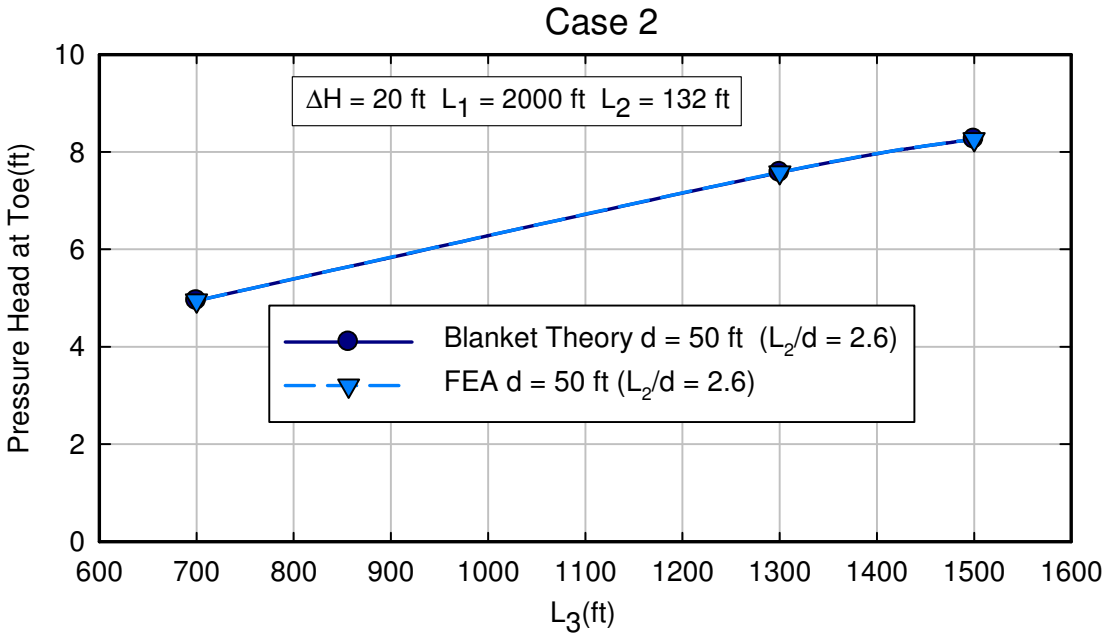

Figure AIII- 4 Excess head (h_o) or pressure head beneath blanket at toe for Case 2 calculated using FEA and blanket theory for different values of L_3 for d = 50 ft.

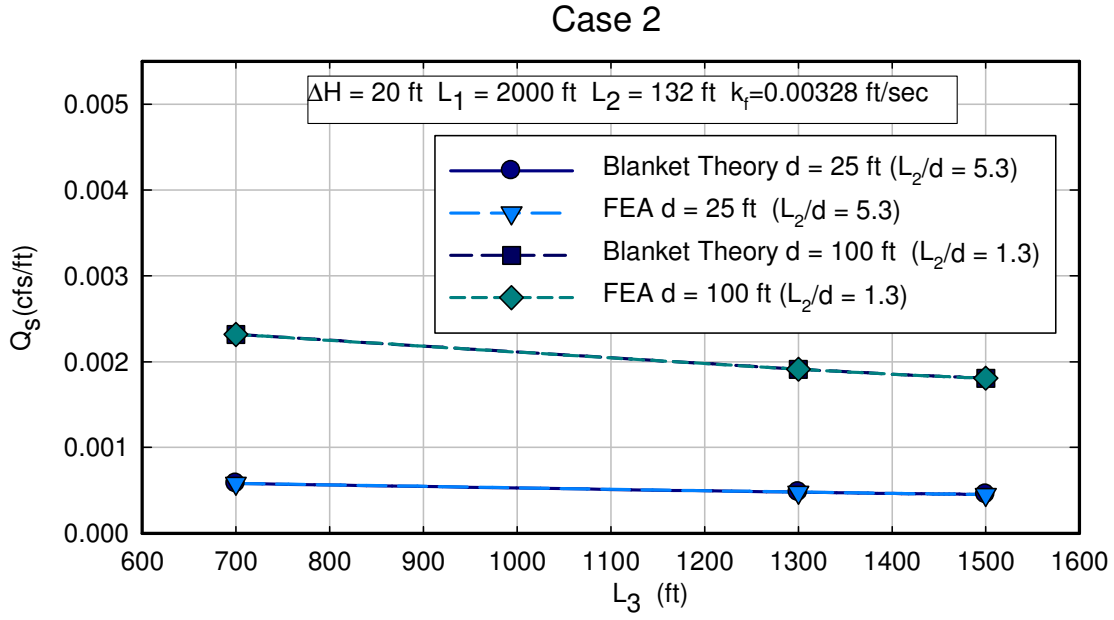

Figure AIII- 5 Calculated values of flow per unit length (Q_s) from blanket theory and finite element analysis for different values of L_3 for Case 2 having k_f as 0.00328 ft/sec.

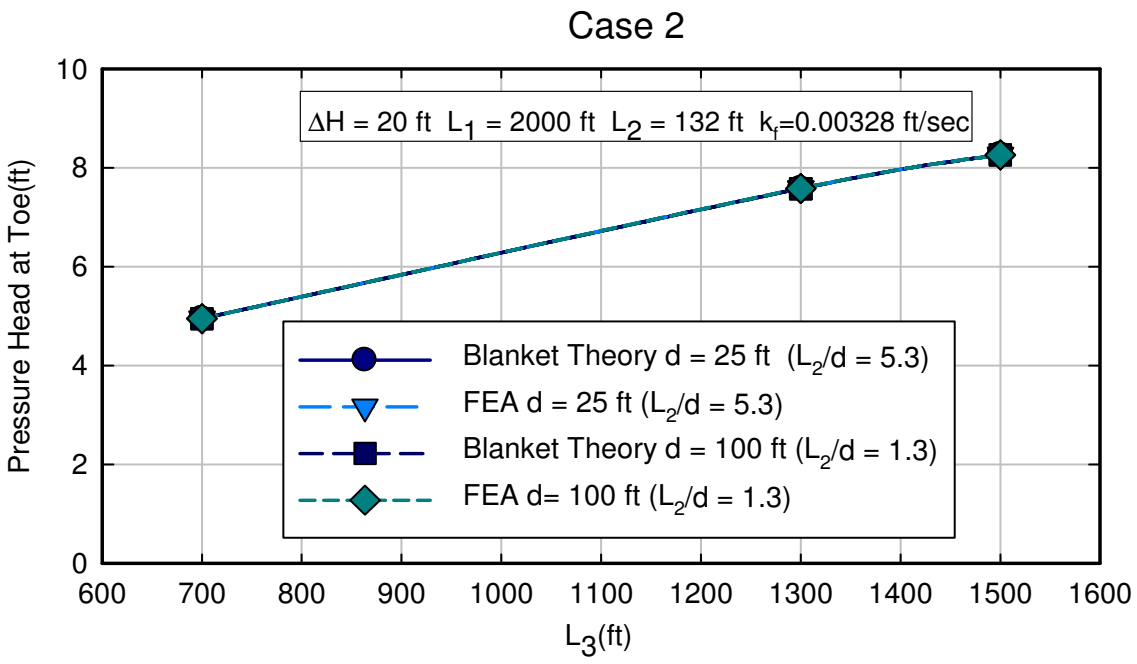

Figure AIII- 6 Excess head (h_o) or pressure head beneath blanket at toe for Case 2 calculated using FEA and blanket theory for different values of L_3 for k_f as 0.00328 ft/sec.

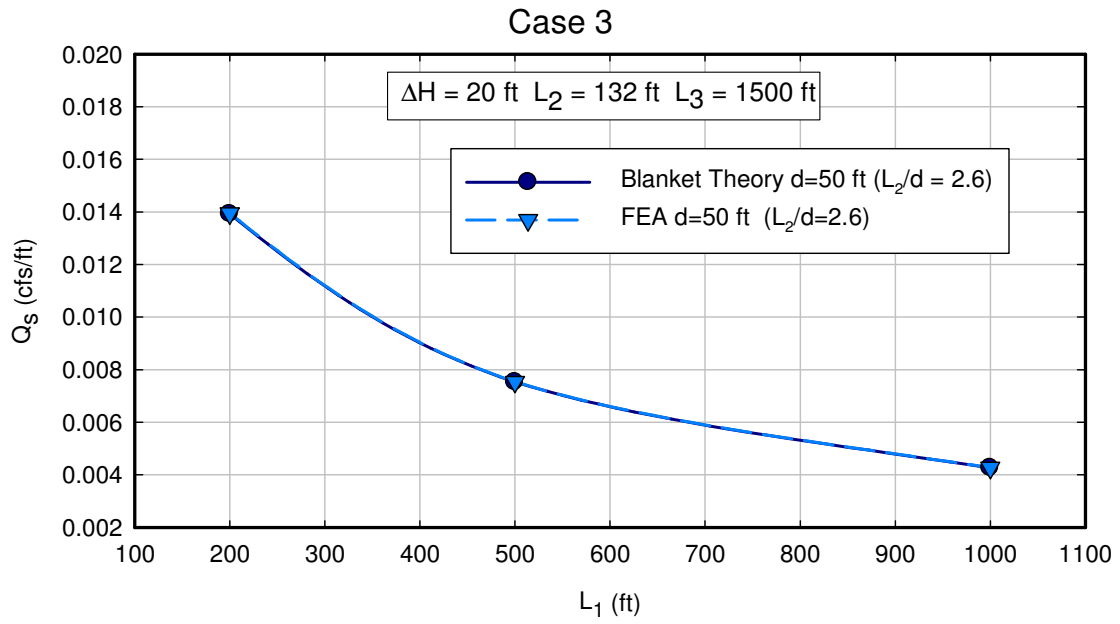

Figure AIII- 7 Calculated values of flow per unit length (Q_s) from blanket theory and finite element analysis for different values of L_1 for Case 3.

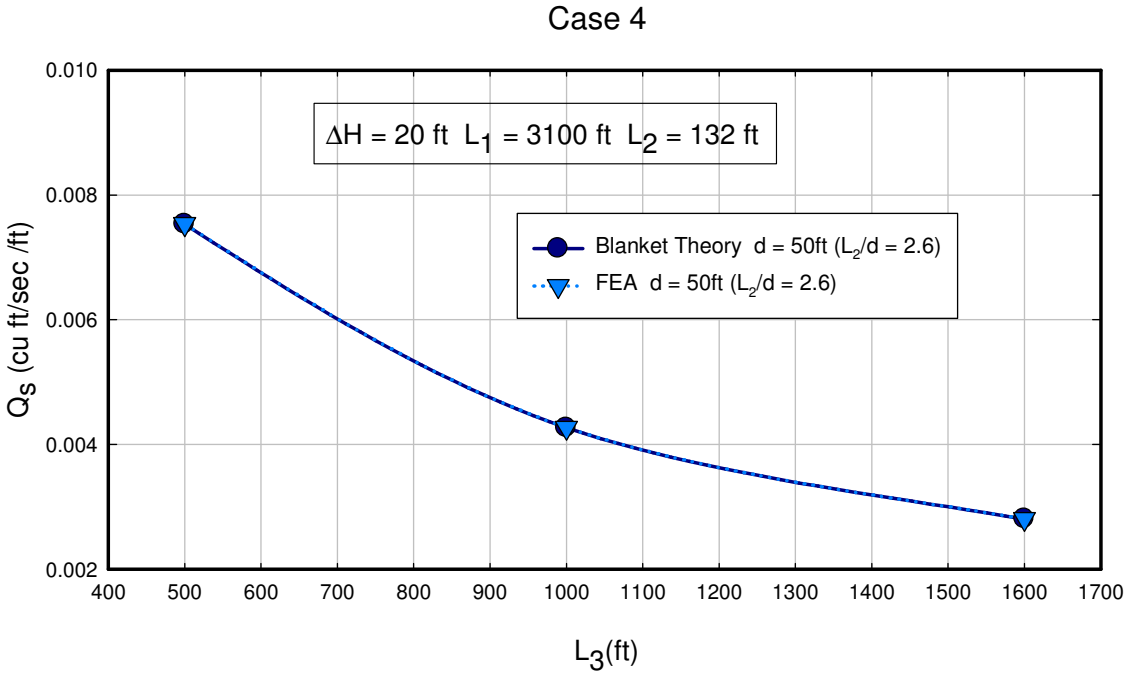

Figure AIII- 8 Calculated values of flow per unit length (Q_s) from blanket theory and finite element analysis for different values of L_3 for Case 4.

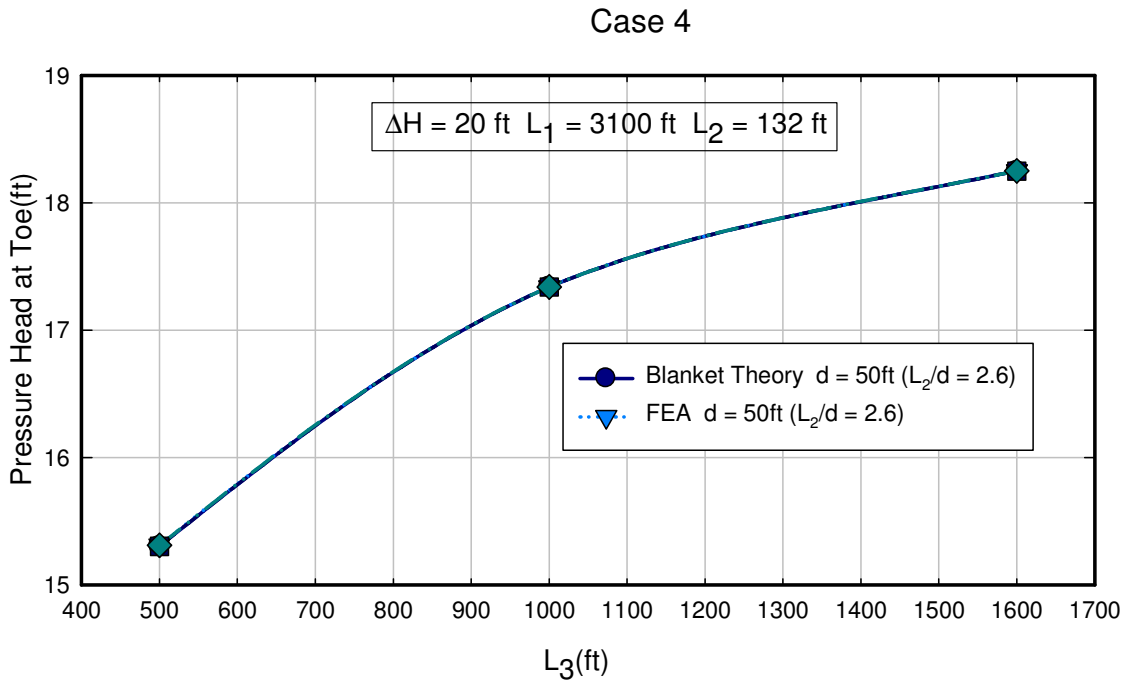

Figure AIII- 9 Excess head (h_o) or pressure head at toe calculated using FEA and blanket theory for different values of L_3.

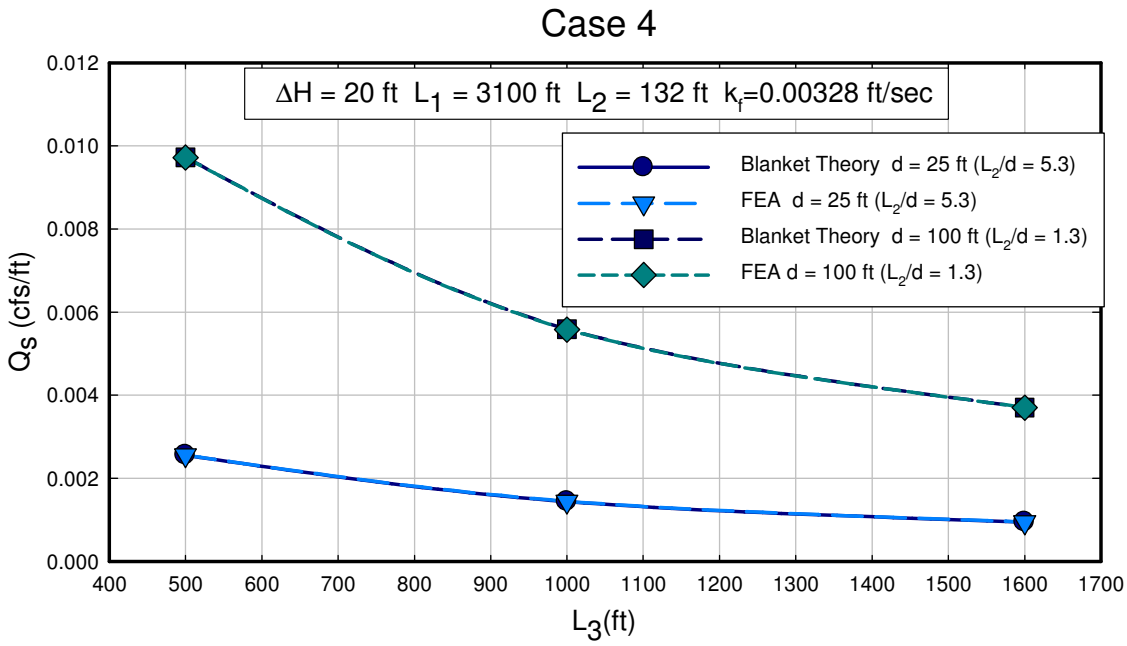

Figure AIII- 10 Calculated values of flow per unit length (Q_s) from blanket theory and finite element analysis for different values of L_3 for Case 4 having k_f as 0.00328 ft/sec.

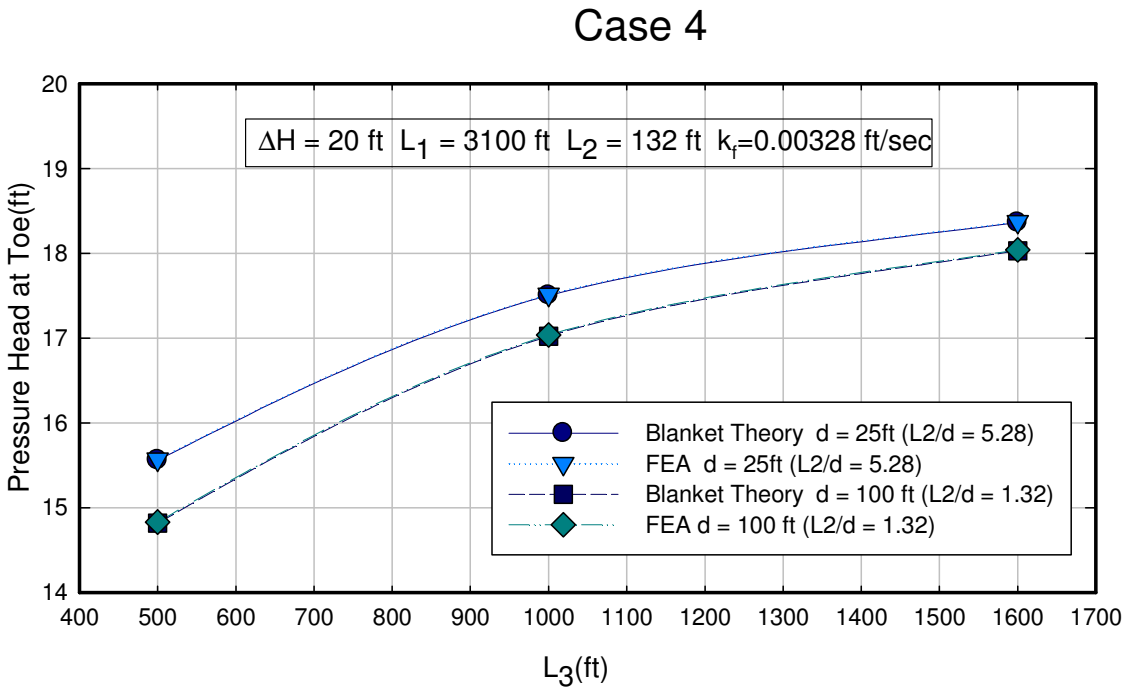

Figure AIII- 11 Excess head (h_o) or pressure head at toe calculated using FEA and blanket theory for different values of L_3 having k_f as 0.00328 ft/sec.

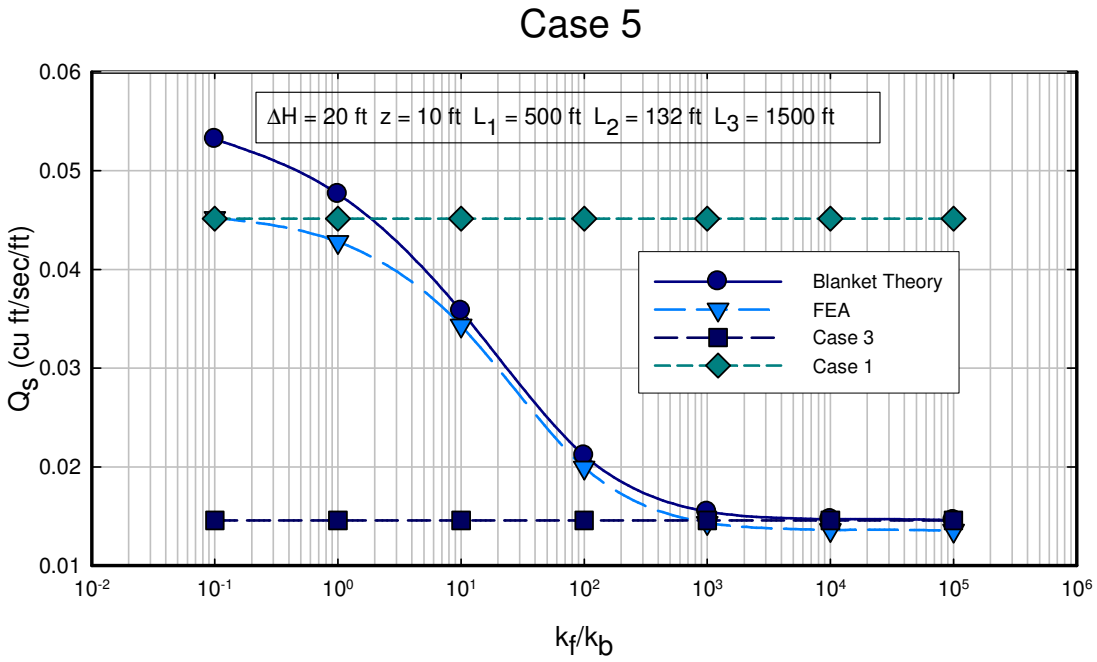

Figure AIII- 12 Calculated values of flow per unit length (Q_s) for various permeability ratios from blanket theory and finite element analysis for Case 5 for z_b = 10 ft and L_1 = 500 ft.

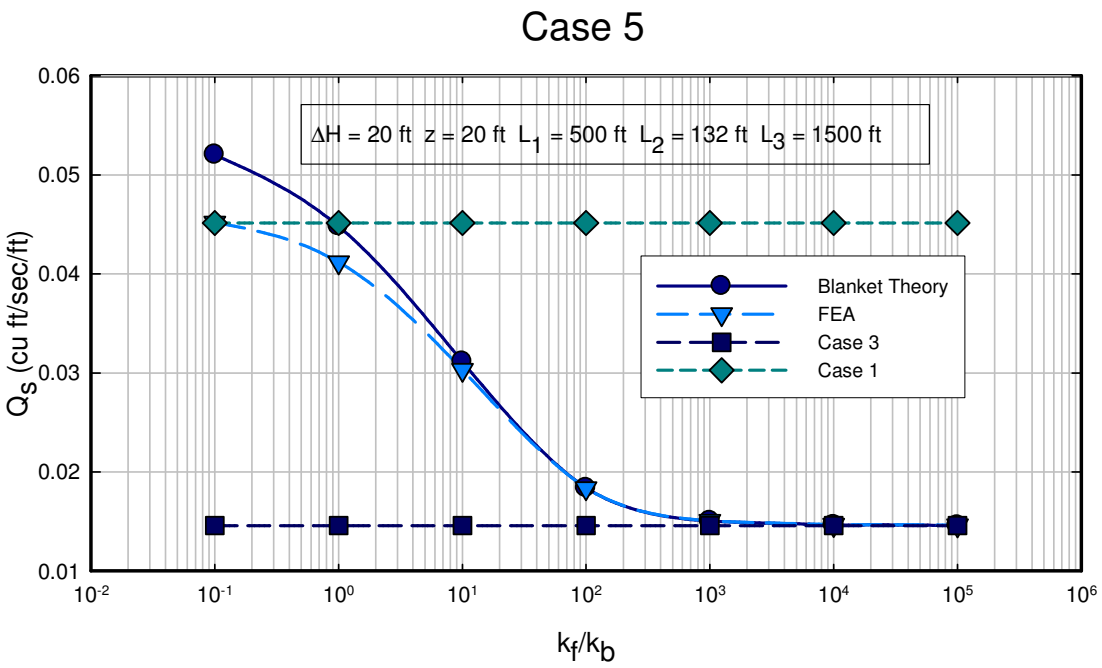

Figure AIII- 13 Calculated values of flow per unit length (Q_s) for various permeability ratios from blanket theory and finite element analysis for Case 5 for z_b = 20 ft and L_1 = 500 ft.

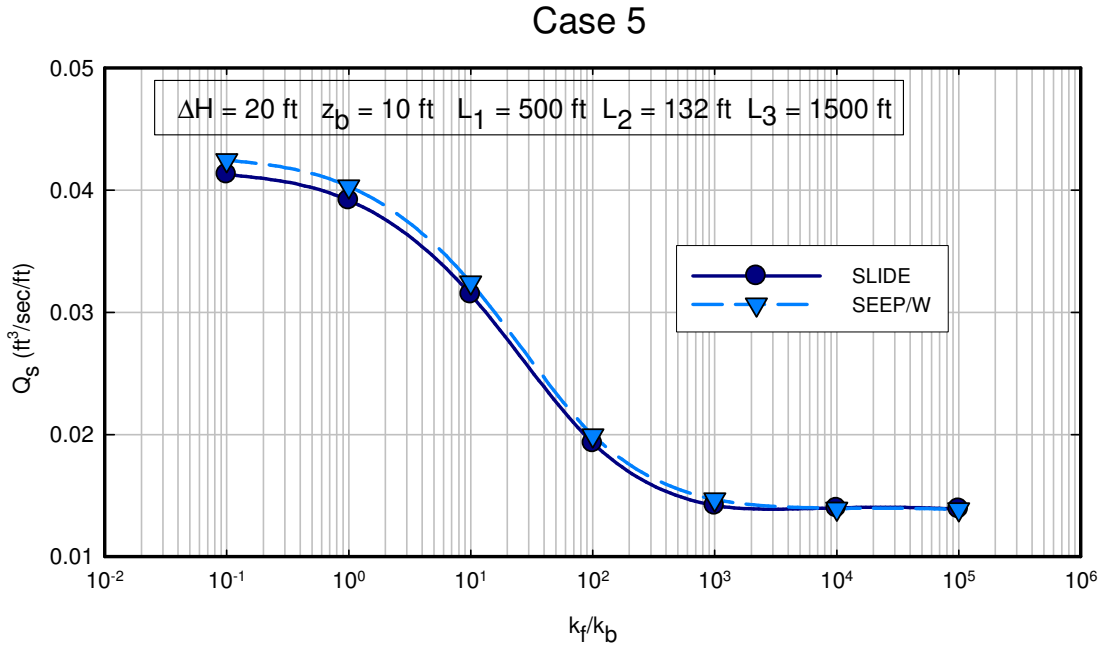

Figure AIII- 14 Calculated flows for SLIDE and SEEP/W for Case 5.

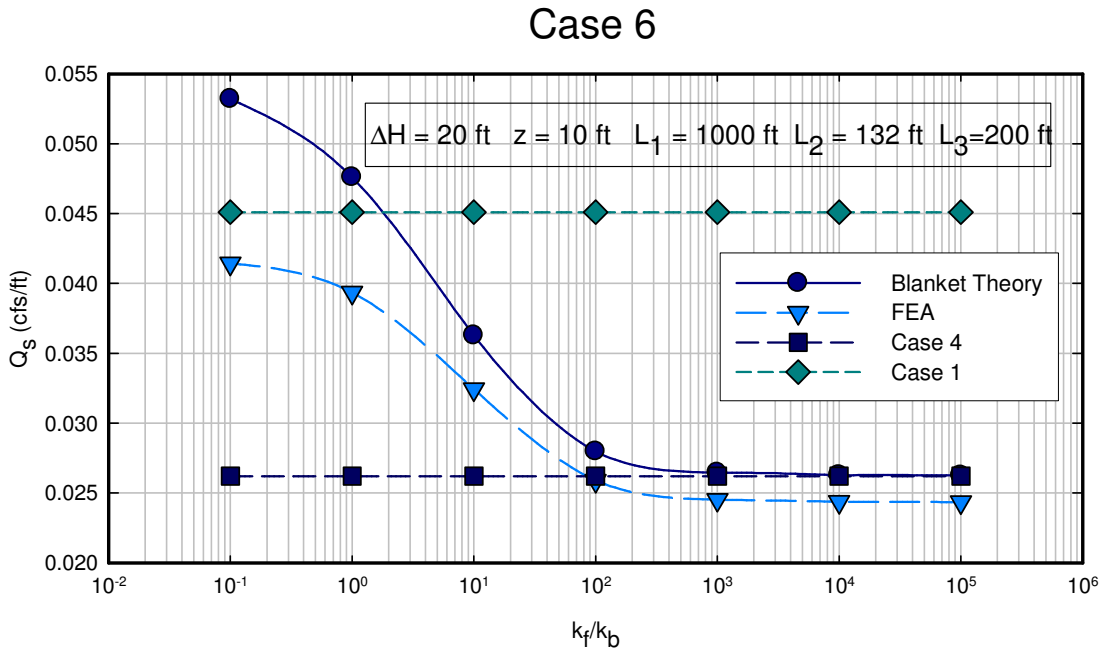

Figure AIII- 15 Calculated values of flow per unit length (Q_s) for various permeability ratios from blanket theory and finite element analysis for Case 6 for z_b = 10 ft and L_3 = 200 ft.

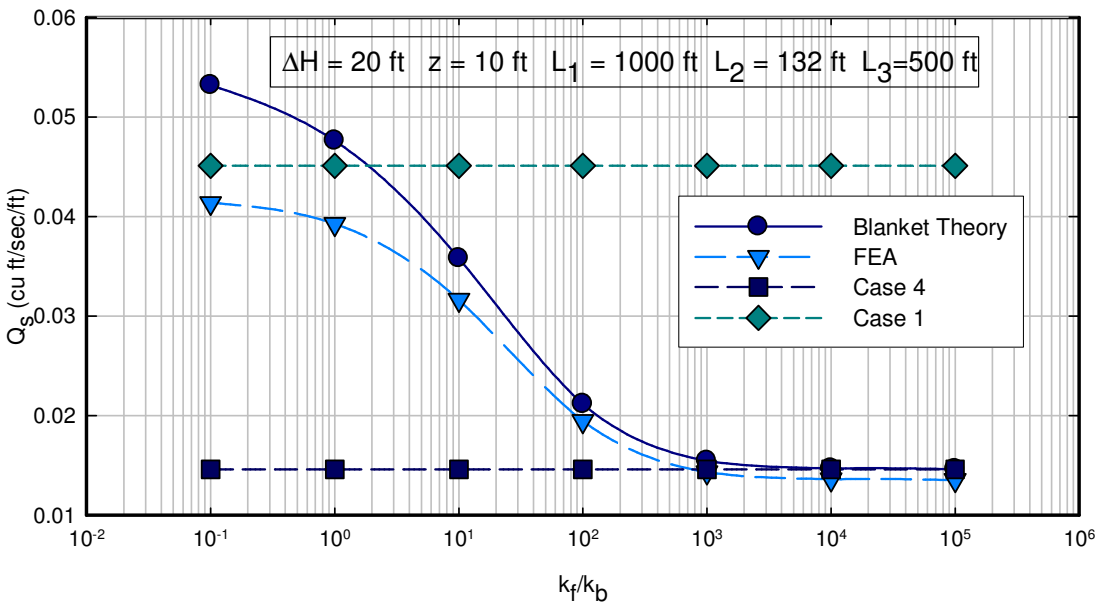

Figure AIII- 16 Calculated values of flow per unit length (Q_s) for various permeability ratios from blanket theory and finite element analysis for Case 6 for z_b = 10 ft and L_3 = 500 ft.

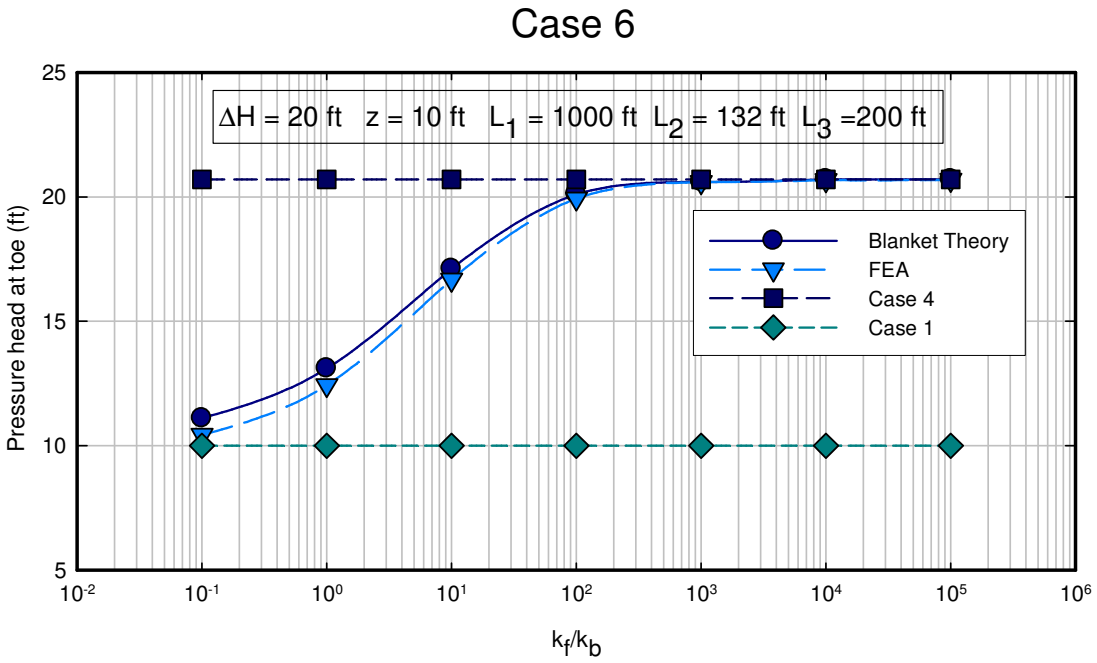

Figure AIII-17 Excess head (h_o) or pressure head beneath blanket at toe for Case 6 calculated using FEA and blanket theory for different permeability ratios for z_b = 10 ft and L_3 = 200 ft.

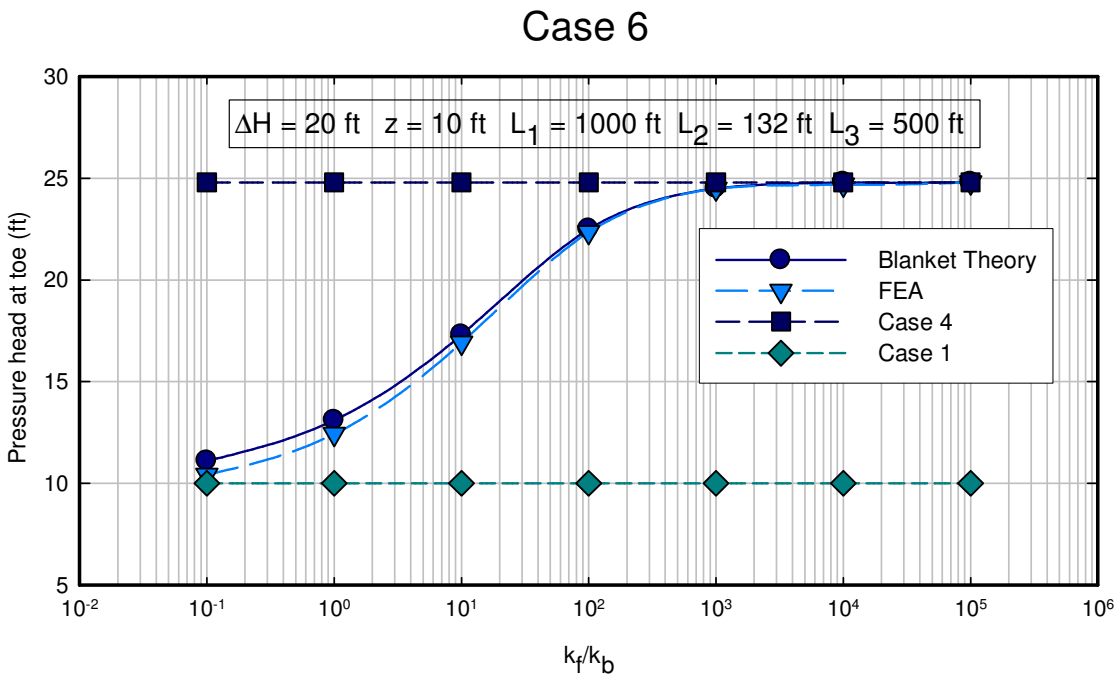

Figure AIII-18 Excess head (h_o) or pressure head beneath blanket at toe for Case 6 calculated using FEA and blanket theory for different permeability ratios for z_b = 10 ft and L_3 = 500 ft.

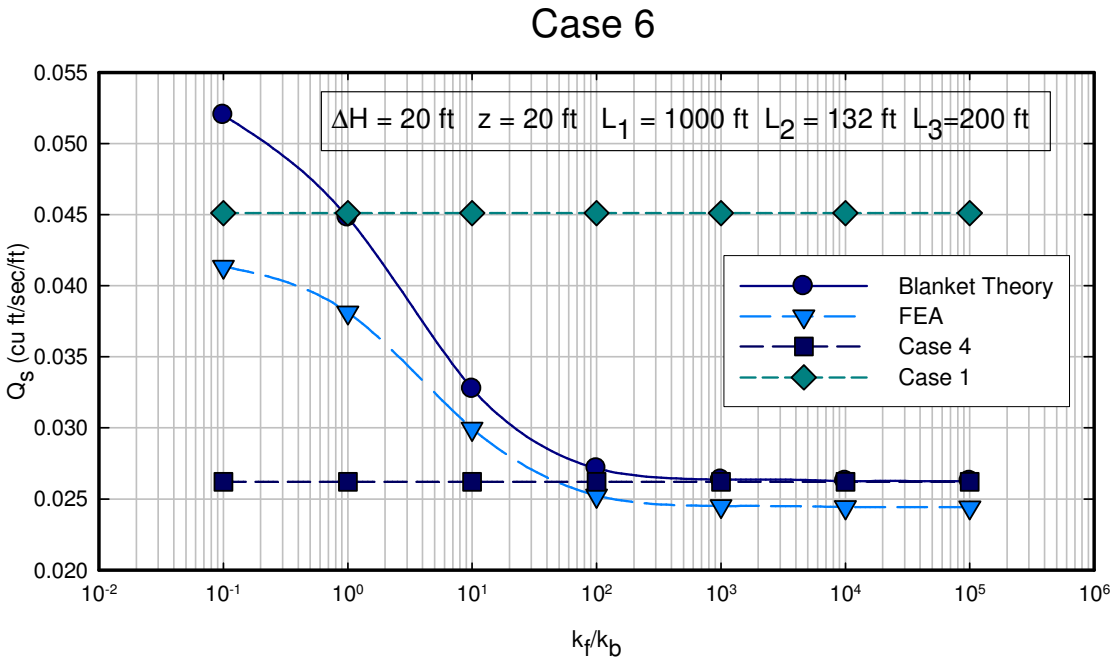

Figure AIII-19 Calculated values of flow per unit length (Q_s) for various permeability ratios from blanket theory and finite element analysis for Case 6 for z_b = 20 ft and L_3 = 200 ft.

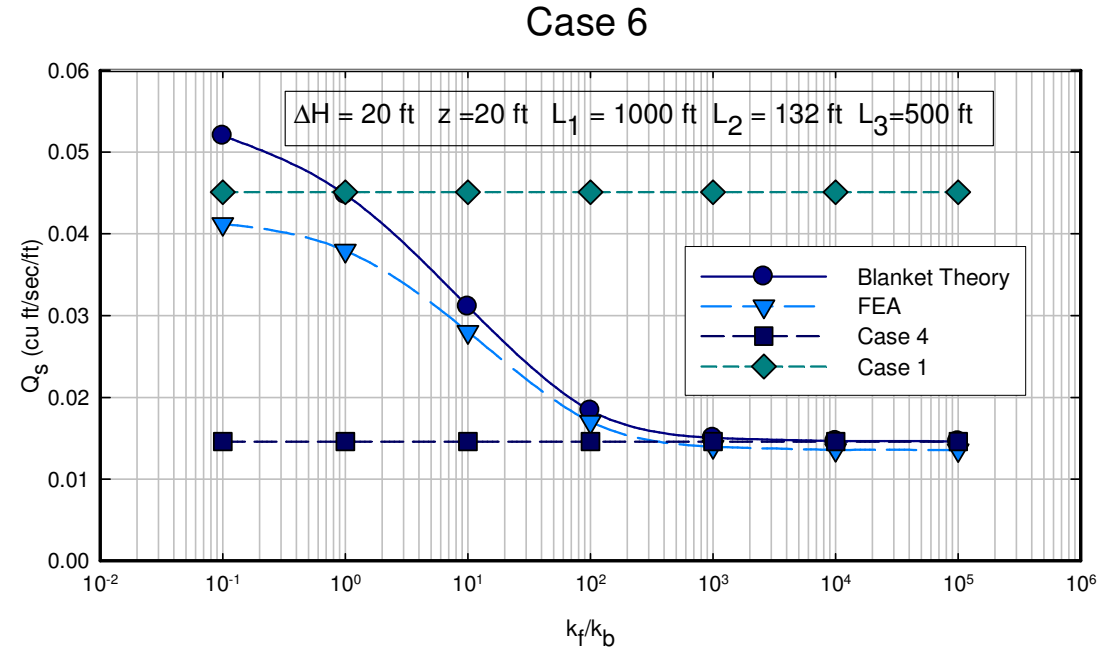

Figure AIII- 20 Calculated values of flow per unit length (Q_s) for various permeability ratios from blanket theory and finite element analysis for Case 6 for z_b = 20 ft and L_3 = 500 ft.

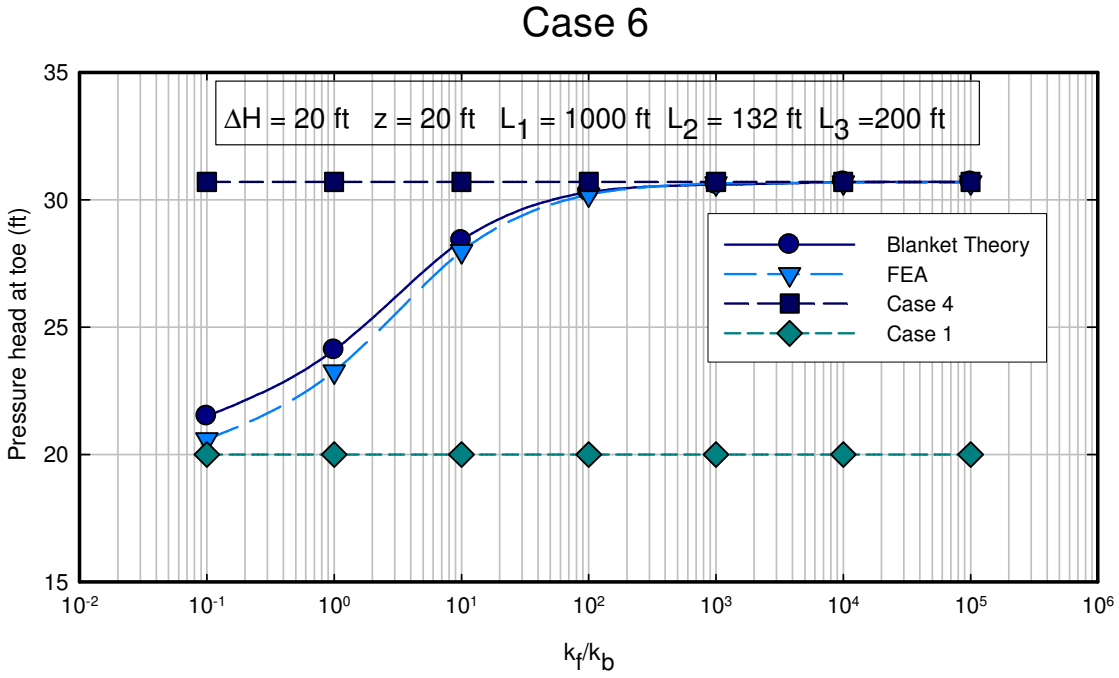

Figure AIII- 21 Excess head (h_o) or pressure head beneath blanket at toe for Case 6 calculated using FEA and blanket theory for different permeability ratios for z_b = 20 ft and L_3 = 200 ft.

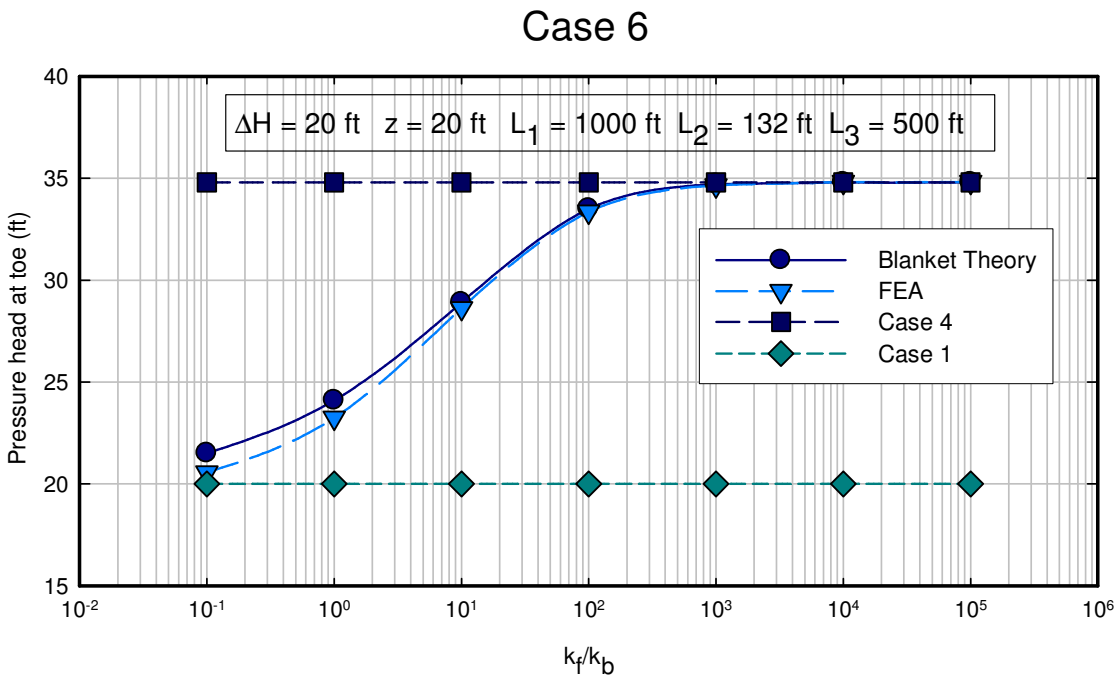

Figure AIII- 22 Excess head (h_o) or pressure head beneath blanket at toe for Case 6 calculated using FEA and blanket theory for different permeability ratios for z_b = 20 ft and L_3 = 500 ft.

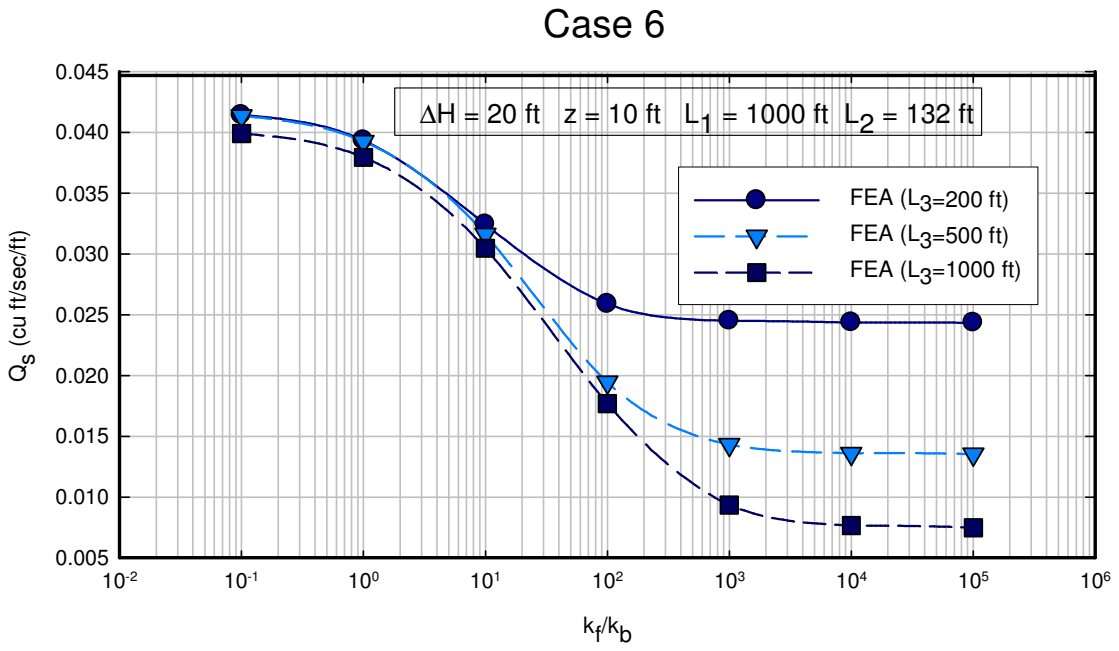

Figure AIII- 23 Comparison of flows for different values of L_3 for Case 6 for z_b=10 ft.

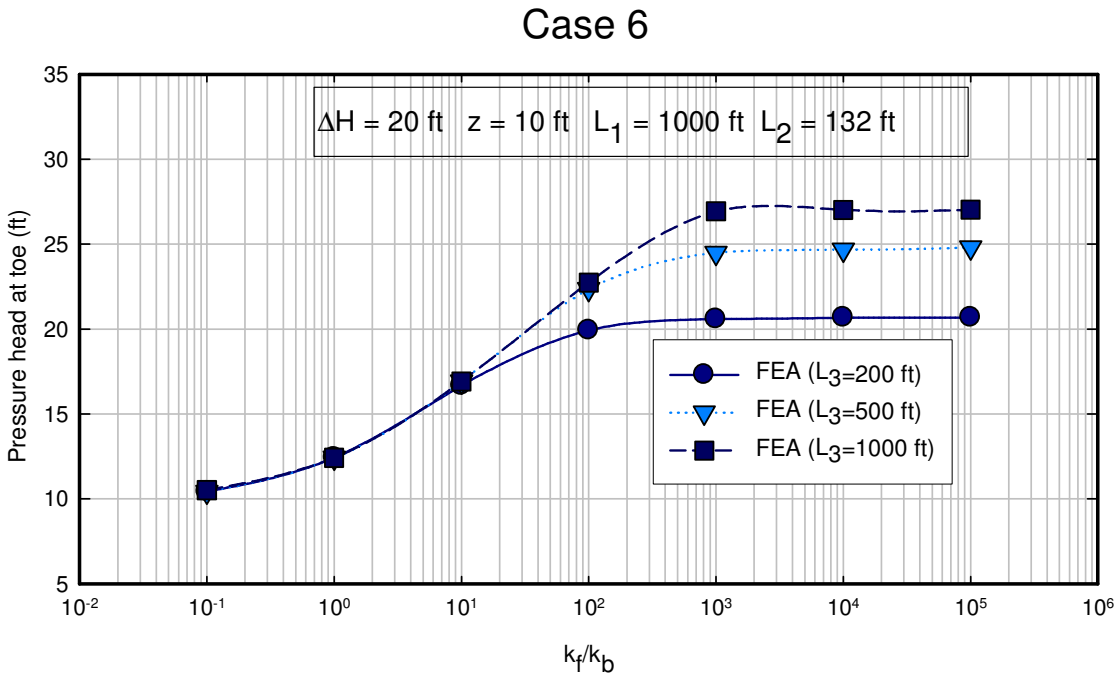

Figure AIII- 24 Comparison of excess head (h_o) for different values of L_3 for Case 6 for z_b=10 ft.

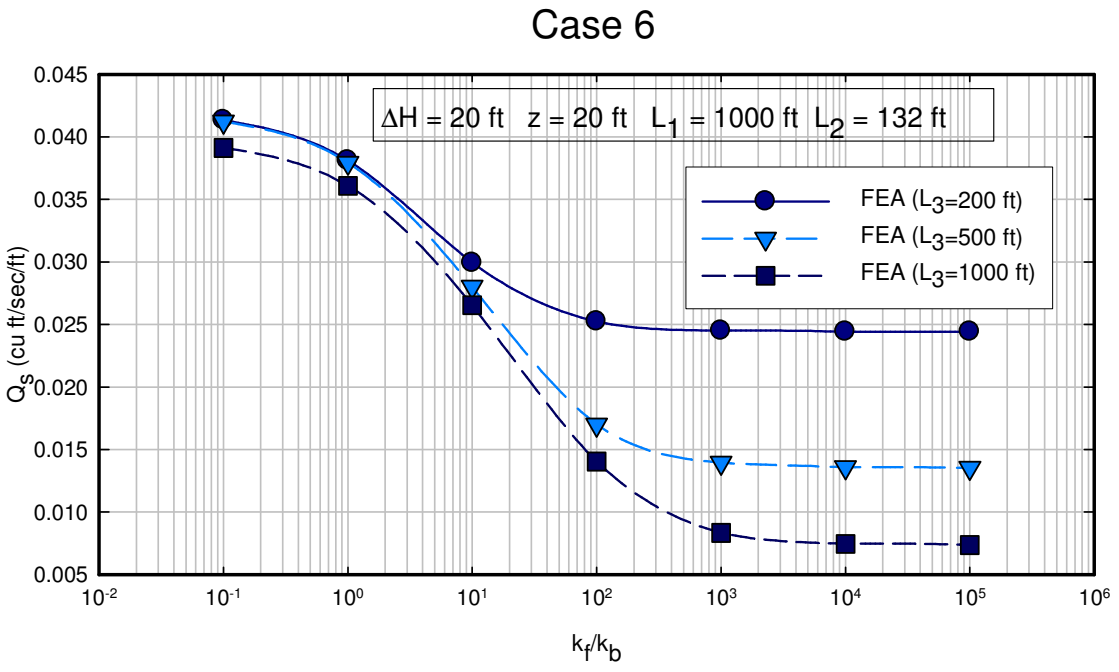

Figure AIII- 25 Comparison of flows for different values of L_3 for Case 6 for z_b=20 ft.

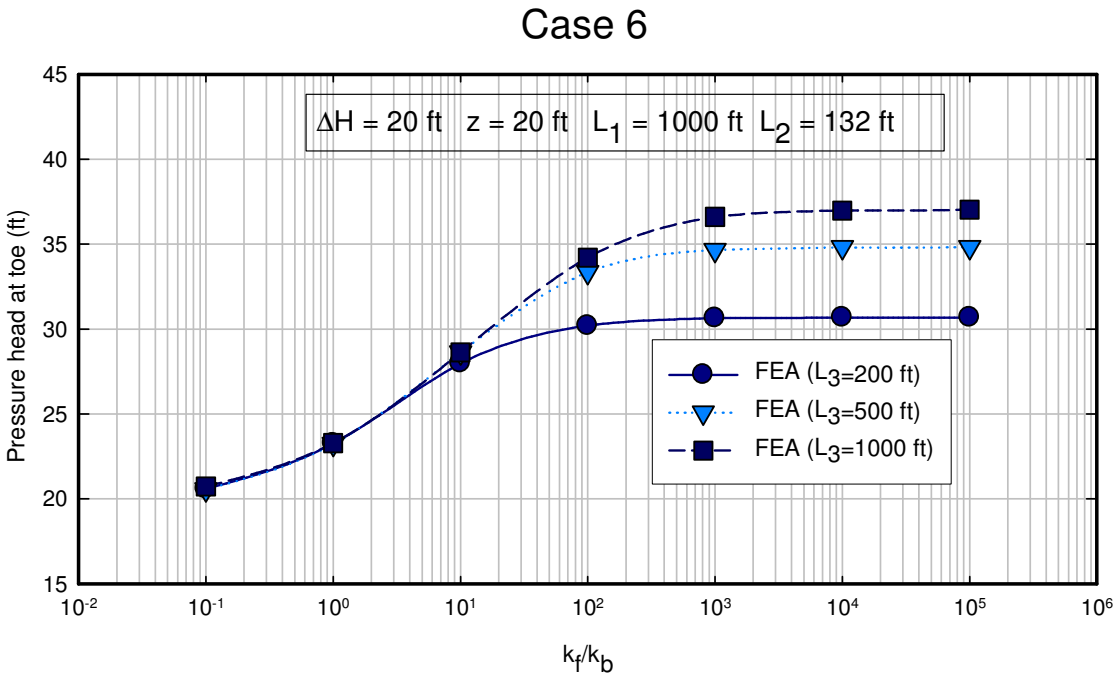

Figure AIII- 26 Comparison of excess head (h_o) for different values of L_3 for Case 6 for z_b=20 ft.

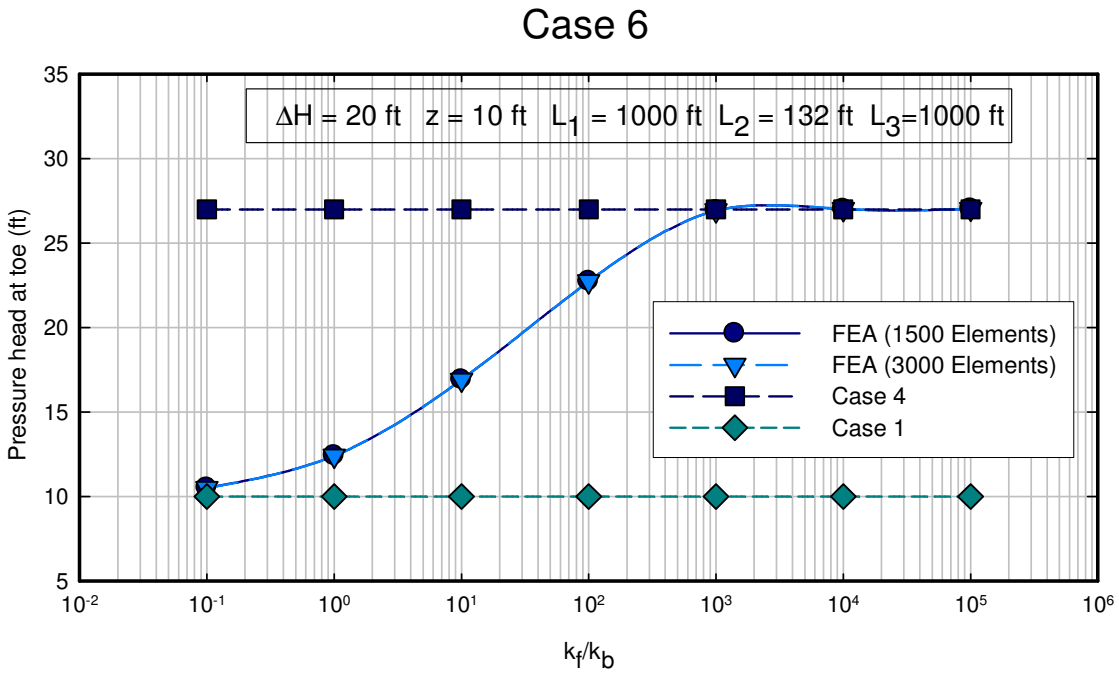

Figure AIII- 27 Calculated excess head (h_o) for Case 6 showing the effect of number of elements.

Appendix B

Finite Element Seepage Analysis of the London Avenue Canal Load Test

Report submitted to the U. S. Army Corps of Engineers (2010)

Authors

Abeera Batool[1] and Thomas L. Brandon[1],

[1]*Dept. of Civil and Environmental Engineering, Patton Hall, Virginia Polytechnic Institute and State University (Virginia Tech), Blacksburg, VA 24061 USA*

Introduction

An extensive study was done by the US Army Corps of Engineers (USACE) following the events of Hurricane Katrina to investigate the causes of failures of I-walls and levees. This included the analyses conducted by Interagency Performance Evaluation Taskforce (IPET) to assess the performance of the Hurricane Protection System in New Orleans and Southeast Louisiana. The USACE also conducted a load test along the portion of the London Avenue Canal to better understand the performance of I-walls in that region. The intention was to hydraulically load the I-wall and measure pore pressures and displacements in the vicinity of the I-wall through extensive instrumentation. A section considered to be critical was selected along the London Canal and the test was conducted on a 150 ft section of the I-wall and the levee from August 18 to September 1, 2007. A cofferdam was constructed to isolate the wall panels, and the water level inside the cofferdam was raised in increments while all instruments were monitored. The types of data collected during the test included canal water levels, pore pressures, rotation and displacement of I-wall panels, and horizontal and vertical movement of the ground surface.

The purpose of this research was to assess the collected data related to seepage and to develop a seepage model that would be applicable to the London Avenue Canal and portions of the Orleans Avenue Canal where the soil conditions are similar. Three-dimensional (3D) seepage analyses were conducted, and the model was calibrated with the field test data to determine the best soil properties and hydraulic boundary conditions. However, the boundary conditions of the load test were not ideal, and impacted the observed parameters during the test. A summary of best combination of various soil properties and hydraulic boundary conditions is presented and the results were generalized for the more common two-dimensional (2D) seepage analyses. Modeling of the load test presented some complex scenarios and additional analyses would be helpful in better comprehension of the situation.

Causes of failure of London Canal I-walls during Hurricane Katrina

Two breaches occurred in the London Avenue Canal I-wall after Hurricane Katrina. These were the north breach (on the east side of the canal at Robert E. Lee Boulevard) and the south breach (on the west side of the canal at Mirabeau Avenue) as shown in Figure B-1. A detailed assessment of these breaches was presented in the report prepared by Interagency Performance Evaluation Taskforce (IPET 2007). A brief summary of the causes of failure of London Canal I-walls from IPET report will be outlined here.

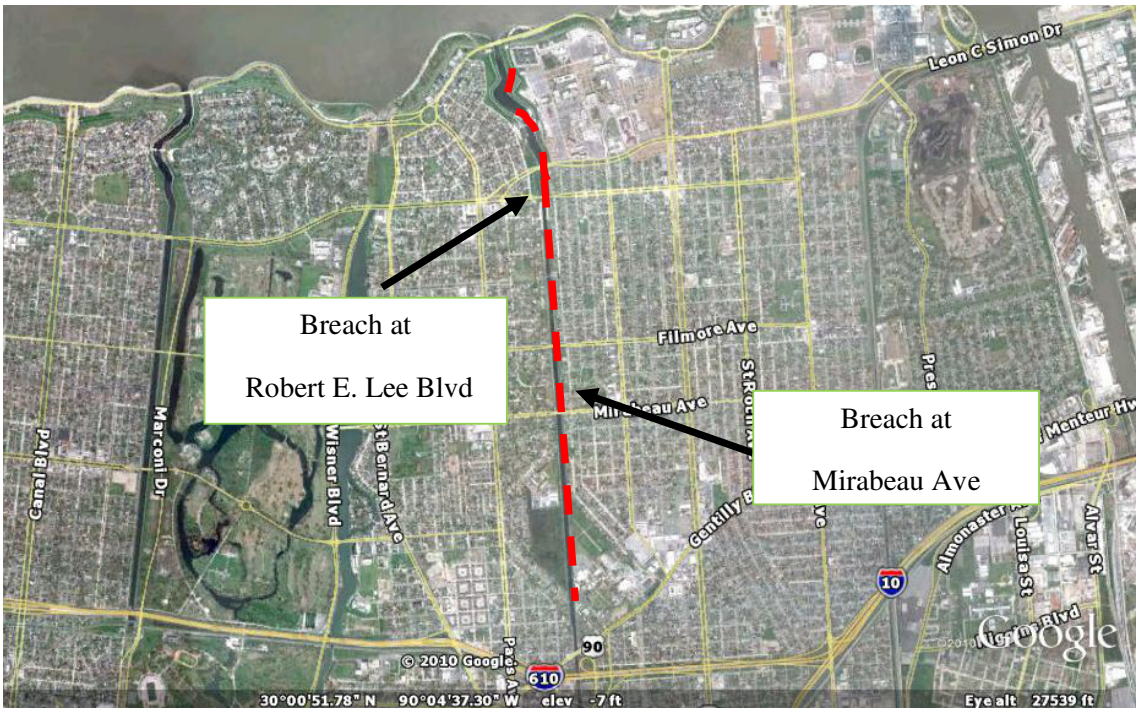

Figure B-1 Location of breaches developed in London Avenue Canal during Hurricane Katrina (Google Earth –used under fair use, 2013).

IPET Assessment of London Avenue Canal Failures

Several breaches in the flood protection system of New Orleans were the result of the failure of I-walls during Hurricane Katrina. The breaches in both the London Avenue Canal and the 17th Street Canal were triggered by the formation of gap between the I-wall and the levee fill. However, the failure mechanisms were different at the London Avenue Canal as compared to the 17th Street Canal due to the dissimilar soil conditions. The 17th Street Canal I-wall had a predominately clayey foundation while London Canal I-wall had a continuous sand stratum at a relatively shallow depth overlain by a marsh layer and the clayey levee fill. The presence of the sand layer may have resulted in a direct hydraulic connection between the water in the canal

through the sand layer exposed at the bottom of the canal or through the gap between the I-wall and the levee embankment.

Detailed seepage and stability analyses were performed during the IPET study to understand the failure mechanisms resulting in the north and the south breaches in the London Canal I-wall (IPET 2007). The IPET study also involved the use of centrifuge models to better understand the failure mechanisms. These analyses indicated that high uplift pressure on the base of the levee and the marsh layer was a key factor in the failures at both the south and the north breaches of the canal. At both locations, these high uplift pressures probably resulted in the development of a rupture through the marsh layer and hydraulic gradients large enough to cause erosion of the sand (IPET 2007). Figure B-2 is from the IPET report indicating the breaches in the London Avenue Canal and summarizing the failure mechanisms.

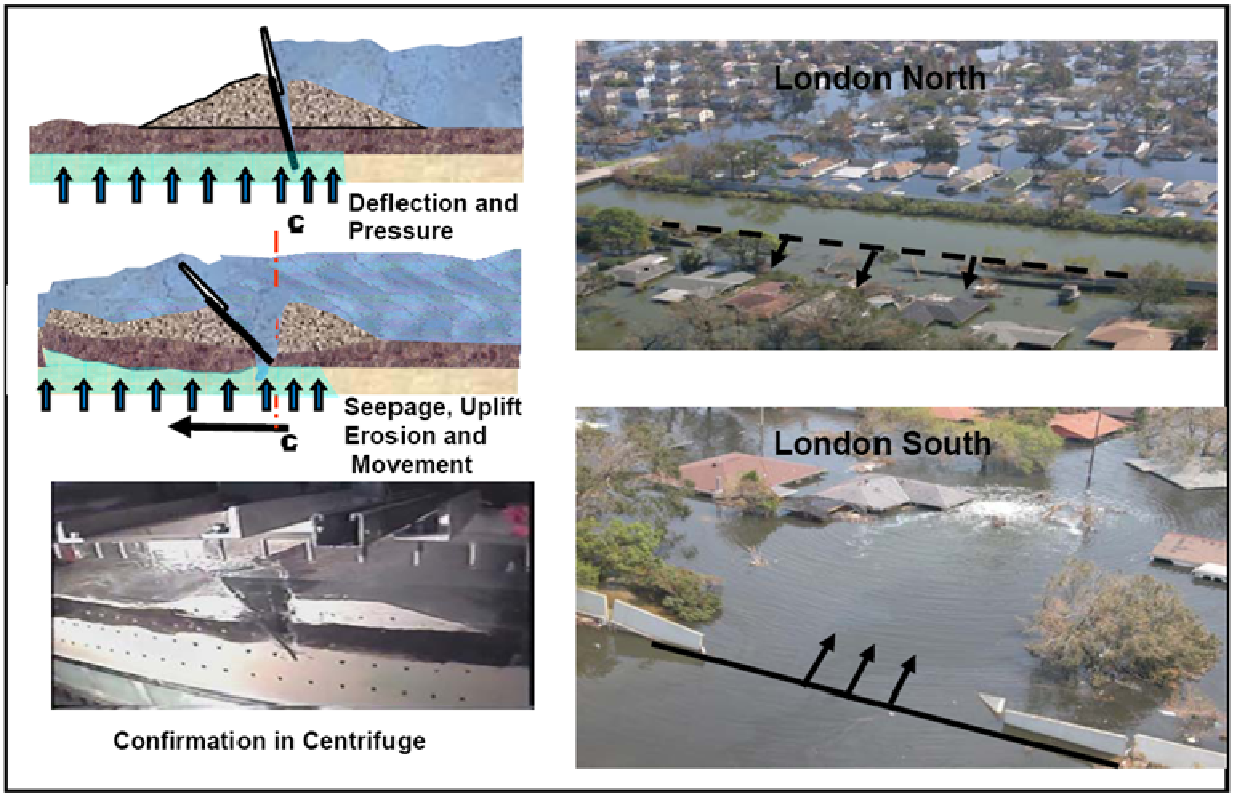

Figure B-2 North and south breaches developed in London Avenue Canal I-wall due to deflection of I-wall caused by high uplift pressures and erosion, and confirmed by centrifuge pumping (IPET 2007- used under fair use, 2013).

The principal mode of failure was different in the north and the south breach of the London Avenue Canal. At the south breach area, the sand was dense with a high friction angle, and the initial calculated factors of safety against instability were greater than 1, even with the high pore pressures resulting from a hydraulic connection of the canal water to the underlying sand layer. However, as erosion was initiated due to the high gradients at the toe of the levee, the factor of safety was reduced significantly by erosion and piping, which removed large quantities of the foundation soil, thus resulting in instability at this location. Thus, the major factors that contributed to the south breach were erosion and piping in localized zones caused by increased hydraulic gradients, especially in the areas where rupture through the marsh layer occurred. This

failure scenario is supported by the fact that the failure started in a small area, and the failure was relatively narrow.

At the north breach, the sand was in a looser state and had a lower friction angle. Although, piping and erosion were still contributing factors, the probability of instability was higher at this section. The high pore pressures developed within the sand would have been sufficient enough to cause the instability even without the loss of soil due to erosion and piping. This is supported by the wider north breach when compared to the south breach, indicating the lesser role of intense piping and erosion in a localized zone. Although piping and erosion were significantly involved in the failure, instability due to the presence of the loose sand was the major failure mechanism at the north breach. It should be noted that the I-wall on the east side of the canal, directly across from the north breach, was also severely distressed and was replaced after Hurricane Katrina as part of Task Force Guardian.

Description of I-Wall Load Test

The USACE decided to conduct a load test along a portion of the London Avenue Canal to better understand the failure mechanisms that resulted in the breaches along the canal. A brief summary of the design and operation of the load test is presented below.

A site was selected for the load test based on an assessment of the soil stratigraphy relying on scant pre-Katrina borings, the dimensions of the levee embankment sections (crest width and slope angle), and the availability of adequate space for conducting the test. Based on the information available at the time, Station 111+00 on the east bank (south of Robert E. Lee Blvd.) was considered to be critical and the load test was performed at this location. The site location is

shown in Figure B-3. A detailed geotechnical investigation was completed immediately prior to the load test to provide information about the soil profile and the engineering properties of the soil layers. This information was used for the design of the load test in such a manner that it could be safely conducted without risking the integrity of the existing flood protection system.

A sheet pile cofferdam was constructed to isolate a section of the I-wall from the rest of the canal. The cofferdam was about 150 ft long and 35 feet wide and the centerline of the cofferdam was located at 5772 Warrington Drive aligned with a vacant lot. The top elevation of the cofferdam was +8.00 ft NAVD88 as the maximum water elevation to be tested inside the cofferdam was +7.50 ft NAVD88. The cofferdam isolated five of the 30 ft long wall panels for testing.

Figure B-3 Location of site for London Avenue Canal load test (from Google Maps- used under fair use, 2013).

PZ-35 sheet piles and HP 14x73 piles were available to the USACE from other projects and were used in the construction of the cofferdam. The cofferdam fully penetrated the pervious layer of beach sand to be effective as a cut-off system. The connection between the cofferdam sheet piles and the existing I-wall was critical in maintaining watertightness, and details of this connection can be found in a later section of this report. A pump system was also incorporated into the

design to quickly dewater the cofferdam. It was supported by a sluice gate included in the cofferdam, which further addressed rapid unloading issues.

The water level was raised in increments while the instrumentation was automatically monitored. Each water level was maintained until it was judged, using both displacement and pore pressure measurements, that a steady state condition had been achieved. A plan view of the location of the instruments is shown in Figure B-4. The types of data collected during the test included canal water levels, pore pressures, rotation and displacement of I-wall panels, and horizontal and vertical movement of the ground surface.

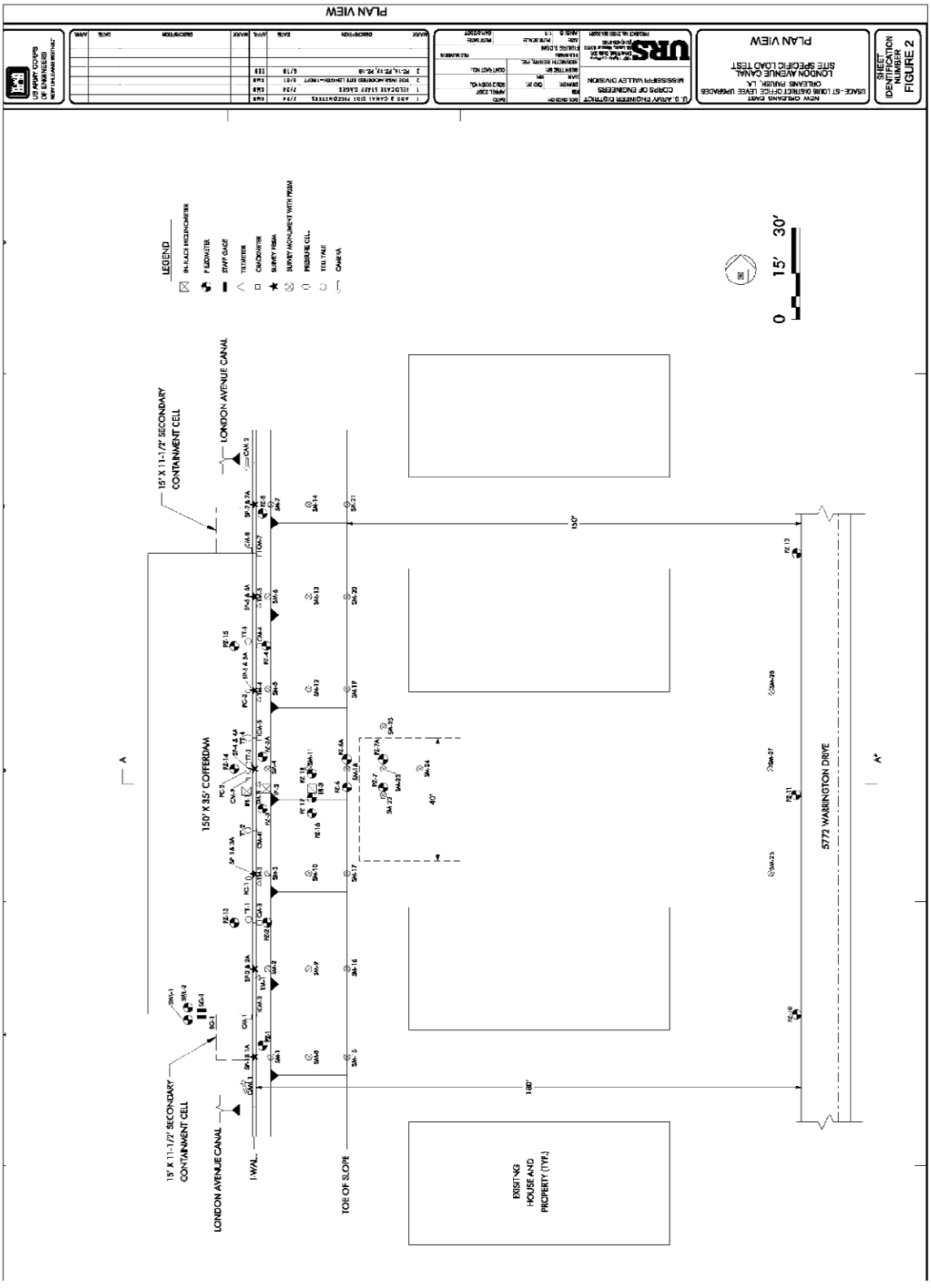

Figure B-4 Plan view of instrumentation layout (Conroy 2008- used under fair use, 2013).

Phase I and Phase II Test Series

The five wall panels were hydraulically loaded by increasing the water level in the cofferdam and observing the response of the I-wall and the levee. This loading process took place in two separate phases or stages. Phase I of the load test was performed to isolate the formation and propagation of the gap between the I-wall and the levee. The cofferdam was installed through the canal-side levee fill and marsh layers, and fully penetrated the beach sand layer. This geometry effectively replicated the condition of having an impervious material at the bottom of the canal. For the water level inside of the cofferdam to have an effect on the pore pressures in the sand layer, the hydraulic connection would have to be made through the gap next to the sheet pile I-wall. There was a concern that there may have been a potential for the hydraulic connection to be made at the location where the sheet pile cofferdam was inserted through the soil. Bentonite powder and pellets were placed inside of the cofferdam in the vicinity of the sheet pile in an attempt to ensure that no short-circuiting of the flow occurred.

The water level was raised in 0.5 ft increments and the responses of the instruments were monitored. As the data was collected, it was transmitted to a technical team located in a trailer 1200 ft from test site. The technical team assessed the data and determined (1) if steady state conditions had been achieved, and (2) if the water level inside of the cofferdam could safely be raised. Once it was deemed that steady state conditions had indeed been achieved, based on pore pressures, wall and ground displacements, wall tilt, etc., the water level was increased by 0.5 ft. The final water level achieved was 7 ft (NAVD88).

The Phase II loading geometry was intended to model a condition where there was a hydraulic connection with the cofferdam water level and the beach sand layer at the bottom of the canal.

Twenty-nine slotted pipes were installed along the inside face of the cofferdam. The change in pore pressures in the silty sand and beach sand layers during the Phase II portion of the load test would be the result of the hydraulic connection made by these injection wells. The data reduction and loading procedure used in the Phase I portion of the test was also used for the Phase II portion of the test.

In this report, a numerical model was developed for the Phase II loading considering the injection wells. The model was calibrated using Phase II results. Five piezometers (PZ-3A, PZ-6, PZ-7, PZ-14 and PZ-17) located at the center of the test section were used for calibration. These piezometers provided the highest pore pressures measured, and were less influenced by the boundary conditions of the test section.

Shown in Figure B-5 and Figure B-6 are the measured total heads for the different piezometers (including the selected piezometers for calibration) as a function of the water level inside of the cofferdam for Phase I and Phase II, respectively.

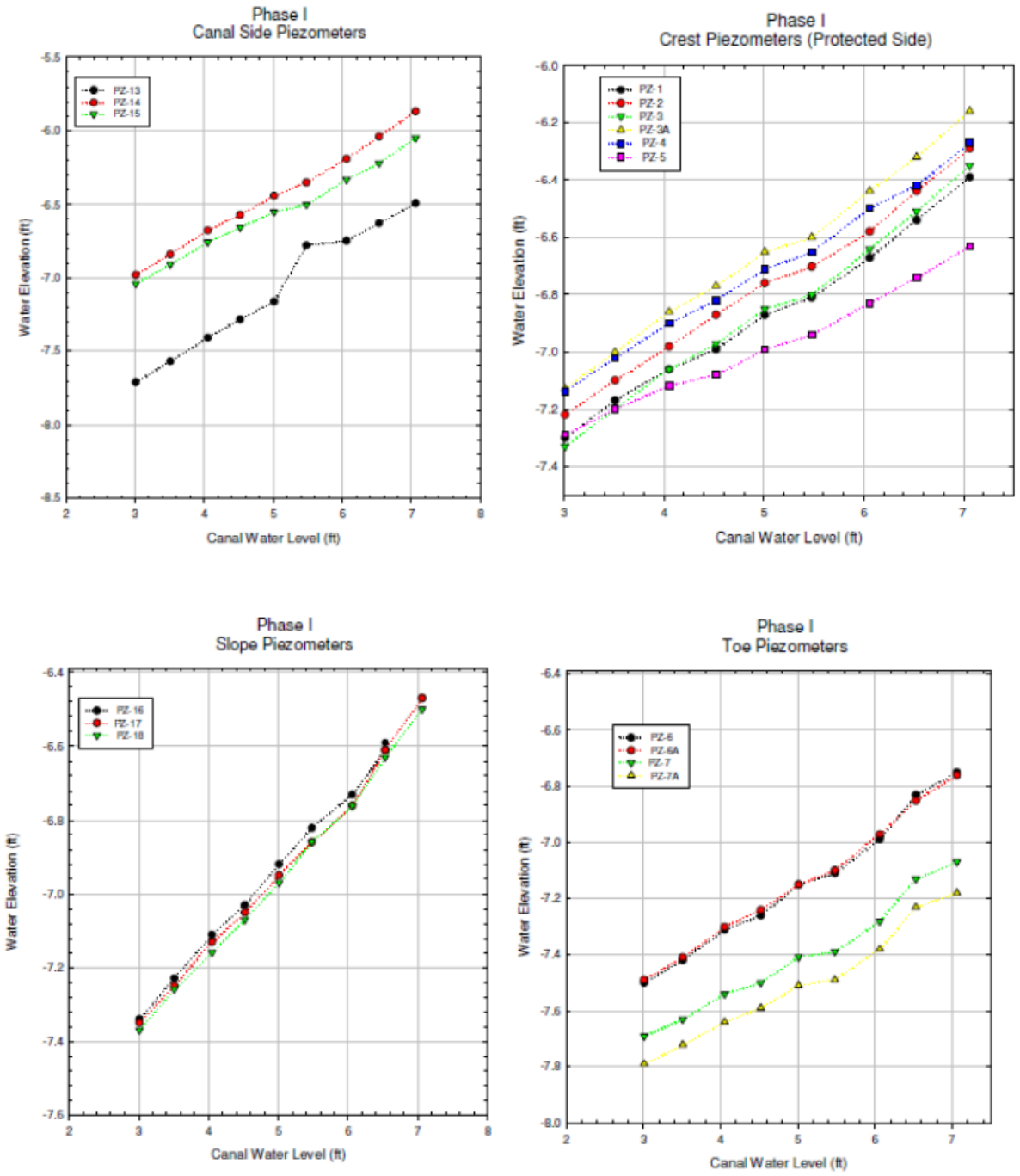

Figure B-5 Piezometer readings for different canal (cofferdam) water levels for different piezometers for Phase I of the load test.

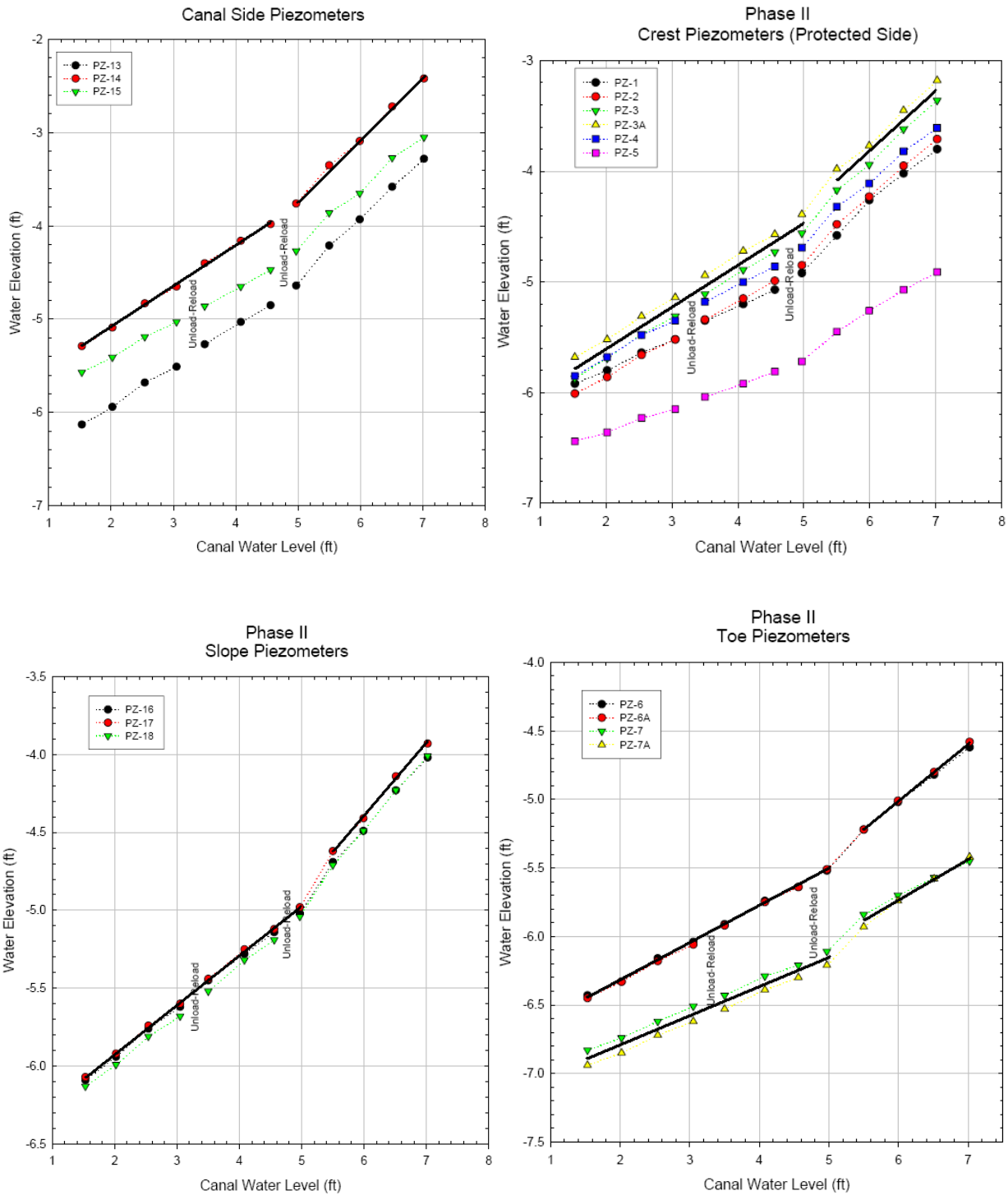

Figure B-6 Piezometer readings for different canal (cofferdam) water levels for different piezometers for Phase II of the load test.

Permeability of Load Test Soils

Soil permeability is perhaps the most important parameter in a seepage analysis. The results of such analyses vary significantly with the value of the coefficient of permeability assigned to the soil. Since the objective of this report is to develop a seepage model for the London Avenue Canal load test, which is complicated in nature, the permeability of the soil becomes even more significant when numerically modeling the actual field test.

The London Avenue Canal load test is a three dimensional seepage problem where the effect of different canal water levels is being studied. Details about the modeling issues will be presented in the modeling section of this report. The stratigraphy at the test site includes levee fill material, a marsh layer, a silty sand layer, a beach sand layer, and a bay sound clay layer. Table B-1 presents the approximate elevation of the top and the bottom of each layer in addition to the approximate layer thickness. Figure B-7 is a simplified cross section of the test site showing the soil layers.

Table B-1 Soil stratification at the London Avenue Canal load test site.

Soil Layer	Elevation		Thickness (ft)
	From	To	
Levee fill	2.1*	-5.7	7.8
Marsh	-5.7	-12.0	6.3
Silty sand	-12.0	-21.0	9.0
Beach Sand	-21.0	-46.0	25.0
Bay sound clay	-46.0	-67.0	21.0

*Crest elevation of the levee

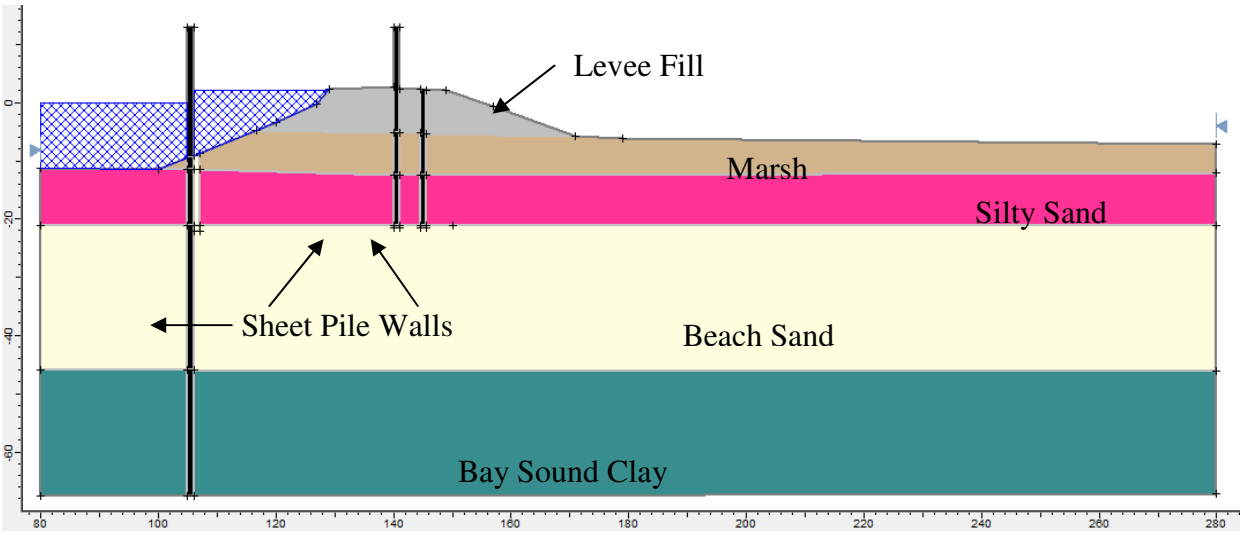

Figure B-7 Cross section of the levee indicting different soil layers.

The levee fill, marsh, and bay sound clay are organic and mineral clays and the permeabilities of these layers will be discussed collectively. In addition to the soil layers, assigning the correct permeability to the sheet pile walls is also important and is discussed later in detail.

The following data were examined for estimating the values of permeability of each layer when available:

- Boring logs and gradation curves
- Piezometer installation logs and falling head permeability test results
- Pumping test data

The majority of the available information was for the silty sand and beach sand layers as opposed to the organic and mineral clay layers.

Beach Sand

The permeability of beach sand can be estimated using published correlations with the grain size distribution. Sieve analyses were performed on samples obtained from different borings. The different methods considered to estimate the permeability of the beach sand are described below.

Hazen's Formula

Hazen (1911) presented the following formula to determine the permeability of loose, clean, filter sands based on the gradation of the soil:

$$k = C_H {D_{10}}^2$$

where,

k = permeability (cm/sec)

C_H = Hazen's empirical coefficient (normally taken as 100)

D_{10} = particle size corresponding to which 10% soil is finer (cm)

Hazen developed this formula specifically for the design of clean sand filters having a coefficient of uniformity less than 2 (Terzaghi and Peck 1964) and having less than 5% passing the no. 200 sieve (Holtz and Kovacs 1981). The value of permeability obtained from this formula should only be considered as approximate because a slight amount of fines can greatly affect the permeability of the soil. Carrier (2003) reports that values of C_H found in geotechnical engineering literature range from 1 to 1000, which provides an indication of the approximate nature of the method.

The classification of the gradation test samples was considered to distinguish between beach sand and silty sand layers. The classifications were based on the New Orleans District (MVN) soil classification system. According to the old MVN classification, if percentage passing the No. 200 sieve was less than 10%, the soil was classified as poorly-graded sand (SP) or beach sand, otherwise, the classification was silty sand (SM). The new MVN classification system has reduced the fines threshold to 5% to distinguish between SP and SM. However, according to ASTM D2487, which is generally used in practice, the percentage of fines will be less than 5% for poorly graded sand (SP) and more than 12% for silty sand (SM). Soils having a percentage of fines between 5% and 12% will have a dual classification symbol of SP-SM, assuming that the fines classify as a silt. The ASTM classification system was used in this report, and the samples having 5% to 12% fines were separated from both the beach sand (SP) layer and silty sand (SM) layer to obtain more accuracy in the permeability estimates. A plot of D_{10} versus elevation for the samples obtained from the test site is shown in Figure B-8.

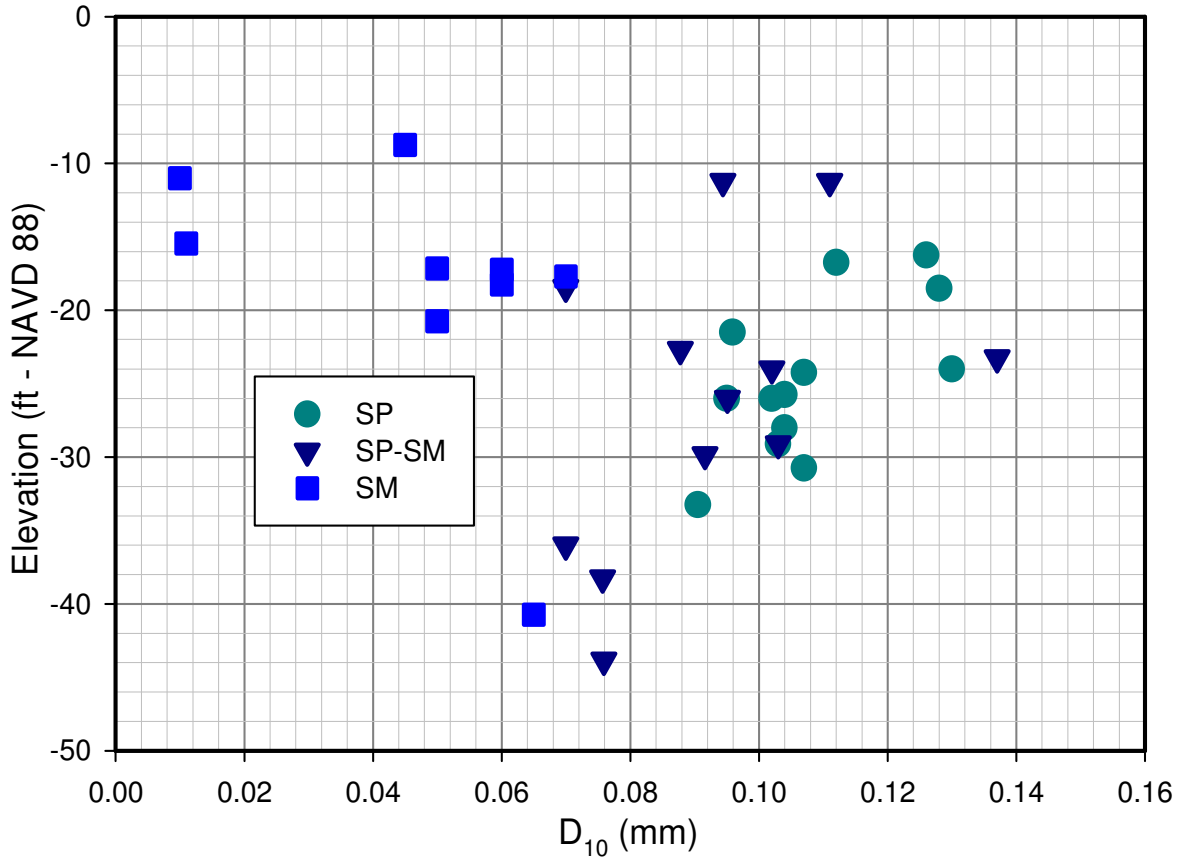

Figure B-8 Plot of effective size (D_{10}) and elevation for sands at the load test site.

The permeability of each sample of the beach sand was calculated and the average value is obtained as **3.8 x 10^{-4} ft/sec** (**1.16 x 10^{-2} cm/sec**) based on Hazen's Formula.

Kozeny-Carman Method

Kozeny (1927) and Carman (1956) developed the most detailed formula to relate particle sizes to the permeability of soils. A simplified form of their method is given by Duncan et al. (1972) and is as follows:

$$k = \frac{580 \emptyset_s{}^2 n^3 d_m{}^2}{(1-n)^2}$$

where,

k = Permeability (cm/sec)

Φ_s = Particle shape factor

n = Porosity

d_m = Mean surface diameter (cm)

$$d_m = {}^{1}\Big/_{\sum \frac{x_i}{d_i}}$$

where,

x_i = Fraction of particles between two sieve sizes

d_i = Average particle size between two sieve sizes (cm)

This method is useful as it considers the average particle size between two sizes and indicates that the smallest particles will have more influence on the permeability value. The effect of shape of the particle (e.g., rounded versus angular) is also considered in this formula by the incorporation of the particle shape factor.

The above relationships were used to come up with the permeability value for the beach sand. The required parameters were obtained from the gradation curves. The shape factor was considered as 1 based on the assumption that soil particles were spherical in nature. Similarly, the porosity value was estimated to be 0.33 based on the available information. The average permeability value for beach sand obtained from the Kozeny-Carman relationship is about **4.79 x**

10^{-4} ft/sec (**1.46 x 10^{-2}cm/sec**). Figure B-9 shows the comparison of permeability values obtained from both the Hazen's Formula and the Kozeny-Carman relationship.

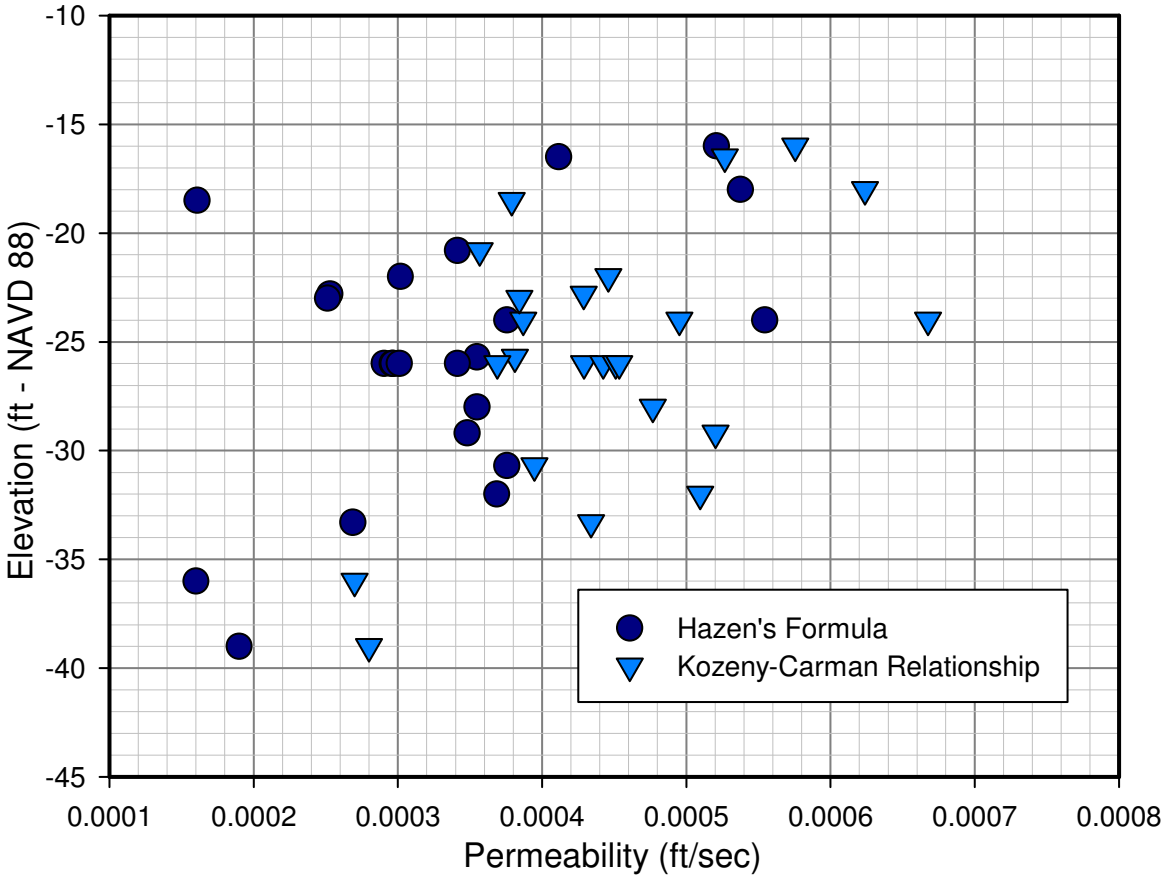

Figure B-9 Comparison of permeability values from the Hazen's Formula and Kozeny-Carman relationship for beach sand.

Some other methods using gradation information, like the ones suggested by Powers and Burnett (1986), Slichter (1905) and Kenney et al. (1984) were also reviewed. Although all the methods based on grain sizes give only approximate values of permeability, some are more approximate than others. For example, the charts developed by Powers and Brunett assume 50% relative density for the soil samples. Since no information was available regarding the relative density, this method was not used. Similarly, Kenney et al. consider D_5 (particle size corresponding to

where 5% soil is finer), and since the gradation curves did not extend to this value, the curves were not extrapolated as the permeability values obtained in this manner may not be accurate. For these reasons, it is believed that the Kozeny-Carman method is probably the best method to estimate the permeability value on the basis of grain size as it considers more parameters than the others. Carrier (2003) recommended that Kozeny-Carman method should be adopted in practice as opposed to Hazen's Formula for this reason.

Field Pumping Test

Field tests are recognized to provide the most representative value of permeability of the soil as they reflect the actual site conditions and are not limited by the sample sizes or disturbance caused during sampling. A field pumping test was conducted at Pratt Park near the London Avenue Canal starting on February 3, 2006. It was a step-drawdown pump test in which a total drawdown of approximately 9 ft was targeted. Figure B-10 shows the array of observation wells present near the pumping well. The locations of these observation wells are useful for determining the pattern of the cone of depression in the vicinity of the pumping well.

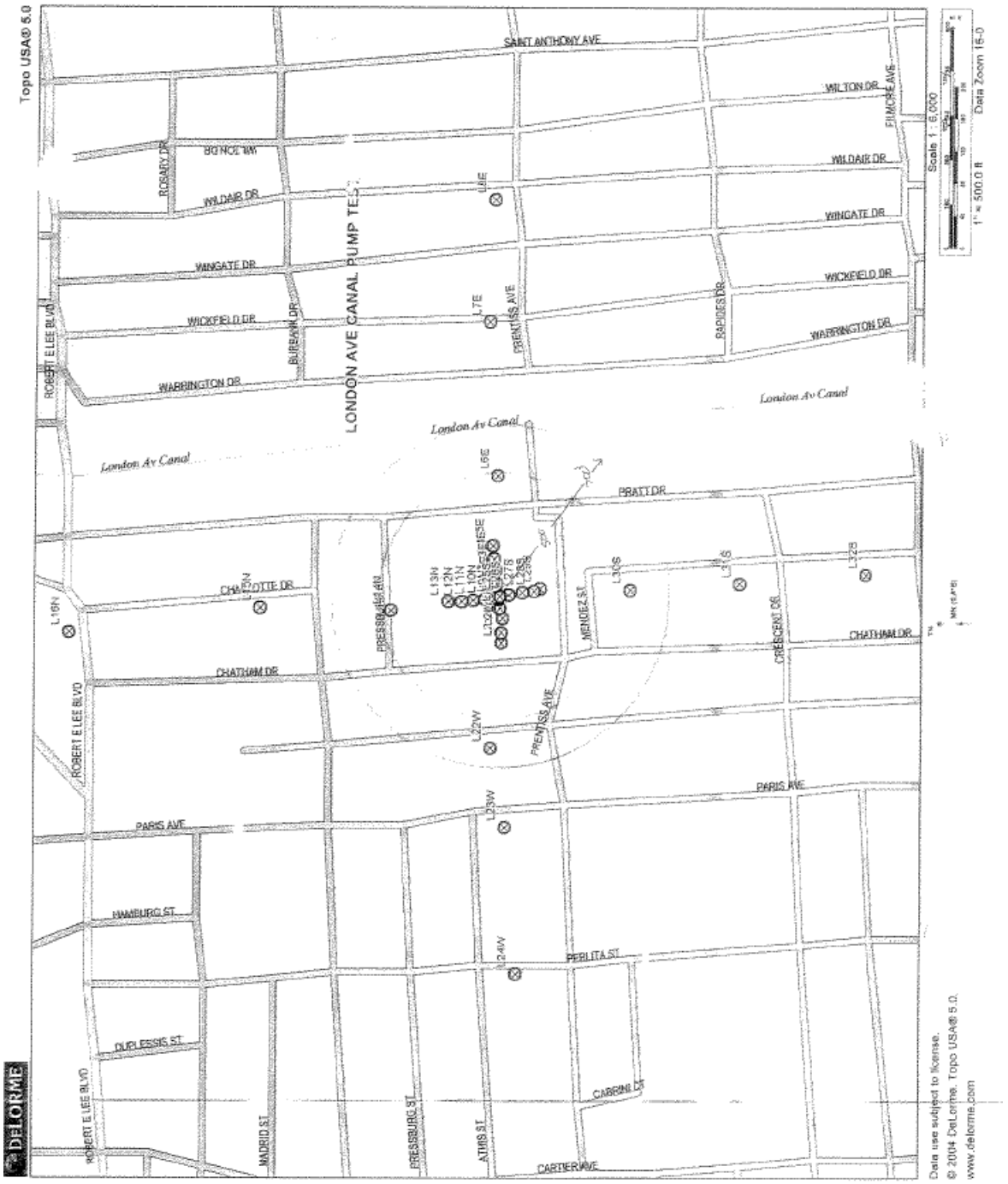

Figure B-10 Schematic showing the location of pumping and observation wells (USACE 2006- used under fair use, 2013).

Curves of drawdown versus elapsed time were generated for all the observation wells. These plots were automated for observation wells within 200 ft of the pumping well. Manual plots were generated for farther distances. The plot for the north transect is shown in Figure B-11.

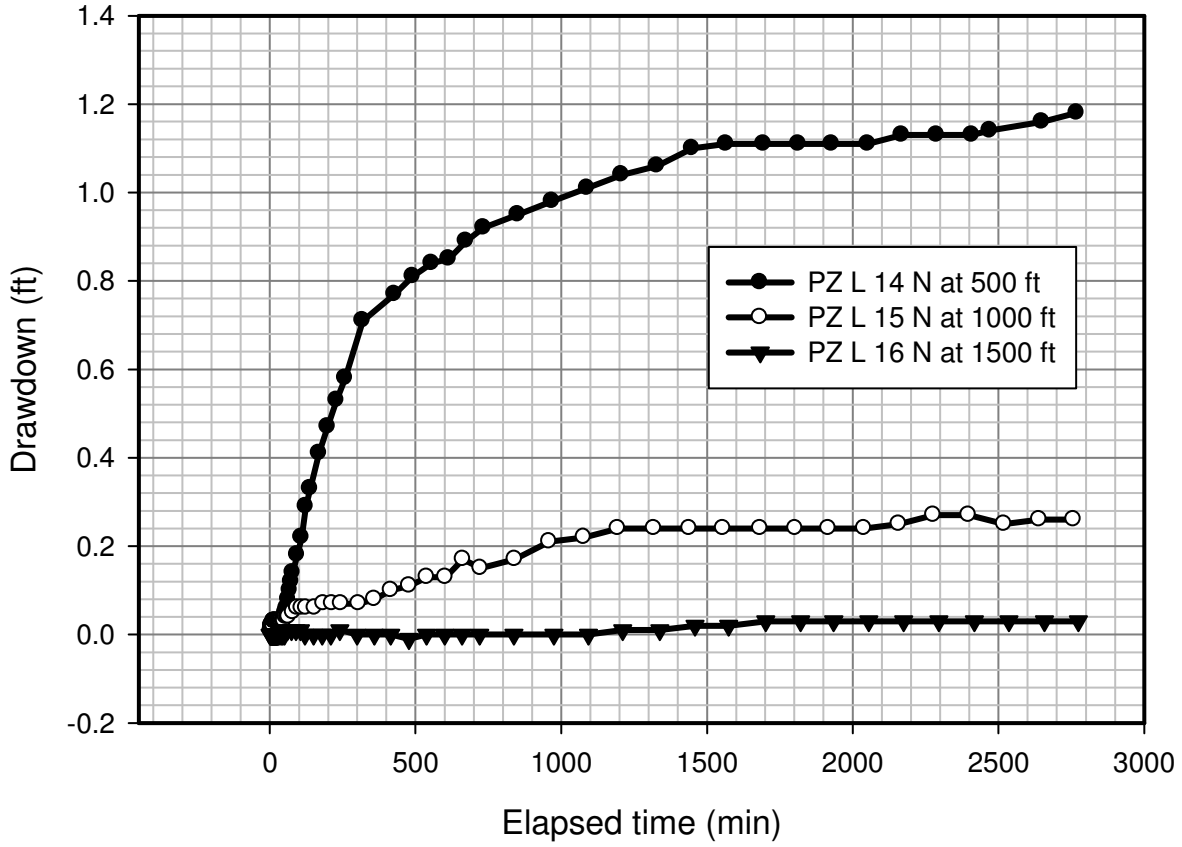

Figure B-11 Plot of drawdown and elapsed time for observation wells located at 500, 1000 and 1500 ft from the pumping well.

Similar curves were developed for observation wells transecting the pumped well in the south, east and west directions. The observation well located at the distance of 1500 ft from the pumping well (PZ L 16 N) showed almost no drawdown indicating that there was no influence of pumping on the groundwater level at this distance.

The permeability values were determined considering the transient conditions of flow to the well and observing the progress of drawdown over time. The following assumptions were made to determine the appropriate method for solution:

1. The aquifer is confined, homogeneous and isotropic.
2. The aquifer is of infinite areal extent.
3. There is no vertical flow entering the aquifer.
4. All flow is directed radially toward or away from the origin.
5. There is no areal recharge applied to the aquifer.
6. The well has an infinitesimal radius and is 100% efficient.

The two methods that were used to determine the permeability value from the pumping test considering the transient flow conditions are:

1. The Theis Method (Curve Matching Method)
2. The Cooper-Jacob Method

The permeability values were calculated from both the drawdown and recovery phases of the well data. All the previously reported calculations were verified. The details of these two methods can be found in most hydrogeological texts. However, a brief summary of these methods (Driscoll 1986) and the equations that were used to determine the permeability value from the pumping test are outlined here.

The basic equation used to determine the permeability value from pumping test is:

$T = kb$

Where,

T = Transmissivity [L^2/T]

b = Thickness of the aquifer [L]

k = Permeability [L/T]

The Theis and Cooper Jacob methods are used to determine the properties of the aquifer including transmissivity from which the permeability value can be easily calculated.

The Theis Method (Curve Matching Method)

The governing equation from the Theis Method is:

$$s = \frac{Q}{4\pi T} W(u)$$

Where,

s = Drawdown [L]

Q = Pumping Rate [L^3/T]

T = Transmissivity [L^2/T]

$W(u)$ = Well function of u (the Theis function or simply well function)

Similarly, u is found as:

$$u = \frac{r^2 S}{4Tt}$$

Where,

r = Distance from pumping well to where drawdown is recorded [L]

S = Storage Coefficient

t = Time since the beginning of pumping [T]

The value of $W(u)$ can be easily found in the hydrogeology literature for different values of u. If the properties of the aquifer are known, then the drawdown can be found by calculating u and then finding the well function, and then solving for the drawdown using the Theis equation. However, explicit solutions of the above equations are not possible if the properties of the aquifer are not known. The Theis method involves the matching of the two types of curves in this case. One is hypothetical in nature, and involves the plotting of the theoretical values of $W(u)$ versus $(1/u)$ as shown in Figure B-12. This curve is then matched with time versus drawdown curve for the actual field condition (with both axes as log scales). The values of T and S can be calculated from this graphical method if all other variables are known. Then permeability values can be calculated using the transmissivity and thickness of aquifer as explained earlier. The step by step graphical procedure is explained below:

1. Plot the time versus drawdown curve based on the data obtained from the pump test.
2. Mark the match point on the Theis curve. Usually, it is taken at $W(u)$ equal to 1 and $(1/u)$ equal to 1 for ease of calculations.
3. Fit the drawdown curve with the Theis curve by super-imposing them and then read off the values of corresponding drawdown and time.
4. Use the values obtained above to determine the aquifer properties like T and S.

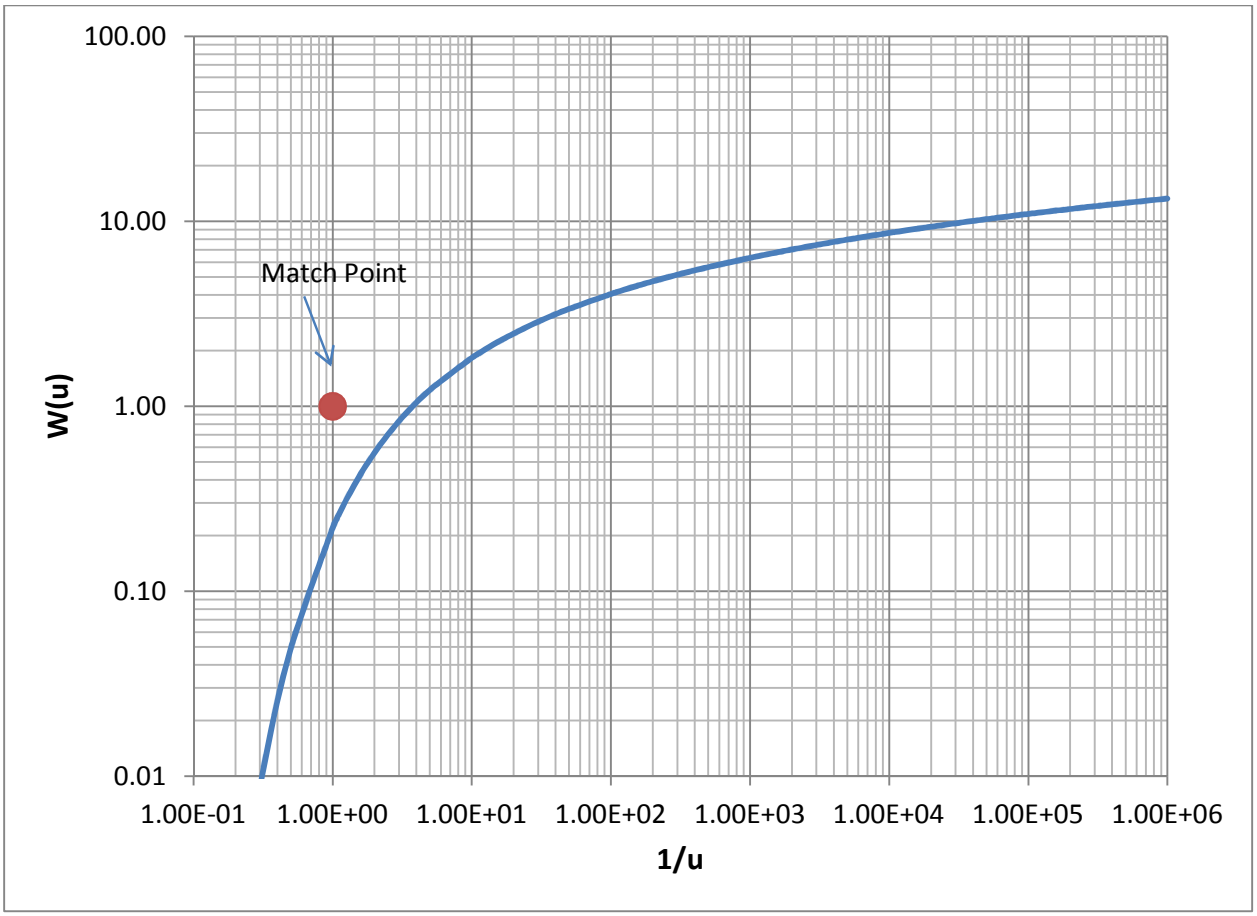

Figure B-12 Theis curve for matching the field data to calculate the aquifer properties.

The use of various computer programs has made it easy to come up with the transmissivity and storage coefficient values. These programs take drawdown versus time as input, develop the curves, and match it with the Theis curve to give the aquifer properties from which permeability can be easily calculated.

The Cooper-Jacob Method

The well function can be approximated by Cooper-Jacob method if

$$u = \frac{r^2 S}{4Tt} < 0.01$$

This condition is met when the time is large enough that there is no appreciable change in the drawdown. This approximation simplifies the analysis, as curve matching is not required anymore as was the case in Theis method. The Cooper-Jacob approximation can be used by considering *Time-Drawdown* method as well as the *Distance-Drawdown* method. The equations for each of these methods are summarized below:

Time-Drawdown Method

The transmissivity and storage coefficient equations can be simplified to the following forms considering the Time-Drawdown method using the Cooper-Jacob approximation:

$$T = \frac{2.303 Q_w}{4\pi \Delta s}$$

and

$$S = \frac{2.25 T t_o}{r^2}$$

Where

Q_w = Well Discharge [L^3/t]

Δs = Drawdown per cycle of (log) time-drawdown curve [L]

t_o = Time corresponding to zero drawdown

r = Distance from pumping well to where drawdown is recorded [L]

The time versus drawdown curve is plotted on a semi-log scale and Δs is calculated for one log cycle from this curve. Transmissivity, and ultimately permeability, can be easily calculated from this method.

Distance-Drawdown Method

When there are multiple observations wells, the Distance-Drawdown method is used to come up with aquifer properties. All observation wells should be measured at the same time. The transmissivity and storage coefficient equations can be simplified to the following forms using the Cooper-Jacob approximation:

$$T = \frac{2.303 Q_w}{2\pi \Delta s}$$

and

$$S = \frac{2.25 T t}{r^2}$$

Where all the parameters are same as defined above, except t is used instead of t_o in this case.

t = Time at which the observation is made for all the observation wells.

Similarly, permeability values can be obtained using the transmissivity equation as explained in the earlier sections.

Permeability Values from the Field Pumping Test for Beach Sand

The permeability values obtained from the field pumping test for the beach sand layer are summarized in Table B-2. The Theis Method and Time-Drawdown Method using Cooper-Jacob approximations were used to come up with the permeability values.

Table B-2 Summary of permeability values calculated from field pumping test.

Observation well			**Permeability**		**Method**
Name	**Location from Pumping well**				
	X (ft)	**Y (ft)**	**cm/sec**	**ft/sec**	
n10	50	0	0.0108	3.54×10^{-4}	Theis
n10	50	0	0.0113	3.71×10^{-4}	Cooper & Jacob
n11	100	0	0.0118	3.87×10^{-4}	Theis
n11	100	0	0.013	4.27×10^{-4}	Cooper & Jacob
n12	150	0	0.0136	4.46×10^{-4}	Theis
n12	150	0	0.0149	4.89×10^{-4}	Cooper & Jacob
n13	200	0	0.0156	5.12×10^{-4}	Theis
n13	200	0	0.0163	5.35×10^{-4}	Cooper & Jacob
n10	50	0	0.0136	4.46×10^{-4}	Theis (Recovery)
n11	100	0	0.0136	4.46×10^{-4}	Theis (Recovery)
n12	150	0	0.0156	$5.12x\ 10^{-4}$	Theis (Recovery)
n13	200	0	0.0179	5.87×10^{-4}	Theis (Recovery)
s26	50	0	0.0108	3.54×10^{-4}	Theis
s26	50	0	0.0113	3.71×10^{-4}	Cooper & Jacob

Observation well			Permeability		Method
Name	Location from Pumping well				
	X (ft)	Y (ft)	cm/sec	ft/sec	
s27	100	0	0.0136	4.46×10^{-4}	Theis
s27	100	0	0.0149	4.89×10^{-4}	Cooper & Jacob
s28	150	0	0.0171	5.61×10^{-4}	Theis
s28	150	0	0.0179	5.87×10^{-4}	Cooper & Jacob
s29	200	0	0.0236	7.74×10^{-4}	Theis
s29	200	0	0.0226	7.41×10^{-4}	Cooper & Jacob
s26	50	0	0.0136	4.46×10^{-4}	Theis (Recovery)
s27	100	0	0.0156	5.12×10^{-4}	Theis (Recovery)
s28	150	0	0.0179	5.87×10^{-4}	Theis (Recovery)
e02	50	0	0.0103	3.38×10^{-4}	Theis
e02	50	0	0.0113	3.71×10^{-4}	Cooper & Jacob
e03	100	0	0.0124	4.07×10^{-4}	Theis
e03	100	0	0.0136	4.46×10^{-4}	Cooper & Jacob
e04	150	0	0.0149	4.89×10^{-4}	Theis
e04	150	0	0.0163	5.35×10^{-4}	Cooper & Jacob
e05	200	0	0.0171	5.61×10^{-4}	Theis
e05	200	0	0.0206	6.76×10^{-4}	Cooper & Jacob
e02	50	0	0.0136	4.46×10^{-4}	Theis (Recovery)
e03	100	0	0.0149	4.89×10^{-4}	Theis (Recovery)
e04	150	0	0.0179	5.87×10^{-4}	Theis (Recovery)

Observation well			Permeability		Method
Name	Location from Pumping well				
	X (ft)	Y (ft)	cm/sec	ft/sec	
e05	200	0	0.0206	6.76×10^{-4}	Theis (Recovery)
w18	50	0	0.0103	3.38×10^{-4}	Theis
w18	50	0	0.0103	3.38×10^{-4}	Cooper & Jacob
w19	100	0	0.0118	3.87×10^{-4}	Theis
w19	100	0	0.013	4.27×10^{-4}	Cooper & Jacob
w20	150	0	0.0136	4.46×10^{-4}	Theis
w20	150	0	0.0156	5.12×10^{-4}	Cooper & Jacob
w21	200	0	0.0149	4.89×10^{-4}	Theis
w21	200	0	0.0171	5.61×10^{-4}	Cooper & Jacob
w18	50	0	0.0136	4.46×10^{-4}	Theis (Recovery)
w19	100	0	0.0136	4.46×10^{-4}	Theis (Recovery)
w20	150	0	0.0164	5.38×10^{-4}	Theis (Recovery)
w21	200	0	0.0180	5.91×10^{-4}	Theis (Recovery)

The average value of permeability for beach sand from the field pumping test is approximately **4.88×10^{-4} ft/sec (1.49×10^{-2} cm/sec).**

The overall permeability of the beach sand from the above discussion can be estimated as **4.9×10^{-4} ft/sec (1.5×10^{-2} cm/sec).** This is the value obtained from field pumping test and is comparable to the value obtained from the Kozeny-Carman method.

Silty Sand

A 9 ft thick layer of silty sand (SM) was present above the beach sand layer at the London Avenue Canal load test site. The presence of this layer was not known during the site selection or the design of the field test, and this layer was judged to have significantly influenced the field test results. The use of the correct value of permeability for this layer is very important in the development of the seepage model because it will greatly affect the results. Similar to the beach sand, the permeability of the silty sand was also estimated using the gradation curves developed from the same borings as discussed above.

Permeability Values from Gradation Curves

Hazen's Formula and the Kozeny-Carman method were used to determine the permeability of the silty sand from the gradation curves. The details of these methods have already been provided in the beach sand section of the report. However, Hazens's Formula is not well suited to determine the permeability of the silty sand (SM). This is because Hazen developed his method to determine the permeability of clean sand filters with a coefficient of uniformity of less than 2 and for soils having less than 5% fines as explained earlier. The percentage of fines for silty sand is more than 12% according to ASTM D2487 and more than 5% according to the new MVN classification. Hazen's Formula is still frequently used in practice to determine the permeability of all types of soils, but its limitation should be kept in mind while applying these values. The permeability of silty sand from Hazen's Formula was calculated for completeness but not much emphasis was given to the calculated value. The value from Hazen's Formula for silty sand layer is approximately **9.15×10^{-5} ft/sec** (**2.79×10^{-3} cm/sec**).

The permeability was also calculated for silty sand layer from Kozeny-Carmen method using the shape factor of 0.45 based on the assumption of particle shape as "angular" and porosity of 0.33. This method is not appropriate for clayey soils but is applicable to soils having non-plastic fines contents (i.e. silts) (Carrier 2003). The value was calculated as **4.95 x 10^{-5} ft/sec** (**1.51 x 10^{-3} cm/sec**) from the Kozeny-Carman method**.** Figure B-13 shows a comparison of permeability values obtained from the Hazen's Formula and Kozeny-Carman relationship for the silty sand layer.

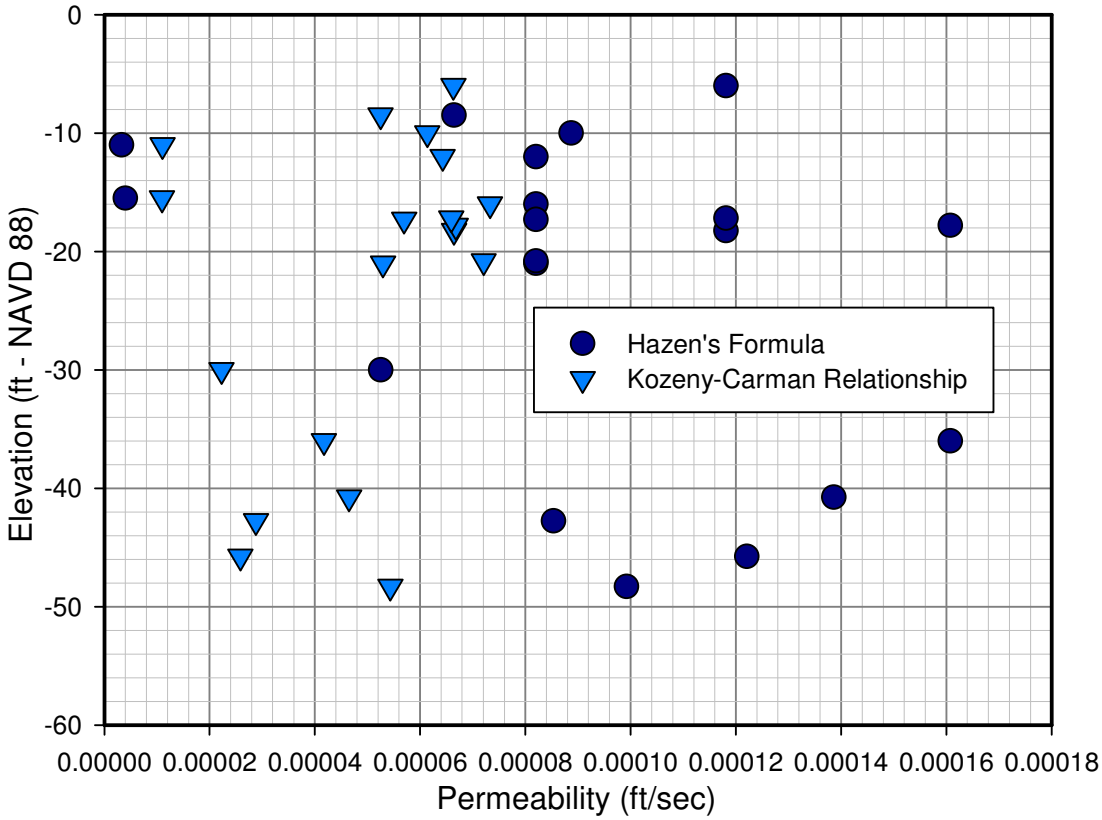

Figure B-13 Comparison of permeability values from Hazen's Formula and the Kozeny-Carman relationship for silty sand.

There is more dispersion in the values of permeability obtained from Hazen's Formula as compared to the Kozeny-Carman method as evident in the above plot.

Falling Head Tests or Slug Tests

The open-standpipe piezometers were installed at the load test site as explained in a previous section. The falling head tests were conducted on 15 piezometers namely PZ 1, 2, 3, 3A, 4, 5, 6, 6A, 7, 7A, 8, 9, 10, 11, and 12. This is perhaps the best method to determine the permeability of silty sands as it is a field method and involves fewer assumptions and limitations than correlations and laboratory test methods. The use of the appropriate relationship to determine the permeability from the variable head test is a function of the condition of boreholes (cased or uncased, flush bottom or not flush) and type of stratum. The relationship that was used to determine the permeability of the silty sand layer from the falling head test results is as follows (Cedergren 1989):

$$k = \frac{r^2}{2L} ln\left(\frac{L}{R}\right)\left[\frac{ln(h_1/h_2)}{(t_2 - t_1)}\right]$$

Where,

r = Radius of the standpipe

R = Radius of the borehole

L = Uncased length of the borehole

Figure B-14 is useful in understanding the remaining parameters.

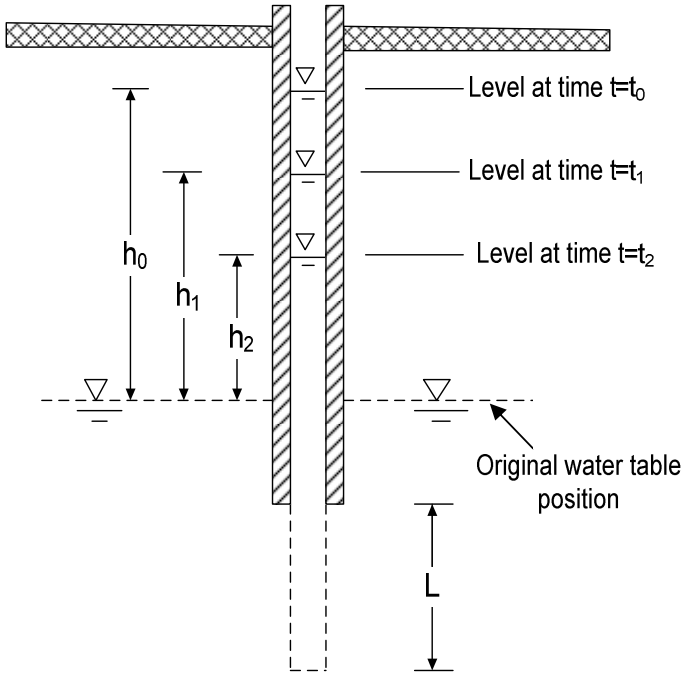

Figure B-14 Schematic of the falling head test.

The mud rotary method was used to install the piezometers for the London Canal load test. The diameter of each piezometer was 2 inches and sand filters were used. However, the use of above equation is only appropriate if the plot of head ratio (h_t/h_o) versus time (t) on the semi-log scale for any piezometer is linear. This plot indicates the test reliability whereby a linear relationship shows minimum disturbance and reliable results. On the other hand, a non-linear relationship indicates the clogging or other disturbances retarding flow into the formation. Therefore, the first step to determine the value of permeability from falling head tests is to separate the reliable sets of piezometers from the non-reliable ones by generating these plots. Two such plots are shown in Figure B-15 indicating each of the cases where the data from the piezometers is deemed acceptable or unacceptable to determine the value of permeability for silty sands.

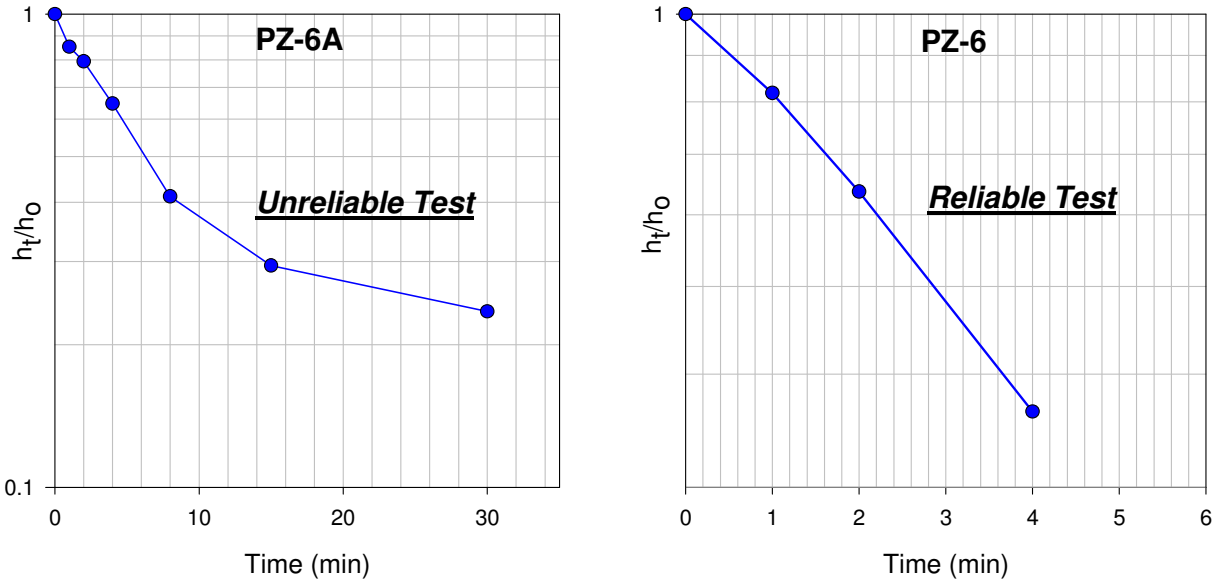

Figure B-15 Plot of head ratio versus time showing reliability of the falling head test.

Similar reaction plots indicate that piezometers 1, 2, 4, 5, 6, 7, 7A, 8 and 11 can be used to determine the value of permeability from the falling head test while piezometers 3, 3A, 6A, 9, 10 and 12 are not considered acceptable for this purpose. The data from the falling head tests, as well as the average value of permeability for each of the piezometers, is summarized in Table B-3.

Table B-3 Summary of the results from falling head tests for each piezometer.

PZ No.	Initial Reading (ft)	Elapsed Time (min)	Depth to Water (ft)	Filter Elevation (ft)		Average k (ft/sec)	Comment
				From	To		
1	9.9	0 1 2 4	0 6.8 9.5 9.9	-25	-19	6.44×10^{-5}	Accepted
2	10	0 1 2	0 8 10	-25	-19	6.46×10^{-5}	Accepted
3	10.3	0 1 2 4 8 15 30 60 120	0 1.1 1.7 2.7 4.65 5.65 7.95 9.8 10.2	-25	-19	2.35×10^{-6}	Rejected
3-A	10.4	0 1 2 4 8 15 30 60	0 3.1 4.2 5.7 7.7 9.25 9.8 10.4	-25	-19	6.42×10^{-6}	Rejected
4	10	0 1 2 4	0 8 9.85 10	-25	-19	8.42×10^{-5}	Accepted
5	9.85	0 1 2 4	0 7.5 9.2 9.85	-25	-19	5.45×10^{-5}	Accepted
6	1.4	0 1 2 4 8 15	0.3 0.5 0.7 1 1.2 1.4	-20	-14	9.35×10^{-6}	Accepted

PZ No.	Initial Reading (ft)	Elapsed Time (min)	Depth to Water (ft)	Filter Elevation (ft)		Average k (ft/sec)	Comment
				From	To		
6-A	1.7	0 1 2 4 8 15 30 60	0 0.25 0.35 0.6 1 1.2 1.3 1.7	-20	-14	2.94×10^{-6}	Rejected
7	1.7	0 1 2 4 8 15 30	0 0.3 0.5 0.7 1.55 1.65 1.7	-20	-14	7.42×10^{-6}	Accepted
7-A	1.8	0 1 2 4 8 15 30	0 0.4 0.7 1.1 1.7 1.75 1.8	-20	-14	9.04×10^{-6}	Accepted
8	5.25	0 1 2 4	0 4.75 5 5.25	-21	-15	5.28×10^{-5}	Accepted
9	5.4	0 1 2 4	0 4.8 5.1 5.25	-21	-15	3.74×10^{-5}	Rejected
10	1.4	0 1 2 4	0 1.3 1.35 1.4	-30	-24	5.78×10^{-5}	Rejected
11	1.5	0 1 2 4	0 1 1.4 1.5	-26	-20	5.03×10^{-5}	Accepted
12	1.7	0 1 2 4	0 1.5 1.6 1.7	-28	-22	4.91×10^{-5}	Rejected

The average value of permeability based on the reliable piezometers is determined as **4.63 x 10^{-5} ft/sec** (**1.41 x 10^{-3} cm/sec**) from the falling head test.

The overall permeability of the silty sand based on the above discussion can be estimated as approximately **4.75 x 10^{-5} ft/sec** (**1.45 x 10^{-3} cm/sec**). However, this value is just an initial estimate because of the limited amount of data available for the silty sand. The permeability of the silty sand will be one of the values that will be iterated in the development of the numerical seepage model.

Organic and Mineral Clays

Three types of clays were encountered in the vicinity of the load test and their permeabilities will be collectively considered in this section. These layers were a 7.8 ft thick levee fill, a 6.3 ft layer of marsh and 21 ft thick layer of bay sound clay. The permeability of the levee fill and the bay sound clay was estimated as **3.28 x 10^{-8} ft/sec** (**1.0 x 10^{-6} cm/sec**) based on the general guidelines available for the fine-grained soils (Terzaghi and Peck 1964). These values are similar to those used by IPET in their post-Katrina analysis of the failures that occurred in the London Canal.

The presence of the peat and organic clay layers in the marsh can be identified by plotting the measured water contents from the undisturbed borings versus depth. The water content of New Orleans area soils increases with increasing organic content. Layers of peat and organic clay are often identified by an increase in water content of about 50% to 70% for "mineral" clays to over 100% for organic clays to over 200% for peat. Shown in Figure B-16 are the water contents versus depth for borings LCSLT-1U and LCSLT-3U. The water content measured in LCSLT-1U exceeds 100% at depths of about 8 ft to 13 ft. Boring LCSLT-3U also shows the presence of

organics soils from a depth of about 7 ft to 12 ft. The marsh layer appears to be mainly comprised of peaty soils, and the permeability was evaluated by assessing information available for such soils.

However, scant data are available regarding the permeability values of New Orleans area peat soils. In general, the permeability of peat can be high in a normally consolidated condition at low effective stresses. If a peat is consolidated by placing a fill on top of it, the permeability drastically decreases during consolidation. MacFarlane (1959) reported a decrease in permeability from 1.3 x 10^{-5} ft/sec (4 x 10^{-4} cm/sec) to 2.6 x 10^{-10} ft/sec (8 x 10^{-9} cm/sec) for a peat that was subjected to an 8 psi stress for 7 months. Owing to the fibrous nature of some peat deposits, the permeability in the vertical direction might be expected to be less than the permeability in the horizontal direction.

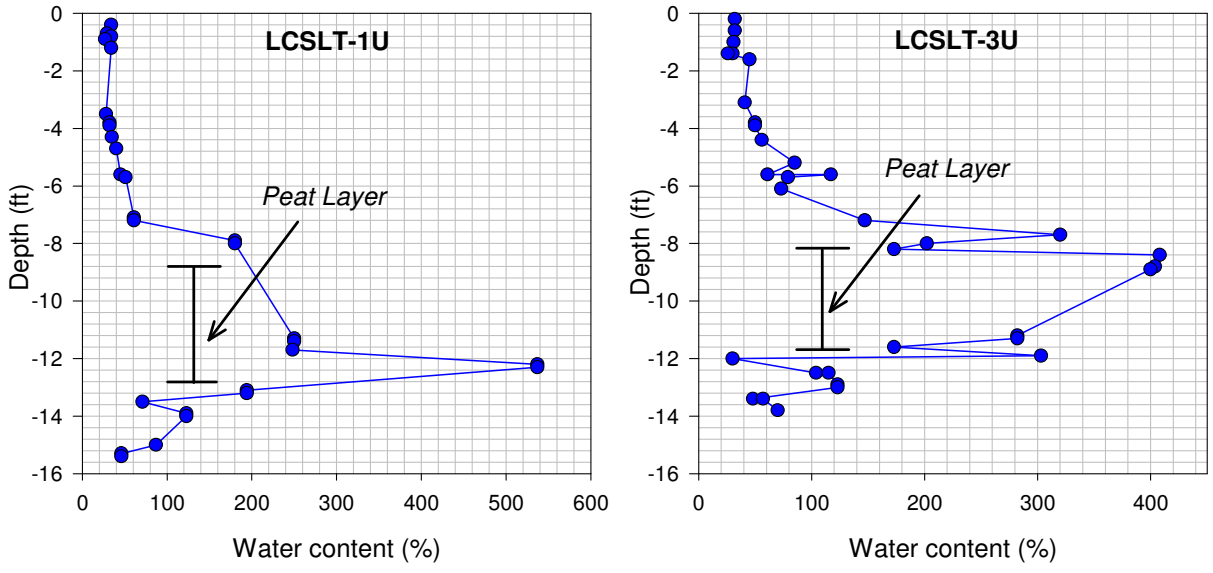

Figure B-16 Water contents versus depth for borings LCSLT-1U and LCSLT-3U.

As part of the IPET study, consolidation tests results were evaluated, and permeability values were determined based on the measured coefficient of consolidation. This procedure is outlined in EM 1110-2-1901 (USACE manual for Seepage Analysis and Control for Dams). The resulting values would represent the permeability in the vertical direction, and are shown in Figure B-17. The permeability values ranged from a maximum of 3.28×10^{-7} ft/sec (10^{-5} cm/sec) for low consolidation pressures, to values as low as 3.28×10^{-10} ft/sec (10^{-8} cm/sec) for a consolidation pressure equal to 4000 psf.

Soil Testing Engineers (STE) of Baton Rouge conducted flexible wall permeability tests on undisturbed specimens of peat from the south bank of the ICWW by the Paris Road Bridge in 1993. The test specimens had in situ water contents ranging from 179% to 632% and dry densities ranging from 8 to 24 pcf. STE conducted tests on specimens that were trimmed in both a horizontal and vertical orientation in order to measure the anisotropy of permeability. The arithmetic average of the horizontal permeability values was 2.41×10^{-7} ft/sec (7.35×10^{-6} cm/sec) and the average of the vertical permeability values was 1.21×10^{-7} ft/sec (3.68×10^{-6} cm/sec). These values result in a permeability ratio (k_h/k_v) equal to 2. If a logarithmic average of the permeability values is calculated, both the horizontal and vertical permeabilities are equal to 6.56×10^{-8} ft/sec (2×10^{-6} cm/sec), with a resulting permeability ratio of unity. The horizontal and vertical permeability values measured by STE are also plotted in Figure B-17.

The Fugro geotechnical laboratory in Houston performed flexible wall permeability tests on peat specimens obtained from the east bank of the IHNC in 2007. Horizontal and vertical permeabilities were measured at effective stresses of 430, 860, and 1440 psf. Only two specimens were tested. The vertical permeabilities ranged from 3.1×10^{-9} ft/sec (9.3×10^{-8}

cm/sec) to 1.25 x 10^{-9} ft/sec (3.8 x 10^{-8} cm/sec), and the horizontal permeabilities ranged from 2.6 x 10^{-8} ft/sec (8 x 10^{-7} cm/sec) to 4.9 x 10^{-9} ft/sec (1.5 x 10^{-7} cm/sec). The average permeability ratio for these tests was about 8. These data are also plotted on Figure B-17.

Weber (1969) measured the permeability of peats in the California Delta using field tests, and the values that he obtained are also plotted on Figure B-17. These values would be predominately horizontal permeability values. The peats in the California Delta are more fibrous than those in the New Orleans area, so these values would probably represent an upper bound.

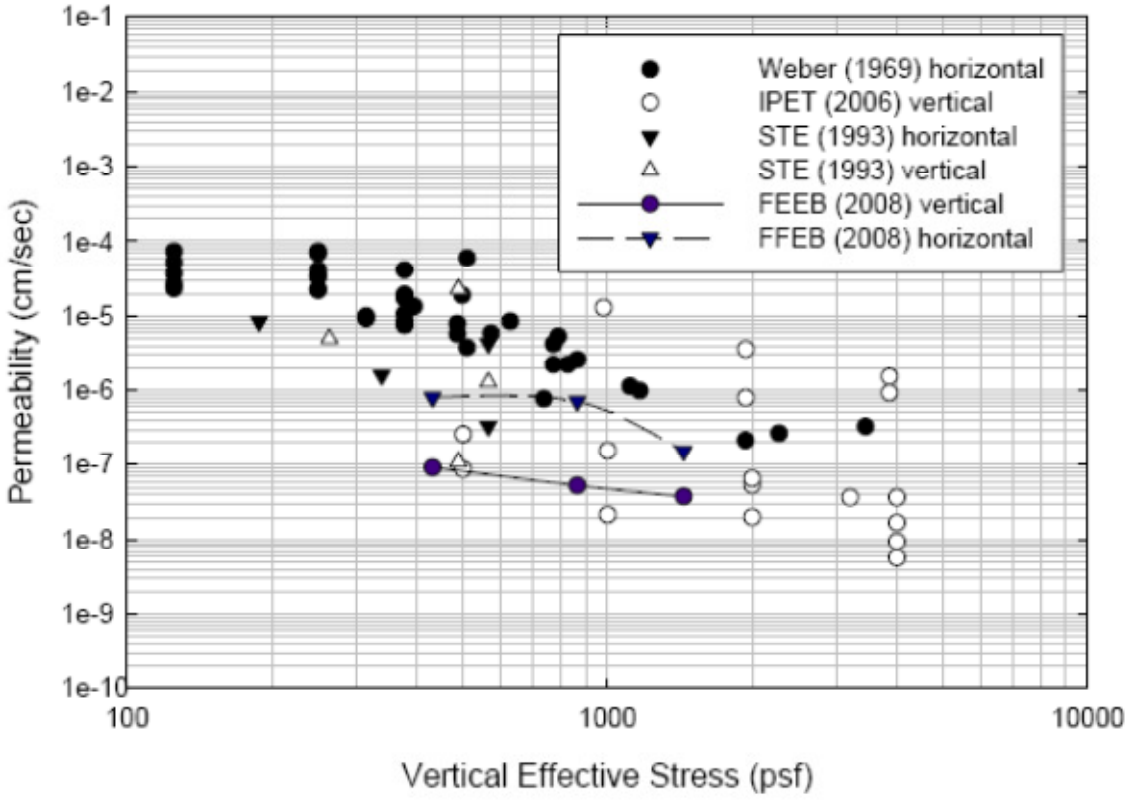

Figure B-17 Permeability values for peat determined from consolidation tests, field tests, and flexible wall permeameter tests.

A levee that is about 7.5 ft tall would produce a vertical effective stress on the peat layer of about 750 psf or greater. Based on the information included in Figure B-17, a permeability less than or

equal to about 10^{-6} cm/sec (3.28 x 10^{-8} ft/sec) would be expected for this value of vertical effective stress.

Anisotropy of permeability was not considered for the marsh layer while modeling the load test and a permeability value of **3.28 x 10^{-7} ft/sec** (**1.0 x 10^{-5} cm/sec**) was assigned with an anisotropic ratio of 1. This can be justified because it was observed through transient and steady state seepage analyses that the pore pressures within the pervious stratum and uplift pressures on the base of the top stratum are independent of the permeability value of marsh layer and levee fill, if these materials are at least two orders of magnitude less pervious than the sands (Duncan et al. 2008).

Permeability of Sheet Pile Walls

The sheet piles of the cofferdam and I-walls have to be modeled while performing the finite element analysis of the test section. This can be done by either assigning an appropriate boundary condition or considering the sheet pile material as having some permeability value. The purpose of the sheet pile is to generally control seepage problems and act as a seepage barrier or a cut-off wall, as well as to control water levels in case of the cofferdam. The sheet pile for both I-wall and cofferdam was modeled as a virtually impervious material with a very low permeability value ($<10^{-100}$ ft/sec) during the modeling of the test section. A brief literature review was done to qualify this modeling technique.

PZ-22 hot rolled sheet piles were mostly used in the existing I-wall system of the London Avenue Canal. The portion of the I-wall extending above the crest of the levee was also encased in concrete for some of the sections along the canal. PZ-35 sheet piles were used for the

cofferdam. The cofferdam fully penetrated the pervious layer of beach sand in order to perform as a cut-off barrier. The connection between the cofferdam and the existing I-wall was a critical detail to make it watertight. A 2 ft excavation along the path of the sheet pile was completed to clear away the debris that might otherwise have impeded the installation process. Bentonite pellets and powder were placed along the inside face of the sheet pile for the entire length of the cofferdam to prevent any seepage entrance along the sheet pile wall. The watertight connection between the sheet pile and existing I-wall was achieved by welding a flat piece of steel to the last PZ-35 cofferdam sheet pile and embedding this into the monolith joint of the concrete I-wall. This joint was further strengthened by reinforcing it with a partial circumference of a pile pipe welded onto the canal side of the sheet pile and filling it with non-shrink grout. The watertightness was achieved by bolting neoprene sheets to both sides (canal side and interior) of the joint. Jet grout columns were installed to establish the structural connection between the cofferdam sheet pile and sheet pile of existing I-wall.

The steel itself can be considered as completely impervious. However, the overall permeability of the sheet pile is greatly dependent on the hydraulic resistance of the steel sheet pile joints (Sellmeijer et al. 1995). Sellmeijer found that the permeability of the joint decreases as a function of time. This behavior is observed in all types of joints, independent of the filler material. The factors contributing to this trend could be rearrangement of the filler material in the joint, collection of small pieces of debris or soil in the pores of the joint, as well as formation of small air bubbles in the joint pores. The permeability value is greatly reduced in the case of filled joints as compared to unfilled ones. The use of hydrophilic sealants in the interlocks of sheet piling reduces the permeability of the joint. The ability of the sealant to expand several times its

volume when coming in contact with water can effectively seal the interlocks (Yeats 2004). In addition, welded joints will result in a completely impervious structure.

The use of hot rolled sheet piles when compared to the cold rolled sheet piles is also preferable for providing a seepage barrier as hot rolled sheet piles are less permeable (Starr 2000). The cold rolled sheets have a looser fit, which does not provide a tight interlock, thus making it less desirable for watertight applications. ArcelorMittal (one of the largest steel producing companies in the world) carried out a collaborative research project[1] to determine the rate of seepage through steel sheet pile walls for various types of joints considering the concept of joint resistance and also provided guidelines to make sheet pile behave as a completely impervious structure.

Two hydraulic tests were conducted at the University of Waterloo to measure the hydraulic conductivity of the cut-off walls (Starr 2000). The PZ-22 steel sheet pile was used as a cut-off wall and the permeability value obtained from the test was approximately 1.5×10^{-7} cm/sec (4.9×10^{-9} ft/sec). However, additional tests were conducted using the sealed joints which further reduced the permeability of the sheet pile wall to as low as approximately 3.28×10^{-12} ft/sec (1.5×10^{-10} cm/sec). It should be noted that the Starr study was a short-term study, and would not have measured the reduction in permeability with time. The true permeability of the sheet pile I-wall at the test site would be much lower than that measured by Starr since it has been in

[1] The detailed document is available at ArcelorMittal website at the following link http://www.arcelormittal.com/sheetpiling/uploads/files/AMCRPS_Impervious_EN.pdf

operation for many years. Other investigators (Cividini et al. 2007) have assumed that sheet piles were impervious in numerical models.

Numerical Modeling of the Test Section

The purpose of developing a numerical model for the London Avenue Canal load test site is to determine the soil parameters and hydraulic boundary conditions that can be used in subsequent assessments of the London Avenue Canal, as well as portions of the Orleans Canal and other canals that have similar site conditions.

The initial approach adopted was to model the canal as a two dimensional (2D) problem. It was assumed that the canal test section was sufficiently long (150 ft) as to adequately simulate 2D conditions. It was later judged that assessing the load test as a 2D problem may provide unconservative results, and a more robust 3D analysis was required.

Calibration of 2D FE Model with Field Test

The 2D modeling was performed for the load test geometry using the finite element seepage program incorporated into SLIDE 6.0 (Rocscience 2010). The 2D finite element model of the London load test is shown in Figure B-18. The boundary conditions required for the 2D finite element analysis were the flood-side constant head boundaries, with a head value assigned to the canal water elevation outside of the cofferdam; and the appropriate water elevation inside of the cofferdam. No-flow boundary conditions were assigned to the flood-side vertical boundary since it was considered to be located at the center of the canal. A potential seepage face was assigned on the landside horizontal ground surface since the position of the phreatic surface was not known.

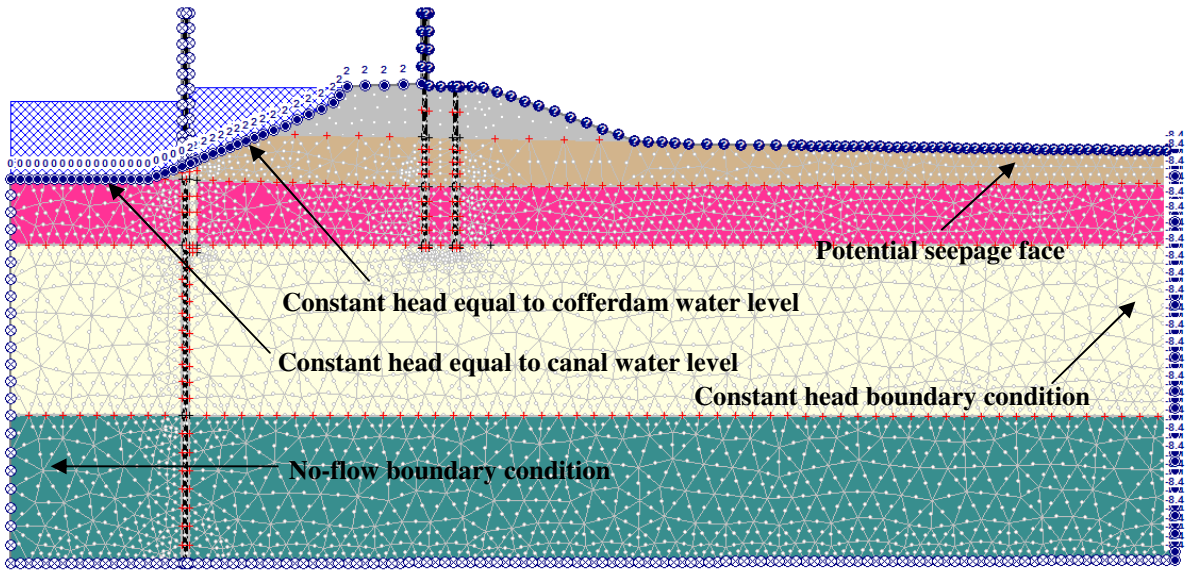

Figure B-18 2D Finite element model showing the mesh generated for the analysis.

One of the most important boundary conditions is the protected-side constant head boundary. Both the horizontal position and the value of the assigned head were iterated within reasonable limits to calibrate the model with the field test. These limits were governed by the street piezometers that were located in the vicinity of the load test indicating normal groundwater elevations in the area. There are two options for modeling the sheet piles of the cofferdam and the I -wall, either assigning them a no-flow boundary condition or assigning them a very low permeability, thus making them behave as impervious barriers. These were modeled by assigning them a very low permeability ($<10^{-100}$ ft/sec). However, the portion of the cofferdam extending above the levee was assigned a no-flow boundary condition to differentiate between the canal and the cofferdam water levels. It should be noted that the canal water level has no influence on the results in the 2D analysis.

The permeability of each layer was assigned based on the discussion presented earlier in the report, except the permeability of the silty sand layer. The permeability of the silty sand layer,

position of the protected-side boundary, and the value of the head at this boundary, were the main variables used to calibrate the model with the actual field data.

The water level inside the cofferdam was raised in increments to simulate the field test conditions and then the pore pressures were compared with the recorded field data for each increment. The 2D analyses also involved modeling of the gap that was formed between the I-wall and the levee for cofferdam water levels of greater than 5 ft. This was achieved by assigning specific nodes as constant head nodes equal to the cofferdam water level along the I-wall up to the bottom of the marsh layer. More details regarding modeling the gap formation will be provided later. Reasonable pore pressure results were obtained from the 2D model.

Multiple iterations were completed to arrive at the best combination for the calibration. The values of the parameters that gave the best match with the field piezometer readings are as follows:

- Permeability of the silty sand layer = 4.9×10^{-5} ft/sec.
- Horizontal distance of the protected-side boundary from the I-wall = 110 ft
- Total head at protected-side boundary = -8.4 ft (about 1.2 ft below the ground surface)

The total head distribution for the cofferdam water level of 2 ft from the 2D finite element analysis for the above conditions is shown in Figure B-19.

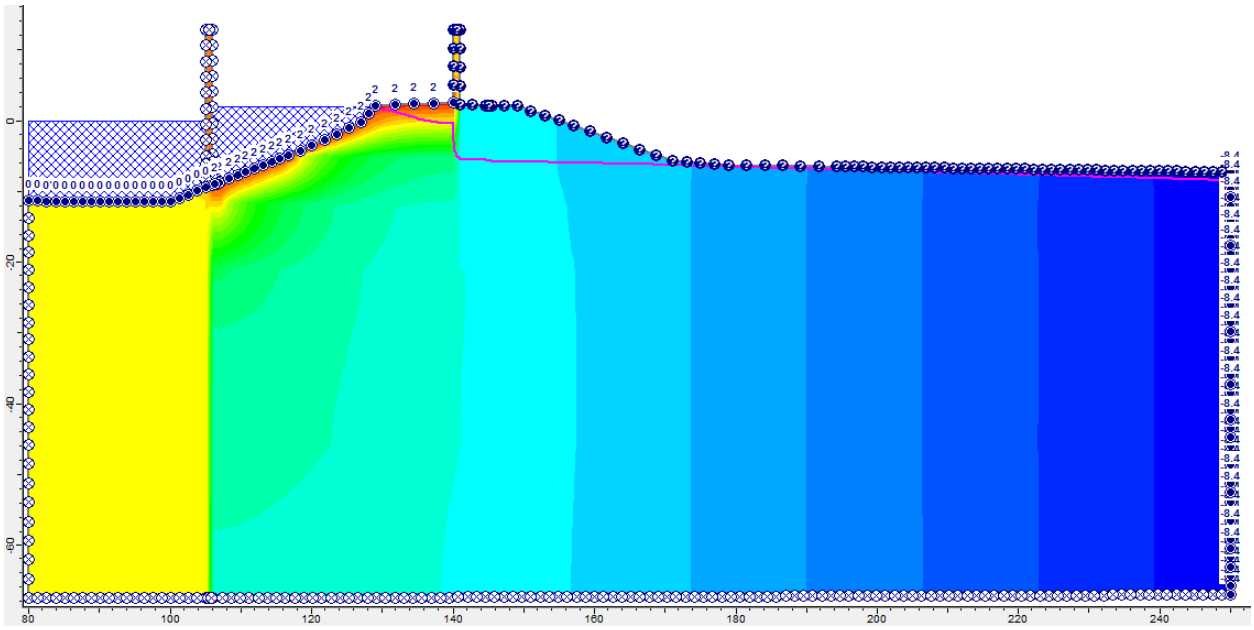

Figure B-19 Output of 2D finite element analysis showing the total head distribution for the canal water level of 2 ft.

3D vs. 2D Analysis

Two-dimensional analysis of seepage problems is very common in geotechnical engineering practice. It was used as a starting point for the more complex analyses conducted as part of this project once the nature of the load test and behavior of the site was fully understood from this analysis. It was easy to vary the parameters and to observe their effects on the pore pressures at various locations in 2D analysis and was comparatively less time consuming. The London Avenue Canal load test could have been accurately modeled as a 2D problem under perfect circumstances (e.g. if the boundary conditions provided essentially a 2D flow situation). However, it was believed that the following factors made the load test differ from the ideal conditions:

1. The flood-side extent of the test section did not go to the center of the canal which would have been a no-flow boundary condition. This also led to some complicated hydraulic boundary conditions on the flood side of the I-wall.
2. The test section was only 150 ft long and the edges of the cofferdam would affect the readings of the piezometers. In general, the highest pore pressures were measured in the center of the section. The pore pressures measured at the boundaries were smaller as compared to the center of the cofferdam as shown in Figure B-20.

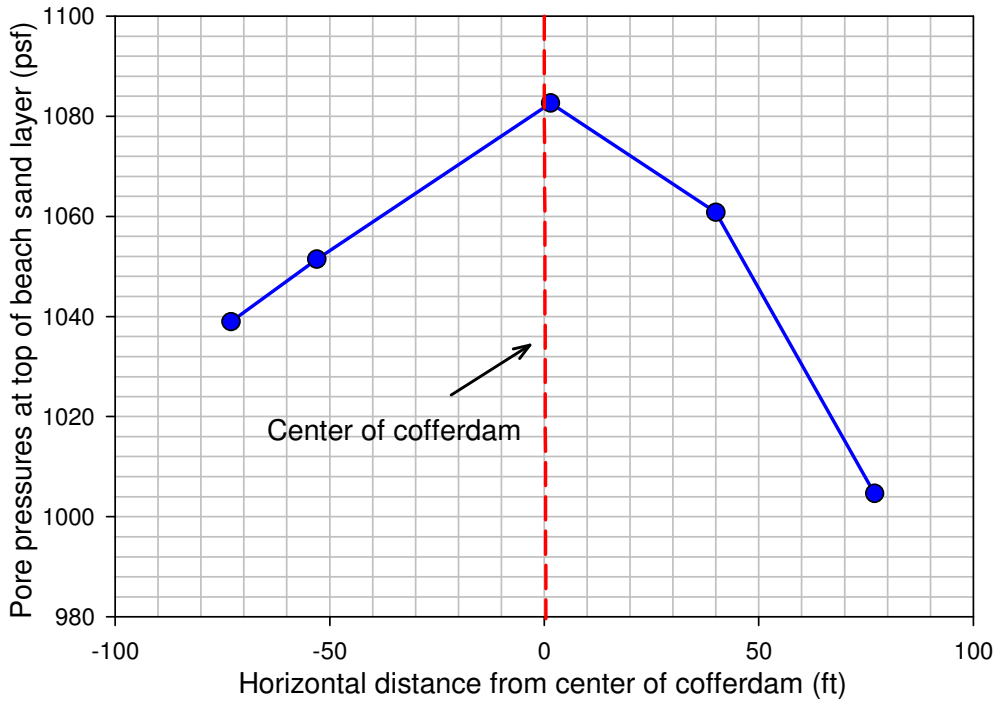

Figure B-20 Pore pressure distribution along the length of the cofferdam for canal water level of 4 ft.

3. The pore pressures may have been influenced by changes in the canal water level as well as the changes in the water level inside of the cofferdam.
4. The displacement of the wall was greatest at the center of the section, and decreased toward the boundaries as shown in Figure B-21. The influence of a “gap” short-circuiting

the flow would be dependent on the wall displacement. This would cause an additional influence on the measured pore pressures.

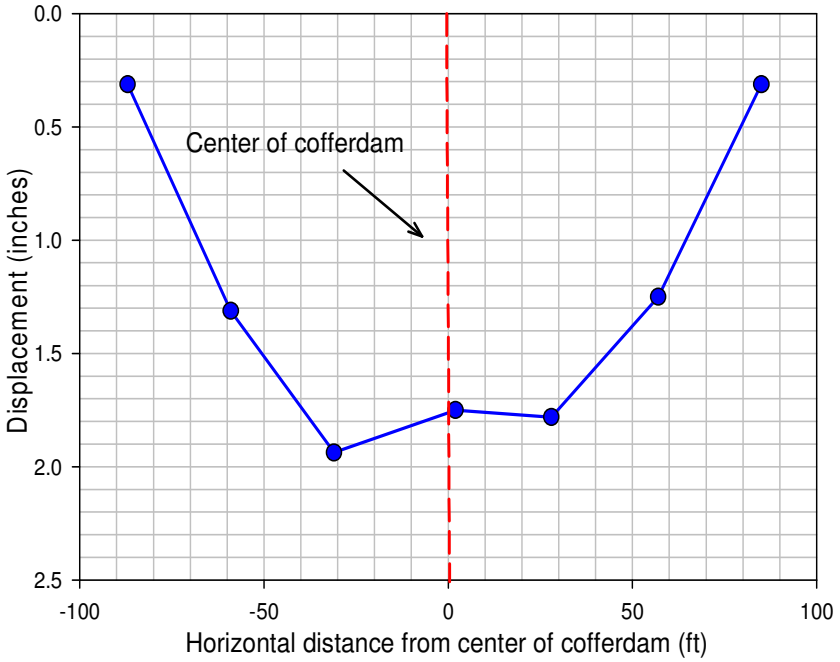

Figure B-21 Distribution of displacement at the top of the wall along the length of the cofferdam for canal water level of 7 ft for the Phase II portion of the test.

5. The permeability and general behavior of the injection wells that were used in Phase II may have changed during the course of the test due to clogging, etc. It was not possible to accurately mode the injection wells in 2D.

Based on the above information, it can be inferred that the London Avenue Canal load test was less than an ideal 2D test, and 3D modeling was necessary to capture the actual field conditions. This will be explained further in the following sections.

Modeling Approach

The most important deviations from the ideal 2D condition were the limited length of the test section and the complex flood-side boundary conditions. The limited length of the test section would cause the measured pore pressures during the test to be less than those that would be expected for a full canal load test for several reasons. First, as shown in Figure B-20, the pore pressures at the boundaries of the test section are much less than those at the center. This can be attributed to the fact that the boundary pore pressures can be affected by the canal water level, and not just the water level inside of the cofferdam. Also, the pore pressures would be influenced by the deflection of the I-wall. If the I-wall deflects enough to cause a hydraulic connection of the canal (cofferdam) water and a subsurface pervious layer, pore pressures would be expected to increase. For a full canal test, the deflection of each wall panel would be the same, assuming that the stiffness of the protected-side embankment fill was approximately the same. However, for the load test, only 5 panels were loaded, and the end panels were effectively "pinned." This would cause displacements, and likely pore pressures, to be greatest at the center or midpoint of the test section.

The limited extent of the test section toward the centerline of the canal would also influence the measured pore pressures. The designers tried to address this by having a Phase I and Phase II loading procedure. During the Phase I loading, the main contribution to the increase in pore pressures in the pervious layers would be mainly the creation of a "gap" along the flood side of the I-wall. The installation of the injection wells prior to the Phase II loading was done to simulate a condition where there was a hydraulic connection at the bottom of the canal to the outcropping of the pervious layers. For the Phase II loading, the pore pressures in the pervious

layers should have been mainly due to the hydraulic connection made by the wells, and less due to the formation of a gap between the I-wall and levee fill. Both the Phase I and Phase II boundary conditions instill some uncertainty in the numerical model.

The above factors led to the conclusion that pore pressures measured during the load test at various locations did not represent the pressures that would have been developed for a full canal test if the water level inside the entire canal was raised.

The following two-step procedure was initially adopted for the analysis of the London Avenue Canal load test:

1. Develop a simple three-dimensional (3D) model of the load test to incorporate the effects of the third dimension and to correct the pore pressures obtained from the test. Ideally, a constant correction factor could have been applied to all measured centerline pore pressures.
2. Build a two-dimensional (2D) model of the load test geometry and calibrate it with the corrected piezometer readings obtained from the 3D model of step 1.

The 3D analyses were started and the model was made consistent with the load test geometry. However, after running several 3D analyses, it was concluded that the initial thought process may not have been correct. The first step, to correct the pore pressures obtained from the load test by developing the 3D model, was logical. On the other hand, developing the 2D model of the test geometry was not reasonable. This is because the 2D model of the load test geometry did not capture the actual load test conditions in which the influence of the third dimension cannot be ignored. The comparison of the 2D model of the load test geometry with the actual field

condition was flawed because it was as if two different scenarios were compared. Changing the boundary conditions in the 2D model to accurately calculate the "corrected" pore pressures added too much uncertainty to the results.

A more appropriate procedure that was adopted to do the analysis for the London Canal load test is summarized in the following steps:

1. Calibrate the 3D model using the actual load test geometry and measured pore pressures. This calibration will increase confidence in the 3D model. This calibration is done using a parametric analysis and will be explained in a later section.
2. Use the parameters obtained from the calibrated 3D model of step 1 to develop a 3D model of the "ideal" or full canal load test.
3. Compare the pore pressures obtained from the models developed in steps 1 and 2. This will be of value in attaining either a single number or pore pressure distribution that should be multiplied with the observed piezometer readings to come up with the correct piezometer values that should have been observed if the load test was ideal.
4. Develop a 2D model of the full canal load test using the parameters obtained from the 3D modeling. As the 3D and 2D models will be the same for the full canal load test conditions, comparison of the pore pressures from these two models can be used as a final check.

The final modeling incorporates a 2D model with the full canal load test geometry which is calibrated with the actual load test through 3D modeling. This approach would eliminate the effects of the geometrical limitations of the load test and would ultimately provide the

appropriate soil properties and hydraulic boundary conditions to be used in the finite element model for the London Avenue Canal and other canals with similar subsurface conditions.

Verification

The 3D modeling of the test section is vital as explained in the preceding section. This can be demonstrated by plotting the streamlines from the 3D analysis as shown in Figure B-22 and Figure B-23. These figures show flow around the cofferdam, which would result in a head difference at the piezometers adjacent to the cofferdam. 3D effects would be observed due to the limited length of the cofferdam.

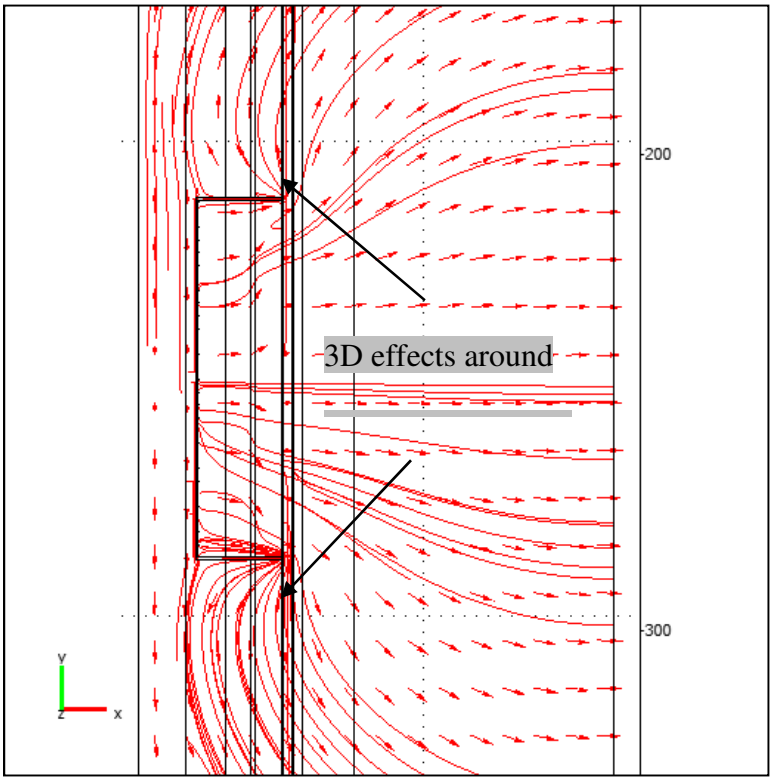

Figure B-22 Plan view of the streamlines in the vicinity of the cofferdam.

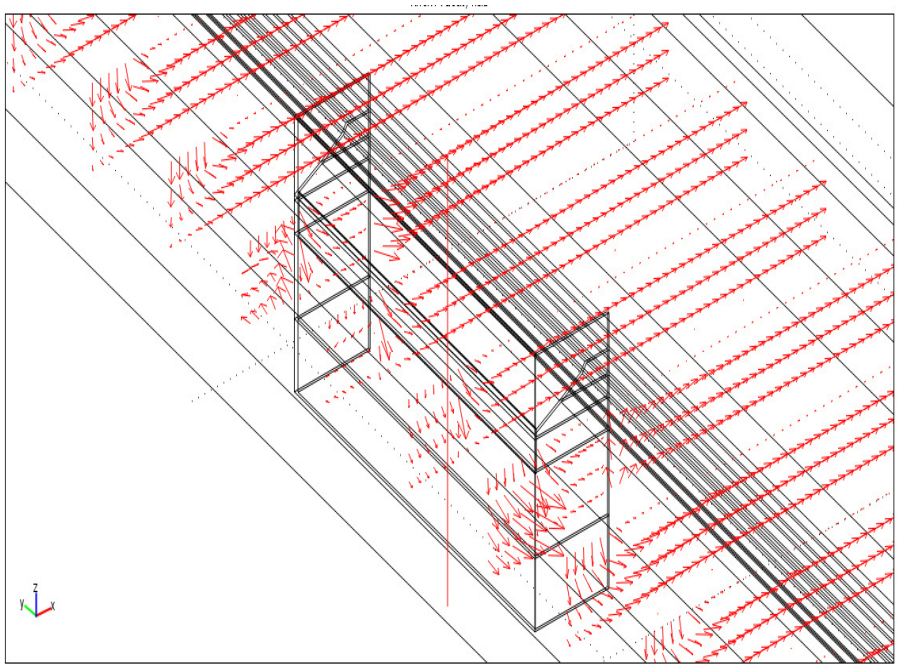

Figure B-23 Perspective view of the streamlines in the vicinity of the cofferdam.

This type of effect cannot be accommodated using a 2D analysis where there is no need to extend the model toward the flood side of the cofferdam and no-flow boundary condition can be shifted to the location of the cofferdam. Therefore, the actual canal water level outside the cofferdam is not captured in 2D modeling. However, Figure B-24 shows that an increase in total head was observed with an increase in canal water level for 3D analyses. The canal water level adjacent to the cofferdam influenced the piezometer readings during the load test as indicated by the 3D analyses of the load test geometry and its effect cannot be ignored.

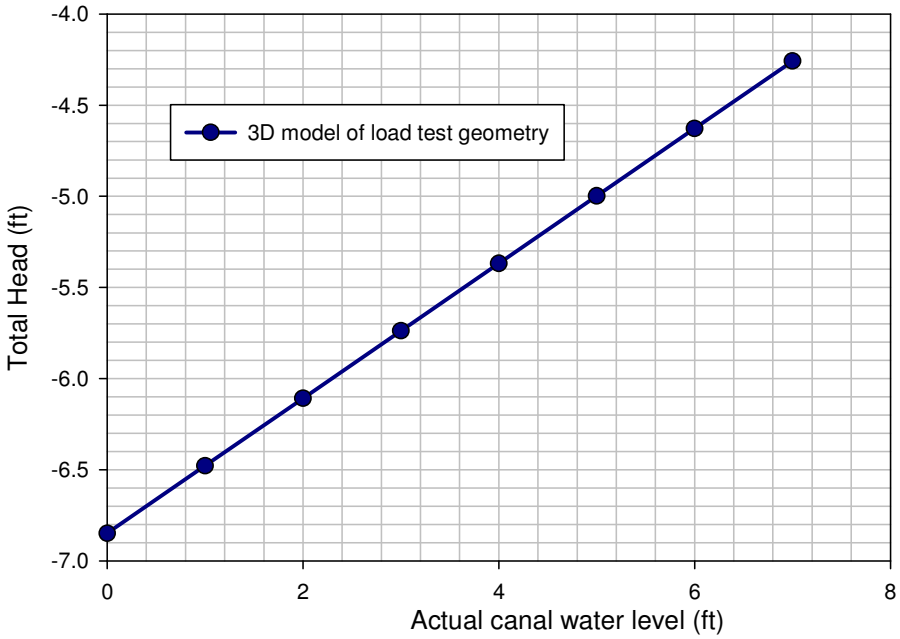

Figure B-24 Variation of the total head at the toe of the levee captured by the 3D analyses for different canal water levels keeping the cofferdam water level at 4 ft.

3D Analysis and Optimization

The 3D seepage analyses were performed using a finite element program called COMSOL Multiphysics (version 3.5). The Earth and Science Module of this program was used to perform the seepage analysis. Initially, a 2D seepage model was developed in COMSOL and then the output from this model was compared with SLIDE. It was observed that almost identical results were obtained from both programs for the total head at the top of the beach sand layer as shown in Figure B-25.

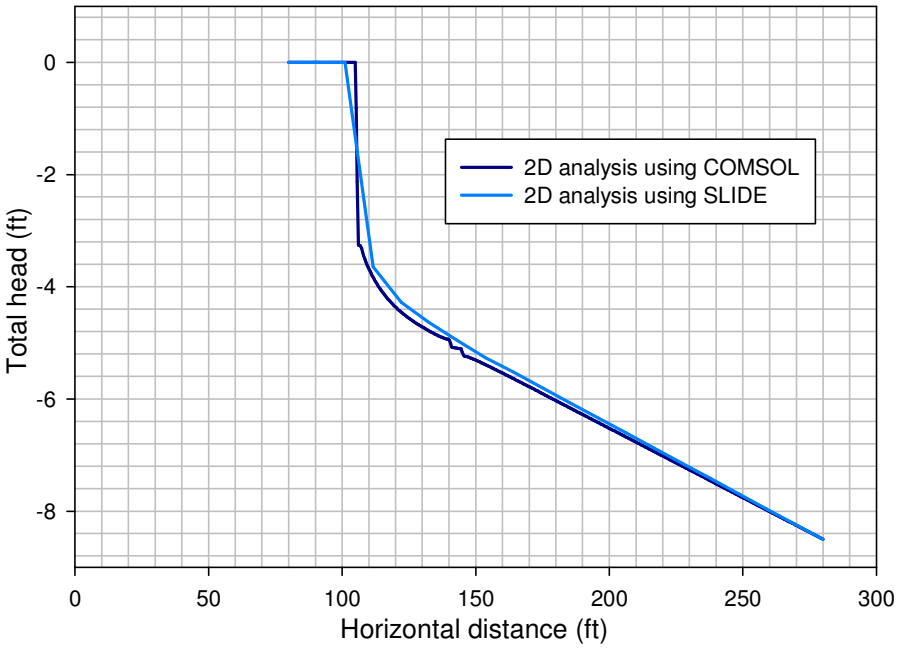

Figure B-25 Comparison of total heads from 2D analyses performed with SLIDE and COMSOL at the top of the beach sand layer.

The 3D model was made consistent with the load test geometry as shown in Figure B-26. It was decided to start with a very simple 3D model of the levee resting on the single layer of soil and having a sheet pile at the center of the levee crest. The model was made progressively more complex by adding the cofferdam, different soil layers (as present at the test site), and injection wells, so that the final model would be a true 3D representation model of the test section.

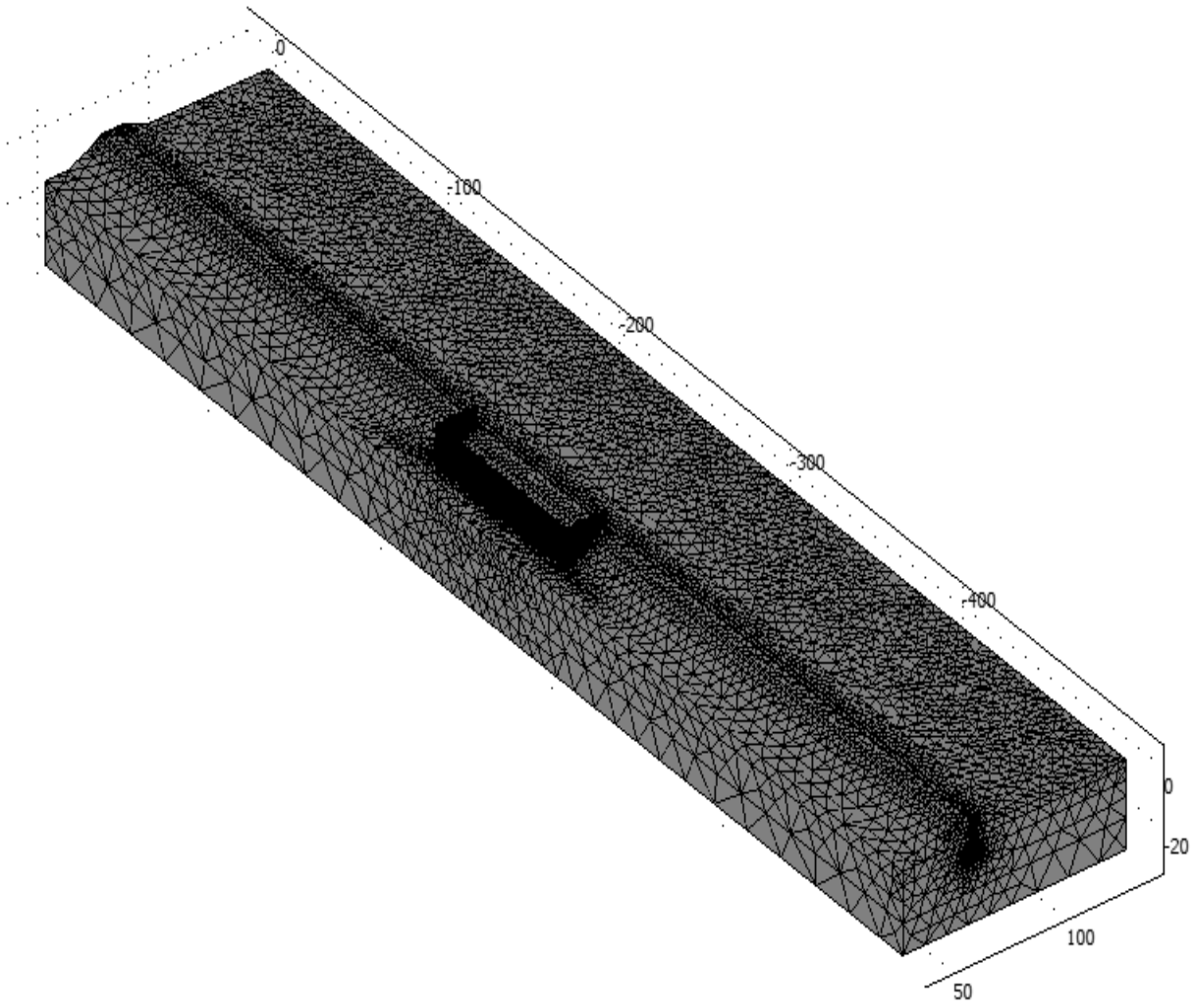

Figure B-26 3D finite element model of the load test geometry.

Phase II of the test was considered while modeling the load test as explained earlier. The injection wells were also modeled to replicate the field conditions showing the hydraulic connection between the water in the cofferdam and the underlying sand stratum. These were relatively difficult to discretize as the injections wells were dimensionally a very small feature with a large aspect ratio when compared to the domain in general. Figure B-27 and Figure B-28 show an orthogonal view of the injection wells as well as the elements comprising these wells in the plan view, respectively. It was also required to assign an appropriate permeability to the

injection wells in the seepage model. The injection wells were slotted PVC pipes to provide hydraulic connection to the beach sand layer. The initial thought was to assign this permeability equal to that of the beach sand layer. However, 3D analyses showed that assigning the permeability equal to that of the beach sand layer did not result in any significant change in total head when the cofferdam water level was increased. This indicated that the permeability of the injection wells during the load test was higher than the beach sand that allowed more flow into the sand layer resulting in significant change in total head with a change of cofferdam water level. The additional analyses were conducted and assigning the permeability of the injection wells as 0.049 ft/sec resulted in reasonable results and this value was used in all the subsequent analyses.

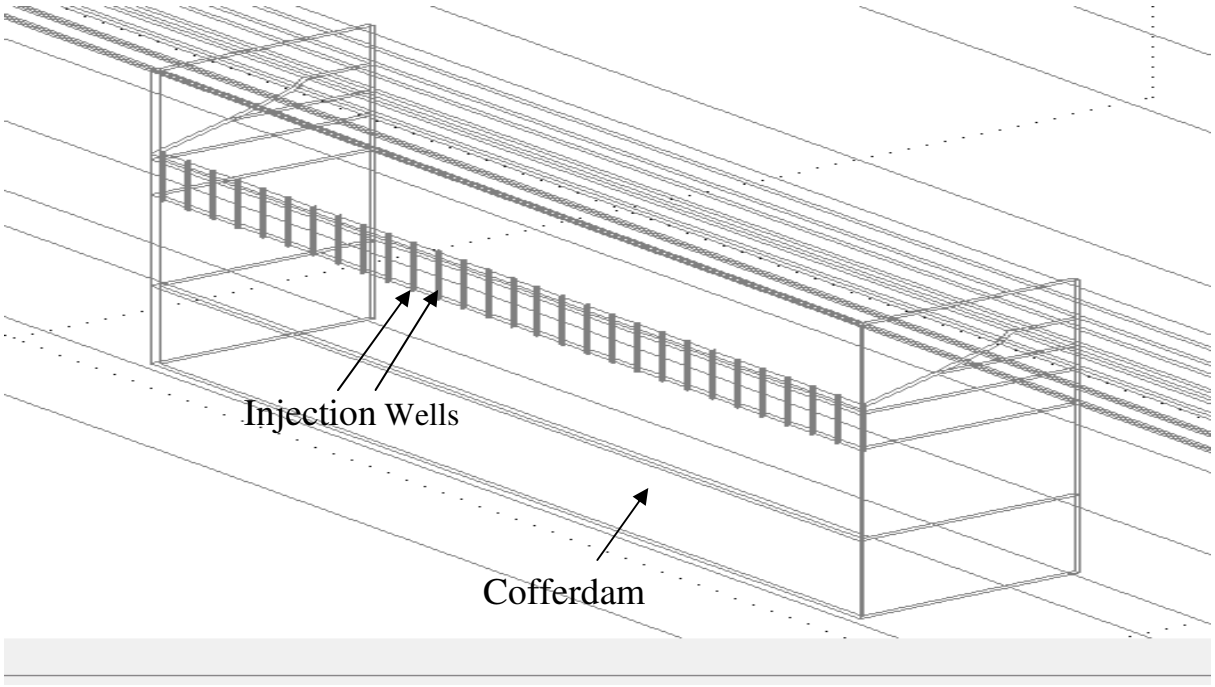

Figure B-27 3D view of injection wells and cofferdam.

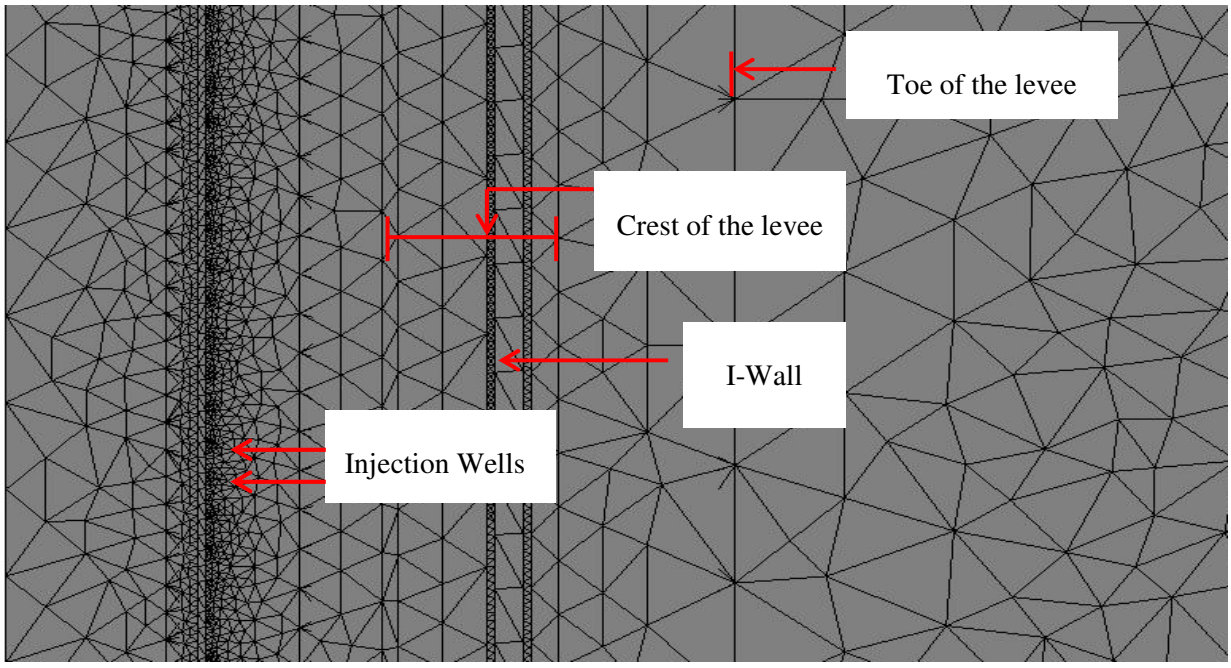

Figure B-28 Plan view showing meshing of injection wells.

After the geometry was developed, the boundary conditions were assigned. Figure B-29 shows the boundary conditions assigned to the 3D model used to simulate the load test geometry.

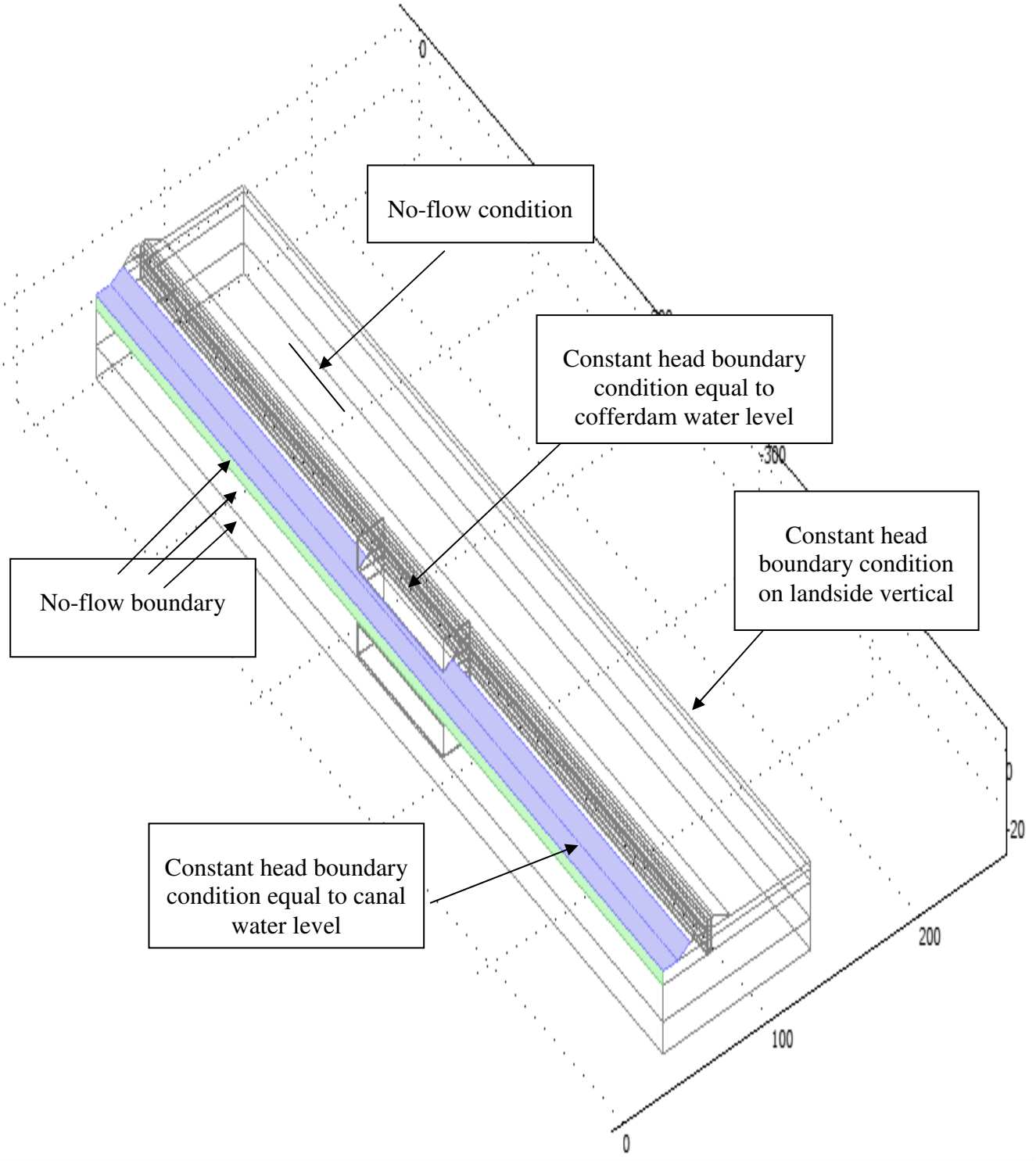

Figure B-29 Boundary conditions used in the 3D model of the London Avenue Canal load test.

A considerable effort was made to determine the hydraulic boundary conditions in the vicinity of the London Avenue Canal from the 3D seepage model by calibrating the model with the measured load test data. Different parameters, as described later, were varied and the total heads were compared with the piezometer values from the field test at the known locations. Contours of total head for one of the 3D analyses are shown in Figure B-30.

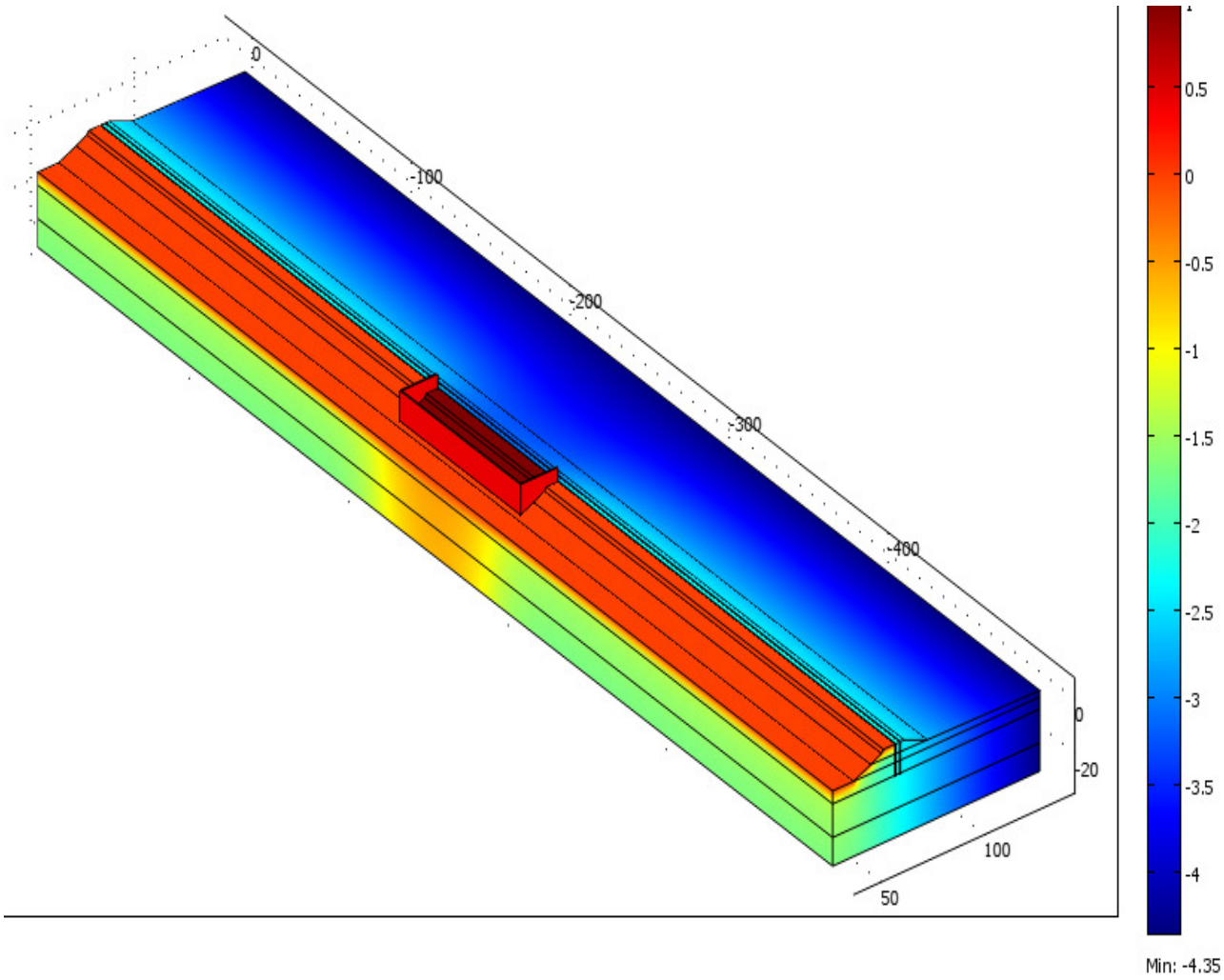

Figure B-30 Output of 3D finite element model showing total head distribution.

The initial analyses adopted a “trial and error” approach that was very time consuming, and it became obvious that the procedure would be more efficient if a parametric analysis of the 3D

model was performed and statistical data were obtained. After numerous runs used to determine the general effect of changing the soil properties and boundary conditions on the total heads at the piezometer locations, it was inferred that the following variables were the most important and required iteration in the analysis:

1. Permeability of silty sand layer.
2. Horizontal distance of the landside boundary from the I-wall.
3. Total head applied to the landside vertical boundary.

The range that the above parameters can logically vary was selected and step sizes were determined for each parameter. Note that the horizontal distance of landside boundary is considered from the toe of the levee in the upcoming discussion, which is located at about 40 ft from the I-wall. The ranges and step sizes are summarized in Table B-4.

Table B-4 Summary of the ranges of parameters to be iterated in parametric analysis.

Parameter	Min Value	Max Value	Step	No. of Runs
Vertical Landside BC	-7.2 ft	-12.2 ft	1 ft	6
Horizontal distance to vertical constant head boundary	100 ft	1000 ft	100 ft	10
Canal Water Level	2 ft	4 ft	1 ft	3
Permeability of silty sand (ft/sec)	1×10^{-6}	1×10^{-3}	1×10^{-6} 5×10^{-6} 1×10^{-5} 5×10^{-5} 1×10^{-4} 5×10^{-4} 1×10^{-3}	7

Based on the number of parameters given in Table B-4, the total number of runs was 1260. The next step is to generate curves for different combinations of variables to come up with the optimum values. One such schematic curve is shown for illustration purposes in Figure B-31.

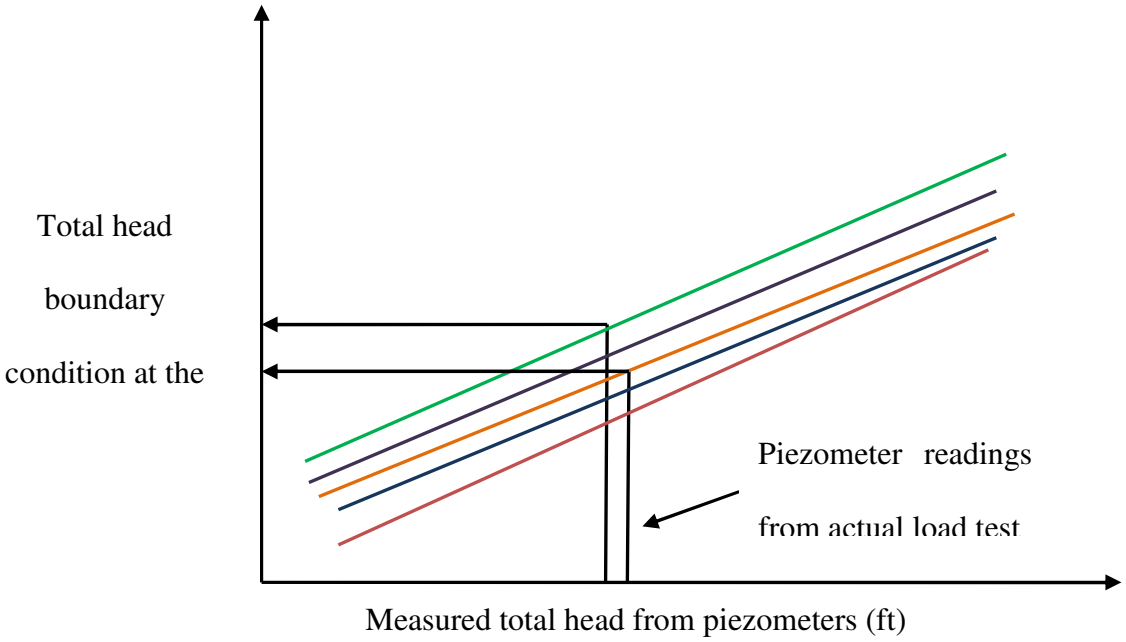

Figure B-31 Schematic plot for one of the combinations generated from parametric analysis.

In the schematic shown above, each line represents the variation of total head calculated at the location of one of the selected piezometers for different values of the total head boundary condition at the landward edge of the domain. The piezometer readings from the actual load test are known; therefore, using the corresponding piezometer line obtained from the 3D model, the boundary condition that is required to achieve the load test readings can be determined. This is done for all five selected piezometers and will produce a range of the head values to be assigned on the landward side for one combination. Plots similar to that shown above will be generated by varying the domain width, boundary conditions, canal water levels and permeability of the silty sand layer. Table B-5 will be generated to summarize the output for all of the combinations.

Table B-5 Summary of the outputs for landside vertical boundary conditions for each combination from parametric analysis.

Combination no.	Horizontal distance of landside boundary	CWL	k of silty sand	Range of total heads for vertical BC	Mean of total heads for vertical BC	Standard deviation of total heads for vertical BC
1						
2						
210						

All 1260 runs must be completed for a full application of the approach described above. However, 210 combinations can be obtained from these 1260 runs by varying the parameters shown in Table B-5 as each plot (based on each combination) will be generated using 6 different values of the landside vertical boundary condition (as shown in Figure B-31). The next step is to use optimization techniques to arrive at the best combinations for the calibration of the 3D model with the London Avenue Canal load test.

Another valid approach is to do multiscale optimization for all three variables, i.e., permeability of silty sand layer, position of the landside vertical boundary, and total head at the landside vertical boundary. This may require more involved statistical analysis but it is also a viable method. However, the approach regarding the optimization on the landside vertical boundary condition was adopted in this study and the numerical runs were carried out in a systematic manner. A summary of the 3D parametric analyses is presented in the following section.

Parametric Analysis

The parametric analysis was performed to obtain the statistical data to find the optimum model for the London Avenue Canal load test. One of the plots, similar to that described above, is shown in Figure B-32. This plot was constructed, making use of the initial estimates obtained from the 2D analysis, in order to check the viability of the approach.

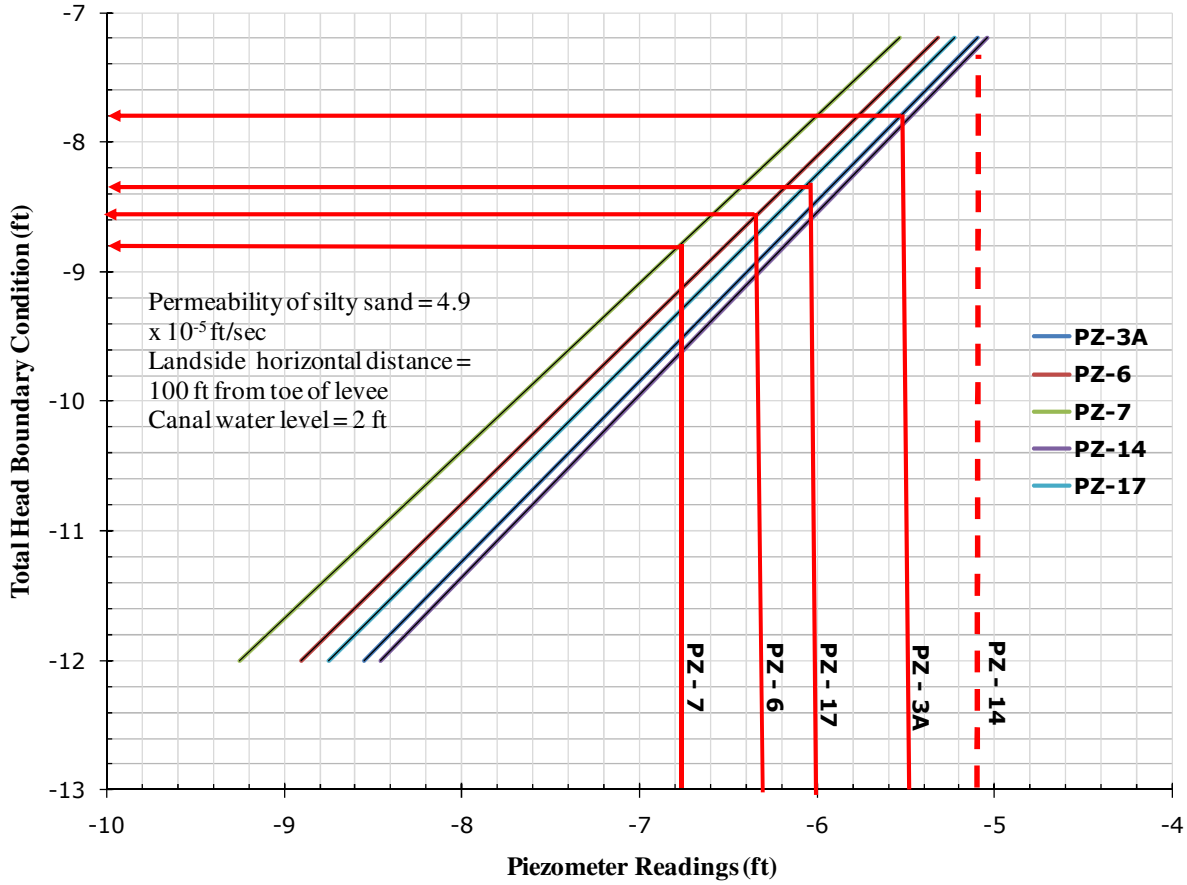

Figure B-32 Plot generated to obtain a range of total heads to be used as the landside vertical boundary condition for the permeability of the silty sand layer equal to 4.9 x 10^{-5} ft/sec, a landside horizontal distance of 100 ft from toe of the levee and a cofferdam water level of 2 ft.

It can be seen that the range of the appropriate head values for the boundary can be determined by comparison with the actual piezometer readings on the x-axis. It can be observed from the above plot that Piezometer 14 (PZ-14), located towards the canal side, was problematic as it did not fall within the range of the generated curves for this combination. The reasons for this will be explained later when discussing the optimization of the data. Conversely, there remains the possibility that the anomalous results of PZ-14 may be the case only for the above combination of parameters and there may exist a better combination for predicting the total heads closer to the field data for all the piezometers. Therefore, the use of parametric analysis to examine all the combinations becomes a valuable tool.

Performing the numerous runs of the 3D model for the parametric analysis is a time consuming process, but the merits and efficiency justify the use of this method. Similar plots as shown in Figure B-32 were generated for all other combinations to assist in the statistical analysis. The purpose of generating such plots was to determine the range of best possible values as explained above. Table B-6 shows a summary of the results for different combinations which can be used to determine the range of values for the landside vertical boundary condition.

Table B-6 Summary of the results for the landside vertical boundary conditions for each combination from the parametric analysis generated using COMSOL.

Combination no.	Horizontal distance of landside boundary (ft)	CWL (ft)	k of silty sand (ft/sec)	Range of total heads for vertical BC (ft)			Mean of total heads for vertical BC (ft)	Std. Dev. of total heads for vertical BC
				min	max	Difference		
1	100	2	1.00×10^{-6}	-8.87	-8.70	0.17	-8.81	0.079
2	100	3	1.00×10^{-6}	-8.83	-8.61	0.22	-8.71	0.083
3	100	4	1.00×10^{-6}	-8.73	-8.45	0.28	-8.59	0.107

Combination no.	Horizontal distance of landside boundary (ft)	CWL (ft)	k of silty sand (ft/sec)	Range of total heads for vertical BC (ft)			Mean of total heads for vertical BC (ft)	Std. Dev. of total heads for vertical BC
				min	max	Difference		
4	100	2	5.00×10^{-6}	-9.41	-9.09	0.32	-9.25	0.125
5	100	3	5.00×10^{-6}	-9.25	-9.00	0.25	-9.14	0.106
6	100	4	5.00×10^{-6}	-9.14	-8.91	0.24	-9.02	0.089
7	100	2	1.00×10^{-5}	-9.92	-9.41	0.51	-9.67	0.187
8	100	3	1.00×10^{-5}	-9.73	-9.31	0.42	-9.56	0.159
9	100	4	1.00×10^{-5}	-9.54	-9.28	0.26	-9.45	0.106
10	100	2	5.00×10^{-5}	-12.09	-10.55	1.54	-11.32	0.555
11	100	3	5.00×10^{-5}	-11.91	-10.45	1.46	-11.21	0.521
12	100	4	5.00×10^{-5}	-11.73	-10.43	1.30	-11.08	0.463
13	100	2	1.00×10^{-4}	-13.42	-11.08	2.34	-12.19	0.848
14	100	3	1.00×10^{-4}	-13.28	-10.99	2.29	-12.11	0.823
15	100	4	1.00×10^{-4}	-13.13	-10.98	2.16	-12.00	0.775
16	100	2	5.00×10^{-4}	-17.08	-11.87	5.22	-13.86	1.952
17	100	3	5.00×10^{-4}	-17.15	-11.81	5.34	-13.87	1.992
18	100	4	5.00×10^{-4}	-17.22	-11.84	5.39	-13.85	2.022
19	100	2	1.00×10^{-3}	-18.38	-11.72	6.66	-13.90	2.589
20	100	3	1.00×10^{-3}	-18.55	-11.66	6.90	-13.92	2.678
21	100	4	1.00×10^{-3}	-18.73	-11.68	7.05	-13.91	2.766
22	200	2	1.00×10^{-6}	-9.98	-9.77	0.20	-9.90	0.083
23	200	3	1.00×10^{-6}	-10.02	-9.75	0.27	-9.88	0.098
24	200	4	1.00×10^{-6}	-10.00	-9.66	0.34	-9.84	0.136
25	200	2	5.00×10^{-6}	-11.03	-10.02	1.01	-10.69	0.396
26	200	3	5.00×10^{-6}	-10.96	-10.69	0.27	-10.83	0.113

Combination no.	Horizontal distance of landside boundary (ft)	CWL (ft)	k of silty sand (ft/sec)	Range of total heads for vertical BC (ft)			Mean of total heads for vertical BC (ft)	Std. Dev. of total heads for vertical BC
				min	max	Difference		
27	200	4	5.00×10^{-6}	-10.93	-10.63	0.30	-10.78	0.106
28	200	2	1.00×10^{-5}	-12.06	-11.48	0.58	-11.78	0.211
29	200	3	1.00×10^{-5}	-11.92	-11.46	0.46	-11.73	0.177
30	200	4	1.00×10^{-5}	-11.79	-11.51	0.28	-11.66	0.128
31	200	2	5.00×10^{-5}	-16.38	-14.21	2.18	-15.25	0.783
32	200	3	5.00×10^{-5}	-16.09	-14.17	1.92	-15.17	0.687
33	200	4	5.00×10^{-5}	-14.94	-13.23	1.71	-14.09	0.608
34	200	2	1.00×10^{-4}	-16.67	-14.07	2.60	-15.31	0.943
35	200	3	1.00×10^{-4}	-18.52	-15.38	3.13	-16.91	1.128
36	200	4	1.00×10^{-4}	-18.42	-15.47	2.95	-16.86	1.059
37	200	2	5.00×10^{-4}	-24.52	-17.10	7.42	-19.94	2.778
38	200	3	5.00×10^{-4}	-24.73	-17.13	7.60	-20.06	2.832
39	200	4	5.00×10^{-4}	-24.94	-17.29	7.65	-20.15	2.873
40	200	2	1.00×10^{-3}	-26.27	-16.82	9.45	-19.92	3.676
41	200	3	1.00×10^{-3}	-26.62	-16.84	9.78	-20.05	3.800
42	200	4	1.00×10^{-3}	-26.98	-16.99	9.99	-20.15	3.922
43	300	2	1.00×10^{-6}	-10.95	-10.73	0.23	-10.87	0.091
44	300	3	1.00×10^{-6}	-11.07	-10.78	0.30	-10.92	0.108
45	300	4	1.00×10^{-6}	-11.11	-10.74	0.37	-10.93	0.152
46	300	2	5.00×10^{-6}	-12.62	-12.27	0.35	-12.44	0.146
47	300	3	5.00×10^{-6}	-12.60	-12.31	0.29	-12.46	0.124
48	300	4	5.00×10^{-6}	-12.63	-12.28	0.35	-12.45	0.125
40	300	2	1.00×10^{-5}	-14.25	-13.58	0.67	-13.92	0.244

Combination no.	Horizontal distance of landside boundary (ft)	CWL (ft)	k of silty sand (ft/sec)	Range of total heads for vertical BC (ft)			Mean of total heads for vertical BC (ft)	Std. Dev. of total heads for vertical BC
				min	max	Difference		
50	300	3	1.00×10^{-5}	-15.14	-14.60	0.53	-14.92	0.204
51	300	4	1.00×10^{-5}	-14.05	-13.72	0.33	-13.90	0.148
52	300	2	5.00×10^{-5}	-20.75	-18.16	2.59	-19.45	0.931
53	300	3	5.00×10^{-5}	-21.61	-19.17	2.44	-20.44	0.872
54	300	4	5.00×10^{-5}	-19.47	-17.30	2.17	-18.40	0.770
55	300	2	1.00×10^{-4}	-24.32	-20.14	4.17	-22.12	1.513
56	300	3	1.00×10^{-4}	-25.24	-21.17	4.07	-23.16	1.465
57	300	4	1.00×10^{-4}	-24.17	-20.34	3.83	-22.15	1.376
58	300	2	5.00×10^{-4}	-32.73	-22.86	9.87	-26.64	3.694
59	300	3	5.00×10^{-4}	-34.07	-23.97	10.10	-27.87	3.767
60	300	4	5.00×10^{-4}	-33.41	-23.24	10.17	-27.04	3.820
61	300	2	1.00×10^{-3}	-34.98	-22.44	12.54	-26.56	4.878
62	300	3	1.00×10^{-3}	-36.52	-23.54	12.98	-27.80	5.042
63	300	4	1.00×10^{-3}	-36.04	-22.79	13.25	-26.99	5.201
64	400	2	1.00×10^{-6}	-11.87	-11.63	0.25	-11.79	0.098
65	400	3	1.00×10^{-6}	-12.05	-11.74	0.32	-11.88	0.116
66	400	4	1.00×10^{-6}	-12.15	-11.75	0.40	-11.95	0.161
67	400	2	5.00×10^{-6}	-14.16	-13.77	0.39	-13.97	0.161
68	400	3	5.00×10^{-6}	-14.19	-13.86	0.33	-14.03	0.139
69	400	4	5.00×10^{-6}	-14.26	-13.89	0.38	-14.07	0.135
70	400	2	1.00×10^{-5}	-16.40	-15.62	0.77	-16.02	0.282
71	400	3	1.00×10^{-5}	-16.32	-15.70	0.62	-16.06	0.236
72	400	4	1.00×10^{-5}	-16.25	-15.88	0.37	-16.08	0.171

Combination no.	Horizontal distance of landside boundary (ft)	CWL (ft)	k of silty sand (ft/sec)	Range of total heads for vertical BC (ft)			Mean of total heads for vertical BC (ft)	Std. Dev. of total heads for vertical BC
				min	max	Difference		
73	400	2	5.00×10^{-5}	-25.25	-22.16	3.09	-23.68	1.113
74	400	3	5.00×10^{-5}	-25.11	-22.15	2.96	-23.69	1.059
75	400	4	5.00×10^{-5}	-23.99	-21.35	2.64	-22.68	0.940
76	400	2	1.00×10^{-4}	-30.03	-24.88	5.15	-27.32	1.868
77	400	3	1.00×10^{-4}	-29.97	-24.95	5.03	-27.40	1.810
78	400	4	1.00×10^{-4}	-29.92	-25.19	4.73	-27.43	1.700
79	400	2	5.00×10^{-4}	-40.98	-28.63	12.35	-33.36	4.620
80	400	3	5.00×10^{-4}	-41.43	-28.81	12.63	-33.70	4.704
81	400	4	5.00×10^{-4}	-41.90	-29.18	12.72	-33.93	4.777
82	400	2	1.00×10^{-3}	-43.74	-28.07	15.67	-33.22	6.091
83	400	3	1.00×10^{-3}	-44.44	-28.23	16.21	-33.55	6.295
84	400	4	1.00×10^{-3}	-45.14	-28.58	16.56	-33.84	6.497
85	500	2	1.00×10^{-6}	-12.73	-12.30	0.43	-12.48	0.176
86	500	3	1.00×10^{-6}	-12.98	-12.63	0.35	-12.80	0.125
87	500	4	1.00×10^{-6}	-13.12	-12.69	0.43	-12.91	0.177
88	500	2	5.00×10^{-6}	-15.64	-14.98	0.66	-15.31	0.259
89	500	3	5.00×10^{-6}	-15.72	-15.36	0.36	-15.54	0.163
90	500	4	5.00×10^{-6}	-15.84	-15.41	0.42	-15.63	0.151
91	500	2	1.00×10^{-5}	-18.48	-17.62	0.85	-18.05	0.312
92	500	3	1.00×10^{-5}	-19.81	-17.74	2.07	-18.78	0.805
93	500	4	1.00×10^{-5}	-18.39	-17.98	0.41	-18.18	0.190
94	500	2	5.00×10^{-5}	-31.70	-28.03	3.68	-29.87	1.325
95	500	3	5.00×10^{-5}	-29.58	-26.11	3.47	-27.84	1.240

Combination no.	Horizontal distance of landside boundary (ft)	CWL (ft)	k of silty sand (ft/sec)	Range of total heads for vertical BC (ft)			Mean of total heads for vertical BC (ft)	Std. Dev. of total heads for vertical BC
				min	max	Difference		
96	500	4	5.00×10^{-5}	-29.45	-26.36	3.08	-27.90	1.095
97	500	2	1.00×10^{-4}	-37.70	-31.60	6.10	-34.65	2.211
98	500	3	1.00×10^{-4}	-35.65	-29.70	5.95	-32.68	2.141
99	500	4	1.00×10^{-4}	-35.61	-30.01	5.60	-32.81	2.010
100	500	2	5.00×10^{-4}	-51.19	-36.40	14.79	-43.79	5.535
101	500	3	5.00×10^{-4}	-49.77	-34.63	15.14	-42.20	5.644
102	500	4	5.00×10^{-4}	-50.34	-35.10	15.25	-42.72	5.724
103	500	2	1.00×10^{-3}	-54.47	-35.71	18.76	-45.09	7.297
104	500	3	1.00×10^{-3}	-53.34	-33.92	19.41	-43.63	7.543
105	500	4	1.00×10^{-3}	-54.20	-34.36	19.84	-44.28	7.785

The above table is for half of the combinations that were described earlier (Table B-4). Although, analyses were completed for all 1260 runs, it was established that locations of the protected side domain boundary in excess of 500 ft provided very unreasonable results. Therefore, it was decided to exclude these runs from the above table.

The head value of the protected-side boundary that was required to obtain the same total head as measured during the field test was calculated for each piezometer in the same manner as shown in Figure B-32. This approach determined the required head boundary condition for each individual piezometer such that using this value of head in the numerical model predicted the exact measured pore pressure. The result is a set of five values for each combination since five different piezometers were considered for calibration purposes. The difference between the maximum and minimum value of the calculated total head was the range in which the boundary

condition needed to be assigned to get a match of the pore pressures predicted from the model with the field readings for that particular combination. After obtaining the results for the cofferdam water levels shown in Table B-6, the data were sorted such that the combinations having the same parameters were combined for different cofferdam water levels because the final aim was to obtain the best combination calibrated to all the water levels at the same time.

The average head value of the landside vertical boundary was calculated considering fifteen values from five piezometers for three different water levels for each combination of the vertical boundary horizontal distance and the permeability of the silty sand. The analysis was run again using the average value as calculated above and the total heads at the selected piezometer locations were again calculated. These values should be similar to the measured values in the field because the landside vertical boundary condition assigned in the final analysis had been back-calculated from plots similar to Figure B-32, which was developed for each combination as explained earlier.

The analyses thus far were done considering the cofferdam water levels up to 4 ft only. The measured values of the piezometers (Figure B-6) indicated a change in slope for the observed readings occurred at a cofferdam water level of about 5 ft. This indicated the development of the gap between the levee and the I-wall. In order to obtain the required boundary conditions for seepage analyses, it was decided to calibrate the model with the field test for the lower water levels only because the 3D model would be closer to the field conditions before the development of the gap.

It should be noted that the seepage analysis does not predict the formation of the gap. In order to predict the formation of the gap, and its associated effect on the pore pressures, a coupled

analysis, incorporating the stress-strain properties of the I-wall, levee fill, and other materials, would be required.

The modeling of the gap in the seepage analysis is an empirical procedure. After obtaining the optimum combination of boundary conditions, the analyses were repeated for higher water levels by incorporating the gap between the levee and the I-wall in the seepage model as constant head nodes along the sheet pile. The depth of the gap is determined by a trial-and-error procedure by incrementally changing nodes from no-flow to constant head until the pore pressures at the piezometer locations are matched.

After all combinations were analyzed, the results were carefully examined to begin the optimization process. At first, the ranges of the required vertical boundary condition were considered for the initial elimination of some of the combinations. The combinations that gave the smallest variation of the head at the protected-side boundary for all the piezometers for three different cofferdam water levels were considered to be the optimum. It was observed that analyses using horizontal distances of the landside boundary greater than 200 ft from the toe of the levee were giving a greater variation of the required head at the boundary. Therefore, distances of 100 ft and 200 ft from the toe of the levee were considered for further optimization.

The processed data indicated that the silty sand permeability values of more than 1 x 10^{-4} ft/sec for a horizontal distance of 100 ft resulted in unreasonably low protected-side boundary heads (more than 5 ft below the ground surface). The permeability value of the silty sand was further reduced to 1 x 10^{-5} ft/sec if the horizontal boundary distance of 200 ft was used in the model. The range of silty sand permeability is typically considered on the order of 10^{-5} to 10^{-7} ft/sec (3.05 x 10^{-4} to 3.05 x 10^{-6} cm/sec), so the results of the 3D model seemed reasonable. After reaching the

above conclusion, additional runs were made between the limits of 1 x 10^{-7} ft/sec (3.05 x 10^{-6} cm/sec) and 1 x 10^{-6} ft/sec (3.05 x 10^{-5} cm/sec) to further refine the permeability estimate. In addition, it was established that the distance of 100 ft from the toe of the levee seemed to agree best with the field conditions and further analyses were performed for this length only.

The analyses were conducted using the mean value of the head at the far protected-side boundary for each value of permeability within this range. Initially, all five piezometers (PZ-3A, PZ-6, PZ-7, PZ-14 and PZ-17) were used in the optimization. However, after carefully reviewing the data, it was observed that PZ-14 was not following any particular trend and seemed to provide erratic results. PZ-14 was a canal-side piezometer that was located inside the test section between the cofferdam and the I-wall. This piezometer was particularly sensitive to the cofferdam water level and also to the irregular flow around the cofferdam which existed due to its limited length as verified earlier. This piezometer was also very near to the I-wall and may have been affected by the rapid change in total heads (and total stresses) in the area around the sheet pile. This was further verified by observing the plots for the required head at the protected-side domain boundary which indicated that PZ-14 was falling outside the selected range of -7.2 ft and -12.2 ft for many cases, as shown in Figure B-32. Similar plots were generated to obtain the required value of permeability of the silty sand which would result in the same pore pressures from the model as measured in the field. These plots also indicated that PZ-14 would fall outside the limits of acceptable values for silty sand for most of the cases. One such plot is shown in Figure B-33.

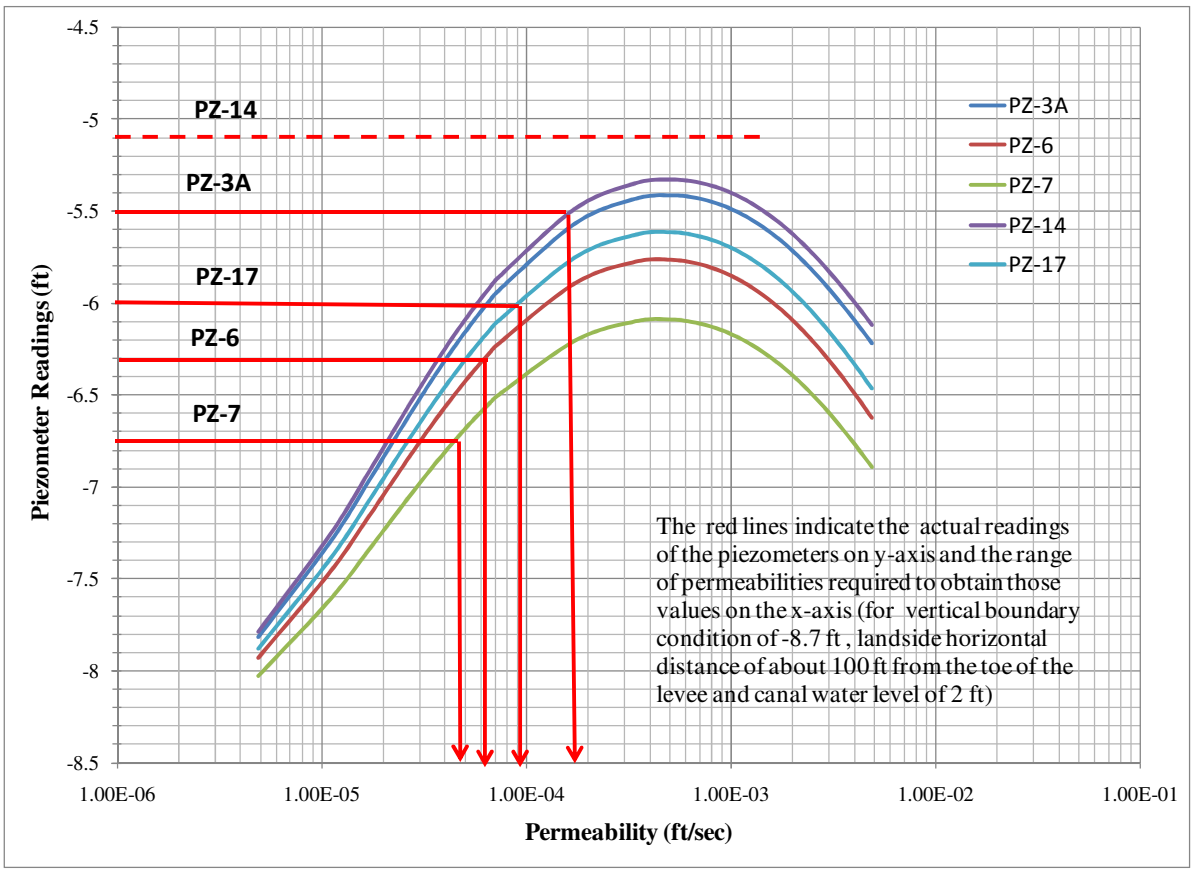

Figure B-33 Plot generated to obtain range of permeabilities to be used for silty sand layer for landside vertical boundary condition of -8.7 ft, landside horizontal distance of 100 ft and cofferdam water level of 2 ft.

It is clear from the above plot that PZ-14 is problematic and does not fall within the range of the generated curves. This indicates that an error was present in the readings and using this piezometer in the calibration process would result in unrealistic calculated boundary conditions in some cases. All other piezometer readings were within the reasonable limits of the field data. Therefore, it was decided not to give much emphasis to PZ-14 during the calibration process of the model. The data were obtained, and error, percent error, sum of absolute errors, variance and standard deviation were calculated for each value of permeability.

A viable method of selecting the best combination of parameters is to identify those that produce the minimum values of sum of absolute errors, variance and standard deviation. Table B-7 summarizes the results of the analyses as well as the errors, variance and standard deviations for a boundary distance of 100 ft from the toe of the levee.

Table B-7 Summary of the analysis results and calculations of errors, variances and standard deviations for a horizontal boundary distance of 100 ft.

CWL (ft)	BC (ft)	K (ft/sec)	Piezometer Readings from numerical model (ft)					Absolute Error (ft)					% Absolute Error					Sum of Absolute Error	Vairance	Standard deviation
			PZ 3A	PZ-6	PZ-7	PZ-14	PZ-17	PZ 3A	PZ-6	PZ-7	PZ-14	PZ-17	PZ 3A	PZ-6	PZ-7	PZ-14	PZ-17			
2	-8.58	1.0E-07	-5.52	-6.18	-6.70	-5.01	-5.85	0.02	0.12	0.05	0.09	0.10	0.42	1.91	0.78	1.72	1.75	1.11	1.31	1.14
3			-5.24	-5.95	-6.52	-4.68	-5.59	0.09	0.10	0.02	0.03	0.01	1.66	1.58	0.32	0.57	0.19			
4			-4.95	-5.73	-6.34	-4.34	-5.33	0.20	0.02	0.04	0.14	0.08	4.18	0.36	0.71	3.35	1.57			
2	-8.64	5.0E-07	-5.51	-6.18	-6.70	-5.00	-5.84	0.01	0.12	0.05	0.10	0.11	0.21	1.97	0.71	2.03	1.89	1.09	1.18	1.08
3			-5.22	-5.95	-6.53	-4.66	-5.58	0.07	0.10	0.03	0.01	0.02	1.43	1.65	0.39	0.22	0.35			
4			-4.94	-5.72	-6.35	-4.32	-5.32	0.19	0.03	0.05	0.12	0.07	3.92	0.44	0.77	2.95	1.40			
2	-8.70	1.0E-06	-5.50	-6.17	-6.71	-4.98	-5.83	0.00	0.13	0.04	0.12	0.12	0.00	2.05	0.65	2.32	2.03	1.07	1.10	1.05
3			-5.21	-5.95	-6.53	-4.65	-5.57	0.06	0.10	0.03	0.00	0.03	1.21	1.72	0.45	0.11	0.50			
4			-4.92	-5.72	-6.35	-4.31	-5.32	0.17	0.03	0.05	0.11	0.07	3.68	0.52	0.84	2.59	1.24			
2	-9.14	5.0E-06	-5.48	-6.19	-6.78	-4.93	-5.83	0.02	0.11	0.03	0.17	0.12	0.40	1.67	0.51	3.26	2.07	1.18	0.90	0.95
3			-5.19	-5.97	-6.61	-4.60	-5.57	0.04	0.08	0.11	0.05	0.03	0.78	1.33	1.67	1.16	0.53			
4			-4.90	-5.74	-6.43	-4.26	-5.31	0.15	0.01	0.13	0.06	0.06	3.21	0.09	2.10	1.40	1.20			
2	-9.56	1.0E-05	-5.46	-6.22	-6.86	-4.89	-5.83	0.04	0.08	0.11	0.21	0.12	0.75	1.28	1.65	4.16	2.06	1.39	1.47	1.21
3			-5.17	-5.99	-6.69	-4.55	-5.57	0.02	0.06	0.19	0.10	0.03	0.39	0.92	2.86	2.18	0.54			
4			-4.88	-5.77	-6.51	-4.21	-5.31	0.13	0.02	0.21	0.01	0.06	2.77	0.33	3.34	0.22	1.19			
2	-11.20	5.0E-05	-5.39	-6.33	-7.19	-4.67	-5.84	0.11	0.03	0.44	0.43	0.11	2.03	0.54	6.47	8.43	1.86	3.08	10.47	3.24
3			-5.08	-6.10	-7.00	-4.31	-5.57	0.07	0.05	0.50	0.34	0.03	1.27	0.81	7.76	7.36	0.55			
4			-4.78	-5.86	-6.82	-3.95	-5.30	0.03	0.11	0.52	0.25	0.05	0.66	1.97	8.28	6.06	0.94			
2	-12.10	1.0E-04	-5.37	-6.43	-7.40	-4.52	-5.88	0.13	0.13	0.65	0.58	0.07	2.28	2.10	9.68	11.34	1.23	4.46	22.79	4.77
3			-5.05	-6.18	-7.21	-4.13	-5.59	0.10	0.13	0.71	0.52	0.01	1.86	2.22	10.9	11.09	0.14			
4			-4.73	-5.94	-7.02	-3.75	-5.31	0.02	0.19	0.72	0.45	0.06	0.33	3.24	11.4	10.79	1.10			

It was observed that the total heads obtained from the numerical modeling, especially for the lower values of permeability of the silty sand, were generally within 5% of the field values for all the piezometers considered. The minimum value of variance and standard deviation is obtained for the combination having permeability value of silty sand as 5.00 x 10^{-6} ft/sec (1.52 x 10^{-4} cm/sec) and the total head at the protected-side domain boundary set as -9.14 ft. Although, the sum of absolute errors for this combination is slightly more than the combinations having a lower permeability value of silty sand, closer inspection revealed that this combination gave an

overall better agreement for all of the cofferdam water levels. Therefore, this combination was considered to be optimal in terms of the calibration with the load test data.

A finite element seepage and stability analyses of the London Canal breaches was presented in the report prepared by Interagency Performance Evaluation Taskforce (IPET 2007). The values of permeabilities used in the IPET study for various soil layers such as beach sand, levee fill, marsh and bay sound clay were the same as used in the finite element models developed in this report. The horizontal distance to the landside boundary domain was considered about 170 ft from the toe of the levee for the north breach (the closest to the load test) in the IPET report. The landside vertical constant head boundary condition used in the IPET analysis was set as either -8.4 ft or -3.9 ft. These boundary conditions were different from the values obtained from the calibration of the load test data through optimization in this report. No silty sand layer was considered in the cross sections used by the IPET for the seepage analysis. However, the silty sand layer that was encountered at the site of the London Avenue Canal load test greatly affected the pore pressures and influenced the boundary conditions for the finite element model.

A summary of best values of various parameters for the seepage analyses obtained from the calibration of the load test data is shown in Table B-8.

Table B-8 Summary of best values of various parameters for finite element seepage analysis of the London Canal obtained from calibration of the load test data.

Parameters	Value	
	Calculated from laboratory and field tests	**Calculated from optimization**
Permeability of the levee fill	3.28×10^{-8} ft/sec (1.00×10^{-6} cm/sec)	-
Permeability of the marsh layer	3.28×10^{-7} ft/sec (1.00×10^{-5} cm/sec)	-
Permeability of the silty sand layer	-	5×10^{-6} ft/sec (1.52×10^{-4} cm/sec)
Permeability of the beach sand layer	4.9×10^{-4} ft/sec (1.5×10^{-2} cm/sec)	-
Permeability of the bay sound clay layer	3.28×10^{-8} ft/sec (1.00×10^{-6} cm/sec)	-
Permeability of the sheet pile wall	$< 10^{-100}$ ft/sec ($< 3.05 \times 10^{-99}$ cm/sec)	-
Landside vertical boundary condition	-	-9.14 ft (1.94 ft below the ground surface)
Horizontal distance to the landside boundary domain from I-wall	-	140 ft

The analyses were further run for the higher cofferdam water levels with the gap between the levee and the I-wall incorporated in the seepage model. A uniform gap was considered along the entire length of the cofferdam for all canal water levels beyond 5 ft. This assumption would not be totally correct because of the non-uniform displacements measured for the I-wall as shown in Figure B-21. During the field test, the gap would have initiated at the center of the test section and progressed towards the edges as the cofferdam water level increased. Therefore, this procedure of modeling of the gap would only be approximate. The behavior of the field test could be more accurately modeled considering the soil-structure interaction along with the seepage analysis, which was beyond the scope of this study.

The gap was initially considered to the top of the silty sand layer, but the output for such analysis showed that the total heads increased linearly with the canal water level with the same slope as before (as for lower canal water levels without the gap). This indicated that the gap between the I-wall and the levee down to the top of the silty sand layer was not sufficient to influence the pore pressures to the degree that was measured. Therefore, it was assumed that the silty sand layer would have the ability to sustain a gap, and the gap was extended into the silty sand layer. The depth of the gap did not extend all the way to the beach sand layer because that would have resulted in very significant increase of pore pressures. The results showed that the total heads obtained from the finite element model were within approximately 8% of the field data after the development of the gap. These results seemed reasonable considering the limitations of the seepage model in capturing the gap formation. Figure B-34 to Figure B-38 show the comparison between the total heads calculated from the 3D seepage model and the observed readings from the actual load test.

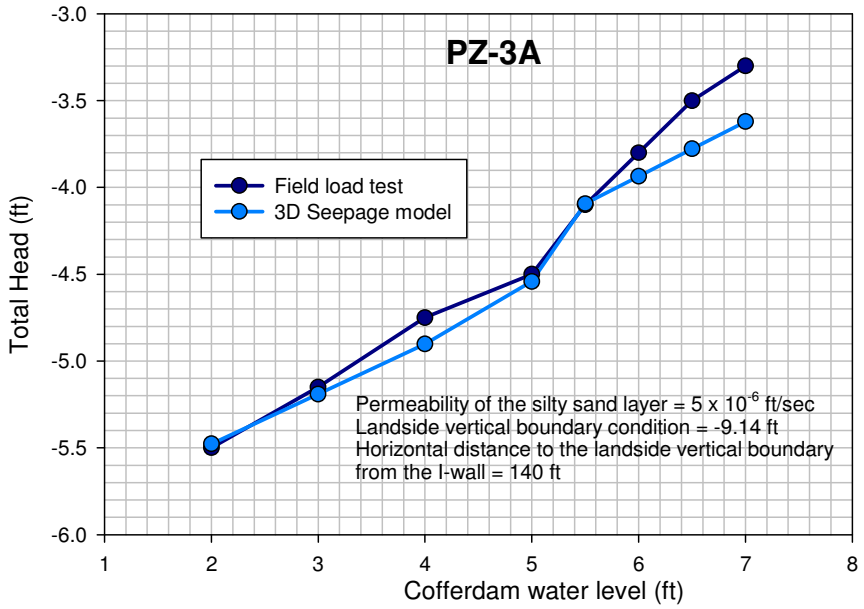

Figure B-34 Comparison of total heads obtained from London Avenue Canal load test and 3D seepage model for PZ-3A.

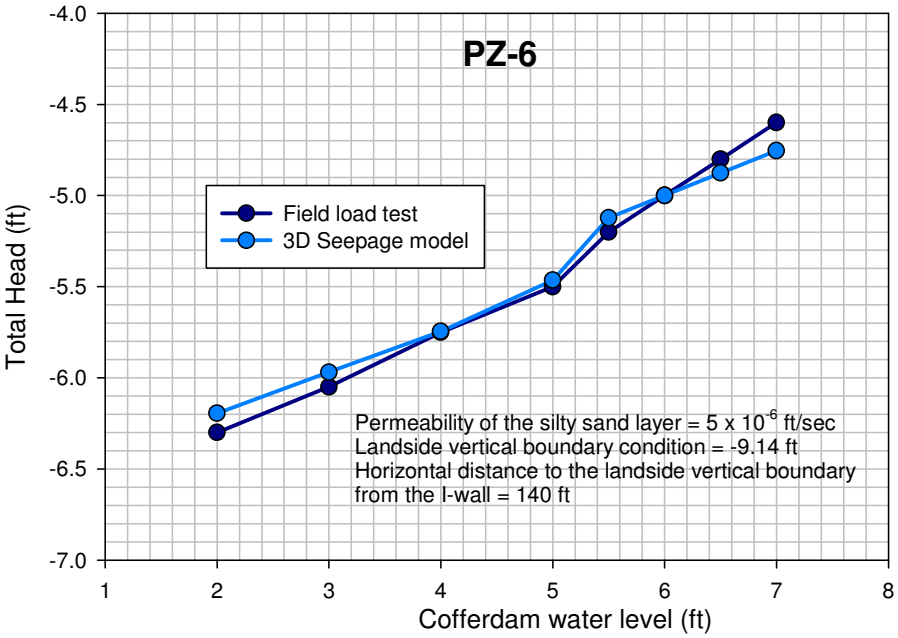

Figure B-35 Comparison of total heads obtained from London Avenue Canal load test and 3D seepage model for PZ-6.

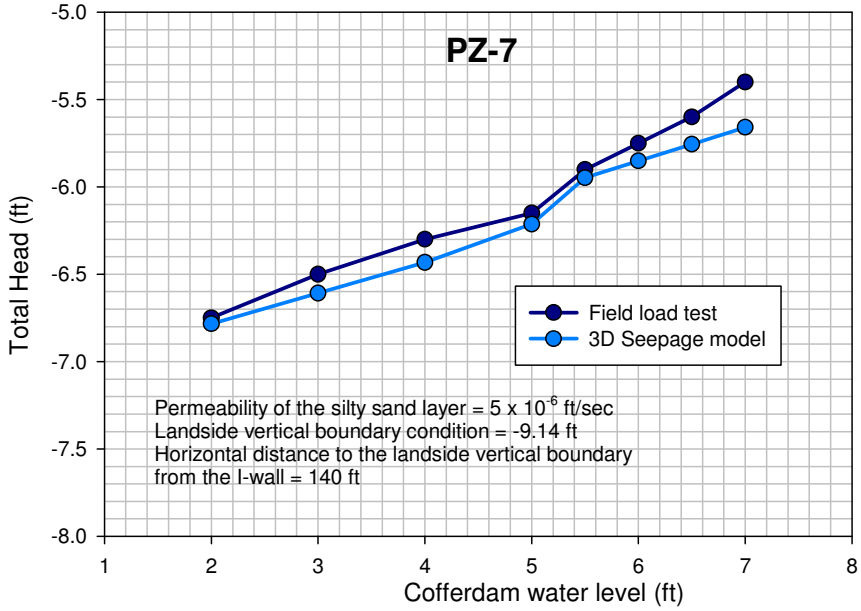

Figure B-36 Comparison of total heads obtained from London Avenue Canal load test and 3D seepage model for PZ-7.

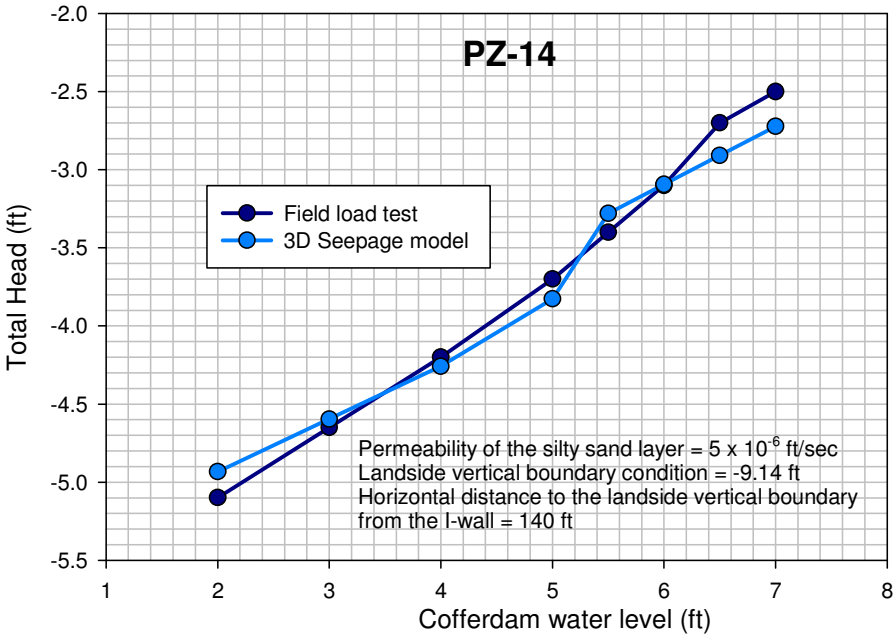

Figure B-37 Comparison of total heads obtained from London Avenue Canal load test and 3D seepage model for PZ-14.

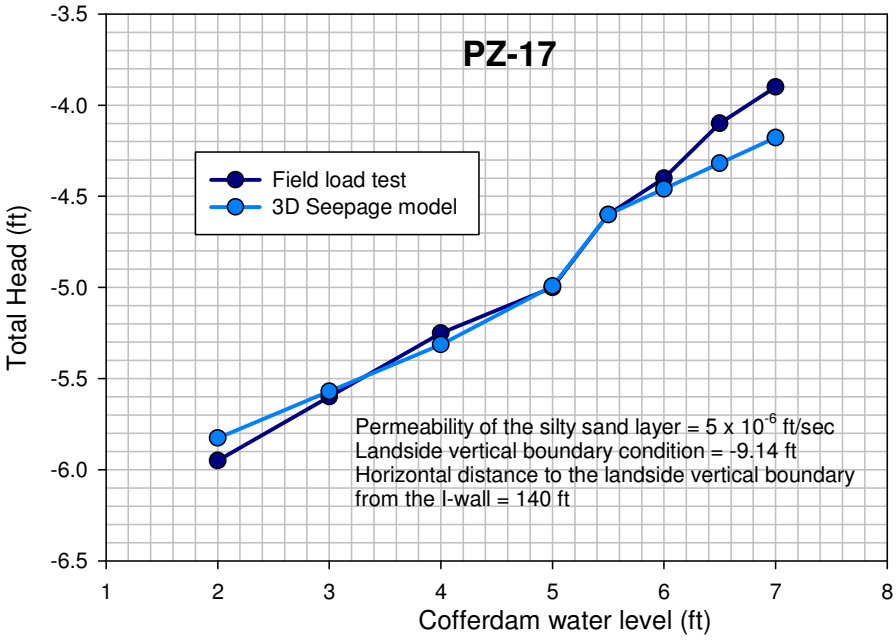

Figure B-38 Comparison of total heads obtained from London Avenue Canal load test and 3D seepage model for PZ-17.

The above results indicate that the 3D seepage model predicts the pore pressure measured during the field test with considerable accuracy. This was especially true prior to the formation of the gap. After the gap has formed, some errors in calculated pore pressures may be incurred owing to the limitations associated with modeling the gap in the current seepage analyses.

2D Analysis of Full Canal Load Test Geometry

The next step was to construct a seepage model for the full canal load test geometry assuming that there were no boundary effects (e.g., the entire canal was loaded). The results from 2D and 3D analyses should be the same if the test was conducted under such ideal conditions.

The 2D and 3D models of the full canal load test were compared and identical results were obtained indicating that both the models were working properly. It was decided to use a 2D

model for further analyses because the final aim was to specify the boundary conditions and material parameters for a 2D model that can be generalized along the London Avenue Canal and sites having similar conditions.

The boundary conditions and soil parameters obtained by calibrating the 3D seepage model with the actual load test were used in the 2D analyses. These included the permeability value of silty sand as 5.00×10^{-6} ft/sec (1.52×10^{-4} cm/sec), a constant head of -9.14 ft assigned to the protected-side domain boundary, and a landside horizontal distance of about 140 ft from the I-wall. The output from the 2D model for such boundary conditions for the selected piezometers is shown in Figure B-39.

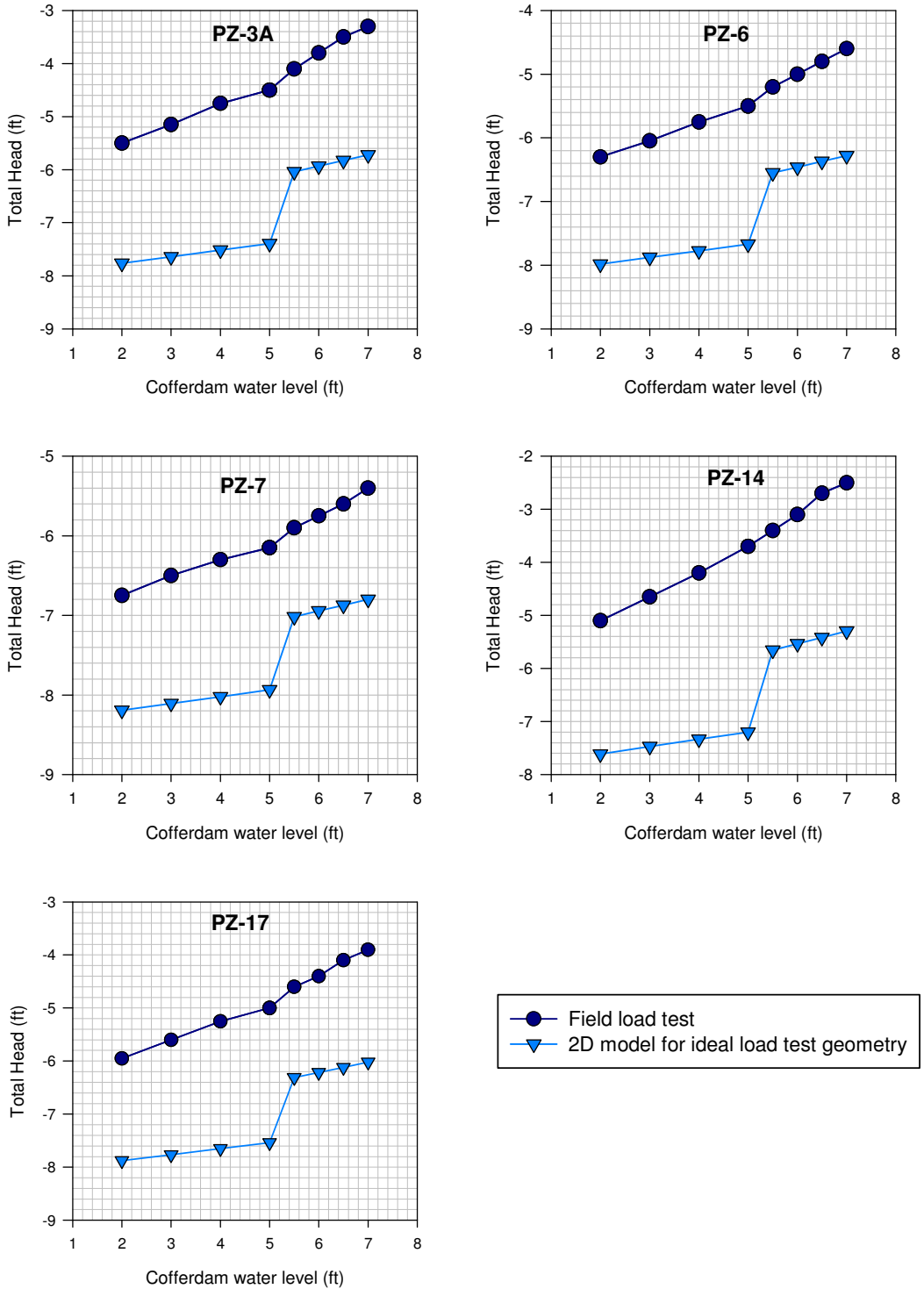

Figure B-39 Comparison of total heads obtained from London Avenue Canal load test and 2D model of full canal load test for the selected piezometers.

The 2D finite element results can be viewed as the results that would have been expected at the test site location if a full canal test had been conducted. The total heads (pore pressure) obtained from the 2D analyses of the full canal load test were lower than the observed values in the field during the load test. This indicated that the load test was conservative in that the measured pore pressures were higher than those that would have been expected for a full canal load test.

It was inferred that the injection wells considered in the Phase II of the load test were a vital component of the 3D seepage model. These injection wells provided a hydraulic connection to the bottom of the canal layer and resulted in higher pore pressures in the pervious layer (beach sand). However, no such injection wells would be present in a full canal load test. Since the permeability of the silty sand layer was much less than the permeability of these injection wells, no hydraulic connection was established in the 2D model. Therefore, this 2D model is a replica of the field condition when the bottom of the canal is "silted in," which differs from the Phase II load test conditions.

These results are also supported by the fact that the silty sand layer was determined to be two orders of magnitude less pervious than the underlying beach sand layer, so great deal of head loss would take place in the silty sand layer and therefore lower pore pressures would be observed in the beach sand layer. Therefore, these factors resulted in lower pore pressures in the 2D model as compared to the actual load test or the 3D model of the load test geometry, and thus making the load test conservative for these particular conditions.

However, the conclusion that the load test was overall conservative cannot be generalized based solely on the above results. It was observed that the pore pressures developed in the beach sand layer were greatly influenced by the value of the permeability of the silty sand. The load test

would have been unconservative if the permeability of the silty sand layer was even modestly higher than the value used in the above analyses. This was verified by conducting the 2D analyses using the value of the silty sand layer equal to the initial estimated value of 4.75×10^{-5} ft/sec (1.45×10^{-3} cm/sec) from the boring data (as explained in permeability section). The total heads obtained from these analyses for the selected five piezometers are shown in Figure B-40. There was a significant increase in the measured total heads as the silty sand was considered one order of magnitude more pervious. This indicated that the permeability of the silty sand layer is a very important factor in the calculated results. The boundary conditions obtained from the 3D seepage analyses in this study are site specific and care must be exercised in generalizing these conditions. The knowledge of the permeability of the soil strata especially becomes very important if a soil of intermediate permeability like silty sand is encountered because it significantly affects the pore pressures in the pervious layer.

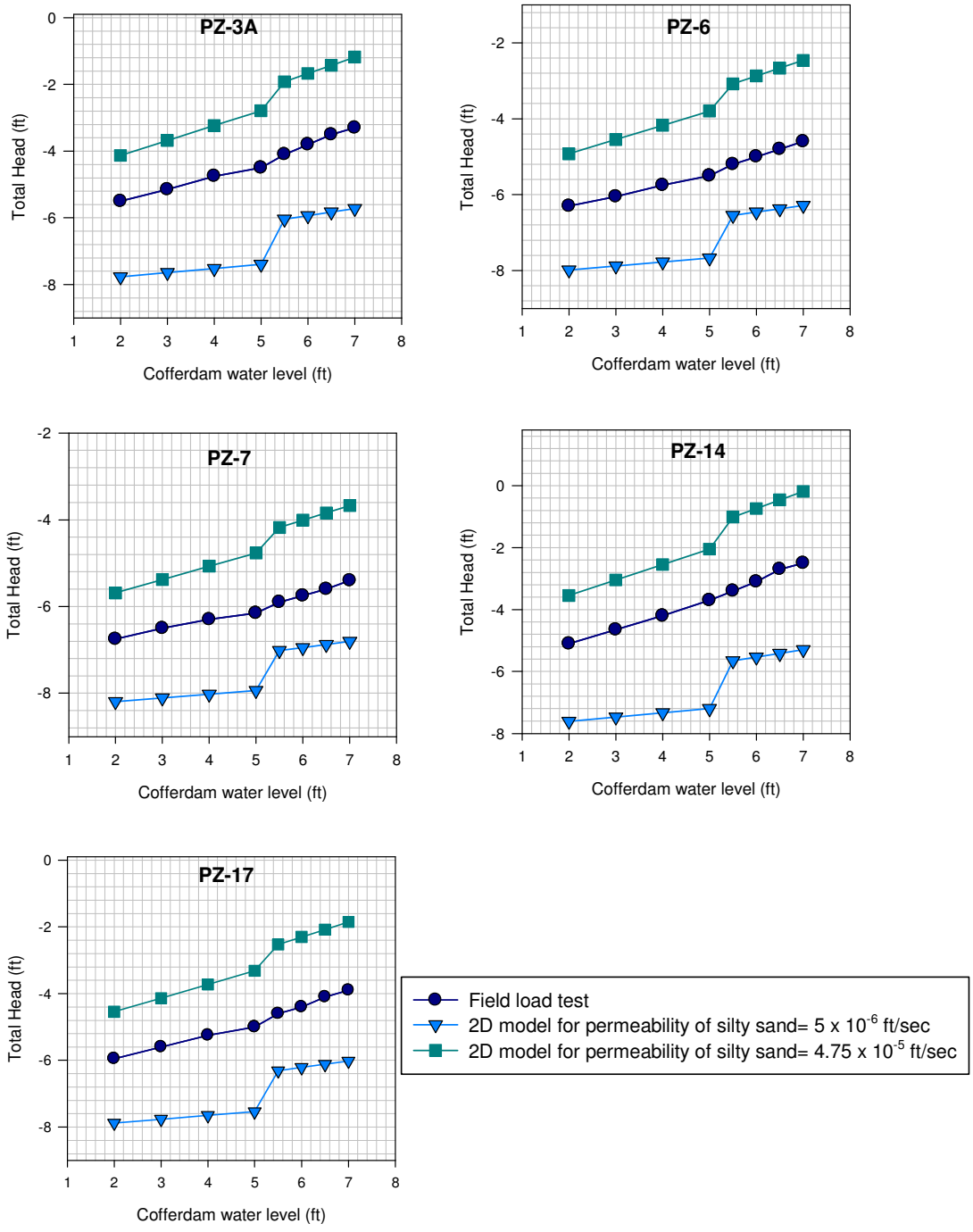

Figure B-40 Comparison of total heads obtained from London Avenue Canal load test and 2D model of full canal test for silty sand permeabilities of 5 x 10^{-6} ft/sec and 4.75 x 10^{-5} ft/sec.

Summary and Conclusions

An analysis was performed of the London Avenue Canal load test in order to arrive at a finite element seepage model. The available exploration and field test data were evaluated to estimate the appropriate soils parameters. The greatest uncertainty was judged to exist in the permeability of the silty sand layer, the location of the constant head protected side domain boundary, and the value of the head at this boundary.

Initial analyses showed that the boundary conditions of the load test deviated too much from a two-dimensional (2D) flow condition, and that accurate results would not be obtained using a 2D finite element analysis to calibrate the seepage model to the load test results. Because of this, a 3D finite element procedure was used to model the true geometrical nature of the load test.

A statistical optimization procedure was used for the determination of the best possible values of the permeability of the silty sand layer, the location of the constant head protected side domain boundary, and the value of the head at this boundary. This approach required over 1200 finite element runs to be conducted, but the results allowed correct prediction of the centerline pore pressures measured during the Phase II portion of the load test.

Based on this analysis, the parameters listed in Table B-9 are recommended for future analyses of London Avenue Canal, and other canals having similar subsurface conditions. The values listed in the table are similar to those used in the IPET analyses, but slightly less conservative.

Table B-9 Recommended seepage analysis parameters for the London Avenue Canal.

Parameters	Value	
	Calculated from laboratory and field tests	**Calculated from optimization**
Permeability of the levee fill	3.28×10^{-8} ft/sec (1.00×10^{-6} cm/sec)	-
Permeability of the marsh layer	3.28×10^{-7} ft/sec (1.00×10^{-5} cm/sec)	-
Permeability of the silty sand layer	-	5×10^{-6} ft/sec (1.52×10^{-4} cm/sec)
Permeability of the beach sand layer	4.9×10^{-4} ft/sec (1.5×10^{-2} cm/sec)	-
Permeability of the bay sound clay layer	3.28×10^{-8} ft/sec (1.00×10^{-6} cm/sec)	-
Permeability of the sheet pile wall	$< 10^{-100}$ ft/sec ($< 3.05 \times 10^{-99}$ cm/sec)	-
Landside vertical boundary condition	-	-9.14 ft (1.94 ft below the ground surface)
Horizontal distance to the landside boundary domain from I-wall	-	140 ft

Recommendations for Further Study

The London Avenue Canal load test was a landmark effort to measure the full-scale behavior of an I-wall system. The extensive instrumentation resulted in large quantities of data being collected. The amount, type, and quality of data collected are unprecedented in regards to previous field tests conducted on I-wall structures.

The analysis presented in this report represents a significant first effort in understanding the seepage behavior of I-walls and other flood protection systems. A robust analysis procedure was developed that allows determination of unknown parameters, critical to performing a seepage analysis, to a high degree of reliability.

Owing to the limited scope of this first effort, many questions regarding both seepage and gap development remain. It was not possible to assess the model for pore pressures that measured away from the centerline of the test section. It was shown in the report that the boundary effects of the test section caused significant variation in measured pore pressures along the axis of the I-wall. The validity of the 3D analysis can further be assessed by extending the analysis to other piezometers monitored during the field test.

The Phase II results were the focus of the analysis presented in this report since a greater pore pressure response was measured in the beach sand layer. The hydraulic boundary conditions for the Phase I loading were complicated in that the only possible hydraulic connection with the silty sand and beach sand layers would have been through the formation of a gap. It would be valuable to reconcile the pore pressures measured during the Phase I loading with the 3D model to correctly predict field pore pressures for both phases.

Understanding the formation of the gap is difficult using only a seepage analysis. If correct pore pressures can be predicted prior to the formation of the gap, then the gap can be modeled empirically by changing the nodes next to the sheet pile as a function of cofferdam water level until the pore pressures match. This approach was used in this report, but it was only an approximation since it was assumed the gap formed equally for the entire length of the test section. This was demonstrated not to be the case based on the acquired field test data.

The best understanding of I-wall behavior would be gained from a soil-structure interaction analysis looking at the gap formation as a function of the stress-strain behavior of the backfill soils. This type of analysis, coupled with the seepage analysis, would be very valuable in developing design procedures for I-walls.

References

Carman, P. C. (1956). *Flow of gases through porous media*, Butterworths Scientific Publications, London.

Conroy, P. (2008). "London Avenue site specific load test report." Technical Report, U.S. Army Corps of Engineers, St. Louis, MO.

Carrier, W.D. (2003). "Goodbye, Hazen; Hello, Kozeny-Carman." *J.Geotech. Engrg*., 129(11), 1054.

Cedegren, H.R. (1989). *Seepage, drainage, and flow nets*, Wiley, London.

Cividini, A. and Gioda, G. (2007). "Back-Analysis Approach for the Design of Drainage Systems." *International Journal of Geomechanics*, **7**(5), 325-332.

COMSOL (2010). "Introduction to COMSOL Multyphysics: Version 3.5." Reference Manual and Tutorial, COMSOL Inc, Burlington MA.

Driscoll, F.G., (1986). *Groundwater and Wells*, Johnson Filtration Systems Inc.

Duncan, J.M., Witherspoon, P.A., Mitchell, J. K., Watkins, J., Hardcastle, J.H., and Chen, J.C. (1972). "Seepage and Groundwater Effects Associated with Explosive Cratering." *Report on TE-72-2*, University of California, Berkeley.

Duncan, J. M., Brandon, T. L., Wright, S. G., and Vroman, N. (2008). "Stability of I-walls in New Orleans during Hurricane Katrina." J.Geotech. Engrg., 134(5), 681–691.

Hazen, A. (1911). ''Discussion of 'Dams on sand foundations' by A. C. Koenig.'' *Trans. Am. Soc. Civ. Eng.,* 73, 199–203.

Holtz, R. D., and Kovacs, W. D. (1981). *An introduction to geotechnical engineering*, Prentice-Hall, Englewood Cliffs, N.J.

Interagency Performance Evaluation Task Force (IPET). (2007). "Performance evaluation of the New Orleans and Southeast Louisiana Hurricane protection system." *Final Rep. of the Interagency Performance Evaluation Task Force*, U.S. Army Corps of Engineers, (www.ipet.army.mil).

Kenney, T.C., Lau, D. and Ofoegbu, G.I. (1984). "Permeability of compacted granular materials." *Canadian Geotechnical Journal*,21, 726-729.

Kozeny, J. (1927). ''Ueber kapillare Leitung des Wassers im Boden.'' *Wien, Akad. Wiss.,* 136(2a), 271.

MacFarlane, I. C. (1959). "A review of the engineering characteristics of peat." *Am. Soc. Civil Engineers Proc., Jour. Soil Mechanics and Found. Div*., V. 85, no. SMI, pt. 1, 21-35.

Powers, J. P. and Burnett, R.G. (1986). "Permeability and the Field Pumping Test," *Proceedings of IN SITU '86, ASCE Speciality Conference,* Blacksbrg, Virginia.

Rocscience, Inc. (2010). "Slide v6.0–2D limit equilibrium slope stability analysis." Toronto.

Sellmeijer, J.B., Cools, J.P.A.E., Decker, J., and Post, W.J. (1995). "Hydraulic Resistance of Steel Sheet Pile Joints." *J.Geotech. Engrg.*, 121(2), 105–110.

Slichter, C.S. (1905). "Field measurements of the rate of movement of underground waters." *Water-Supply and Irrigation Paper No. 140,* U.S. Geological Survey, Washington, D.C.

Starr, R.C. (2000). "Field hydraulic test of a rectangular enclosure comprised of Bethlehem steel PZ 22 sheet piling." *Waterloo Center for Groundwater Research.*

Terzaghi, K., and Peck, R. B. (1964). *Soil mechanics in engineering practice*, Wiley, New York.

USACE (2006). "London Avenue Aquifer Pumping Test." Report by US Army Corps of Engineers.

URS (2007). "Structural and foundation response measured during the site specific load test on the London Avenue Outfall Canal I-wall/levee." Report submitted to US Army Corps of Engineers.

Weber, W. G., Jr. (1969) "Performance of Embankments Constructed over Peat," Journal of the Soil Mechnics and Foundatons Division, ASCE, January 1969, pp. 53-76.

Yeats, M. (2004). "Hydraulic performance - transmissivity and permeability." CMI Technical White Paper, (www.cmiengineer.com/whitepapers/hydraulic.pdf).